OTDM network processing using all-optical and electro-optical devices

Ian David Phillips

Doctor of Philosophy

The University of Aston in Birmingham

March, 1998

The University of Aston in Birmingham

OTDM network processing using all-optical
and
electro-optic devices

Ian David Phillips

Doctor of Philosophy

1998

Abstract

The current optical communications network consists of point-to-point optical transmission paths interconnected with relatively low-speed electronic switching and routing devices. As the demand for capacity increases, then higher speed electronic devices will become necessary. It is however hard to realise electronic chip-sets above 10 Gbit/s, and therefore to increase the achievable performance of the network, electro-optic and all-optical switching and routing architectures are being investigated.

This thesis aims to provide a detailed experimental analysis of high-speed optical processing within an optical time division multiplexed (OTDM) network node. This includes the functions of demultiplexing, 'drop and insert' multiplexing, data regeneration, and clock recovery. It examines the possibilities of combining these tasks using a single device. Two optical switching technologies are explored. The first is an all-optical device known as a 'semiconductor optical amplifier-based nonlinear optical loop mirror' (SOA-NOLM). Switching is achieved by using an intense 'control' pulse to induce a phase shift in a low-intensity signal propagating through an interferometer. Simultaneous demultiplexing, data regeneration and clock recovery are demonstrated for the first time using a single SOA-NOLM.

The second device is an electroabsorption (EA) modulator, which until this thesis had been used in a uni-directional configuration to achieve picosecond pulse generation, data encoding, demultiplexing, and 'drop and insert' multiplexing. This thesis presents results on the use of an EA modulator in a novel bi-directional configuration. Two independent channels are demultiplexed from a high-speed OTDM data stream using a single device. Simultaneous demultiplexing with stable, ultra-low jitter clock recovery is demonstrated, and then used in a self-contained 40 Gbit/s 'drop and insert' node. Finally, a 10 GHz source is analysed that exploits the EA modulator bi-directionality to increase the pulse extinction ratio to a level where it could be used in an 80 Gbit/s OTDM network.

Keywords: optical time division multiplexing (OTDM), demultiplexing, 'drop and insert' multiplexing, data regeneration, clock recovery, semiconductor optical amplifier-based nonlinear optical loop mirror (SOA-NOLM), electroabsorption (EA) modulator

Acknowledgements

I would firstly like to thank my *mum* and *dad* for their encouragement in pursuing my interests. Thanks also goes to *Chrissy* for her understanding and support, and who foolishly agreed to help correct my grammar in this thesis. A personal thanks to *Dave*, *Sara*, *Nickie*, *John* and *Colin*, my flat-mates during my time at Aston, who with *Stella*, we spent many nights discussing the finer points of life. A special thanks to *Jo* who let me stay in her flat while I was writing this thesis.

A big thank you to my supervisor *Prof. Ian Bennion*, who always had time to read my work, and who gave me space and encouragement to develop my own ideas. Thanks also must go to all the members of the Photonics Research Group at Aston, past and present. Especially to *Paul Harper*, *Richard Fallon*, *Finlay Knox*, *Lorna Everall*, *etc...* the experimentalists among us, for their co-operation while sharing equipment. Thank you also to *Allister Pattison* for passing on his experimental skills, and to *Pete Kean* with whom I worked closely in the lab, and who helped me develop my research skills. A special thanks to *Andrew Gloag* for his help and suggestions, and in particular for his idea on exploiting the bi-directionality of an EA modulator to achieve clock recovery. A final thanks within the group to *Bert Biggs* for his help and expertise, and for keeping the lab running smoothly.

I would also like to thank BT Laboratories Fibre Systems Group for the CASE award, and for access to the *HIGHWAY* test bed used in Chapter 7. Thank you to *Andrew Ellis* my industrial supervisor, for his invaluable help and experience. Thank you also to *Dave Moodie* for supplying the state-of-the-art electroabsorption modulators without which, the majority of this work would not have been possible. Thank you also to *Dominique Marcenac* for his help with the theoretical analysis on the system performance requirements within an OTDM network.

Finally I would like to thank EPSRC for their funding throughout my PhD.

Statement of Originality

Except where indicated above, or by reference, all of the ideas and results presented in this thesis are solely attributed to the author. Similarly, the author participated in the design and implementation of all experiments presented except where explicitly indicated.

Contents

Table of figures

Abbreviations

AM	Amplitude Modulator
ASE	Amplified Spontaneous Emission
BER	Bit Error Ratio
CW	Continuous Wave
DFB	Distributed FeedBack
DSF	Dispersion Shifted Fibre
EA	Electro-Absorption
ECMLL	External Cavity Mode-Locked Laser
EDFA	Erbium-Doped Fibre Amplifier
FPSLA	Fabry-Perot Semiconductor Laser Amplifier
FWHM	Full-Width Half-Maximum
FWM	Four-Wave Mixing
GHz	Gigahertz
GVD	Group Velocity Dispersion
HEMT	High Electron-Mobility Transistor
ISI	Inter-Symbol Interference
MHz	Megahertz
MQW	Multi-Quantum Well
MSSI	Mid-Span Spectral Inversion
MZ-SOA	Mach Zehnder-Semiconductor Optical Amplifier
MZ	Mach Zehnder
Nd^{3+}	Neodymium
NLS	Nonlinear Schrödinger (equation)
NOLM	Nonlinear Optical Loop Mirror
NOM	Nonlinear Optical Medium
NRZ	Non-Return-to-Zero
OTDM	Optical Time Division Multiplexing
PDF	Probability Density Function
PDH	Plesiochronous Digital Hierarchy
PLL	Phase Locked Loop
Pr^{3+}	Praseodymium
PRBS	Pseudo-Random-Bit-Sequence
RZ	Return-to-Zero
SBS	Stimulated Brillouin Scattering
SDH	Synchronous Digital Hierarchy
SLALOM	Semiconductor Laser Amplifier Loop Mirror
SM	Single-Mode
SNR	Signal-to-Noise Ratio
SOA	Semiconductor Optical Amplifier
SOA-NOLM	Semiconductor Optical Amplifier-based Nonlinear Optical Loop Mirror
SPM	Self-Phase Modulation

SRS	Stimulated Raman Scattering
TDM	Time Division Multiplexing
THz	Terahertz
TOAD	Terahertz Optical Asymmetric Demultiplexer
TWSLA	Travelling-Wave Semiconductor Laser Amplifier
WDM	Wavelength Division Multiplexing
XPM	Cross-Phase Modulation

Chapter 1

Introduction

1.1 The Information Age

The telecommunications industry is experiencing an exponential increase in demand for bandwidth. This is mainly due to the explosive growth of the *internet* or *world wide web*, which was triggered by the practical realisation of inexpensive and powerful personal computers supporting multimedia technology and based on simple graphical interfaces. Such technology has been widely adopted by the business community, and is becoming increasingly common in the home. Information can be sent in seconds, from one side of the globe to the other. This can take the form of a simple text message, to complex video clips and sound bites. Information ranging from your favourite football team, to a complex data sheet on the latest integrated circuit, are routinely found on the *internet*. With the correct telecommunications infrastructure, the diversity and the number of possible services will be endless.

The current telecommunications network within Great Britain represents a gradual evolution from a coaxial analogue network, to a digital network consisting of slow speed switching systems interconnected by relatively high-speed optical transmission lines. Much of the network is based around the 'plesiochronous digital hierarchy' (PDH), and is very cost effective at carrying a large number of telephone circuits [1]. However, with the increased use of data transmission, the PDH architecture suffers from insufficient provision for carrying network management information, and difficulties that arise when demultiplexing individual channels from a high-speed data stream. To overcome these disadvantages, and to allow the telecommunications network to evolve to meet the demand placed upon it, the 'synchronous digital hierarchy' (SDH) was conceived [1]. SDH offers a number of benefits including, the theoretical ability to eliminate the *mux-mountain* associated with PDH, SDH ring architectures that allows 'add-drop

multiplexers', and improved network protection strategies. SDH also offers improved network management functions through software control, and most importantly network standardisation between different manufactures, although network management maybe lost. The main goal of a standardised SDH architecture is to improve network functionality, not necessarily to increase network capacity.

Historically, as higher data rates have been required, the technical solution has been to employ further stages of time division multiplexing (TDM). The maximum data-rate of optical systems that can be realised using TDM is still limited by the bandwidth of the electronics in the terminal equipment, currently 10 Gbit/s, with 40 Gbit/s devices under development [2 3, 4, 5].

Optical technology should pay an important role in the reduction of the electronic processing requirements within a telecommunications network, by routing groomed data traffic in the optical domain direct to the destination. This introduces the concept of optical paths interconnected across the current, highly meshed network. This avoids the need for large electronic processors at intermediate network locations. The development of capacity is not the only goal, flexibility and development of optical routing is also important. To this end, technologies should develop and be integrated with, and enhance those already existing. Future telecommunications networks must be transparent, to allow for further upgrades in capacity through improved terminal equipment, dynamically re-configurable to match traffic requirements, and fault-tolerant, with self-maintaining nodes to simplify network management.

To meet these requirements, and as an alternative to TDM, optical multiplexing can be used to produce systems with a overall capacity well in excess of anything produced by electronic multiplexing. Two main methods of optical multiplexing have been adopted; these are optical time division multiplexing (OTDM), and wavelength division multiplexing (WDM).

1.2 Optical Multiplexing and Photonic Networks

1.2.1 Wavelength division multiplexing

WDM exploits the normally untapped attribute of a single mode fibre : its potentially unlimited bandwidth. Considering the operational range of the erbium-doped fibre amplifier (EDFA) centred around 1550 nm, a potentially addressable bandwidth of 30 nm (5 THz) exists. With WDM a number of channels at different wavelengths are multiplexed onto a single fibre, whilst keeping the bit rate of individual channels low enough to minimise dispersion effects. The concept is illustrated in Figure 1-1, which shows the main components in a WDM system. Here, a number of different wavelength lasers are each modulated by a different electrical tributary. A multiplexer is used to combine the different wavelengths onto a signal fibre. At the far end a demultiplexer is used to separate out the individual wavelengths, such that individual detection of channels maybe performed. Additionally, in-line optical amplifiers maybe used.

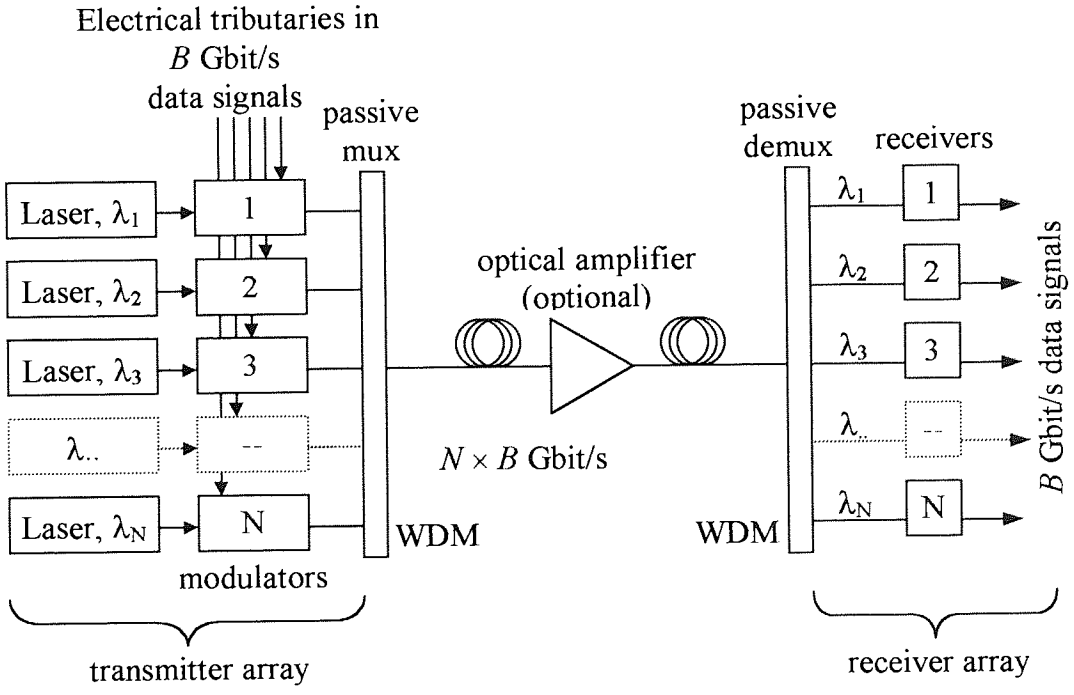

Figure 1-1. A point-to-point WDM link.

The ease with which it is possible to multiplex and demultiplex wavelengths has led to the extension of WDM beyond point-to-point systems, to complex network configurations. WDM networks use the signal wavelength to provide optical routing

through a series of network nodes. Each node allows one or more channels (wavelengths) to be demultiplexed (dropped), and either detected locally, or routed to a remote location. Different channels at the same wavelengths can then be inserted into the vacant wavelength slots. This is commonly termed 'add-drop multiplexing' or 'drop and insert multiplexing'. When such a network is combined with electronic space switches, the network can be made dynamically re-configurable, and so adapt to the changing demands placed upon it.

WDM has been investigated extensively for both point-to-point transmission systems [6], as well as optical networks [7, 8, 9, 10, 11]. Provided the bit-rate of individual channels is kept low enough to minimise dispersion effects, WDM can be used to expand the capacity of a point-to-point system with only a small increase in complexity. This is emphasised by comparing a single channel NRZ system with that of a WDM system operating at the same aggregate data rate. The maximum dispersion limited transmission distance of a 10 Gbit/s NRZ system would be approximately 50 km, assuming $D = +15$ ps/nm/km. However, a 4×2.5 Gbit/s WDM system would increase the maximum transmission distance by a factor of 16, to greater than 600 km.

For moderate line rates (≤ 2.5 Gbit/s) over short distances (< 600 km), WDM, due to its passive nature, provides the simplest implementation of optical multiplexing [12]. Indeed, a number of Dense-WDM systems are now commercially available, including a 100 Gbit/s (40×2.5 Gbit/s) WDM system from *Ciena Inc.* that allows single-span transmission over 70 km, or periodically optically amplified transmission up to 400 km [13]. However, for high capacity long distance links, system design becomes more complex. Present work focuses on how the number of wavelength channels and the transmission distance, i.e. the system capacity, is limited by nonlinear induced crosstalk from stimulated Raman scattering (SRS) and four wave mixing (FWM) [14]. The gain flatness of optical amplifiers and the spectral dependence of optical filters within the system must also be taken into account [15]. The effects of filter and amplifier concatenation also becomes important, and the end-to-end bandwidth of a system must

be considered when performing wavelength allocation. The potential of WDM to update the current installed network has been shown by the transmission of thirty-two, 10 Gbit/s channels (320 Gbit/s) over 500 km of standard single-mode fibre with an amplifier spacing of 125 km [16]. An equally impressive result is the transmission of a 533 Gbit/s (50×10.66 Gbit/s) data stream over 1655 km of dispersion shifted fibre with an amplifier spacing of 50 km [17].

1.2.2 Optical time division multiplexing

With OTDM, each channel is transported and switched according to a time-slot at a single wavelength [18, 19]. Figure 1-2 shows a point-to-point OTDM system, where a picosecond optical pulse source is split into N individual pulse streams.

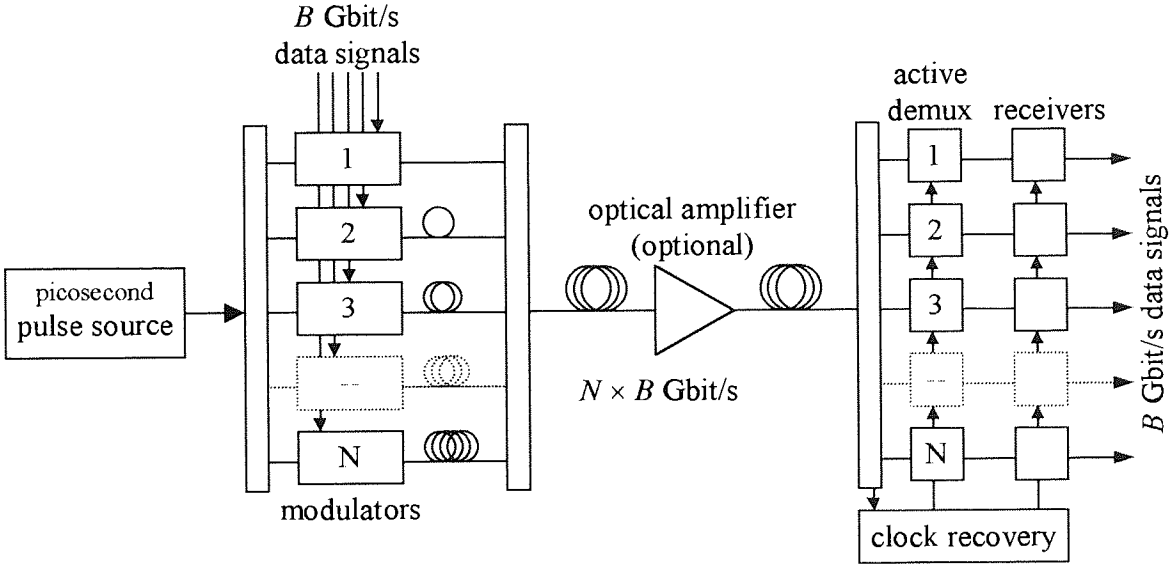

Figure 1-2. A point-to-point OTDM link.

Each pulse stream is individually modulated by a B Gbit/s electrical data signal (e.g. 10 Gbit/s for STM-64), resulting in N optical channels. Each channel is delayed by a specified fraction of the clock period before being recombined to produce an aggregate data rate of $N \times B$ *Gbit/s*. To avoid crosstalk between these interleaved channels, the laser source must be capable of generating pulses significantly shorter than the bit period at the highest multiplexed line-rate in the system. Optical amplifiers maybe used to maintain the correct signal power, ensuring a sufficient signal-to-noise ratio (SNR) for

error-free operation. Chromatic dispersion can be handled in many ways. One method is to balance the net system dispersion over the system length so that it is zero (dispersion management) and another technique is to use soliton transmission. Both methods are discussed in more detail in Chapter 2. At the receiver, the incoming OTDM data stream is actively demultiplexed, and each channel is individually detected. Clock recovery is necessary to synchronise the demultiplexing units to the aggregate signal.

OTDM can not simply be regarded as a further level of multiplexing in the existing SDH structure, because it is based on bit interleaving, whereas SDH uses byte interleaving to achieve higher data rates. Thus, access to SDH overhead information is only possible when the OTDM channels are demultiplexed. The advantage of OTDM is that it avoids the electronic bottleneck, and is best suited to high-capacity transmission systems (e.g. backbone core network), with lower speed electronic or passive WDM networks only acting on individual tributaries.

Developing these ideas further into an OTDM network, a generalised OTDM node (see Figure 1-3) can be broken into a number of functional parts.

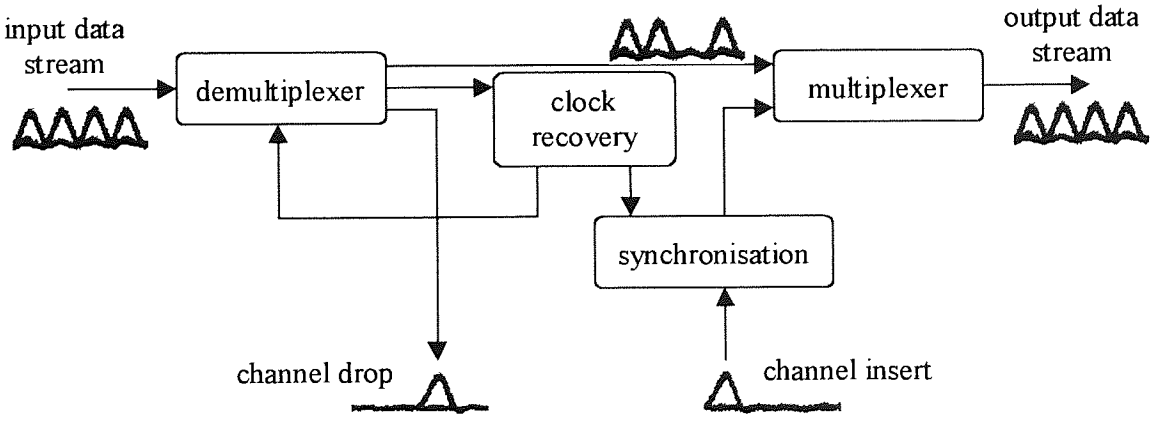

Figure 1-3. The functional units from which an OTDM network node can be constructed.

Traffic enters a node through a demultiplexing unit, which drops out every n^{th} channel. This channel may be detected at the node, or transported to a remote location. Remaining channels are transported to the multiplexing unit, where one or more channels may be inserted to replace the dropped optical data signal, which again may originate from a transmitter or a remote node. This is commonly termed a 'drop and insert'

operation. Clock recovery and synchronisation are necessary to drive the demultiplexing unit and ensure correct channels go into vacant time-slots.

The functional units from which an OTDM network could be constructed are a picosecond optical pulse source, a data encoder, a multiplexer, a demultiplexer, a clock recovery and synchronisation unit, and a receiver. Chapter 3 will give the requirements of the above functional units, and discuss various technological solutions.

1.3 Overview of Thesis

This thesis aims to provide a detailed experimental analysis of high-speed optical processing within an OTDM network node. This includes the functions of demultiplexing, 'drop and insert' multiplexing, data regeneration, and clock recovery. It examines the possibilities of combining these tasks using a single device. Two optical switching technologies are explored. The first is an all-optical device known as a 'semiconductor optical amplifier-based nonlinear optical loop mirror' (SOA-NOLM). Switching is achieved by using an intense 'control' pulse to induce a phase shift in a low-intensity signal propagating through an interferometer. The second device is an electroabsorption (EA) modulator, where an optical signal propagating through such a device can be selectively absorbed by modulating the reverse bias voltage.

The subject area of optical communications is vast; therefore a degree of familiarity with basic optical propagation principles is assumed. Where appropriate, the reader is directed towards commonly available texts for further reading. However, Chapter 2 outlines the properties of single mode optical fibres, which limit the maximum achievable transmission distance, (i.e. attenuation, dispersion, and nonlinearity). It also discusses methods of overcoming these limitations, including nonlinear or soliton transmission.

Chapter 3 outlines the key functional units that are required within an OTDM network. It discusses the requirements of a picosecond optical pulse source, and then compares the most common sources, before presenting experimental results on the characterisation

of two sources that are used throughout this thesis. It then outlines the processes of demultiplexing and 'drop and insert' multiplexing, and describes the most promising devices that have been used to successfully achieve these functions. The importance of data regeneration is considered both in a point-to-point network and in a 'drop and insert' node. Base-rate clock recovery from an OTDM data stream operating at a higher line-rate is considered. Both all-optical and electro-optical techniques are discussed, and the advantages and disadvantages of each method are outlined. Finally, OTDM system impairments are considered. Emphasis is made on the strict requirements of the extinction ratio and duty cycle of the optical source and demultiplexer, and conclusions are drawn from theoretical simulations. The effect of timing jitter between the recovered base-rate clock and the incoming OTDM data stream is also analysed.

Chapter 4 introduces the semiconductor optical amplifier (SOA), and its particular use as a nonlinear element within an OTDM network. The nonlinear processes of gain saturation and gain recovery are considered, and the experimental characterisation of two SOA devices is presented. The basic operating principles of an SOA-NOLM are described, including how such a device can be used to achieve all-optical demultiplexing and data regeneration. The remainder of the chapter describes two different SOA-NOLM configurations; each containing an SOA that was characterised earlier in the chapter. Each configuration is used in Chapter 5 to experimentally analyse the use of such a device to perform high-speed data regeneration at 2.5 Gbit/s and 10 Gbit/s. By simply changing the drive frequency of the optical source, 10 Gbit/s to 2.5 Gbit/s demultiplexing is achieved with data regeneration. The remainder of Chapter 5 combines the switching properties of the SOA-NOLM with its inherent sampling capability, allowing simultaneous demultiplexing, data regeneration, and clock recovery using a single device [20, 21].

Chapter 6 provides an overview of the EA modulator. Current applications are considered and the physical operation of the device is discussed, including device design and limitations. The remainder of the chapter considers the use of an EA modulator as a

picosecond pulse source, and as a high-speed optical switch. Experimental results are presented that agree closely with theory.

To date, the EA modulator has been used in a unidirectional configuration; however, there is no inherent reason for this limitation. Chapter 7 describes four novel experiments that use the EA modulator in a bi-directional configuration. Within an OTDM node for full demultiplexing, a separate modulator is required for each OTDM channel. The first experiment presents results on the use of an EA modulator to demultiplex two independent 10 Gbit/s channels from a 40 Gbit/s OTDM data stream [22]. By using one of the data channels as an error signal in a phase locked loop configuration, a 10 Gbit/s channel can be demultiplexed from a 40 Gbit/s OTDM data stream while simultaneously recovering the base-rate electrical clock [23]. By exploiting the bi-directionality of the EA modulator, independent control can be achieved between the switching and clock recovery processes. The setup exhibits excellent stability, ultra-low timing jitter, and no additional switching penalty. Operation above 100 Gbit/s is predicted possible using the same equipment. The third experiment demonstrates the use of an EA modulator in a self-contained 40 Gbit/s 'drop and insert' node [24]. Clock recovery is achieved using the method outlined in the previous experiment, thus demonstrating the flexibility of the technique. A 10 Gbit/s channel is completely removed from a 40 Gbit/s OTDM data stream, and a different channel is subsequently inserted into the vacant time-slot. Each channel is then demultiplexed, and the effects of incoherent interference are analysed. The final experiment in Chapter 7 presents preliminary results on a high-extinction 10 GHz picosecond source. Typically, to obtain a high pulse extinction ratio that is suitable for multiplexing up to 40 Gbit/s or 80 Gbit/s, two synchronously driven EA modulators are cascaded in series. Alternatively, a high extinction pulse can be obtained by using a single EA modulator, and passing the pulse generated on the first pass, back through the same device in the opposite direction.

Finally, in Chapter 8 the material and results presented in this thesis are summarised. A comparison between all-optical and electro-optical switching is made. Conclusions on the direction of future work are then given.

Chapter 2

Theory of optical communications

2.1 Introduction

Two of the main limiting factors for any optical communications system are power budget and dispersion. The first of these is a function of transmitter power, receiver sensitivity and fibre attenuation, whereas the second is more complicated, depending on fibre dispersion and optical source characteristics [25]. Approximately, ninety percent of the optical fibre installed in the UK trunk network was designed to have a dispersion zero in the second telecommunications window at 1.33 μm. This represents a huge investment, and therefore when upgrading it is desirable to utilise the existing fibre base. Ideally, designers would like to operate in the third telecommunications window, where fibre attenuation is a minimum and erbium amplifiers allow periodic gain blocks. Unfortunately, at 1.55 μm the installed fibres have a dispersion of +17 ps/nm/km, which would severely limit the system bandwidth. Various methods have been proposed and experimentally demonstrated to overcome these limitations. Two such techniques are dispersion management and soliton transmission.

Dispersion management in standard fibre systems seeks to ensure that the mean end-to-end linear dispersion in the transmission path is approximately zero. This is achieved by placing dispersion compensating elements at regular intervals within the transmission link. The dispersions of the compensating elements are equal, but of the opposite sign to that of the link. Elements include single-mode dispersion compensating fibre (DCF) such as that developed by *Corning* [26] and have dispersions around –100 ps/nm/km at the expense of higher attenuation around 0.3 dB/km [27], or linearly chirped fibre Bragg gratings [28, 29]. The effectiveness of dispersion management in OTDM systems was first demonstrated in a 40 Gbit/s, unrepeatered OTDM experiment over 80 km [30]. Without equalisation, the 6 ps pulses making up the 40 Gbit/s OTDM data stream

broadened to approximately 500 ps or 20 times the bit period. Dispersion compensation using DCF restored the pulse width to approximately 7 ps, with a system penalty of under 3 dB.

Soliton transmission utilises nonlinear propagation effects, whereby the intensity of the light travelling in the fibre influences its propagation properties in a way that counteracts dispersion and creates a stable non-dispersive pulse [31]. Impressive soliton transmission experiments have included, 10 Gbit/s transmission over 1 million km [32].

The remainder of this chapter outlines the properties of single mode optical fibres, which limit the maximum achievable transmission distance, (i.e. attenuation and dispersion). It also discusses methods of overcoming these limitations, including nonlinear or soliton transmission.

2.2 Properties of Single Mode Fibres

2.2.1 Normalised frequency & cut-off wavelength

A very useful parameter for considering how light travels within an optical fibre, is the normalised frequency or waveguide parameter V, given by [25, 31]:

$$V = \frac{2\pi a}{\lambda}\sqrt{n_1^{\,2} - n_2^{\,2}} \qquad \textbf{Equation 2-1}$$

where a is the core diameter, λ is the operating wavelength, n_1 is the refractive index of the core, and n_2 is the refractive index of the cladding. The normalised frequency defines the number of modes that are able to propagate within the fibre, and is used to measure the degree of guidance at a particular wavelength. A step-index fibre will support only the fundamental mode (LP_{01}) provided V < 2.405; if V is above this value, then more modes may be guided. The cut-off wavelength λ_c for single-mode step-index fibres is given by:

$$\lambda_c = \frac{2\pi a}{2.405}\sqrt{n_1^{\,2} - n_2^{\,2}} \qquad \textbf{Equation 2-2}$$

Standard single-mode step-index fibre has a refractive index difference, $n_1 - n_2$ of ~0.005, and a core radius of $a = 4$ μm, giving a cut-off wavelength $\lambda_c = 1.2$ μm. Single-mode propagation will only be ensured provided $\lambda_c > 1.2$ μm. Such fibre operates with a single-mode at both 1.3 μm and 1.55 μm, the 2nd and 3rd telecommunication windows.

2.2.2 Attenuation

Figure 2-1 shows the measured attenuation spectrum for single mode fibre, together with some of the calculated loss mechanisms. These mechanisms are influenced by fibre material composition, purity, and waveguide structure.

Figure 2-1. The measure attenuation spectrum for an ultra-low-loss single mode fibre. Also indicated are some of the calculated loss mechanisms which contribute the fibres overall attenuation. Note that attenuation is given as dB/km. The optical bandwidth reduces dramatically for long lengths of fibre. From reference [33].

Attenuation can be caused by intrinsic or extrinsic absorption, Rayleigh scattering, bending losses, and nonlinear effects [25]. Intrinsic absorption is caused by interactions between SiO_2 and GeO_2 components within the glass structure and results in electronic absorption in the ultra-violet wavelength region and photon absorption in the infra-red

region. Extrinsic absorption is caused by unwanted materials or impurities within the fibre. Water (OH-ions) are the most dominant absorber in most modern fibres, causing peaks in optical loss at 1.25 μm and 1.39 μm. Modern manufacturing methods are capable of reducing theses effects to almost zero. Rayleigh scattering is the most dominant intrinsic loss mechanism in modern silica fibres, and is caused by microscopic non-uniformity of refractive index of glass. A ray of light is partially scattered into many directions, thus some light energy is lost. At 1.3 μm the attenuation is typically 0.4 dB/km and at 1.55 μm it is 0.2 dB/km. Therefore, if dispersion effects are overcome, operation in the third telecommunications window allows the maximum transmission distance to be almost doubled.

2.2.3 Optical amplifiers

Optical amplifiers allow the direct amplification of light, without the need for optical to electrical conversion. They provide the amplification necessary to overcome the attenuation associated with optical transmission. The performance of an optical amplifier can be assessed according to the following parameters: gain, bandwidth, noise figure, polarisation sensitivity, saturation power, and gain recovery time. There are two main types of optical amplifiers for telecommunications, namely the semiconductor optical amplifier (SOA), and the rare-earth doped-fibre amplifier. The SOA has been almost completely abandoned as the solution for amplification within a point-to-point transmission line [34, 35, 36, 37, 38], but has recently been used extensively as an all-optical processing element [39]. SOA are covered in detail in Chapter 4, and then used experimentally in Chapter 5 to achieve all-optical OTDM network processing. The remainder of section 2.2.3 will cover the basic operating characteristics of the erbium-doped fibre amplifiers (EDFA), which are used extensively in the experiments described throughout this thesis to compensate for device insertion loss.

Fibres for optical amplification are formed by introducing rare-earth ions into silica or fluoride glass during the fabrication process. Several rare-earth ions have been used, each offering amplification in a specific wavelength region: examples include

praseodymium (Pr^{3+}) [40, 41, 42] and neodymium (Nd^{3+}) [43] for operation in the 1.3 μm wavelength region. However, the most widely used is erbium [44, 45], offering wide gain in the 1550 nm wavelength region. The configuration of a typical EDFA is shown in Figure 2-2.

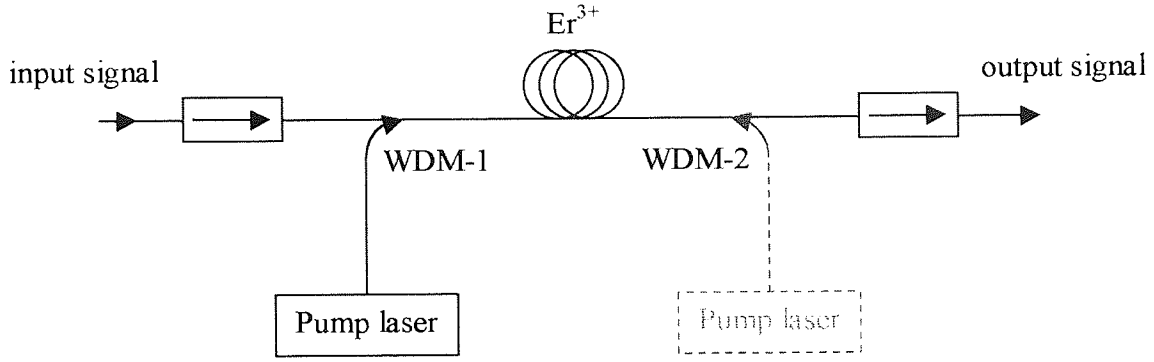

Figure 2-2. Schematic of an erbium doped fibre amplifier.

An EDFA consists of a length (~25 m) of erbium-doped fibre; an optical pump laser to provide the necessary population inversion; an optical isolator to prevent instability from back reflections; and a coupler to combine the signal and the pump in the amplifying fibre. In practice, the pump power can be injected into the erbium fibre by using a number of different configurations. If the pump and signal propagate in the same direction, then the amplifier is said to be forward pumped [45]. Amplifiers of this type have the best characteristics in terms of noise figure and optical gain at a fixed pump power, but suffer from a lower saturated output power. If the pump is injected at the far end of the erbium fibre, then a higher saturated output power is achieved; this is known as reverse pumping [45]. To achieve high gain, low noise figure, and high-saturated output power, then the amplifier can be bi-directionally pumped [45]. The absorption spectrum of erbium is shown in Figure 2-3a, which shows that there are a number of possible pumping wavelengths for achieving the required population inversion. Highest gain is achieved by pumping at either 980 nm or 1480 nm. The shaded bands indicate regions of excited state absorption that reduce the efficiency of the amplification process [46].

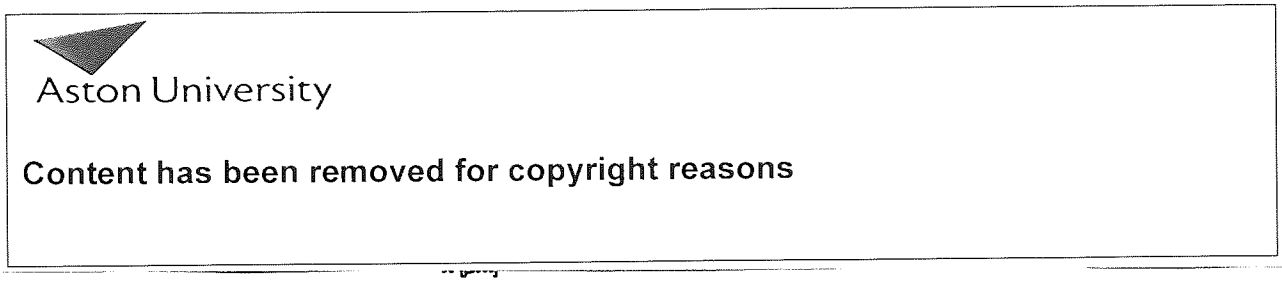

Figure 2-3. (a) Absorption spectrum of erbium; (b) Erbium energy diagram. From reference [46].

The principle of operation can be understood by referring to Figure 2-3b, which shows an energy level diagram of the erbium ion. Considering pumping at 1480 nm, the incoming pump wavelength excites electrons from the ground state E_0 to the higher energy metastable state E_1, creating population inversion. A photon is then emitted when a transition occurs between the metastable state E_1 and the ground state E_0. This can be caused by either random spontaneous decay (causing optical noise), or it can be due to stimulated emission from a signal photon in the 1530-1560 nm wavelength band. A pump photon at 980 nm causes excitation to a higher energy state E_2, from which it decays down to the metastable state E_1, losing energy as it does so. Transitions from the metastable state are similar to the 1480 nm pumping outline above.

Typical gain characteristics are shown below in Figure 2-4. Erbium amplifiers are typically polarisation insensitive, have gains of >25 dB, saturated output power of >10 dBm, and a noise figure of 3–7 dB depending on the pump wavelength and configuration [47].

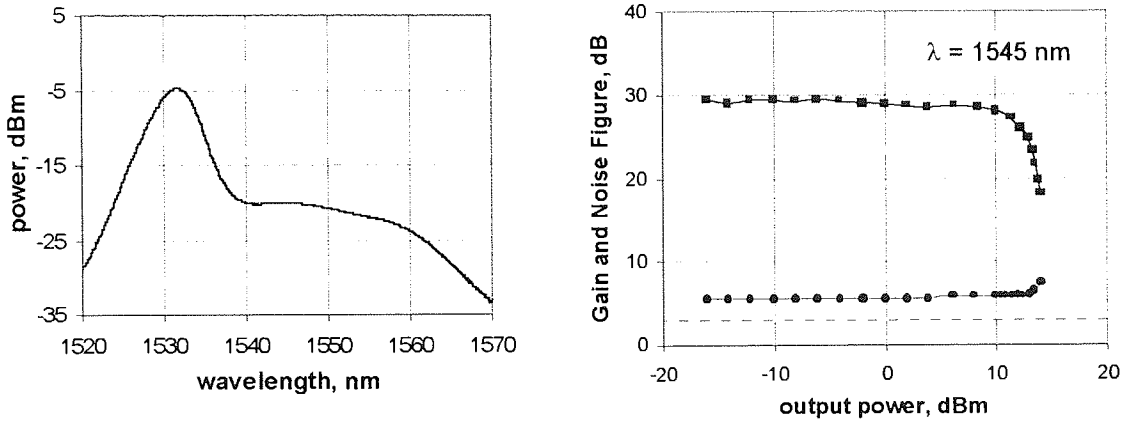

Figure 2-4. EDFA operating characteristics: (a) ASE spectrum; (b) Gain and noise figure as a function of output power at λ = 1545 nm.

A more detailed analysis of erbium-doped fibre amplifiers is discussed by *Desurvire* in [45].

2.2.4 Dispersion

Dispersion mechanisms within the fibre cause broadening of the transmitted light pulses as they travel along its length. As each pulse broadens it will overlap with its neighbour, resulting in inter-symbol interference, which will degrade the SNR and cause a system penalty. Eventually the two pulses will become indistinguishable, and an error-floor will occur. For system design purposes and assuming a maximum 1-dB dispersion penalty, the maximum bit rate-distance product, is given by [48]:

$$B^2 L = \frac{c}{2D\lambda^2} \qquad \text{Equation 2-3}$$

where B is the bit-rate, L is the transmission distance, D is the fibre dispersion, and λ is the operating wavelength. Equation 2-3 is based on the assumption that an idea 'chirp-free' source is used (see section 3.2.1), i.e. the spectral spread associated with the signal is Fourier-transform limited.

Assuming a 10 Gbit/s return-to-zero (RZ) transmission system, with a fibre dispersion $D = +17$ ps/nm/km, operating at 1550 nm, the maximum transmission distance is ~50 km. If the dispersion is decreased to 1 ps/nm/km then the maximum transmission

distance is increased by an order of magnitude to 600 km. This therefore shows the significance of dispersion in an optical communication system. These calculations assume minimal inter-symbol interference, and in practice, the conditions can be relaxed with no significant degradation in system penalty, thereby slightly increasing the maximum transmission distance [25].

Within single mode (SM) fibres, dispersion is an indirect consequence of the finite spectral width of the optical source. A propagation delay exists between different spectral components of the transmitted signal, thus causing broadening. The delay differences are caused by a combination of material dispersion and waveguide dispersion. These two types of dispersion are considered in more detail below.

2.2.4.1 Material Dispersion

Material dispersion is caused by the frequency dependence of the refractive index $n(\omega)$, which results in different frequency components of a transmitted signal suffering from a different delay.

A monochromatic plane wave propagating through a homogeneous material will have points of constant phase which travel at a velocity, v_p:

$$v_p = \frac{\omega}{\beta} = \frac{c}{n}, \text{ and } \beta = \frac{2\pi n}{\lambda} \qquad \text{Equation 2-4}$$

where ω is the optical frequency in rad/s, β is the propagation constant, c is the velocity of light in a vacuum, and n is the refractive index of the material. However, modulated signals have a finite spectral width and consist of a number of plane waves with closely similar frequencies travelling as a packet, see Figure 2-5.

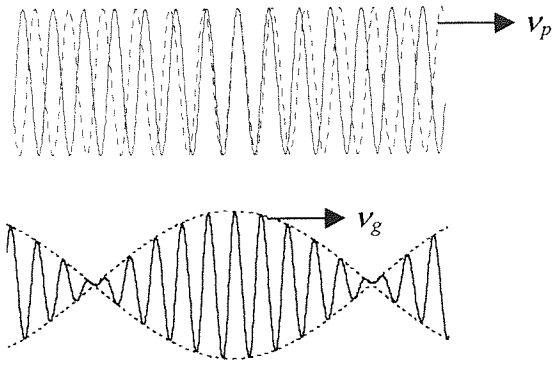

Figure 2-5. Finite spectral width of a modulated signal results in a number of plane waves travelling at a group velocity.

A modulated signal will therefore travel at a group velocity v_g, given by [25]:

$$v_g = \frac{d\omega}{d\beta} = \frac{c}{\left(n - \lambda \frac{dn}{d\lambda}\right)} = \frac{1}{\tau_g} \qquad \textbf{Equation 2-5}$$

The delay of the signal through the material is known as the group delay τ_g and is the inverse of the group velocity (i.e. $\tau_g = 1/v_g$) per unit length. The material dispersion D_m is given by the derivative of the group delay and is caused by the wavelength dependence of the fibre refractive index creating a wavelength dependence of the phase and group velocities [25].

$$D_m = \frac{d\tau_g}{d\lambda} = \frac{d}{d\lambda}\left(\frac{n}{c} - \frac{\lambda}{c}\frac{dn}{d\lambda}\right) = -\frac{\lambda}{c}\frac{d^2n}{d\lambda^2} \qquad \textbf{Equation 2-6}$$

The refractive index $n(\omega)$ can be approximated by the *Sellmeier* equation [31]:

$$n^2(\omega) = 1 + \sum \frac{B_j \omega_j^2}{\omega_j^2 - \omega^2} \qquad \textbf{Equation 2-7}$$

where ω_j is the resonance frequency and B_j is the strength of the *jth* resonance. In the case of optical fibre, the parameters B_j and ω_j are obtained experimentally by fitting to measured dispersion curves. For bulk fused silica, these parameters are found to be [49] $B_1 = 0.696166$, $B_2 = 0.407942$, $B_3 = 0.8974794$, $\lambda_1 = 0.068404$ μm, $\lambda_2 = 0.1162414$ μm, and $\lambda_3 = 9.896161$ μm, where $\lambda_j = 2\pi c/\omega_j$ and c is the velocity of light in a vacuum. The wavelength dependence of the $n(\omega)$ is shown below in Figure 2-6.

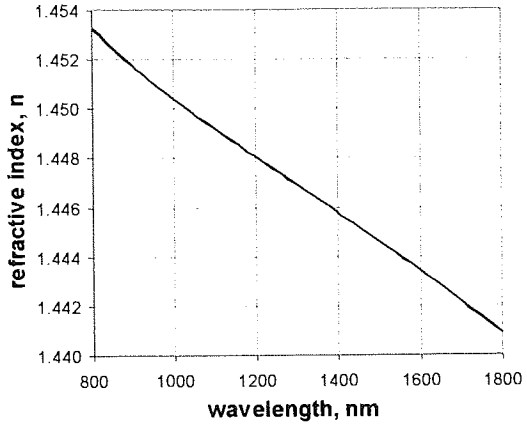

Figure 2-6. Refractive index *n* of bulk silica. Calculated using the Sellmeier equation.

Figure 2-7 shows the group delay τ_g and the material dispersion D_m for bulk silica, calculated using Figure 2-6, Equation 2-5, and Equation 2-6. The group delay has a minimum value of 4.87 μm/km at 1270 nm, and the corresponding material dispersion, D_m has a zero value at the same wavelength. At this wavelength the effects of higher order material dispersion become dominant.

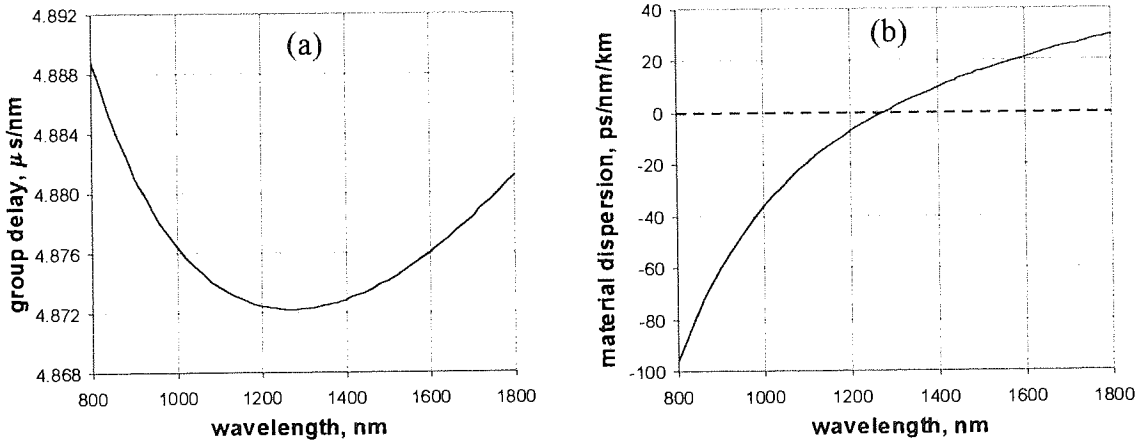

Figure 2-7. (a) Group delay, τ_g, and (b) Material dispersion, D_m.

The curves shown in Figure 2-6 and Figure 2-7 were calculated for bulk fused silica. The material dispersion of actual optical fibres deviates from that shown in the figures, because the fibre core typically contains small amounts of dopants, such as GeO_2. The parameters used to calculate $n(\omega)$ in Equation 2-7, should be changed so that they reflect the appropriate doping level [50].

2.2.4.2 Waveguide dispersion

Material dispersion was related to the wavelength dependence of the refractive index within bulk materials. For the propagation of modes within optical fibre, the dispersive properties of the waveguide structure must also be considered. It is convenient to define the effective refractive index n_{eff}, as [25]:

$$n_{eff} = \frac{\beta}{k}$$ **Equation 2-8**

where β is the propagation constant of the fundamental mode, and k the vacuum propagation constant, $k=2\pi/\lambda$.

The waveguide dispersion can be better understood by considering Figure 2-8a, which shows how the refractive index of the core and the cladding varies with wavelength.

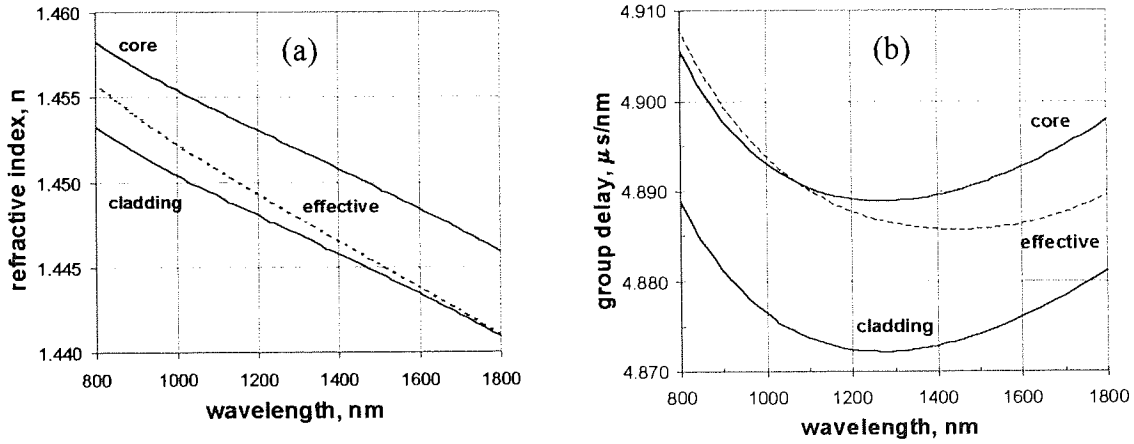

Figure 2-8. (a) Variation of the core, cladding and the effective refractive index; (b) variation of the core, cladding, and effective group delay as a function of wavelength for single-mode fibre.

At short wavelengths, where the V-value is high, the mode is tightly confined to the core and sees an effective refractive index that is close to the core value. At longer wavelengths the spot size increases, and the mode penetrates more into the cladding where it sees a lower effective refractive index. Hence, the effective refractive index will vary over the range $n_2 < n_{eff} < n_1$. It is this variation of the effective index from the core to the cladding that is responsible for waveguide dispersion [51, 52]. Figure 2-8b shows the corresponding effective group delay, where a similar variation occurs between the group delay seen in the core and in the cladding.

The waveguide dispersion D_w, is given by [25]:

$$D_w = -\frac{\lambda}{c}(n_1 - n_2)\frac{d^2 b}{d\lambda^2}$$ **Equation 2-9**

where n_1 and n_2 are the refractive index of the core and cladding, respectively. The variable b describes the effect of the wavelength dependent spot diameter on the propagation, and is given by [25]:

$$b \approx \frac{n_{eff} - n_2}{n_1 - n_2}$$ **Equation 2-10**

Equation 2-10 can be used to determine the effective refractive index. The dependence of b on the normalised frequency V can be approximated within 0.2% for $1.5 \leq V \leq 2.5$, using [53]:

$$b(V) \approx \left(1.1428 + \frac{0.9960}{V}\right)^2$$ **Equation 2-11**

2.2.4.3 Total chromatic dispersion

The total fibre dispersion is shown in the Figure 2-9, and is the sum of the material and the waveguide dispersion.

$$D = \text{material dispersion} + \text{waveguide dispersion}$$
$$= \frac{\lambda}{c}\frac{d^2 n_1}{d\lambda^2} - \frac{\lambda}{c}(n_1 - n_2)\frac{d^2 b}{d\lambda^2}$$ **Equation 2-12**

The total dispersion passes through zero at λ_0, which in standard single-mode fibre is 1.33 μm, the second telecommunications window. When operating near λ_0, third order dispersion needs to be considered [25].

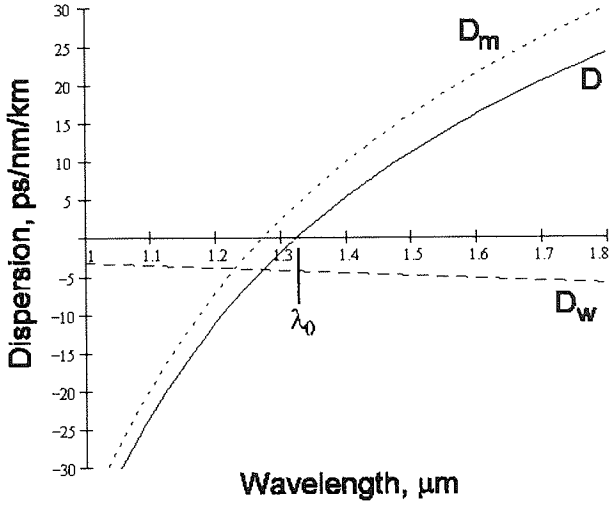

Figure 2-9. The material dispersion parameter (D_m), the waveguide dispersion parameter (D_w) and the total dispersion parameter (D) as a function of wavelength for a conventional single-mode fibre.

The waveguide dispersion can be increased by reducing the fibre core radius, therefore allowing λ_0 to be shifted to the third telecommunications window at 1.55 μm, where silica fibre has minimum loss. This is known as dispersion shifted fibre (DSF) [54]. DSF made by simply reducing the core size tends to have a higher loss compared with that of standard step-index fibre. This problem can be overcome by using graded index profiles, allowing DSF with an attenuation as low as 0.22 dB/km at 1550 nm to be produced [25].

As a pulse broadens without change in spectral width, it acquires a chirp [55]; i.e. the instantaneous frequency differs from the central frequency in a linear manner. If $D < 0$, then the pulse will acquire an up-chirp, where the longer wavelength 'red components' tend towards the leading edge, and travel faster than the shorter wavelengths 'blue components' at the trailing edge. The regime is known as normal dispersion. If however, $D > 0$ then the opposite is true. The pulse acquires a down chirp, and is said to be propagating in the anomalous regime. In other words, the shorter wavelength 'blue components' travel faster than the longer wavelength 'red components'. A pulse therefore acquires a dispersion-induced chirp on propagation. Operation in the anomalous regime can, under the correct conditions lead to the propagation of very stable, non-dispersive pulses known as solitons. The principles of soliton propagation will be discussed in section 2.5.

Mathematically the effects of fibre dispersion can be accounted for by expanding the propagation constant β using the Taylor series about a centre frequency, ω_0 [31].

$$\beta(\omega) = n(\omega)\frac{\omega}{c} = \beta_0 + \beta_1(\omega - \omega_0) + \frac{1}{2}\beta_2(\omega - \omega_0)^2 + \ldots + \frac{1}{m!}\beta_m(\omega - \omega_0)^m$$

Equation 2-13

where ,

$$\beta_m = \left(\frac{d^m\beta}{d\omega^m}\right)_{\omega=\omega_0} \qquad \textbf{m = 0, 1, 2, ... n}$$

The pulse envelope moves at a group velocity, $v_g=1/\beta_1$. This gives rise to the group velocity dispersion (GVD), and is linked to the dispersion coefficient, D by:

$$D = \frac{d\beta_1}{d\lambda} = -\frac{2\pi c}{\lambda^2}\beta_2$$

Equation 2-14

D has the units ps/nm/km, and β_2 has the units ps^2/km.

An important parameter when considering fibre dispersion is known as the dispersion length L_D. L_D is defined as the length over which a transform-limited *gaussian* pulse will double in width, and is given by [31]:

$$L_D = \frac{T_o^2}{|\beta_2|}$$

Equation 2-15

where T_0 is the pulse width at the *1/e* intensity point. For a *gaussian* pulse T_0 is related to the FWHM pulse width by:

$$\tau_{fwhm} = 2(\ln 2)^{1/2} T_0 = 1.665 T_0$$

Equation 2-16

2.2.4.4 Dispersion measurement

Chromatic dispersion can be measured using a number of methods. The simplest technique, is to launch two optical picosecond pulses into the fibre under test, each at a

different wavelength. At the output, a sampling oscilloscope is used to detect the differences in the pulse travel time. The dispersion D is then given by:

$$D = \frac{\Delta t}{\Delta \lambda L}$$ **Equation 2-17**

where Δt is the group delay between the pulses, $\Delta \lambda$ is the difference in wavelength between the two sources, and L is the fibre length.

A more accurate method of dispersion measurement is to use the frequency domain. In this case, the laser diodes are driven with a fixed frequency sine wave (e.g. 100 MHz) [56]. The sine wave $a(t)$ at the fibre output is given by:

$$a(t) = A\cos\left[2\pi f_0 \left(t - t_{gr}\right)\right]$$ **Equation 2-18**

where f_0 is the modulation frequency, and t_{gr} is the group travel time. The change of phase $\Delta \phi$ due to a change of wavelength $\Delta \lambda$ can be measured with a vector voltmeter, and is given by:

$$\Delta \phi = 2\pi f_0 \Delta t_{gr}$$ **Equation 2-19**

where Δt_{gr} is the change in group travel time. From Equation 2-19 the chromatic dispersion can be calculated:

$$D = \frac{\Delta \tau_g}{L \Delta \lambda} = \frac{\Delta \phi}{2\pi f_0 L \Delta \lambda}$$ **Equation 2-20**

The dispersion D is measured in ps/nm/km. In practice, an external cavity tuneable laser source would be used, and the measurement repeated over the wavelength range of interest.

2.3 Birefringence

Single mode fibres are not truly single mode; in fact, they support two degenerate modes polarised in two orthogonal directions [31]. Under ideal conditions of perfect cylindrical geometry and isotropic material, a mode excited with its polarisation in the x-direction will not couple with a mode in the orthogonal y-polarisation. Practically, it is extremely

difficult to fabricate a fibre with a perfect geometry, and mixing of polarisation states occurs.

Figure 2-10. Evolution of light polarisation through a birefringent fibre. From reference [31].

Furthermore, the x- and y- axes will have a slightly different mode propagation constants, β_x and β_y, respectively. This leads to a polarisation dependent group delay, with propagation along one axes faster than the other; this is known as the *fast* axis. The other axis is known as the *slow* axis. The power between the two modes is exchanged periodically, with the period of the evolution is known as the beat length L_B. In standard single-mode fibre, L_B is typically 1 metre. Therefore, light that is launched into a fibre with a linear polarisation will quickly reach an arbitrary state of polarisation. Polarisation preserving fibre intentionally introduces a large amount of birefringence so small random changes do not significantly effect the polarisation. If the polarisation axis of the launched light coincides with the slow or fast axis of the fibre, the polarisation remains unchanged. If the polarisation axis makes an angle with these axes, the polarisation changes continuously along the fibre in a periodic manner with a period equal to the beat length.

2.4 Self-Phase Modulation

Applying an intense electromagnetic field to any dielectric will yield a nonlinear response, which is fundamentally related to the anharmonic motion of the bound electrons that are

under the influence of the applied field. Within optical fibres this phenomenon gives rise to an intensity dependence of the refractive index, given by [31]:

$$n(\omega, I) = n_0(\omega) + n_2 I$$ **Equation 2-21**

i.e. the refractive index of the fibre increases linearly with optical intensity. This has clear implications for high intensity ultra-short pulses, with the centre region of the pulse experiencing a higher refractive index than the lower intensity leading and trailing edges (wings). In standard fibre, $n_0 \approx 1.45$, and $n_2 = 3.2\times10^{-20}$ m^2/W.

As a pulse propagates down the fibre, it acquires a self-induced nonlinear phase shift, which ignoring dispersion effects is given by [57]:

$$\phi_{NL}(t) = -\frac{2\pi n_2 L}{\lambda} I(t)$$ **Equation 2-22**

where L is the length of the fibre, and $I(t)$ is the pulse temporal intensity profile. This effect is known as self-phase modulation (SPM) and gives rise to a frequency chirp (or shift), $\Delta\omega$ which is proportional to the time derivative of the intensity profile of the pulse.

$$\Delta\omega = -\frac{d\phi_{NL}}{dt} = \frac{2\pi n_2 L}{\lambda}\frac{dI}{dt}$$ **Equation 2-23**

Figure 2-11a shows a gaussian pulse and Figure 2-11b the frequency chirp acquired due to SPM; the resulting optical spectrum is also shown.

Figure 2-11. (a) a gaussian pulse; (b) frequency chirp as a result of SPM; (c) corresponding optical spectrum. (Note: for a peak phase shift of 2π). From reference [57].

SPM therefore generates new frequency components, with the higher frequencies generated at the trailing edge of the pulse. This results in spectral broadening. In the normal regime ($D < 0$), in which GVD leads to up-chirp, SPM will produce an enhancement to the dispersion induced temporal broadening. However, in the anomalous regime the down chirping effect of GVD acts in opposition to the effect of SPM. By balancing these two effects, an ultra-stable non-dispersive pulse can be formed, known as a soliton [57, 58]. Soliton transmission is considered in the next section.

The length over which a pulse acquires a nonlinear phase shift of π, is known as the nonlinear length L_{NL}, given by:

$$L_{NL} = \frac{1}{\gamma P_0}$$

Equation 2-24

where $\gamma = \frac{\omega_0 n_2}{c A_{eff}}$

P_0 is the peak power, γ is the nonlinearity coefficient, and A_{eff} is the effective core area of the optical fibre. In standard step-index single-mode fibres, A_{eff} = 80-90 μm^2 at 1550 nm, and in dispersion shifted fibre A_{eff} = 50-60 μm^2. Assuming $n_2 = 3.2 \times 10^{-20}$ m^2/W, γ can vary over the range 2-30 $W^{-1}km^{-1}$, depending on wavelength.

2.5 Soliton Propagation

A new generation of transmission systems exploits rather than fights against the inherent nonlinear intensity dependence of the fibre refractive index, and in doing so achieves transmission distances very much greater than the dispersion limit. The key to these systems is a soliton, which is a non-dispersive stable pulse that occurs as a result of a balance between dispersion and nonlinearity induced in the fibre at high pulse intensities. After a certain distance (soliton distance), solitons do eventually succumb to attenuation, break down and subsequently disperse. However, by placing optical amplifiers at critical intervals along the cable, which are significantly shorter than the soliton distance, then pulse breakdown is avoided. The optical soliton was first predicted theoretically in 1973 [59], and observed experimentally in 1980 [60]. Transatlantic transmission distances (>11,000 km) at 10 Gbit/s have been reported [61], making soliton transmission a promising candidate for use in future generation all-optical transmission networks [62, 63]. The issue with soliton systems is not how far, but how fast they can operate, and at what amplifier spacing.

The propagation of soliton pulses within an optical fibre is governed by the nonlinear Schrödinger equation (NLS), given by [31]:

$$\frac{\partial U}{\partial z} = \underbrace{-\frac{1}{2}\alpha U}_{\text{Fibre Absorption}} + \underbrace{\frac{i}{2}\beta_2 \frac{\partial^2 U}{\partial t^2}}_{\text{Group Velocity Dispersion}} + \underbrace{\frac{1}{6}\beta_3 \frac{\partial^3 U}{\partial t^3}}_{\text{3rd Order Dispersion}} - \underbrace{\gamma |U|^2 U}_{\text{Self Phase Modulation}} \qquad \textbf{Equation 2-25}$$

where U is a slowly varying envelope function, z is the propagation distance, t represents a time frame of reference that moves with the pulse at a group velocity v_g, α is the fibre loss, and γ is the nonlinearity coefficient. To simplify the solution of the equation, fibre attenuation and third order dispersion are often ignored, and the NLS is re-written:

$$i\frac{\partial U}{\partial z} + \frac{1}{2}\beta_2 \frac{\partial^2 U}{\partial t^2} + i\gamma |U|^2 U = 0 \qquad \textbf{Equation 2-26}$$

The precise solution to the above Schrödinger equation is complex, and is typically found numerically or by using inverse scattering transforms [64]. Equation 2-26 can be solved exactly under certain circumstances. One such solution is the optical soliton, which has a hyperbolic secant profile of the form [57, 65]:

$$U(t) = N \operatorname{sech}(t) \qquad \textbf{Equation 2-27}$$

where N is the order of the soliton. Figure 2-12 shows the temporal and spectral evolution of an initial *3 sech(t)* pulse as it propagates along a loss-less fibre. It can be seen that the evolution is periodic with distance, with the pulse width initially narrowing, before subsequently broadening. The opposite is observed in the frequency domain, with new frequency components being first generated, and then destroyed over the same period.

(a)

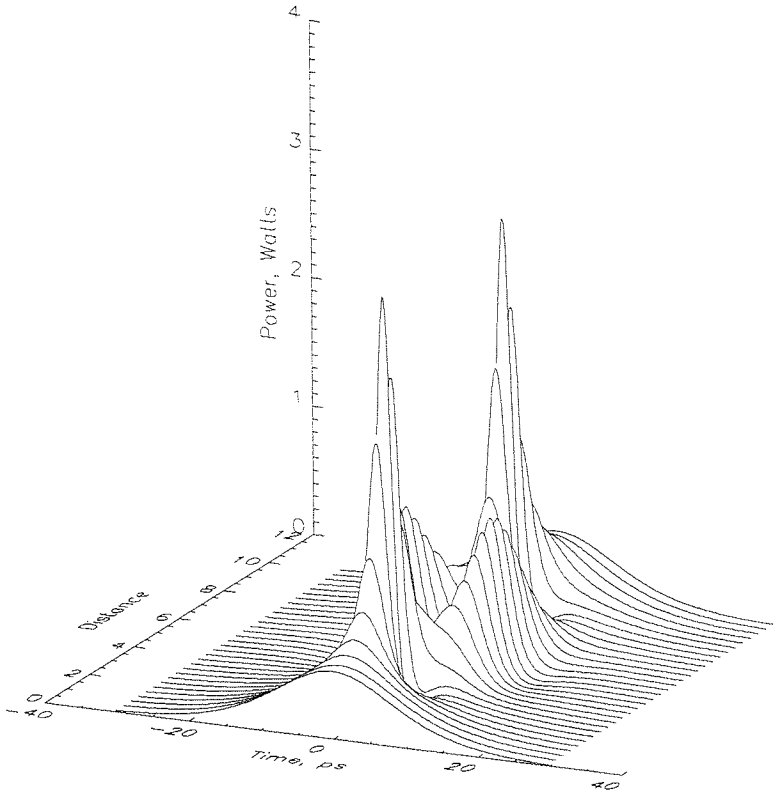

(b)

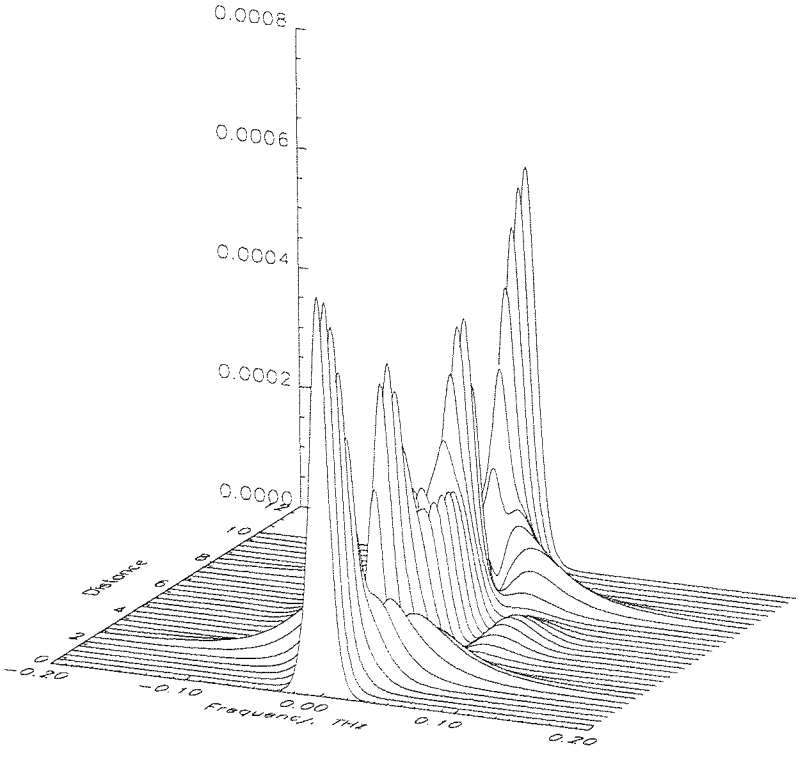

Figure 2-12. Evolution of a *3sech(t)* pulse in the: (a) temporal domain, and the; (b) spectral domain [66].

The length scale of this evolution is known as the soliton period Z_0, and corresponds to the distance it takes the phase of the soliton to evolve by $\pi/4$. The property of creation and destruction of new frequencies is probably one of the most remarkable properties of soliton evolution. The evolution is accompanied by a periodic phase variation, which is also present in the fundamental soliton (N=1), which propagates without change in shape in either the time or frequency domains. There are several important scales for solitons in fibres, in general the required peak power P_{sol} and the soliton period Z_0 are given by [55]:

$$P_{sol} = -\frac{3.098\beta_2}{\gamma\tau^2} = \frac{0.766\lambda^3 A_{eff} D}{\pi^2 c n_2 \tau^2}$$ **Equation 2-28**

$$Z_0 = \frac{0.322\pi^2 c\tau^2}{\lambda^2 D}$$ **Equation 2-29**

where β_2 is the group velocity dispersion, D is the fibre dispersion, γ is the nonlinearity coefficient, τ is the full-width half-maximum (FWHM) pulse width, A_{eff} is the effective core area of the fibre, c is the speed of light in a vacuum, and n_2 is the nonlinear refractive index coefficient.

For a fundamental soliton propagating in standard step-index fibre with a FWHM pulse width of τ (ps), dispersion D (ps/nm/km), the peak power P_{sol} (Watts), pulse energy E (pJ), and soliton period Z_0 (km) are more simply given by [57]:

$$P_{sol} = 1.34\frac{D}{\tau^2}$$ **Equation 2-30**

$$E = 1.53\frac{D}{\tau}$$ **Equation 2-31**

$$Z_0 = 0.42\frac{\tau^2}{D}$$ **Equation 2-32**

Considering a typical 10 Gbit/s system with a FWHM pulse width of 20 ps, and a dispersion $D = +1$ ps/nm/km. The peak power required is 3.5 mW, which is easily achievable using modern optical sources. The linear relationship between the soliton

power and dispersion means that as the dispersion approaches zero, lower powers are needed to generate a soliton.

Soliton formation is dictated by balancing dispersion and nonlinearity. This can be achieved by arranging that the dispersion length L_D (the distance over which a pulse will double its temporal width, see Equation 2-15) and the nonlinear length L_{NL} (the distance to acquire a nonlinear phase shift of π, see Equation 2-24) are equal. Thus, to generate a soliton in a particular fibre, a pulse of the correct peak power and shape is required as dictated by Equation 2-28. In practice, a soliton with the appropriate width will form if the pulse energy is close to the ideal value. The remaining energy will be shed from the pulse on propagation as a dispersive wave [57].

2.6 Soliton System Design

In a practical soliton system, the propagating signal will be subject to an exponential decay in power due to fibre attenuation, which leads to a decrease in nonlinear effects and the balance between GVD and SPM is destroyed. Soliton transmission can be maintained by using either *distributed* [67] or *lumped* all-optical amplification. The design of lumped or periodically amplified soliton systems is considered in detail below.

Figure 2-13 shows a typical soliton design diagram for a 5 Gbit/s system with a dispersion D = 1 ps/nm/km, and whose amplifiers are set to exactly compensate for a fibre loss of 0.2 dB/km. The total system length, L_{sys} is 7000 km, and the amplifier noise figure NF is 5.5 dB.

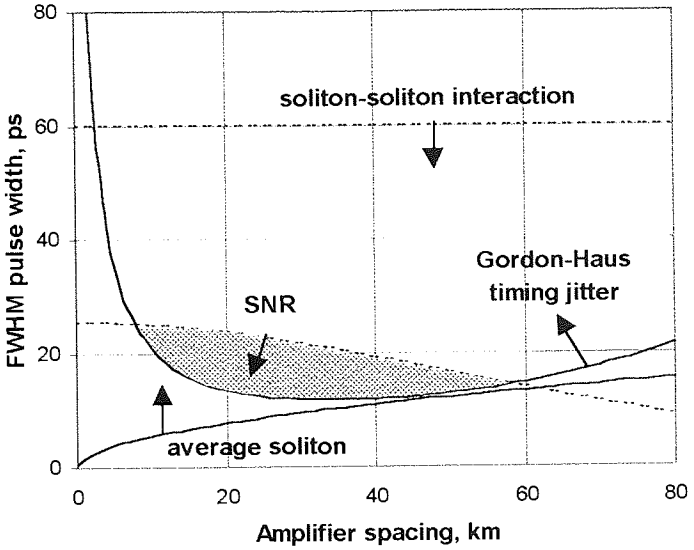

Figure 2-13. Soliton design diagram for a 7000 km system operating at 5 Gbit/s, D=1ps/nm/km, NF=5 dB. Note: the gain of each amplifier is set to directly compensate for the loss in each span.

The two axes show the amplifier spacing Z_a (km) and the soliton FWHM pulse width τ (ps). The figure shows four of the main operating characteristics that are important in soliton design, these are:

- Average soliton model
- Soliton-soliton interaction
- Receiver signal to noise ratio
- Gordon-Haus timing jitter

The shaded area shows the safe operating region, which is centred on a pulse width of 15 ps and an amplifier spacing of 30 km. Each parameter is described in detail below.

2.6.1 Average soliton model

In a practical system, the propagating signal will be subject to fibre attenuation, which is typically overcome using periodic gain blocks. Figure 2-14 shows the variation in pulse energy as a pulse passes through a system where the fibre loss is balanced by periodic amplification.

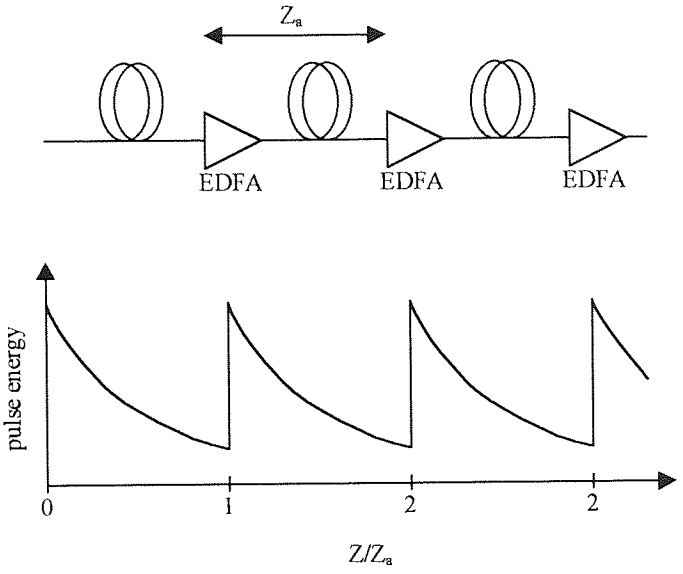

Figure 2-14. Schematic of an optical transmission system, and the corresponding periodic variation in pulse energy.

Over a distance l, the propagating pulse experiences a fibre loss $e^{\alpha l}$, then the gain required at each amplification stage, G, is given by:

$$G = e^{\alpha Z_a} \qquad \textbf{Equation 2-33}$$

where Z_a is the amplifier spacing. Attenuation and subsequent amplification results in large changes in the pulse energy. The integrity of a soliton, (including pulse width) will be maintained provided [57]:

a) The amplifier spacing is small compared to the full soliton period, which is defined as the period over which a loss less soliton changes phase by 2π. This is eight times the traditional soliton period, Z_0. To ensure that this condition is met, the following is typically used [57]:

$$Z_a \leq \frac{8Z_0}{10} \qquad \textbf{Equation 2-34}$$

b) The initial soliton amplitude is such that on average over the soliton period, the amplitude is equal to that of the loss less soliton. This is called the average soliton principle [68].

$$\langle P \rangle = P_{sol}$$ **Equation 2-35**

where P_{sol} is the peak power required for soliton propagation, defined in Equation 2-28, and $\langle P \rangle$ is the path average peak power, given by:

$$\langle P \rangle = P_{in}\left(\frac{G-1}{\ln(G)}\right)$$ **Equation 2-36**

P_{in} is the peak power of the input pulse, and G is the amplifier gain. Equation 2-32 and Equation 2-34 give a simple equation relating the dependence of the pulse width τ on the amplifier spacing Z_a:

$$\tau = \sqrt{\left(\frac{10}{(8)(0.42)}\right) Z_a D}$$ **Equation 2-37**

Equation 2-37 is used to plot a line of inequality on Figure 2-13, and a stable solution exists for the region above the curve.

2.6.2 Soliton-soliton interactions

If two solitons are launched at the same frequency, phase and amplitude, they will impart a phase shift on one another. This is due to the exponentially decaying tail of one pulse, changing the nonlinearity of its neighbour due to XPM. A periodic collapse is observed, see Figure 2-15.

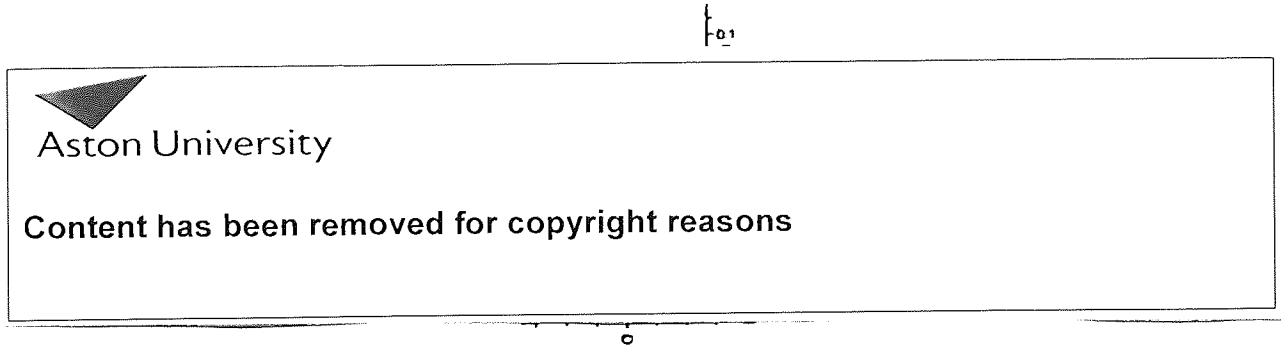

Figure 2-15. Soliton-soliton interaction. Two solitons launched with the same frequency, phase, and amplitude will interact and collapse after period L_c. From reference [57].

The distance over which the interaction occurs is known as the collapse length, given by [70]:

$$L_c = \frac{2\pi Z_0}{4\sec h\left(\frac{1.763T}{2\tau}\right)} \approx Z_0 \exp\left(\frac{1.763T}{2\tau}\right)$$ **Equation 2-38**

where Z_0 is the soliton period defined in Equation 2-29, T is the bit period, and τ is the FWHM pulse width. A soliton system is typically designed to avoid this collapse, and the design rule that L_{sys} is less than $L_c/4$ is adopted. The minimum bit-period is given by:

$$T \geq \frac{2\tau}{1.763}\ln\left(\frac{4L_{sys}}{Z_0}\right)$$ **Equation 2-39**

This condition is independent of amplifier spacing. In a practical communication system, the transmitted signal will be an uncorrelated sequence of random data, soliton interaction effects can be avoided by ensuring that the systems has a large mark-to-space ratio, typically greater than 3:1. This places stringent requirements on the type of soliton source used. Equation 2-39 can be rearranged to give a maximum value of τ for a given system design, and is plotted on Figure 2-14.

2.6.3 Receiver signal to noise ratio

The system must be designed to maintain an acceptable signal to noise ratio (SNR) along the system length, and at the detector [69]. In an optically amplified system, there are four main sources of noise that can contribute to the degradation of the SNR. The first two sources are due to shot noise associated with the signal and with the amplified spontaneous emission (ASE). The third cause of noise is signal-spontaneous beat noise, which is a beating effect between the signal frequency and the ASE frequencies. The final noise source is known as spontaneous-spontaneous beat noise and is due to a beating of the ASE frequencies against themselves. If an appropriate optical bandpass filter is used, then the most dominant noise source is signal-spontaneous beat noise. Assuming, the loss due to fibre attenuation is exactly compensated for by the amplifier gain, and ignoring amplifier coupling losses, then the electrical SNR is then given by [70, 71]:

$$SNR = \frac{\left\langle i_{sig}^2 \right\rangle}{\left\langle i_{sig-spont}^2 \right\rangle}$$
$$= \frac{(eP_{out}/hv)^2}{(2e/hv)^2 P_{out} N_{amp} F_{out} \frac{\Delta f_{elect}}{\Delta f_{opt}}}$$
$$= \frac{P_{out}}{4N_{amp} F_{out} \frac{\Delta f_{elect}}{\Delta f_{opt}}}$$

Equation 2-40

where i_{sig} and $i_{sig\text{-}spont}$ are the detector currents due to the signal and the signal spontaneous beat noise. P_{out} is the average optical power at the output of the amplifier, h is Plank's constant, v is the signal frequency, e is the electronic charge, N_{amp} is the number of amplifiers in the link, Δf_{elect} is the electrical bandwidth of the receiver, Δf_{opt} is the optical bandwidth of the bandpass filter, and F_{out} is the ASE noise power of the amplifier in a single polarisation, and is given by [55]:

$$F_{out} = n_{sp}(G-1)hv\Delta f_{elect}$$

Equation 2-41

where G is the amplifier gain, and the population inversion parameter n_{sp} is directly related to the amplifier noise figure by [55]:

$$NF(dB) = 10\log_{10}(2n_{sp})$$

Equation 2-42

The average power required to support a first order soliton can be derived from Equation 2-36, and is given by [70]:

$$P_{out} = P_{sol}\frac{\tau}{1.76T}\frac{G\ln G}{(G-1)}$$

Equation 2-43

where P_{sol} is the peak soliton power defined in Equation 2-28, T is the bit period, and τ is the FWHM pulse width. The receiver electrical SNR is then given by:

$$SNR = \frac{1.06(G\ln G)D}{4N_{amp} n_{sp}(G-1)^2 hv\Delta f_{elect} T\tau}$$

Equation 2-44

The soliton design diagram shown in Figure 2-13, was calculated assuming the electrical bandwidth of the receiver was set to *0.8/T*, and the SNR was 23 dB, which gives a 7 dB system margin for a BER of 10^{-9}, see section 2.9.

2.6.4 Gordon-Haus timing jitter

In periodically amplified RZ transmission systems, signal-spontaneous beat noise from each amplifier will induce random frequency fluctuations, which are subsequently translated into a timing jitter via fibre dispersion on propagation [72]. This effect is known as Gordon-Haus jitter. The magnitude of the jitter is given by [55]:

$$\left\langle \delta t^2 \right\rangle^{1/2} = \frac{4.14\text{x}10^{-6} n_{sp}(G-1)\left(1-e^{-\alpha Z_a}\right)L_{sys}^3 D}{\alpha Z_a^2 A_{eff}\tau} \qquad \text{Equation 2-45}$$

where L_{sys} (km) is the overall system length, D (ps/nm/km) the fibre dispersion, G is the amplifier gain, α is the fibre loss, Z_a (km) the amplifier spacing, A_{eff} (μm^2) the effective core area, τ (ps) is the FWHM pulse width, and n_{sp} is the population inversion parameter related to the amplifier noise figure by Equation 2-42. In order for the detector at the end of the system not to receive an error, then the pulse must arrive within a time window $\pm t_w$. Assuming gaussian statistics and a BER of less than 10^{-9}, then the timing jitter must be [70]:

$$\left\langle \delta t^2 \right\rangle^{1/2} < \frac{t_w}{6.1} \qquad \text{Equation 2-46}$$

The Gordon-Haus limit is the primary obstacle in achieving high-data rate soliton transmission systems. Efforts to overcome this limit are commonly described as soliton control, where the position of the soliton in time is controlled to prevent errors occurring at the detector when a soliton drifts into the wrong time-slot. Soliton control techniques will be discussed in section 3.5.1. Such techniques have allowed almost unlimited transmission at 10 Gbit/s [77], and transatlantic transmission up to 40 Gbit/s [73, 74].

2.7 Cross-Phase Modulation

Cross-phase modulation (XPM) is a nonlinear phase shift, similar to SPM, but induced by a co-propagating field at either a different wavelength, or polarisation. The total nonlinear phase shift for a field E_1 must be modified to include both SPM and XPM, and is given by [31]:

$$\phi_{TOT} = -\frac{2\pi n_2 L}{\lambda}\left(|E_1|^2 + 2|E_2|^2\right) \qquad \text{Equation 2-47}$$

where $|E_2|^2$ is the intensity of the co-propagating field. From the mathematics, the phase shift due to XPM is twice that of the SPM term for the same intensity. This effect is of great importance in nonlinear all-optical switching, which is discussed in section 3.4.

2.8 Four-wave Mixing

The same nonlinearity that gives rise to the nonlinear refractive index in single-mode fibres also mediates the process of four-wave mixing (FWM) [31]. Quantum mechanically, FWM occurs when photons from one or more waves are annihilated and new photons are created at different frequencies such that the net energy and momentum are conserved during the interaction. This is known as phase matching and in single-mode fibre requires a specific choice of frequencies and refractive indices.

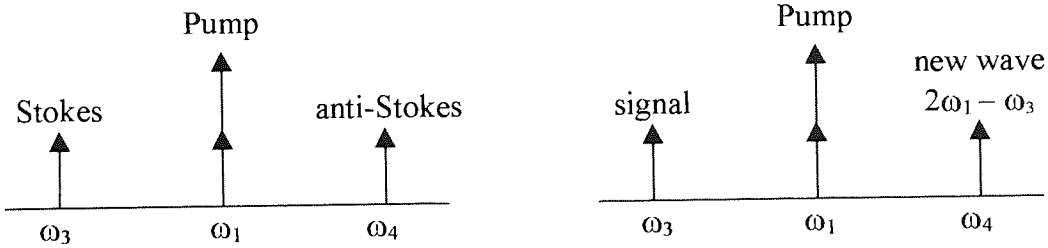

Figure 2-16. Four-wave mixing (FWM); (a) An intense pump at ω_1 will generate Stokes and anti-Stokes waves at ω_3 and ω_4 from noise; (b) If a signal at ω_3 is copropagating with the pump, then ω_3 will be amplified, and a new signal will be generated at ω_4 that is the phase conjugate of the signal at ω_3.

A strong pump wave at ω_1 creates two sidebands located symmetrically at the frequencies ω_3 and ω_4, typically referred to a the Stokes and anti-Stokes bands. If only the pump wave propagates in the fibre and the phase matching condition is satisfied, then the Stokes and anti-Stokes waves at frequencies ω_3 and ω_4 can be generated from noise, see Figure 2-16a. On the other hand, if a weak signal at ω_3 is also launched into the fibre together with the pump so that the two waves copropagate, then the signal at ω_3 is amplified while a new wave is simultaneously generated at ω_4, see Figure 2-16b. The

new signal is the phase conjugate of the original signal and will be generated at a frequency $2\omega_1 - \omega_3$.

Phase conjugation via FWM has been used extensively for signal processing within OTDM networks, and its applications are discussed in more detail in Chapter 3.

2.9 System Performance

There are two competing *binary* formats used to encode a digital signal for optical transmission, namely non-return-to-zero (NRZ), and return-to-zero (RZ). For a comparison of the two data formats see reference [55]. The remainder of this thesis will concentrate on the use of RZ encoding.

The two common ways of assessing the performance of a communications system are:

- Bit error ratio (BER)
- Q-value

The BER is the probability that a data pulse is interpreted incorrectly. An error will occur if a pulse which signifies a "1" is detected at the receiver as a "0", and vice-versa. This may be understood with reference to Figure 2-17, which shows an example of a fluctuating signal received by the decision circuit.

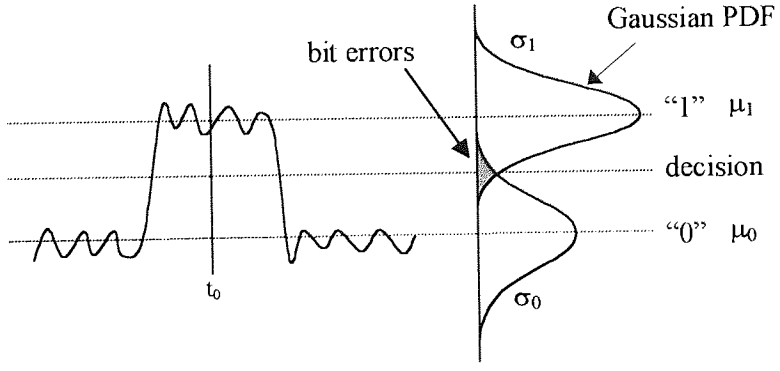

Figure 2-17. Sampling at the detector, and the probability density functions associated with each decision level.

The decision circuit samples the signal at t_0. Each logic state will have a probability density function (PDF), the characteristics of which, depend on transmission

impairments, e.g. noise or dispersion. A decision point is set between the two states, and the BER is determined as the sum of the areas under the tails of the PDFs that appear on the wrong side of the threshold (shaded area). The decision point maybe chosen as the crossing point of the two PDFs to give the lowest BER.

System characterisation will normally measure the BER of the transmitter, which provides a back-to-back indication of the receiver sensitivity. This is conventionally taken, as the optical input power required for a BER of 10^{-9}. The BER measurement is made by connecting the transmitter through a variable optical attenuator directly onto the receiver. As the attenuation is varied, the BER is plotted against the optical power incident on the receiver. A transmission link is then inserted between the transmitter and attenuator, and the BER measurement repeated. Minor transmission impairments will cause a degradation in the receiver sensitivity (optical power at a BER of 10^{-9}); system performance can by recovered by increasing the optical power incident on the receiver. The amount by which the optical power must be increased is known as the system penalty. A system penalty of less than 2 dB is usually tolerable. If however, it becomes impossible to restore the BER by simply increasing the optical power incident on the receiver, then the system is said to have an error-floor, which is unacceptable. Figure 2-18 shows an example of a typical BER measurement, indicating a back-to-back receiver sensitivity, a 1 dB penalty, and an error-floor.

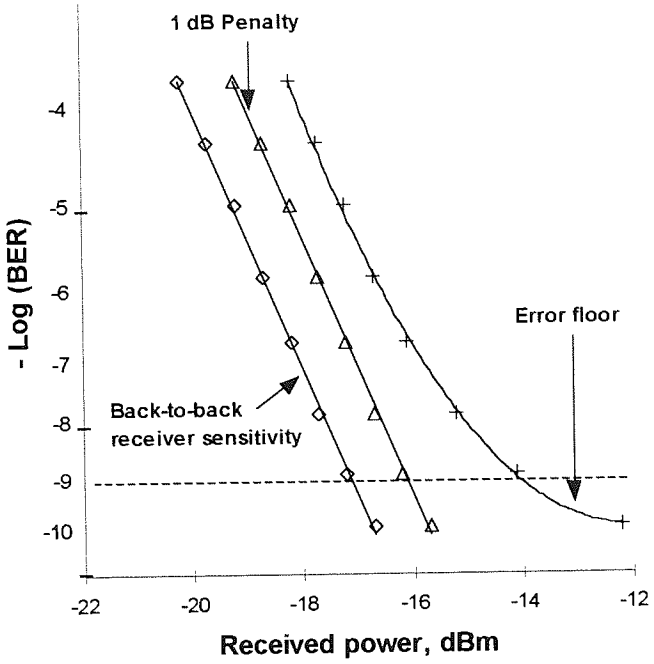

Figure 2-18. Indicates BER for a back-to-back measurement, a 1-dB penalty, and an error-floor.

BER can also be used to characterise the performance of optical components, such as a demultiplexer within an OTDM network.

Q is the electrical SNR ratio at the receiver decision circuit. The system Q can be measured using a sampling oscilloscope, which is triggered by the system clock. The result is an eye diagram, which is an overlay of all possible states produced by a pseudo random bit stream (PRBS). An eye diagram can be use to calculated the system performance, in terms of timing and amplitude jitter, noise, inter-symbol interference, some patterning effects, and BER [75]. System or transmission impairments will appear as a closure of the eye diagram. Assuming gaussian noise, and a decision threshold midway between the *zero* and *one* states, the BER can be estimated from the Q factor using [76]:

$$BER = \frac{1}{2} erfc\left(\frac{Q}{\sqrt{2}}\right) \approx \frac{\exp\left(-Q^2/2\right)}{Q\sqrt{2\pi}} \qquad \textbf{Equation 2-48}$$

Figure 2-19 shows the BER verses Q-value.

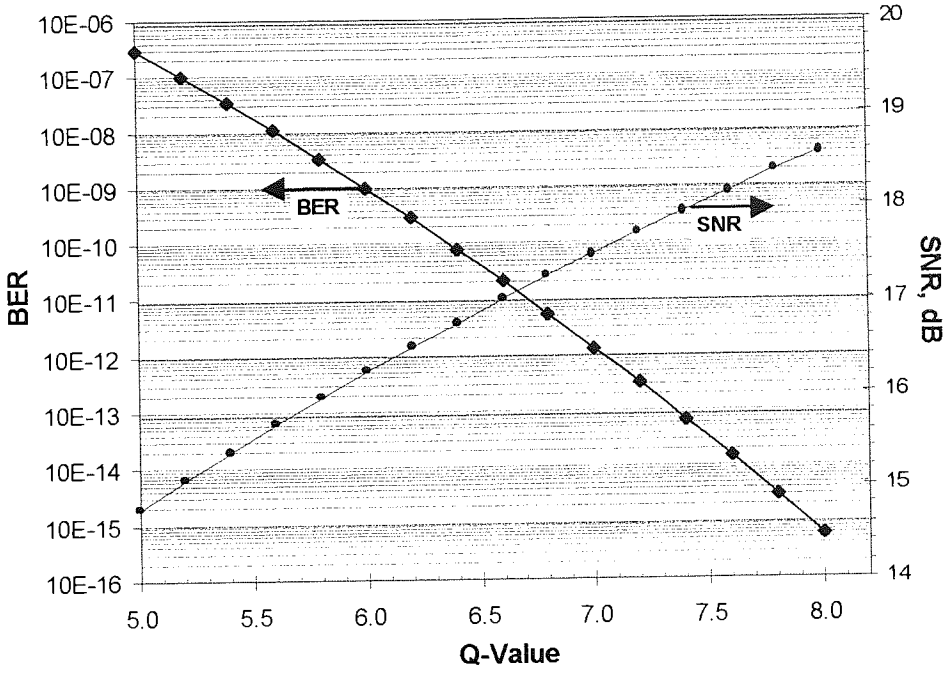

Figure 2-19. Q-value verses bit-error-rate (BER) and signal-to-noise ratio (SNR)

As mentioned, the receiver sensitivity is conventionally defined as a BER of 10^{-9}, which corresponds to a Q of approximately 6. BER becomes lower than 10^{-12} for $Q > 7$. The system Q can be related to the receiver SNR using [55]:

$$SNR = Q\left(1 + Q\sqrt{\frac{B}{\Delta f}}\right)\sqrt{\frac{B}{\Delta f}} \qquad \textbf{Equation 2-49}$$

where B is the data rate and Δf is the receiver bandwidth. To obtain a BER of 10^{-9} then a SNR of 16.4 dB is required at the receiver. A BER of 10^{-15} gives a SNR at the receiver of 18.5 dB.

The method used to measure the Q-value in this thesis relies on the histogram function on an HP5420B 50 GHz digital-sampling oscilloscope, in conjunction with a HP11982A 25 GHz lightwave converter. Here the mean and standard deviation of each logic state are measured. Equation 2-50 is then used to calculate the Q and infer a BER.

$$Q = \frac{\mu_1 - \mu_0}{\sigma_1 + \sigma_0} \qquad \textbf{Equation 2-50}$$

where μ_1 and μ_0 are means of the distributions and σ_1 and σ_0 are the standard deviations of the 'on' and 'off' states respectively. Figure 2-20 shows an experimental example of an eye diagram and its corresponding histogram. The Q is calculated to be 20.1.

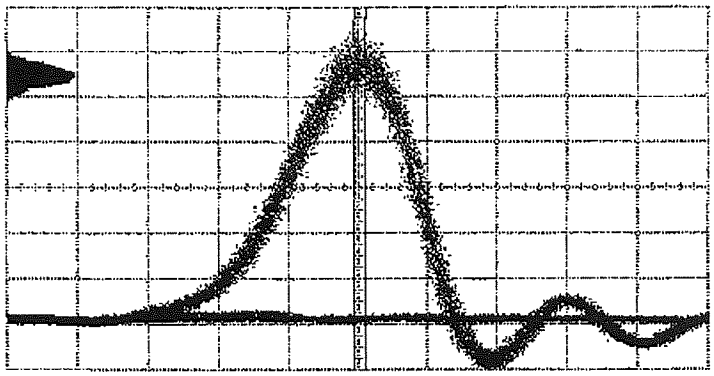

Figure 2-20. Example of an eye diagram, and histogram from a HP digital sampling oscilloscope.

It must be noted that this technique suffers from measurement errors that become particularly significant when measuring high Q's. Sources of error include noise added at the receiver and at the front end of the oscilloscope, quantisation errors, and limited number of sampled bits, dictated by the sampling speed [75]. These effect become increasingly noticeable as the data rate increases, because of the difficulty in manufacturing wide-band high-speed electronics.

To measure BER $>10^{-14}$ to a high degree of confidence will take a number of days. (e.g. at 10 Gbit/s the test time is 14 hours for a degree of confidence of 99.4%). The Q-value therefore becomes a much faster and simpler method of measurement. Both techniques are used in this thesis. Q values are used when measuring the data regeneration described in Chapter 5, and BER are used when measuring the performance of the EA modulator as a demultiplexer and drop and insert multiplexer, see Chapter 7.

2.10 Chapter Summary

This chapter introduced the subject area of optical communications. The maximum achievable transmission distance is limited by fibre attenuation and dispersion. Methods of overcoming these limitations were discussed, including nonlinear or soliton

transmission. System performance can be analysed using either BER measurements, or Q-measurements, or a combination of each. These techniques were described, and the advantages and disadvantages of each method was given.

Chapter 3

Optical time division multiplexing

3.1 Introduction

Within an optical time division multiplexed (OTDM) network, optical pulses at the base-rate are split into a number of channels, and each is separately encoded with data before being re-combined into a single high-speed optical data stream at the line-rate. The data-stream is then transmitted around the network, which consists of a number of network nodes interconnected by optical transmission links. A typical network node is shown in Figure 3-1. Each node needs to perform the following basic processing functions: demultiplexing, 'drop and insert' multiplexing, and clock recovery. Data regeneration may also be required either mid-way through a long transmission path or at the network node to ensure that all channels have the same wavelength and temporal profile.

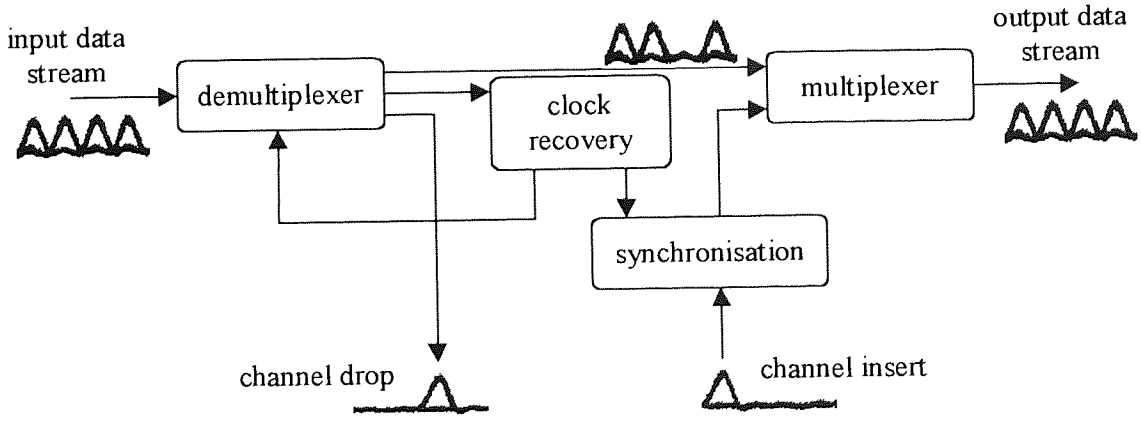

Figure 3-1. An OTDM network node.

This chapter discusses the requirements of an OTDM network, outlining the most promising solutions, stating advantages and disadvantages of each technique. Finally, details are given of system impairments that may occur within an OTDM system.

3.2 Optical Sources

An essential component within an OTDM network is a picosecond optical pulse source, the quality of which has a decisive effect on the maximum achievable transmission distance [77]. Ideally, an optical pulse source should generate return-to-zero (RZ) pulses with a $sech^2$ intensity profile and a time-bandwidth product of 0.315, at a fraction (less than $1/3^{rd}$) of the bit-period (see section 2.5). Most practical sources generate RZ pulses with an intensity profile that only approximates the required $sech^2$ profile. A soliton will still be formed on transmission, provided the peak pulse power is equal or greater than that given in Equation 2-28. A residual amount of energy will be shed as a dispersive wave, appearing as extra noise in the system. Other characteristics that help access the suitability of a source for use in an OTDM network are timing and amplitude jitter, pulse extinction (signal to background intensity), spectral purity and wavelength stability. A practical source that might one day be deployed in the field must also considered for its overall complexity, reliability and long-term stability. These criteria impose very stringent requirements and in practice, a compromise might have to be made.

The following optical sources are typically used to demonstrate OTDM systems: gain-switched distributed-feedback lasers (DFB), external-cavity mode-locked lasers (ECMLL), external modulation of a CW-DFB by an electroabsorption (EA) modulator, and a fibre-ring laser. The following section gives a brief explanation of chirped pulse compression, before discussing the advantages and disadvantages of each of the four main sources, introduced above.

3.2.1 Chirp pulses and compression

A pulse propagating in a dispersive optical fibre will be subject to either an 'up-' or 'down-' linear frequency chirp as it broadens, depending on which dispersion regime (normal or anomalous, respectively) the pulse is propagating in. The broadened pulse

can then be compressed back to its original width, by propagation through a fibre with dispersion of equal magnitude, but opposite sign.

A semiconductor source will typically produce chirped pulses through dynamic changes in the semiconductor refractive index, and not through propagation in fibre. However, provided the chirp is linear, the pulse will behave as if it was chirped through fibre propagation, and can therefore be compressed to form a transform-limited pulse stream. A chirped gaussian pulse can be described by [31]:

$$E(t) = \exp\left(-\frac{(1+iC)}{2}\frac{t^2}{{\tau_0}^2}\right) \qquad \textbf{Equation 3-1}$$

where C is the chirp parameter, and τ_0 is the initial FWHM pulse width. The chirp parameter is given by [31]:

$$C = \sqrt{\left(\frac{\Delta\omega \cdot \Delta\tau}{2.77}\right)^2 - 1} \qquad \textbf{Equation 3-2}$$

where $\Delta\tau$ is the FWHM pulse width, and $\Delta\omega$ is the FWHM spectral width in rad/s, which can be related to the 3 dB spectral width $\Delta\lambda$, using:

$$\Delta\lambda = -\frac{\lambda^2}{2\pi c}\Delta\omega \qquad \textbf{Equation 3-3}$$

The chirp parameter can be estimated by using an optical spectrum analyser to experimentally measure the 3-dB spectral width $\Delta\lambda$, and either a digital sampling scope, or an autocorrelator to measure the FWHM pulse width $\Delta\tau$. If $C > 0$, the instantaneous frequency increases from the leading to the trailing edge (up-chirp), where as the opposite occurs for $C < 0$ (down-chirp). In the absence of frequency chirp ($C = 0$), the spectral width is said to be Fourier transform-limited. For a *gaussian* pulse, $\Delta\nu\Delta\tau = 0.44$, and for a *sech*^{2} pulse, $\Delta\nu\Delta\tau = 0.315$, where $\Delta\nu = \Delta\omega/2\pi$. The FWHM pulse width τ_{out} after propagation over a distance z is related to the initial FWHM pulse width τ_{in} by the relation [31]:

$$\frac{\tau_{out}}{\tau_{in}} = \sqrt{\left(1 + C\frac{2.77\beta_2 z}{\tau_{in}^2}\right)^2 + \left(\frac{2.77\beta_2 z}{\tau_{in}^2}\right)^2} \qquad \text{Equation 3-4}$$

The broadening depends on the relative signs of the GVD parameter β_2 and the chirp parameter C. This is illustrated in Figure 3-2, which plots the broadening factor τ_{out}/τ_{in} as a function of z/L_D for different values of chirp parameter C, where L_D is the dispersion length defined in Equation 2-15.

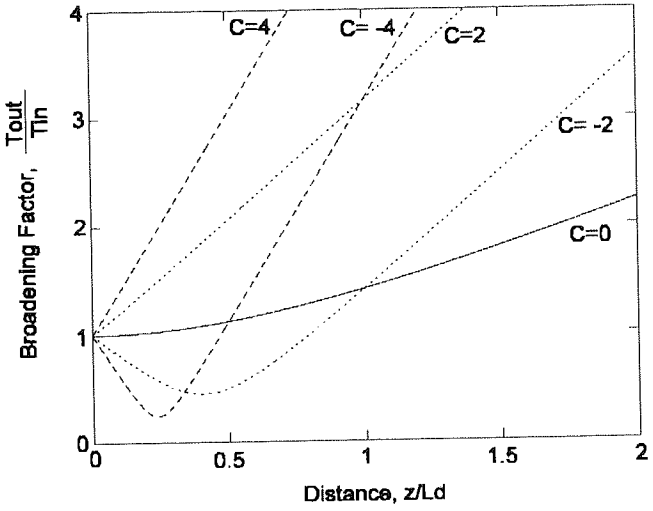

Figure 3-2. Variation of broadening factor with distance for chirped gaussian pulses propagating in the normal dispersive regime, D < 0.

For an initially un-chirped gaussian pulse ($C = 0$), dispersion-induced broadening does not depend on the sign of the parameter β_2. If however $\beta_2 C > 0$ then the pulse broadens monotonically with Z, if however, $\beta_2 C < 0$, the pulse goes through an initial narrowing stage. The pulse width becomes a minimum after a distance, Z_{min} [31]:

$$Z_{\min} = \frac{C}{1+C^2} L_D \qquad \text{Equation 3-5}$$

with the minimum pulse width given by [31]:

$$\tau_{\min} = \frac{\tau_{in}}{\sqrt{1+C^2}} \qquad \text{Equation 3-6}$$

Semiconductor laser devices typically produce pulses with shorter wavelengths 'blue components' at the leading edge, and longer wavelengths 'red components' at the trailing edge of the pulse, (i.e. with negative frequency chirp, $C < 0$). By propagation in

the normal dispersive regime ($D < 0$) the pulses will initially compress before broadening. In practice, chirp compensation is achieved by either propagation through a length of normal dispersive fibre ($D = -80$ ps/nm/km), or by using a more stable specially designed (in terms of wavelength and chirp) chirped fibre Bragg grating [28]. It must be noted that semiconductor sources also typically produce a finite amount of nonlinear chirp that often prevents truly transform-limited pulses from being generated.

3.2.2 Distributed feedback lasers

One of the simplest forms of optical pulse source is a gain-switched DFB [78]. The laser is biased near threshold, and a RF signal is applied, resulting in the generation of short optical pulses. The gain switching mechanism can be understood with reference to Figure 3-3.

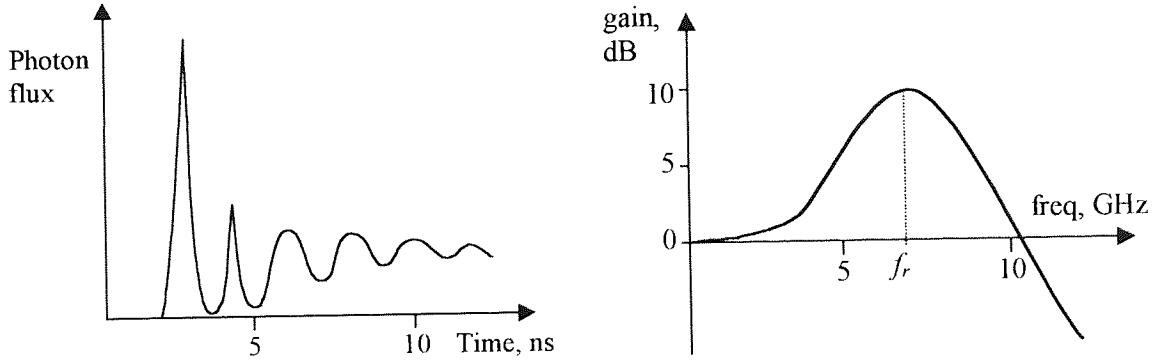

Figure 3-3. Gain switching process; (a) photon output when a large signal is applied to the laser; (b) small signal frequency response of a semiconductor laser.

If the laser is biased slightly below threshold, and then quickly switched high above threshold, then relaxation oscillations will occur in the laser cavity, see Figure 3-3a. These oscillations can be seen in the transfer function shown in Figure 3-3b, as a pronounced resonance peak. The oscillations can be described as follows. An increase in the input current creates, a short time later, an increase in the carrier concentration; after another short delay this leads to an increase in the photon density by recombination; the increase in photon density stimulates further recombination, which after another time delay causes the carrier concentration to fall. The cycle then repeats, resulting in oscillations in the carrier density and the photon output. Gain switching involves

switching the laser on and off at a high-speed so that only the first resonance peak is obtained. Optimum gain switching is achieved by operating at a frequency corresponding to the resonance peak on the transfer function shown in Figure 3-3b. This corresponds to an equilibrium condition between the rate of *electron-hole* recombination and population inversion due to current injection.

The overall timing and wavelength characteristics associated with gain switching are determined by the RF drive frequency and the laser grating. Spontaneous emission which seeds each individual pulse, leads to a high degree of timing (6 ps) and wavelength jitter. Carrier-density variations in the laser-gain region will lead to linear and nonlinear red frequency chirp; consequently, the pulses are far from transform-limited. The linear frequency chirp can be compensated for by compression in dispersion compensating fibre [79], spectral windowing using a bandpass filter [80], and using a semiconductor optical amplifier to simultaneously amplify and induce an equal and opposite frequency chirp [81]. Timing and wavelength jitter can be minimised by feeding part of a previously generated pulse back into the DFB, at the appropriate time. This process is known as reflective self-seeding, where each pulse is seeded by a previous pulse, and not by the random uncorrelated spontaneous emission [82, 83]. The technique has allowed 10 GHz, 8 ps gaussian pulses with a time-bandwidth product of 0.4, and a timing jitter of 500 fs (limited by RF source) to be produced, making them suitable for use in all-optical signal processing [84]. However, residual *nonlinear* chirp limits their use in transmission systems.

3.2.3 Modulation of CW laser by an external modulator

Modulation of a CW laser by an external modulator is a very stable and practical solution to the problem of optical pulse generation. It was first demonstrated using a sinusoidally driven high-speed lithium-niobate ($LiNbO_3$) Mach-Zehnder modulator [85, 86]. Such devices achieve amplitude modulation by utilising the electro-optic effect to induce a phase-shift in one arm of an integrated interferometer; the output of the device has a cos^2 intensity transfer characteristic. Unfortunately, the optical pulses produced by the

technique are relatively broad. One method used to reduce the duty cycle involves the use of pulsed electrical drive circuitry, which results in a significant pulse background pedestal. Methods to reduce this effect typically involve passing the signal through a second, synchronously driven modulator [87]. Combining these factors with other practical disadvantages, including polarisation-sensitivity, and very long-term stability issues associated with the interferometric operation, makes the $LiNbO_2$ modulator far from an ideal choice.

EA modulators are a very promising alternative, offering wide electrical bandwidths, low-drive voltages, polarisation insensitivity, wide wavelength operation, and high extinction ratios. Such devices have been used to generate transform-limited pulses with *sech*^{2} to *gaussian* intensity profiles. They have also been integrated with CW-DFB lasers to produce a single and potentially highly stable reliable, monolithic device. A detailed explanation of the EA modulator is given in Chapter 6 followed by four novel applications detailed in Chapter 7.

3.2.4 External cavity modelocked lasers

An extremely attractive and versatile high-speed transform-limited pulse source is that of the external cavity mode-locked laser (ECMLL) [88, 89], illustrated in Figure 3-4.

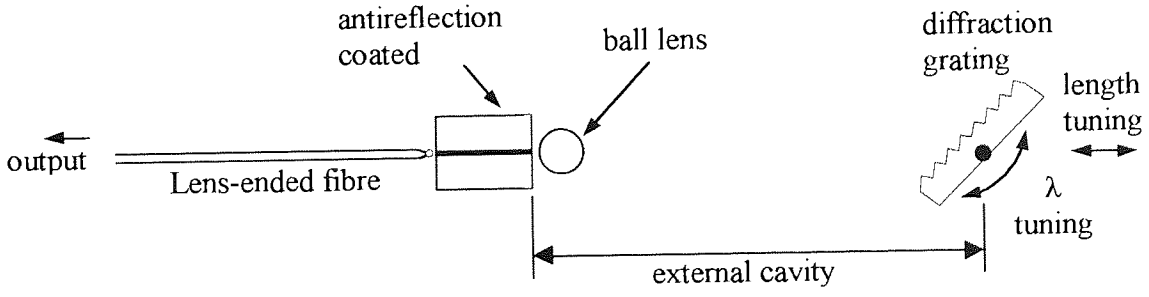

Figure 3-4. Diagram of an actively modelocked external cavity semiconductor laser source.

One facet of a laser diode is AR-coated. A ball lens is used to collimate the output beam into the external cavity onto a diffraction grating that acts as a wavelength-selective external mirror. The lasing emission is filtered from the wide gain-spectrum of the laser-chip, producing a narrow linewidth at the desired wavelength. Wavelength tuning of the

output is achieved by mechanical rotation of the grating such that the lasing wavelength moves with mode-hops from one longitudinal mode to the next. In general, coarse spectral tuning is obtained by rotation of the grating, whilst fine-tuning can be achieved by lateral translation of the grating. An anti-reflective coated lens-ended fibre is used to couple light out of the device.

To generate an optical pulse stream, the laser is biased near threshold and a high-power RF signal is applied, similar to a gain-switched DFB. Active mode-locking is achieved by matching the cavity round-trip time (cavity length) to that of the desired operating frequency (or a harmonic thereof), according to the following equation:

$$f_{\text{mod}} = \frac{c}{2L}$$ **Equation 3-7**

where f_{mod} is the modulation frequency, c is the speed of light in a vacuum, and L is the cavity length. Conceptually, the output from a mode-locked laser can be considered (in the time domain) as a single pulse circulating within the cavity, which gives an output pulse each time it is reflected from the output coupler. The pulse width is dependent on the power and frequency of the RF drive signal; in general, the higher the frequency and the RF power the shorter the pulse width. The characteristics of the diffraction grating also limit the pulse width via inherent spectral filtering. External cavity sources exhibit high-pulse extinction ratios, and typically produce close to transform-limited pulses, with a time bandwidth product of 0.4. They are tuneable in terms of pulse width, repetition-rate, and wavelength. Typical devices operated from 2-10 GHz have pulse widths of 5-40 ps, and wavelength tuning ranges of 1500-1580 nm, making them ideal laboratory sources for use in OTDM demonstrations. Alignment and stability issues are gradually being overcome, and a number of commercial ECMLL operating at < 5 GHz are currently available from companies such as *Lamda Photometrics* or *Santec Corporation.* Attempts to integrate the external cavity with a monolithic waveguide and a Bragg reflector have produced transform-limited 20 ps pulses at 8 GHz [90]. The approach makes the design, stable and compact but removes the benefits of tuneability, making it difficult to synchronise the modelocked frequency to multiples of the SDH line-rates.

3.2.5 Actively modelocked fibre lasers

A more complex alternative to the ECMLL is the fibre-ring laser. This consists of an erbium-doped fibre amplifier (EDFA) as the gain element, a bandpass optical filter to control the operating wavelength, and an amplitude/phase modulator to control the operating frequency. The modulator can be either electro-optic [91], or all-optical [92, 93]. A typical example is shown in Figure 3-5.

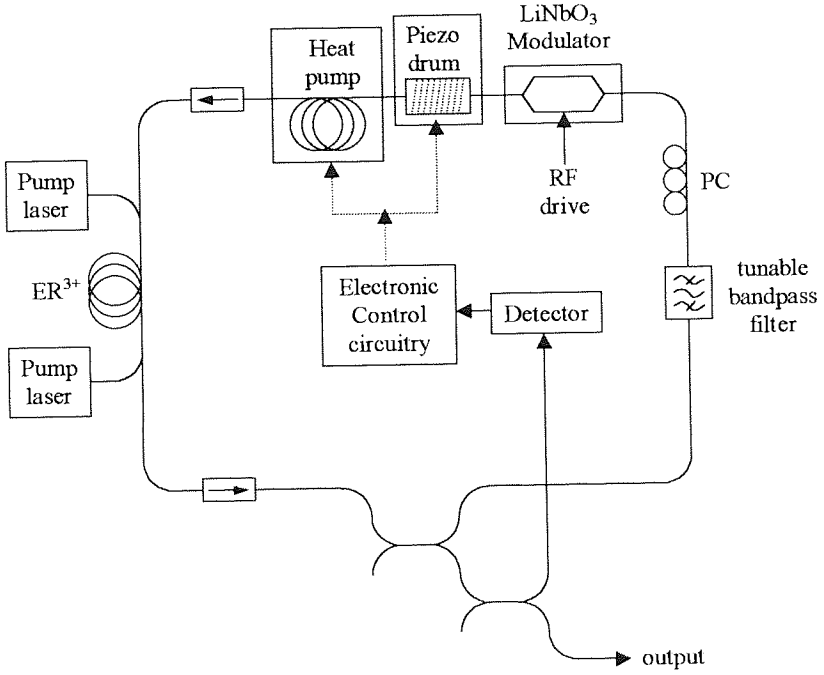

Figure 3-5. Schematic of an actively mode-locked erbium doped fibre ring laser with cavity length stabilisation.

Mode-locking is achieved by matching the cavity round-trip time to that of the desired operating frequency dictated by the modulator. Pulses will experience soliton-shaping effects in the fibre-cavity; pulse energy will be shed, which is subsequently converted into high-quality soliton pulses, by the mode-locking process. Actively mode-locked lasers require the cavity length (typically 100 metres) to be accurately controlled to keep the drive frequency synchronised to a high harmonic of the cavity round-trip time. The tight tolerance can be overcome by monitoring the output and using a standard phase-locked loop configuration [94]. A heat-pump attached to a section of fibre in the cavity is used to compensate for long term drifts in temperature, while vibrations can be overcome by

using a piezoelectric fibre stretcher [95]. Fibre ring lasers have been developed that produce short, sub-10 ps soliton pulses, at frequencies up to 40 GHz [96, 97]. Transmission demonstrations with fibre-lasers produce impressive results that agree closely with ideal transform-limited soliton numerical simulations [77].

A variation of the fibre ring laser, is the linear fibre laser [98]. Cavity length stabilisation can be performed passively using a chirped fibre Bragg grating [28] as one end mirror in the cavity. The grating behaves as a lumped dispersive element within the cavity that allows accurate control of inter-cavity dispersion to produce controllable and well-defined pulse characteristics from the laser output. In addition, the grating acts to self-stabilise the laser in the presence of cavity length variations by changing the grating reflection point and so the cavity feedback wavelength. This is however undesirable because the laser wavelength changes.

Such sources are likely to be confined to the laboratory because of the cavity length fluctuations, and the operating frequency is dictated by the cavity fundamental, making it difficult to operate at a desired SDH frequency. However, a commercial fibre ring laser is available from *PriTel Inc.* that generates 3 ps transform-limited soliton pulses at frequencies up to 20 GHz [99].

3.2.6 Multiplexing techniques

Multiplexing can be active [85] or passive [100]. Active multiplexing uses a number of transmitters each combined using a hierarchy of electro-optic 2×1 switches to produce a single data channel. An example of passive multiplexing is shown in Figure 3-6. A single high-extinction optical source operating at the channel base-rate is amplified and split into a number of channels. Each channel is separately modulated and passed through a different delay line, before being recombined to form a single OTDM data stream.

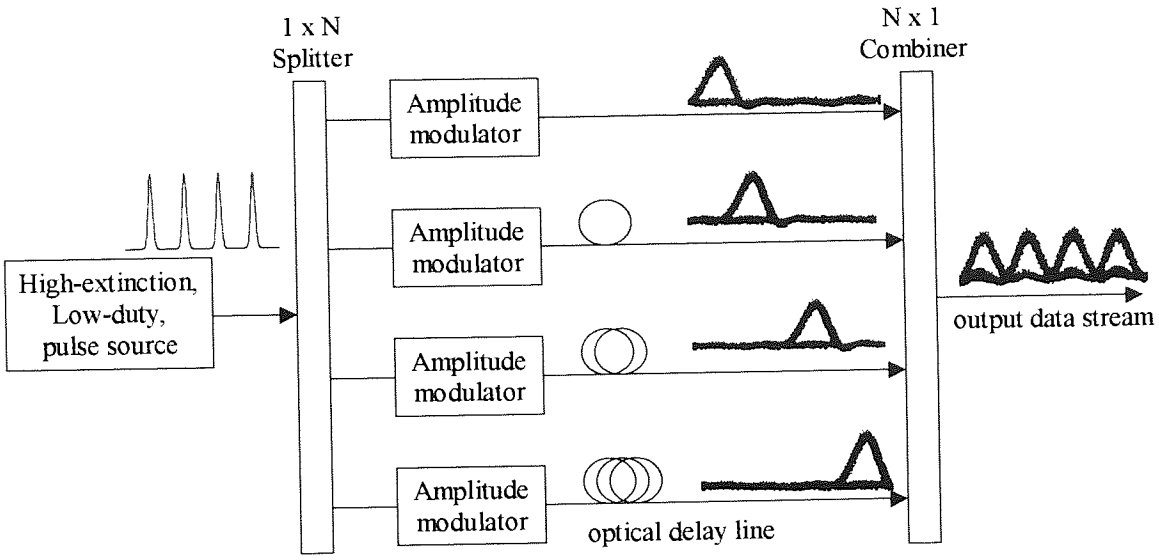

Figure 3-6. An OTDM multiplexer.

In laboratory demonstrations, this technique is usually simplified. The output from the pulse source is typically encoded using a single modulator with a pseudo random bit sequence (PRBS) before being interleaved up to the desired line-rate. Planar light-wave interleavers can be used [101, 102], but do not produce a true PRBS data stream at the required line-rate. To ensure that the PRBS is maintained, then each channel must pass through an arbitrary delay.

3.3 Experimental Characterisation of Pulse Sources

3.3.1 External cavity modelocked laser

A 500 μm long bulk GaInAsP/InP buried heterostructure device with one facet antireflection coated to ~0.05%, was supplied by BT Laboratories. The device was supplied mounted on a submodule in a similar configuration to that described by *Bird* [103], see Figure 3-4. The laser is biased and modulated via a 50 Ω microstrip and a SMA connector. The front facet of the laser is coupled to a single-mode fibre using a tapered fibre lens, and the fibre assembly is laser welded to the body of the module to give stable coupling. The output from the antireflection-coated facet is collimated by an AR coated 2mm-ball lens, which was glued into position using a fast setting ultra-violet curing adhesive. The submodule is mounted on a heat pump, which in turn is mounted

on a base plate. The external cavity is formed using a 600-lines/mm diffraction grating, blazed at 1.6 μm. This grating was mounted using doubled-sided tape onto a Melles Griot NanoFlex™ miniature piezo-electric tilt and translation stage. This is then mounted on an MDE-255M miniature precision translation stage supplied by Elliot Scientific. The grating module, which allows translation, rotation, and tilt was mounted parallel to the collimated output from the laser so that the cavity length could be adjusted between 15 mm and 80 mm.

For a modulation frequency of 10 GHz, the fundamental cavity size would be 15 mm. To simplify the mechanical design, the device was operated at the 4th harmonic, with a cavity length of 60 mm. The fundamental mode spacing of this cavity is 2.5 GHz, allowing mode-locking at 2.5 GHz, 5 GHz, and 10 GHz, with suitable RF drive electronics.

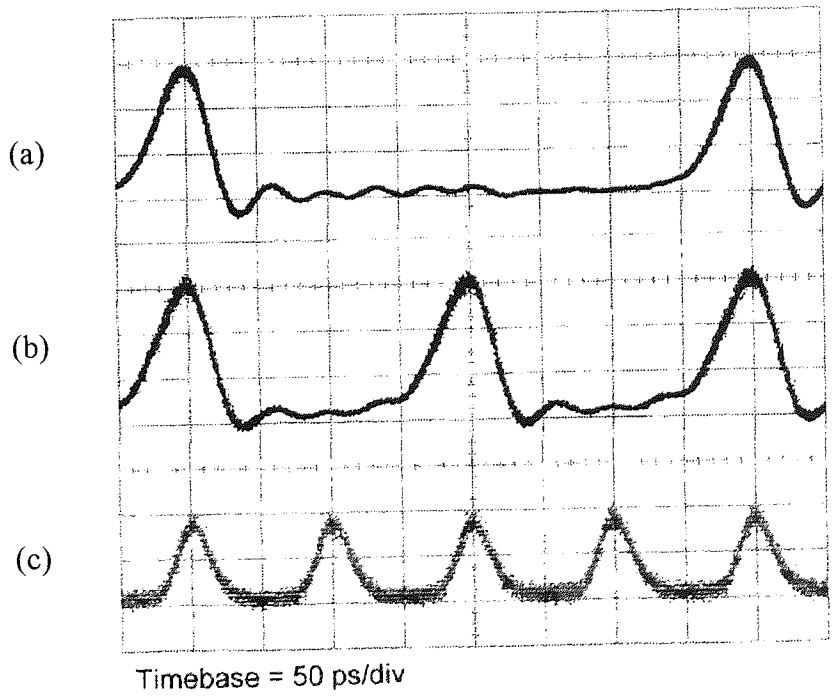

Figure 3-7. Output from an ECMLL laser operated at: (a) 2.5 GHz; (b) 5 GHz; (c) 10 GHz.

Figure 3-7 shows the output from the source at 2.5, 5, 10 GHz respectively. The device was tuneable over the entire erbium bandwidth and exhibited low levels of amplitude jitter. The wavelength of the ECMLL was set to 1534.7 nm. The device was biased near threshold and sinusoidally modulated at 2.5 GHz using a HP synthesiser and a *Mini-*

Cirkits (ZHL-42) DC-3.4 GHz RF amplifier. The pulse and spectral widths were measured using an *Inrad* autocorrelator and an HP70950A optical spectrum analyser. The pulse characteristics were optimised by varying the cavity length, bias current, and RF drive voltage. In general, the shortest pulses were obtained for the largest RF drive voltage, but to avoid damage a maximum drive voltage of 7 V_{p-p} (21 dBm) was applied. Optimum mode-locking was achieved by finely tuning the modulation frequency. Figure 3-8 shows the autocorrelation and optical spectrum of an optimised 2.5 GHz pulse stream, biased at 20.6 mA, with a 7 V_{p-p} RF drive.

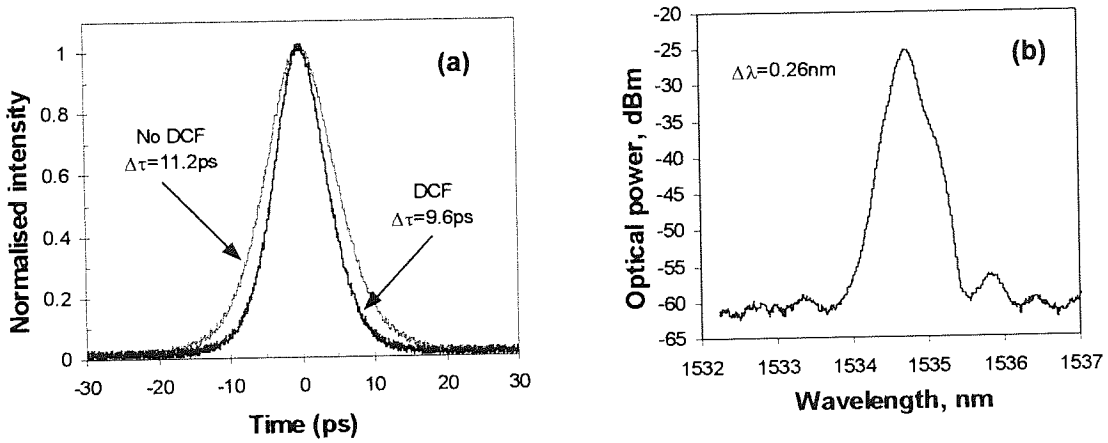

Figure 3-8. Autocorrelation and optical spectrum of the ECMLL. *f*=2.5 GHz, I=20.6 mA, V_{p-p}=7V, λ=1534.7, Δλ=0.263 nm, Δτ=11.2 ps.

The pulse width is ~11.2 ps and the spectral width is 0.263 nm, giving a time-bandwidth product assuming gaussian profile of 0.38. Different lengths of dispersion compensating fibre (DCF) were used to remove any residual linear-chirp and compress the pulse width, see Figure 3-9.

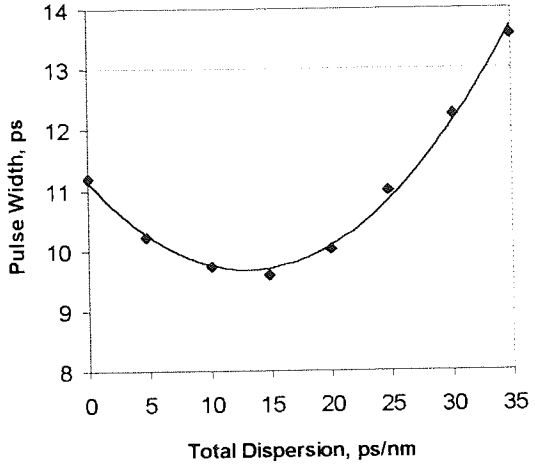

Figure 3-9. Pulse compression of ECMLL using dispersion compensating fibre (DCF). Initial pulse width = 11.2 ps, minimum pulse width = 9.6 ps.

A minimum pulse width of 9.6 ps was obtained using a total dispersion of –15 ps/nm, giving a time-bandwidth product of 0.32.

Pulse-to-pulse timing jitter analysis was performed using a HP70000 series microwave spectrum analyser and a HP70810A high-speed photodiode [104]. The electrical spectrum of a pulse stream consists of a fundamental frequency component, and a series of harmonics at integral multiples, *n* of the pulse repetition rate, see Figure 3-10.

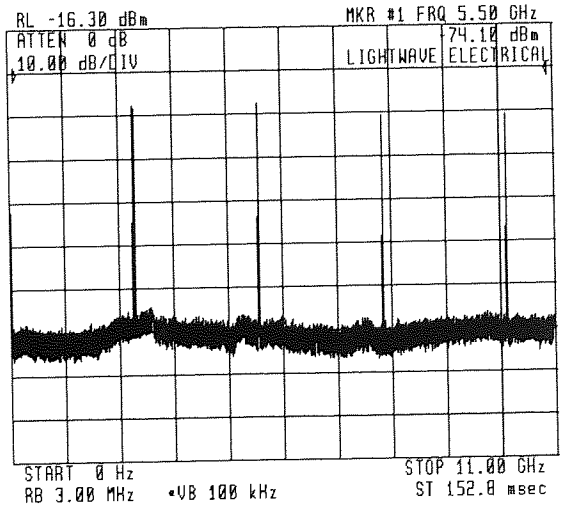

Figure 3-10. An electrical spectrum of a pulse stream, consisting of a fundamental frequency component, and a series of harmonics at integral multiples n of the pulse repetition rate.

Each component has a carrier resting on one or more broad pedestals or noise bands, which result from fluctuations in pulse energy (amplitude noise) and/or from random

variations in the pulse repetition rate (phase noise). The ratio of the area under a noise band to the area under the sharp carrier peak is independent of n for purely amplitude noise, while this ratio increases as n^2 for purely phase noise. In this way, the timing and amplitude jitter can be distinguished, and subsequently calculated. The root mean square (rms) phase fluctuation $\delta\phi(n)$ can be obtained from the ratio of the integrated power in the noise band $P_n(n)$ to the power in the carrier $P_c(n)$ using [104]:

$$\langle \delta\phi(n) \rangle = \sqrt{\frac{P_c(n)}{P_n(n)}} \qquad \text{Equation 3-8}$$

where n represents the harmonic number. The rms timing jitter, $\langle \delta t^2 \rangle^{1/2}$ is given by [104]:

$$\langle \delta t^2 \rangle^{1/2} = \frac{1}{2\pi n f} \delta\phi(n) \qquad \text{Equation 3-9}$$

where f is the repetition rate in Hz. The n^2 dependence of the phase noise means that the calculation of timing jitter will be more accurate, the higher the spectral harmonic used.

The ECMLL laser was modelocked using a 7 $V_{p\text{-}p}$, 2.5 GHz sinusoidal drive, producing ~10 ps pulse, as described earlier. These were detected using a HP70000 series electrical spectrum analyser, which has a frequency range from dc to 22 GHz and was capable of a 10 Hz resolution. Figure 3-11 shows the electrical spectrum of the fundamental, and the first three harmonic components of the ECMLL driven at 2.5 GHz. The frequency scale is 100 kHz/div. Each of the traces shows similar characteristics, with small peaks at f ± 300 kHz are due to interference from the HP5420B digitising sampling oscilloscope. The noise pedestal increases in size as the harmonic number increases.

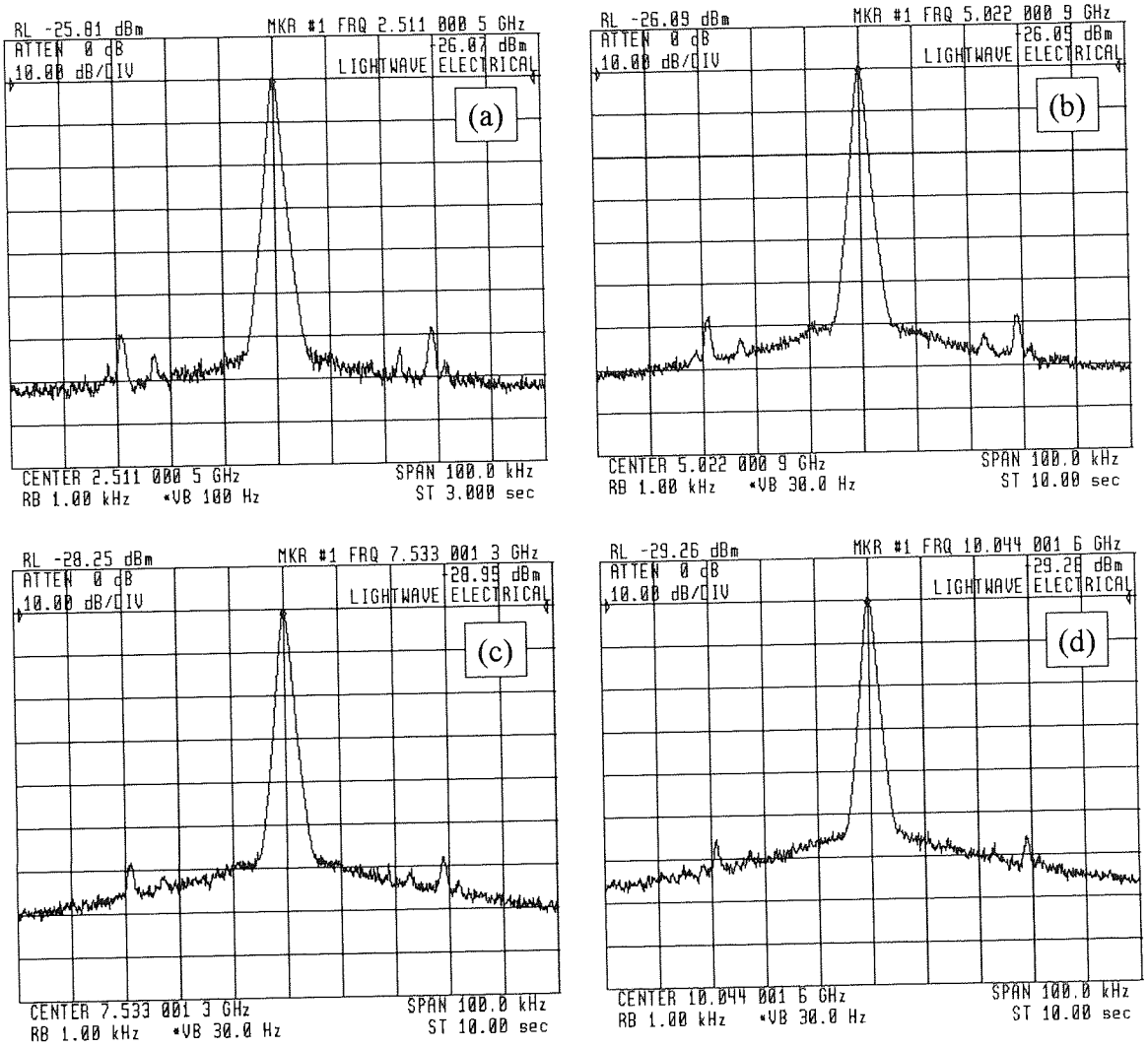

Figure 3-11. Measurement of timing jitter of 2.5 GHz ECMLL, using electrical spectrum analyser: Span=100 kHz/div
(a) f_c= 2.5 GHz, P_c= -25.58 dBm; (b) 1st harmonic, $2f_c$= 5 GHz, P_c= -26.20 dBm;
(c) $3f_c$= 7.5 GHz, P_c= -29.12 dBm; (d) $3f_c$= 7.5 GHz, P_c= -29.32 dBm;

The phase fluctuations for each harmonic were calculated using Equation 3-8, and are shown in Figure 3-12, which shows the $\delta\phi(n)/\delta\phi(1)$ verse n. Using Equation 3-8, the ratio of the phase fluctuation in the n^{th} harmonic to that of the fundamental is a straight line fit, proportional to the harmonic number n, i.e. $\delta\phi(n)/\delta\phi(1)=n$. Data points not on this line indicate amplitude noise components. It is therefore possible to calculate the timing and amplitude jitter components.

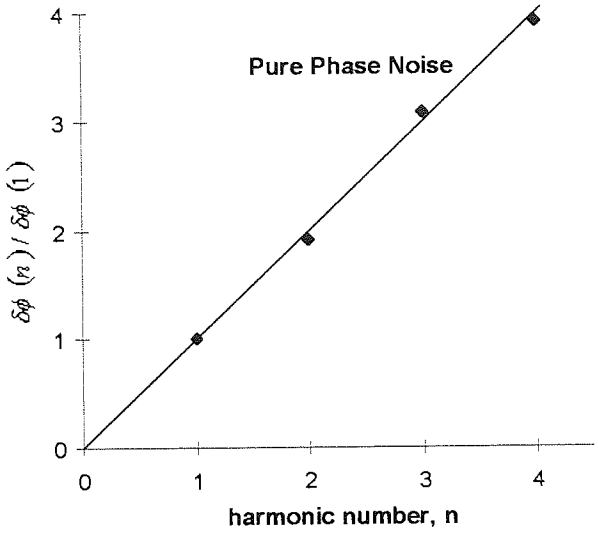

Figure 3-12. Normalised rms phase fluctuations, used to determine amplitude and timing jitter.

The 2.5 GHz pulse stream had a timing jitter of 140 fs, with no significant amplitude jitter.

The above characterisation of the ECMLL was repeated at 10 GHz. Figure 3-13 shows the autocorrelation and optical spectrum of the optimised pulse stream. The laser was biased at 32.4 mA, and modulated with a 9 V_{p-p} 10 GHz sine-wave, derived from a HP83711B synthesiser and a MITEK 10 GHz narrow-band amplifier.

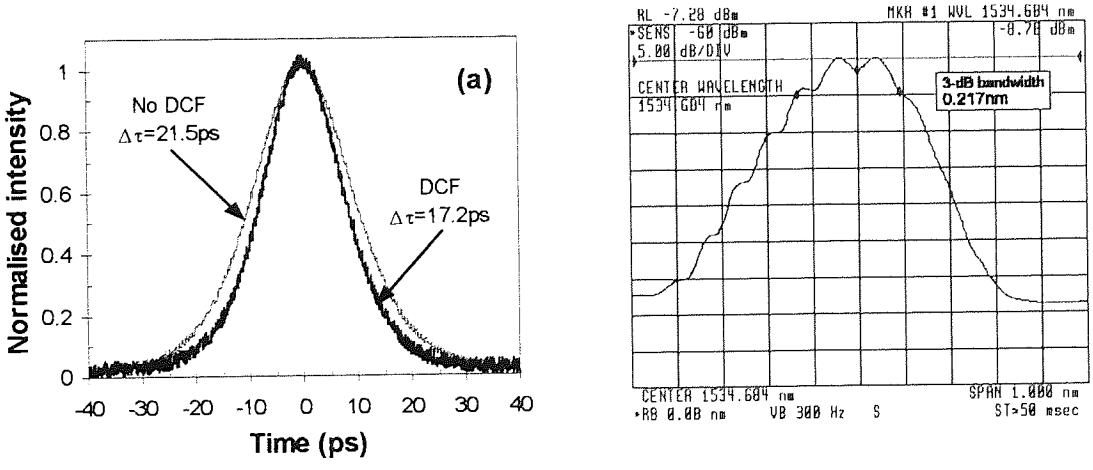

Figure 3-13. Autocorrelation and optical spectrum of the ECMLL, f=10 GHz, I=32.4 mA, V_{p-p}=9V, λ=1534.7, $\Delta\lambda$=0.217 nm, $\Delta\tau$=21.5 ps.

The pulse width was measured to be 21.45 ps and the spectral width was 0.217 nm, giving a time-bandwidth product of 0.59. The individual modes are just visible on the

10 GHz spectrum, indicating good wavelength stability and low timing jitter. The modes could not be seen on the 2.5 GHz spectrum due to resolution limitation of the optical spectrum analyser. DCF (–35 ps/nm) was used to remove residual chirp, producing 17.2 ps pulses and a time-bandwidth product of 0.47. To totally remove the chirp, a total dispersion of –55 ps/nm would have been necessary. This could be achieved using ever a longer length of DCF or a chirped fibre Bragg grating [28, 105]. The timing jitter was measured to be ~280 fs with 3.5% amplitude jitter. The minimum pulse width of an ECMLL should be inversely proportional to the frequency and amplitude of the RF drive signal [106], i.e. the pulse width should be shorter when the ECMLL is driven at 10 GHz. than when it is driven at 2.5 GHz, assuming equal amplitude drive voltages. In practice, this was not observed and this is attributed to the poor frequency response of the bias-T and the packaging of the device itself.

The ECMLL is a very flexible laboratory pulse source in terms of wavelength, pulse width, and frequency. It is however quite complex to setup, although once optimised for a particular wavelength and frequency it is extremely stable for a period of weeks.

3.3.2 Actively stabilised 2.5 GHz fibre-ring laser

The other source used throughout this thesis was a 2.5 GHz fibre-ring laser, constructed by *Finlay Knox* for use in soliton transmission experiments [107]. The setup is shown in Figure 3-14. Gain is provided by an erbium fibre amplifier, which was constructed from ~15 m of Er^{3+} doped fibre, and was reversed pumped via a WDM with a 60 mW, 980 nm laser diode. Residual pump light was coupled out of the cavity using a second WDM. Approximately 10 m of DSF fibre was wrapped onto a piezo-electric drum, which allowed the cavity length to be actively adjusted, to compensate of changes in temperature.

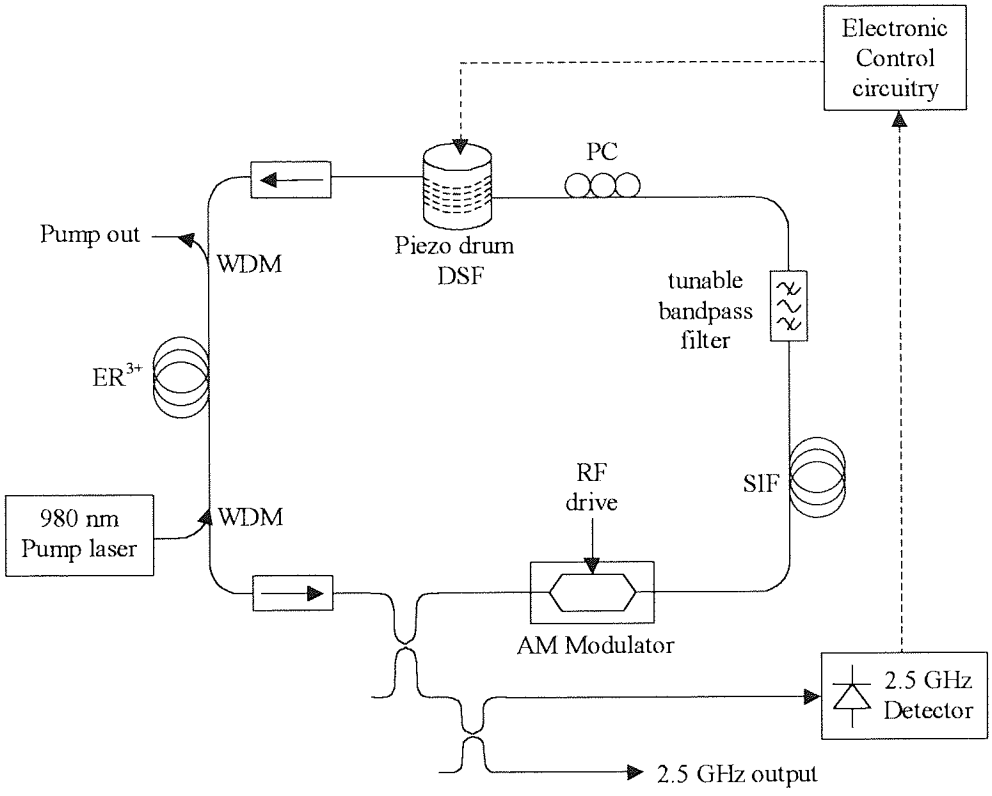

Figure 3-14. Schematic diagram of a 2.5 GHz fibre laser.

Figure 3-15 shows the temporal and spectral characteristics of the pulse source. The autocorrelation shows a pulse width of 15 ps and is a good approximation to the $sech^2$ fit. The spectral width was 0.18 nm, giving a time-bandwidth product of 0.33, indicating that the pulses were very close to transform-limited.

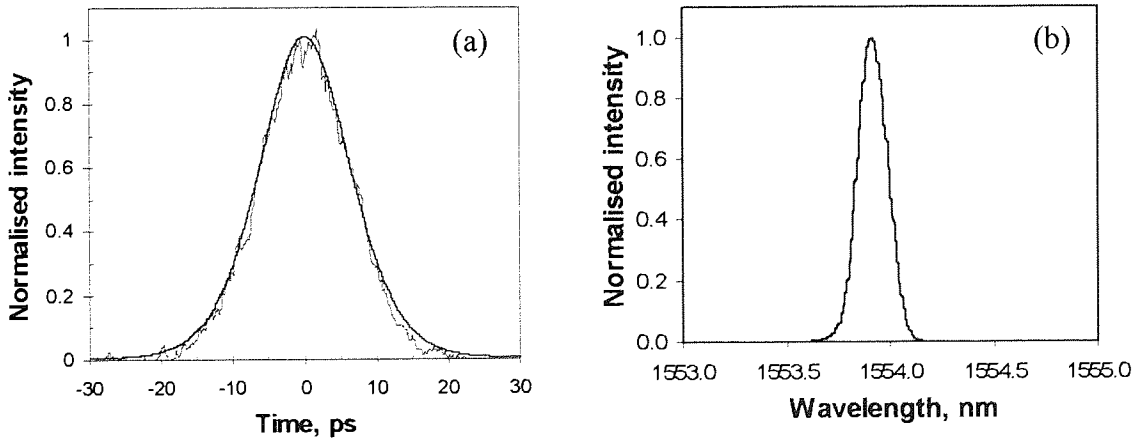

Figure 3-15. Measurements of fibre laser pulse characteristics: (a) autocorrelation, $\Delta\tau$=15 ps; (b) optical spectrum, $\Delta\lambda$=0.18 nm.

The laser required careful adjustments of cavity polarisation and operating frequency to generate optimised modelocked pulses.

The output pulse stream was amplified using an EDFA, and then encoded with a $2^{31}-1$ PRBS data sequence using a HP pattern generator and an *ETEK* 5 GHz $LiNbO_3$ amplitude modulator. The frequency response is shown in Figure 3-16a, and the transmission characteristics are shown in Figure 3-16b. The modulator has a fibre-to-fibre insertion loss of 10 dB.

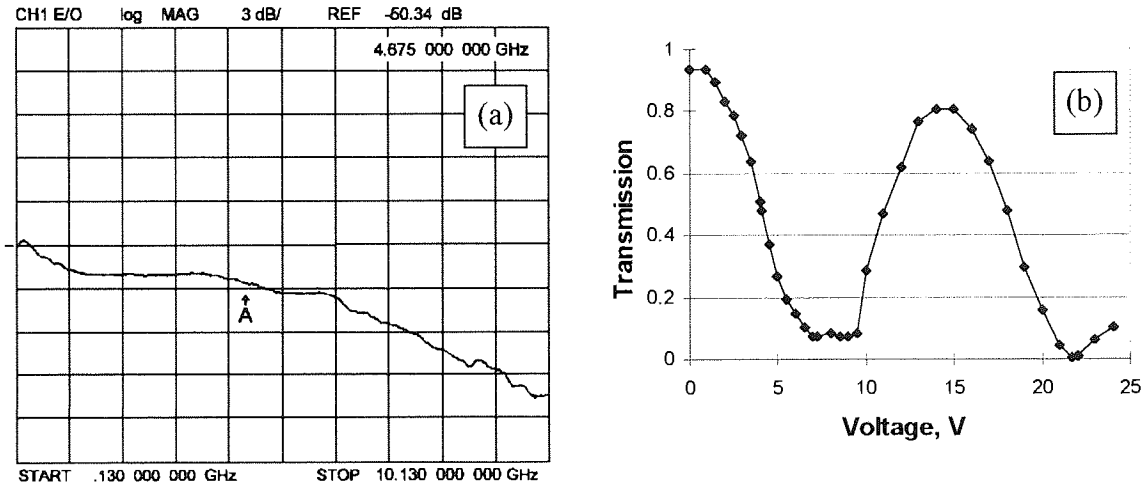

Figure 3-16. Characteristics of ETEK $LiNbO_3$ amplitude modulator; (a) frequency response, 3-dB bandwidth = 4.675 GHz; (b) transmission against bias voltage; Insertion loss = 10 dB.

The 2.5 Gbit/s PRBS data stream was amplified using an EDFA and then passively multiplexed up to 10 Gbit/s using a two stage fibre interleaver. The interleaver is shown in Figure 3-17, and consists of *SIFAM* wavelength flattened 50:50 couplers, variable fibre stretchers, and polarisation controllers. A *SIFAM* polariser was used to ensure that each OTDM channel was linearly polarised.

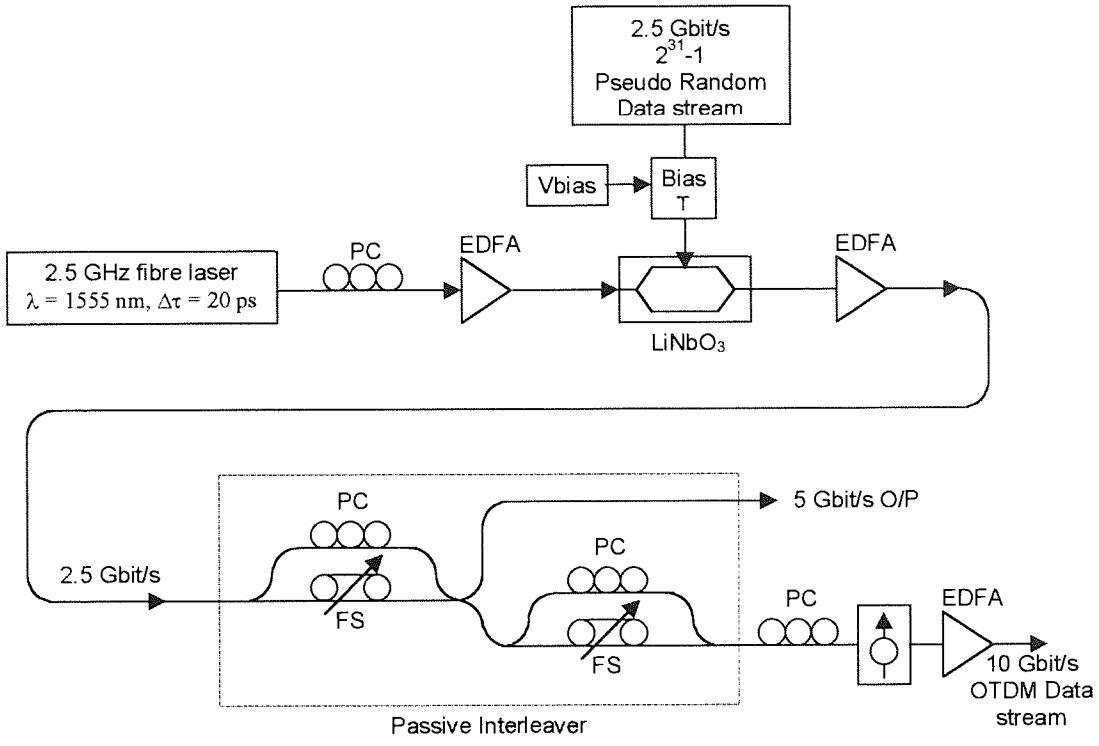

Figure 3-17. Passive fibre interleaver for multiplexing from 2.5 Gbit/s to 10 Gbit/s.

Figure 3-18a shows the 2.5 Gbit/s base-rate data stream, and Figure 3-18b shows the multiplexed 10 Gbit/s OTDM data stream.

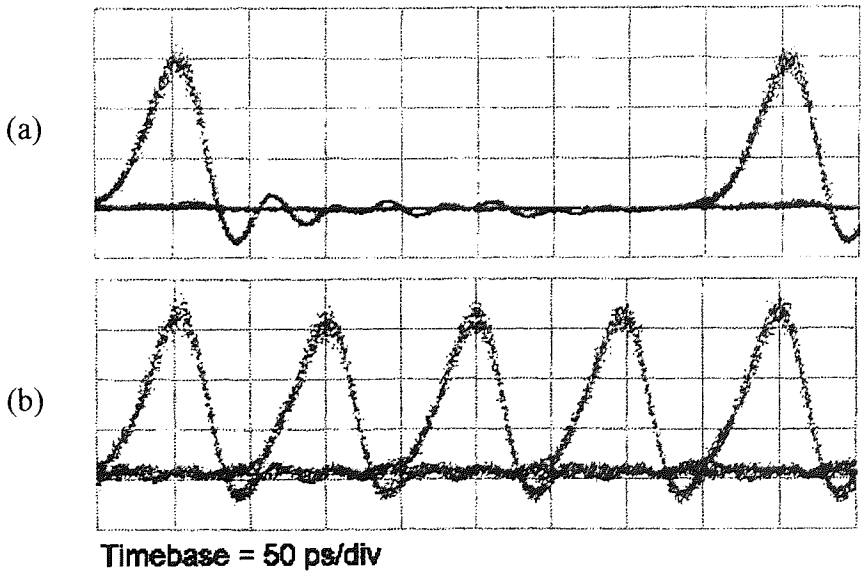

Figure 3-18. (a) 2.5 Gbit/s PRBS data stream generated using HP pattern generator and ETEK 5 GHz $LiNbO_3$ amplitude modulator; (b) Multiplexed 10 Gbit/s OTDM data stream.

3.4 High-speed Optical Switching

This section concentrates on the process of optical switching to perform either demultiplexing or 'drop and insert' multiplexing. It gives an overview of current technologies and their achievements to date.

3.4.1 Demultiplexing and 'Drop and Insert' techniques

Demultiplexing and 'drop and insert' multiplexing must be performed actively, either electro-optically or all-optically [18].

To perform effective 'drop and insert' functionality an optical switch must completely remove a single data stream (the 'drop'), whilst leaving the remaining channels undisturbed. It is then a simple matter to insert a data stream into the vacant time-slot (the 'insert'). Clock recovery is necessary to ensure correct synchronisation of the switching process. If the dropped channel is not completely removed, then crosstalk between the inserted channel and the remaining signal can cause incoherent interference, effectively and irretrievably degrading the system performance. The extinction ratio and the shape of the transmission window are therefore important device parameters. Another issue that must be considered, is the pulse characteristics (in terms of wavelength and temporal profile) of the inserted channel. To allow for accurate demultiplexing, the relative propagation delay between the inserted channel at λ_{insert} and the remaining channels at $\lambda_{remaining}$ must be a small fraction, f of the overall line-rate. For a system with a line-rate $N\times B$ Gbit/s, transmission distance L (km), and dispersion D (ps/nm/km), the wavelength separation should be [55]:

$$\Delta\lambda < \frac{f}{NBDL} \qquad \textbf{Equation 3-10}$$

For $f = 10\%$, $N\times B = 40$ Gbit/s, $D = 1$ ps/nm/km, and $L = 100$ km, this implies a wavelength accuracy of 0.025 nm, or ~3 GHz, which introduces a stringent requirement on source fabrication and specification. If however, 50 km of standard fibre is considered, then $D = 17$ ps/nm/km, and $\Delta\lambda = 0.003$ nm, an almost impossible

requirement. If the inserted channel has a different temporal profile, then energy will be exchanged between channels and a dispersive wave generated, finally limiting the number of nodes that can be cascaded [108]. In order to overcome these limitations, a regenerative 'drop and insert' node may have to be considered. This ensures that the temporal and spectral characteristics of all pulses within the data stream are identical. A regenerative 'drop and insert' node also overcomes limitations of cascadablility that plague analogue 'add-drop multiplexers'. Data regeneration is considered in section 3.5.3 and experimental results of an all-optical regenerator based on an SOA-NOLM, and capable of simultaneously routing information is presented in Chapter 5.

To date, a wide variety of optical demultiplexers, and optical switches that allow 'drop and insert' functionality have been demonstrated. Electro-optic techniques rely on the modulation of an optical signal using a high-speed electrical drive [109]. Conventionally lithium-niobate ($LiNbO_3$) amplitude modulators have been used, which utilise electro-optic effects to induce a phase modulation which is subsequently converted to an amplitude modulation using an optical interferometer; the extinction ratio is therefore periodic with the applied voltage. To overcome device limitations, and meet the stringent requirements in extinction ratio and transmission window profile, two simple methods have been employed. Firstly, two devices have been cascaded in series. The first modulator was biased in such a manner as to demultiplex from 40 Gbit/s down to 20 Gbit/s, and the second modulator biased to demultiplex from 20 Gbit/s down to 10 Gbit/s [110]. Another approach is to drive the device with a RF pulse stream, achieved in practice by harmonically driving the modulator, allowing a 10 Gbit/s channel to be completely removed from a 40 Gbit/s data stream [87, 108]. Both of these solutions increase the network complexity and cost. An alternative device is the EA modulator, where high extinction ratios and low duty-cycles can be achieved by simply increasing the reverse bias [106]. This device performs the necessary electro-optic switching without the need for either cascades of modulators or complex electrical drive circuits. It has been the key demultiplexing component in a number of recent system experiments [74, 111]. The EA modulator is discussed in more detail in Chapter 6,

which outlines the basic operating characteristics of the device. Chapter 7 describes novel experiments that utilise the bi-directional capability of these devices.

Many forms of high-speed all-optical switching rely on the nonlinear Kerr-effect. Optical pulses travelling in a nonlinear medium are subject to a phase-shift, the size of which is dependent on the intensity of the optical signal applied, and is a result of a nonlinear phenomenon known as SPM. Alternatively, if a second (control) pulse is applied, then the interaction and subsequent phase-shift is due to XPM. All-optical techniques include cross-phase modulation and Kerr-rotation in optical fibre [112], four wave mixing (FWM) in both fibre and semiconductor optical amplifiers [113], nonlinear optical loop mirrors [114, 115], semiconductor optical amplifier based nonlinear optical loop mirrors [116], and Mach-Zehnder integrated interferometers [117]. All-optical techniques have the added advantage that they may perform both demultiplexing and 'drop and insert' functionality in a single device. Electro-optic techniques require two synchronously driven modulators, one to perform the demultiplexing and the other to perform the 'drop' functionality. All-optical techniques are discussed in more detail in the following section.

3.4.1.1 Switching by Kerr-induced polarisation rotation

A relatively simple technique of all-optical switching is based on nonlinear polarisation rotation (NPR). NPR is a result of the fibre birefringence (see section 2.3), where the x- and y- axes have a slightly different refractive index. If E_x and E_y are the electric field components of E, in the x- and y- axes of the fibre, then each field E_x and E_y will induce a phase shift on the other due to XPM. This causes a rotation in the polarisation of a propagating signal. A polarisation rotation can also be induced due to XPM by a second field. This effect was exploited to achieve 40 Gbit/s to 5 Gbit/s all-optical demultiplexing [112]. The polarisation of a single optical channel in a OTDM data stream was rotated by 90° using an intense optical clock pulse. An in-line polariser was used to distinguish the rotation and allow demultiplexing. Nonlinear polarisation rotation has also been

exploited in an SOA, allowing a 10 Gbit/s channel to be demultiplexed from a 20 Gbit/s OTDM data stream [118].

3.4.1.2 Switching by Kerr-induced spectral shifts

40 Gbit/s to 5 Gbit/s demultiplexing has been demonstrated using XPM induced spectral shifts [112]. A WDM is used to combine a 5 GHz high power clock pulse stream with a 40 Gbit/s data stream. The signals are then propagated along a length of fibre, where provided correct temporal synchronisation is achieved, then every eighth pulse will experience a net frequency shift of up to 86 GHz (0.69 nm). The net frequency shift varies linearly with, and is limited by the clock pulse pump power [119]. A narrow band optical filter can then be used distinguish this shift, enabling demultiplexing to be achieved. The same technique can be used to simultaneously demultiplex many OTDM channels at once [119]. Here, the frequency shift is determined by the temporal location of the OTDM data stream with respect to a very broad pump pulse, see Figure 3-19.

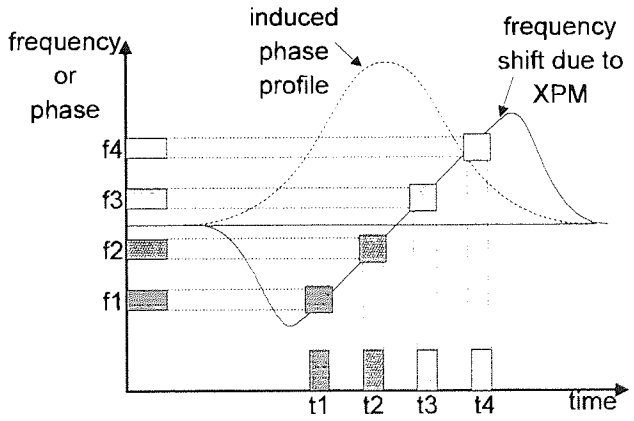

Figure 3-19. XPM frequency shift is determined by temporal location of the data signal with respect to the clock pulse.

Each channel can then be spatially separated using a wavelength selective element such as a grating.

3.4.1.3 Switching by four-wave mixing

Four-wave mixing (FWM) is discussed in section 2.8. If a signal at λ_s copropagates in a nonlinear medium with an intense pump at λ_p and the correct phase matching conditions

are satisfied, then a phase conjugated signal will be generated at a new wavelength ($2\lambda_p - \lambda_s$). If the signal is a high-speed OTDM data stream, and the pump-light is a pulse stream at the base-rate, then the generated signal will represent a demultiplexed channel, which can selected using a bandpass filter [120]. FWM within DSF has allowed a 6.3 Gbit/s data channel to be demultiplexed from a 100 Gbit/s OTDM data-stream [121]. A 6.3 Gbit/s channel has been demultiplexed from a 200 Gbit/s OTDM data stream using FWM in a semiconductor optical amplifier [122]. Even more impressive is the error-free demultiplexing of a 10 Gbit/s channel from a 500 Gbit/s OTDM data stream using FWM in 300 m of polarisation maintaining dispersion shifted fibre [123].

3.4.1.4 Nonlinear optical loop mirror

The nonlinear-optical loop-mirror (NOLM), shown in Figure 3-20a, consists of a fibre directional coupler with its outputs joined by a long loop of fibre. The input signal is split equally between the two arms by the 50:50 coupler, clockwise and anticlockwise components travel through the same optical path and interfere at the coupler. By conservation of energy, the device is normally 100% reflecting, and can be used as an almost perfect mirror [124]. This is the idealised response of the device, and so does not take into account, coupler and fibre losses, and birefringence of the fibre. The birefringence can cause a variation of optical path length with polarisation angle. By adjusting the polarisation of the light in the loop, the NOLM can be totally reflecting or totally transmitting [125].

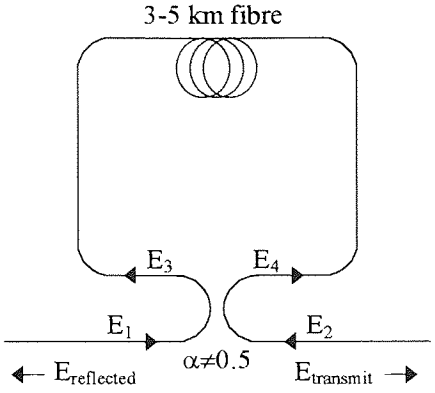

Figure 3-20. Nonlinear optical loop mirror.

To modify the response of the loop, some form of optical path *asymmetry* needs to be introduced. If the coupler splitting ratio is not 50:50 the clockwise and anti-clockwise components acquire a differential phase due to SPM, which is intensity-dependent and so the interference conditions at the coupler vary nonlinearly with incident intensity. The reflectivity of the device is therefore periodic with input intensity, see Figure 3-21 [126].

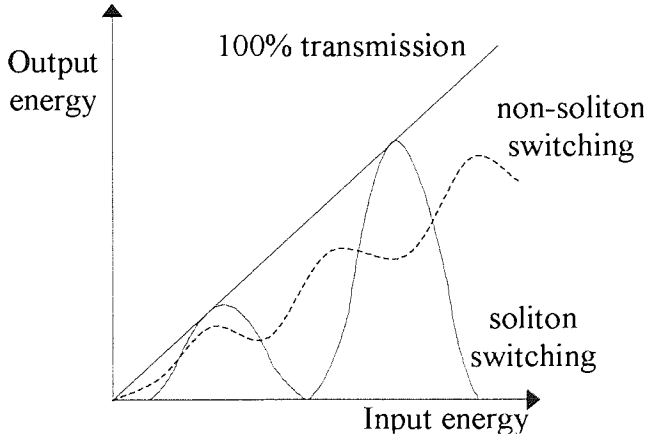

Figure 3-21. Intensity dependence of a NOLMs reflectivity.

The NOLM has two distinct modes of operation. First, when the pulses are long (e.g. ~100 ps), so that the dispersion length is large compared with the loop length, the transmitted pulses suffer distortions due to incomplete switching [127]. Second, when the pulses are short, so that the dispersion length is shorter than the loop length, and soliton effects are important and results in complete switching [128]. The best switching ratio (i.e. the contrast between the linear off and the high-intensity on) occurs for α closest to 0.5, but the switching energy increases correspondingly [126].

A 100% switching ratio can be obtained by introducing a different form of *asymmetry* into the loop. This can easily by achieved by introducing a loss or gain element [129]. An EDFA has been used to preferentially amplify one propagating (clockwise) component over the other, causing an optical path difference and so switching [130]. Recently, a fibre grating has been inserted into the loop, acting as a loss element [131]. One of the most common techniques uses an intense control signal at a different wavelength to induce a nonlinear phase shift via XPM [132, 133]. The principle of operation is shown in Figure 3-22, and discussed below.

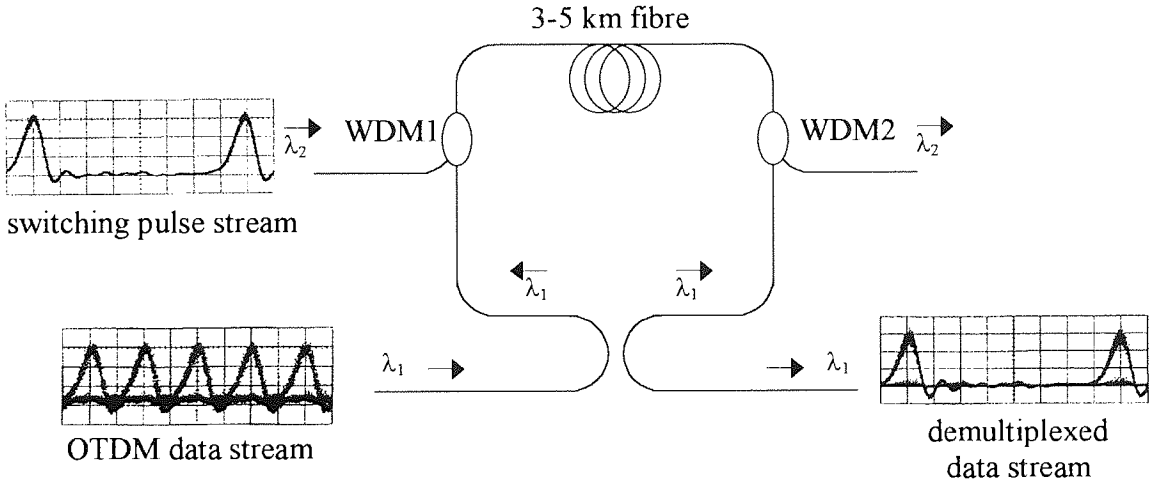

Figure 3-22. Two-wavelength switched NOLM as a demultiplexer. Insets illustrate demultiplexing process.

A low power signal pulse at λ_1 introduced at the input of the NOLM is split into two components travelling clockwise and anticlockwise around the loop. As with the standard NOLM, the pulses will traverse the loop and recombine at the coupler, and be either transmitted or reflected depending on the loop polarisation. A high power control pulse at λ_2 is introduced using WDM1, which traverses the loop and exits at WDM2. As it co-propagates with the clockwise component of λ_1, it imparts a nonlinear phase-shift due to XPM, resulting in incomplete interference of the low power signal on recombination at the coupler, and switching of the NOLM [132]. If a 2.5 GHz high intensity pulse stream at λ_2 is used to switch every 4th channel of a 10 Gbit/s low intensity signal at λ_1, then 10 Gbit/s to 2.5 Gbit/s demultiplexing is achieved.

The configuration requires careful design in order to obtain the correct pulse walk-off for a specified switching window width, for given source wavelengths. This is usually achieved using DSF, and arranging that the wavelength of the control and the signal pulse streams straddle the dispersion zero of the fibre.

The NOLM has been used extensively in applications based on an all-optical network processing [115], including: 100 Gbit/s to 6.3 Gbit/s high-speed demultiplexing [134], optical memory [135], an actively modelocked fibre laser [91, 136] and clock recovery [137]. Other all-optical applications of the NOLM include RZ to NRZ conversion [138], 1.5 μm to 1.3 μm wavelength conversion [139], pulse shaping and pedestal suppression [140], and all-optical logic operations [141].

The NOLM has a number of advantages over other devices in both switching and system applications, be they all-optical or electro-optical. It is simple to construct, and has an inherently balanced interferometer which makes the device relatively stable, even for the long fibre lengths (5-10 km) that are necessary in order to allow practical control pulse powers. In practice, the maximum data-rate is limited by the long lengths of fibre, which lead to a walk-off effect between the control and the signal pulse streams.

An alternative to the standard NOLM is the SOA-NOLM. The long lengths fibre is replaced with a small semiconductor optical amplifier. This improves the device stability, and eases the design constraints caused by pulse walk-off. Chapter 4 outlines the basic characteristics of an SOA and describe some applications of its use in an OTDM network. It goes on to describe in detail, the operation of an SOA-NOLM, which is somewhat different to the fibre-NOLM. Chapter 5 presents experimental results of the use of an SOA-NOLM to achieve simultaneous demultiplexing, data regeneration, and clock recovery.

3.5 Data Regeneration

Periodically optically amplified transmission systems are essentially analogue and, therefore, accumulate transmission impairments over the total transmission path. Timing jitter and amplitude fluctuations will inevitably limit the maximum transmission distance. Other limiting factors are SNR degradations due to group-velocity dispersion and spontaneous-emission generated by optical amplifiers, as well as greatly increased nonlinear effects at higher bit-rates. It is therefore desirable to re-time, re-shape and regenerate the transmitted data, which may be carried out midway through a point-to-point transmission link, or at a 'drop and insert' node within the network. Within a 'drop and insert' node, the inserted data channel may have a slightly different wavelength and temporal-profile from the data stream it is to be inserted into. This can lead to a group velocity mismatch and dispersive wave generation that degrades the receiver sensitivity, and limit the maximum transmission distance [108].

Electronic signal regenerators may be used, but will inevitably introduce a bandwidth limitation on a transmission system. In order to overcome this, all-optical signal processing may be used. The following sections consider the different techniques of data regeneration, outlining the advantages and disadvantages of each.

3.5.1 Soliton control

The primary obstacle in achieving high data-rate transmission is known as the Gordon-Haus effect [142], see section 2.6.4. Signal-spontaneous beat-noise from each amplifier induces random frequency fluctuations in the optical signal. During transmission, these frequency fluctuations are translated into a timing jitter, due to fibre dispersion. The jitter has a mean of zero but a finite variance. Efforts to remove these limits are known as soliton control. The solitons position in time is controlled in order to prevent errors, which may occur when a soliton drifts into a wrong time-slot. Passive and active methods have been proposed, and are described below.

3.5.1.1 Passive soliton control

A very simple technique that reduces the Gordon-Haus effect introduces a simple optical filter directly after every optical amplifier [143, 144]. The filter has a central frequency equal to that of the propagating soliton, and a bandwidth that is typically ten times larger than the soliton bandwidth. The principle can be understood by reference to Figure 3-23.

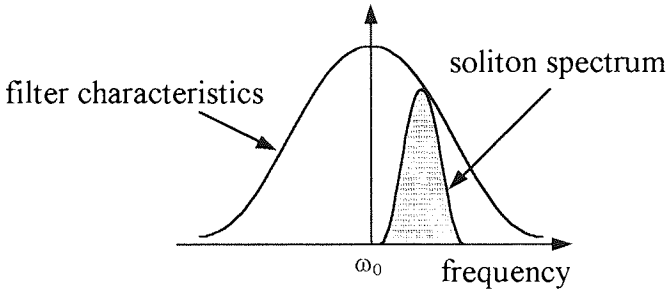

Figure 3-23. Passive soliton control by optical filtering.

As the soliton is periodically amplified, it acquires an unwanted noise component, which results in a new soliton being formed, with a slightly different centre frequency. The filter introduced after the amplifier will selectively attenuate the optical spectrum of the soliton. Provided the filtering is not excessive then a new soliton will form with a centre frequency that is closer to the centre frequency of the filter. The amount of jitter reduction depends on the bandwidth of the filter, and can be greater than 50 % [144].

An improved form of soliton jitter control is known as sliding-guiding filtering [145]. As with the above technique, a passive optical filter is used directly after each amplifier. The centre frequency of each filter is progressively increased (or decreased) along the system length. Due to the ability of a soliton to overcome slight perturbations, then the centre frequency of a soliton will shift in the same direction and follow the centre frequency of the filter. Noise present at the centre frequency of a particular filter in the system, will be attenuated by any subsequent filters. The noise introduced at each amplifier is essentially linear and remains in its original frequency band, thus preventing a build up of ASE and almost completely removing the jitter. This technique has been used to propagate solitons of 20 Gbit/s over 14,000 km [146].

An alternative is the use of a saturable absorber at periodic intervals along the transmission line, which is designed to stabilise the peak amplitude of the solitons. One such device is a self-switched NOLM [147]. The NOLM acts as an intensity filter to remove the dispersive waves inevitably generated by picosecond pulses in periodically amplified systems.

3.5.1.2 Active soliton control

Active soliton control is based on synchronous regeneration by modulating the phase or amplitude (or both) of a soliton, which imposes a frequency shift which counteracts the timing jitter caused by the Gordon-Haus effect [32]. The technique helps enhance error-free transmission whilst also allowing the amplifier spacing to be increased [148]. Typical modulators include $LiNbO_3$ Mach-Zehnders [32], EA modulators [149], or NOLM [150, 151]. However, one of the most attractive techniques of soliton control, in terms of upgradability is known as soliton shepherding [152].

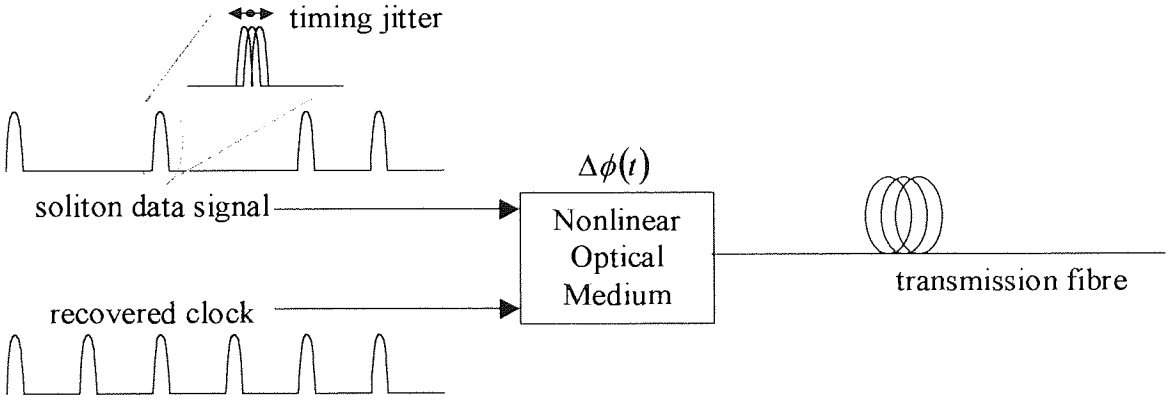

Figure 3-24. Soliton shepherding regenerator concept.

By temporally overlapping a clock and soliton data stream in a nonlinear optical medium (NOM), each clock pulse imposes a nonlinear phase profile on a soliton. This results in a net shift in its carrier frequency, which can be converted into a suitable timing delay through the dispersion of the transmission line. The sign and magnitude of this frequency shift depend on the position of the soliton relative to the clock pulse, and so the clock acts to shepherd the soliton towards the centre of the time-slot defined by the clock pulse. 2.5 GHz soliton transmission using soliton shepherding has been demonstrated over 20,000 km using a re-circulating loop [152]. The single loop span was 100 km

(path average dispersion –1 ps/nm/km), which included 13 km of DSF as the NOM and used XPM as the nonlinear process. The system operated error free, with a 2 dB penalty. A SOA could also be used as a NOM, allowing the system to be integrated. However, the effects of amplifier noise accumulation would need to be investigated.

3.5.2 Electronic data regeneration

Figure 3-25 shows the setup of a typical electronic-based data regeneration technique [153]. The incoming degraded data stream is incident upon a high-speed optical receiver, the resulting electrical signal is amplified, and a percentage is fed to a decision flip-flop, which switches through a clean recovered electrical clock.

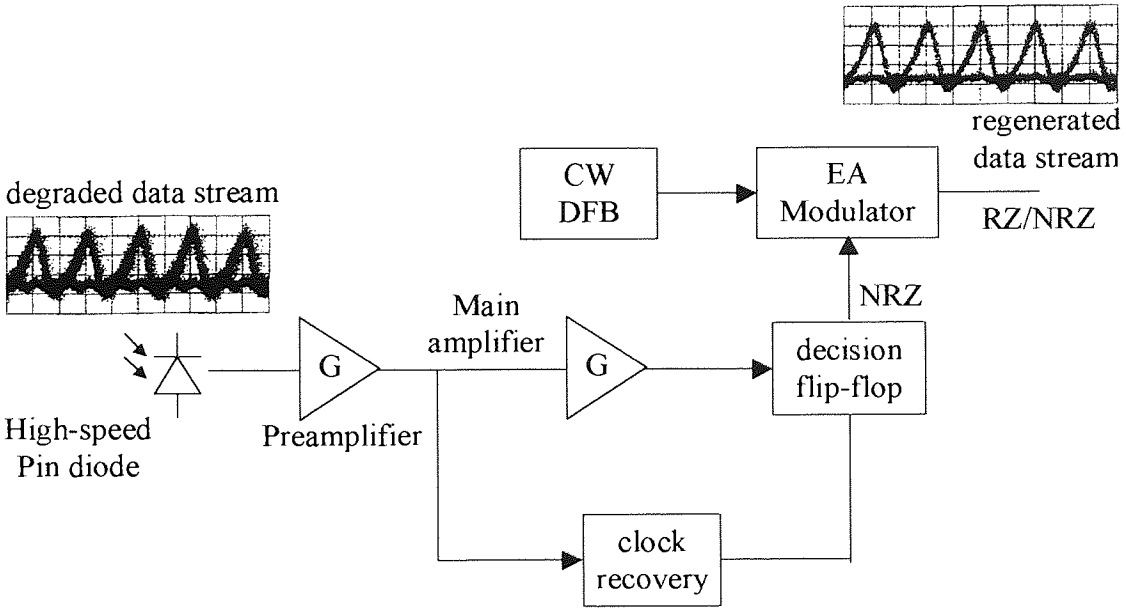

Figure 3-25. Conventional electronic based data regeneration. Insets intended to illustrate regeneration process.

The technique has allowed error-free transmission up to 10 Gbit/s over 400,000 km, with an optical amplifier and regenerator span of 160 km [154]. Excellent regeneration was observed. More recently, 40 Gbit/s electronic data regeneration has been demonstrated using InP high electron-mobility transistor (HEMT) technology [155]. 60 Gbit/s to 30 Gbit/s demultiplexing with data regeneration has also been demonstrated using SiGe technology [156].

3.5.3 All-optical data regeneration

A very promising technique of all-optical data regeneration is that based on a Kerr shutter. All-optical clock recovery was achieved by using the incoming data stream to periodically modulate a fibre ring laser, thus achieving modelocking [157]. The incoming data is subsequently used to switch (and re-code) the high quality pulse stream generated from the fibre laser via Kerr rotation in a length of DSF. This has allowed all-optical data regeneration at 10 Gbit/s [157], and more recently at 40 Gbit/s [158].

Another promising technique of all-optical data regeneration is shown in Figure 3-26, and consists of a standard NOLM, which employs group velocity dispersion in the fibre loop to introduce signal-clock walk-off and generate a square switching window [159, 160, 161]. The incoming degraded data stream is used to switch a high-quality transform-limited pulse into transmission at the output, differing from a standard NOLM demultiplexer (see section 3.4.1.4) where a regular clock is used as the switching signal. The length of the fibre used to achieve the π phase shift is much shorter than the dispersion length and therefore the signal pulse is unaffected by GVD.

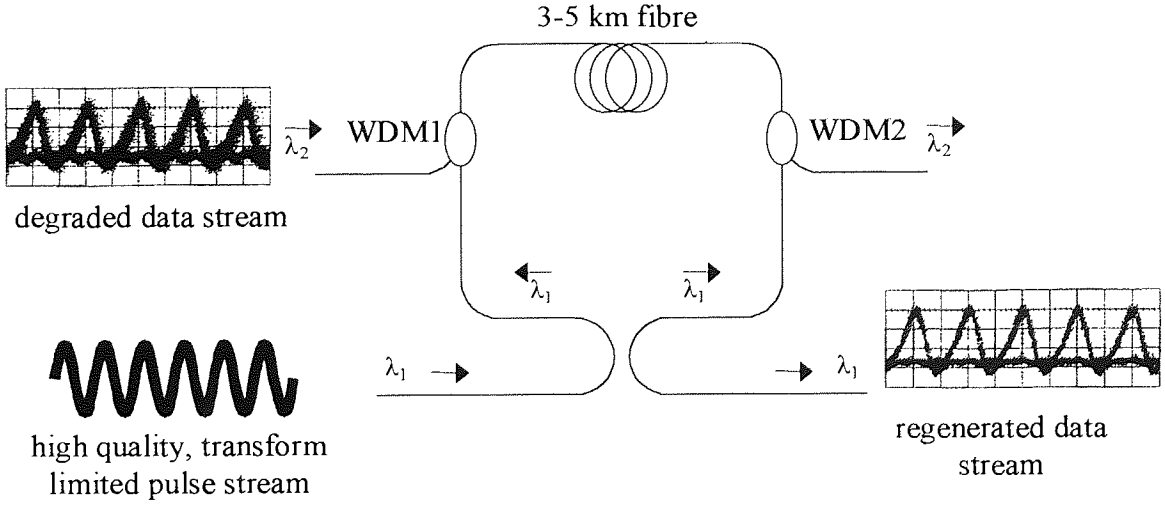

Figure 3-26. All-optical data regeneration using a NOLM. Insets intended to illustrate the regeneration process.

Instead of using a fibre-based NOLM, data regeneration can be performed using an SOA-NOLM [162, 163, 164], or more recently, using an integrated Mach Zehnder (MZ) SOA [165, 218], see Chapter 4. Chapter 5 gives details on a novel experiment where the

SOA-NOLM is used to perform simultaneous demultiplexing, data regeneration and clock recovery using a single device.

3.6 Clock Recovery and Synchronisation

Within OTDM networks, clock recovery must exact a base-rate clock from the transmitted data stream, operating at a higher line-rate. The recovered clock is used for synchronisation of the demultiplexer and the detection process. However, recovery of the OTDM line-rate could be used for the synchronisation of an optical regenerator. In order to prevent degradation of the bit-error-rate (BER) performance of the system, clock recovery techniques must ensure a low jitter between the incoming data stream and the recovered clock.

Clock recovery techniques are diverse and can be classified according to a number of criteria: (i) whether the recovered clock is electrical or optical, (ii) whether the base-rate or line-rate is recovered, and (iii) whether the technique is applied pre- or post-demultiplexer. One important feature of an interleaved OTDM data signal is that it does not necessarily contain a RF component at the base-rate clock frequency, only at the higher line-rate. Clock recovery may be achieved by recovering the line-rate clock signal and performing an optical or electrical clock division process to obtain the base-rate clock signal [166]. The main clock recovery techniques are described below.

3.6.1 Injection-locking

Injection-locking uses the incoming data stream to seed a self-pulsing semiconductor laser [167, 168, 169]. This has allowed clock recovery up to 18 GHz [170], and a 10 GHz clock to be recovered from a 40 Gbit/s [171, 172], and an 80 Gbit/s [173] OTDM data stream. The technique demonstrated a large locking range of ±110 MHz, but suffered from a relatively large timing jitter of greater than 1 ps.

3.6.2 All-optical clock recovery

All-optical clock recovery methods typically involve the modulation of the amplitude or phase of a laser cavity by the transmitted data stream to achieve modelocking [174, 175, 176, 177]. A typical configuration is shown in Figure 3-27, where the incoming data is used to periodically modulate the laser cavity via an interaction with a nonlinear optical medium (NOM) [178]. If the laser round trip time is equal to, (or an integer multiple of) the bit period, then modelocking will be established, and a continuous stream of high quality pulses generated.

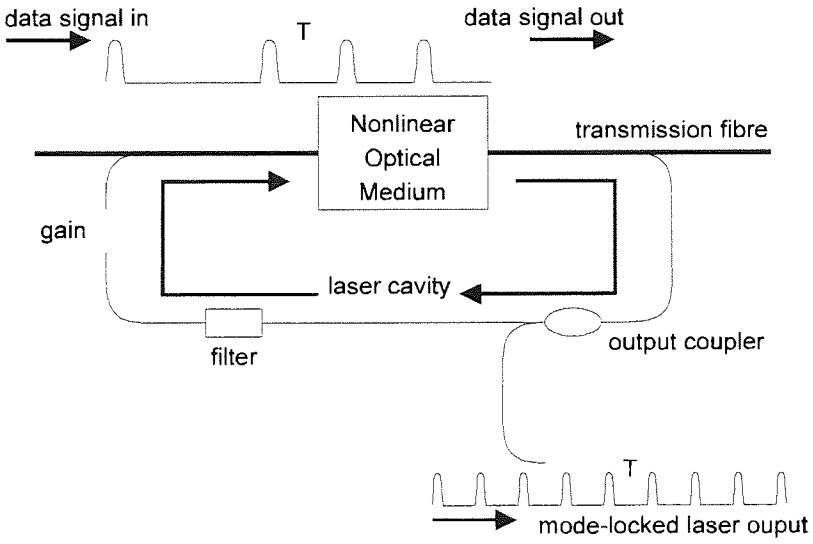

Figure 3-27. All-optical clock recovery circuit using a fibre ring laser.

All-optical methods of clock recovery typically recover the OTDM line-rate. 40 GHz clock recovery has been demonstrated using the Kerr-effect in long lengths (11 km) of optical fibre [174]. The cavity length can be shortened by using an SOA as the NOM, but the maximum operating speed is then limited by the gain recovery of the device. The recovery time can be reduced by reverse optical pumping, allowing 20 GHz clock recovery to be achieved [179]. All-optical clock recovery in fibre ring lasers suffers from stabilisation issues similar to those outlined in section 3.2.5.

3.6.3 Phase-locked loop-based clock recovery

Whilst many of these methods are promising, the most favourable in terms of flexibility and stability are those based on the electronic or optical phase-locked-loop (PLL). PLL techniques typically consist of an optical detector, a locally generated clock derived from a voltage-controlled oscillator (VCO), and a phase detector that can be either optical or electrical. The phase detector is used to determine the frequency mismatch between the incoming data stream and the locally generated clock. The resulting error signal is amplified and filtered in a PLL controller and then used to drive the VCO. In this way, a closed loop is formed, and the frequency of the locally generated clock will stabilise at a point of constant phase with that of the data stream. This allows clock recovery to be achieved, with any fluctuations in phase being constantly corrected for.

PLL techniques can be categorised depending on the type (electrical or optical) of phase detector and whether the PLL is pre- or post- demultiplexer. Each technique has its own advantages and disadvantages and will be described in more detail below. A very attractive and stable method of clock recovery is shown in Figure 3-28. Clock extraction is achieved at the full line-rate prior to demultiplexing, but with a clock output at the system base-rate.

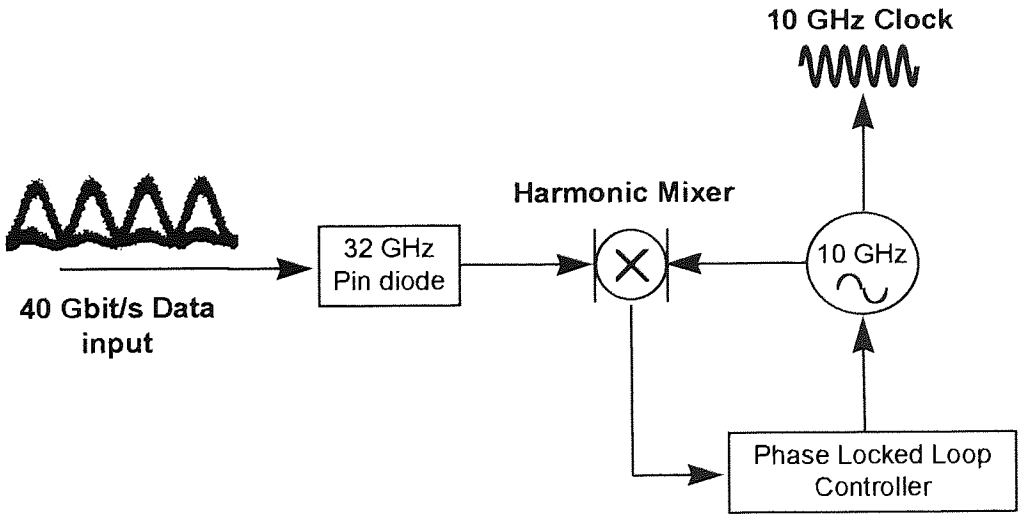

Figure 3-28. Schematic diagram of electronic clock recovery circuits.

A 10 GHz VCO provides the local oscillator input to a harmonic mixer whose nonlinear properties are used to derive the appropriate harmonic for mixing with an incoming 40 Gbit/s data stream detected using a 32 GHz pin diode [84]. Phase comparison is performed at the 40 GHz line-rate. It is anticipated that this technique could be extended for operation up to 100 Gbit/s, providing the conversion efficiency of the harmonic mixer can be optimised for the 10^{th} harmonic, the only problem being the pin diode device packaging. Clock recovery based on this technique is used in section 7.5 to drive a demultiplexer as part of a 3-node OTDM system experiment. The technique has many advantages, in terms of performance and stability. The main disadvantage is that it requires high-speed electronic components, which are often expensive and limit the possibility of future upgradeability.

As mentioned in the introduction, an optimised OTDM data stream does not contain a RF component at the base-rate clock frequency, only at the higher line-rate. An alternative approach is to achieve base-rate clock recovery following the demultiplexer, where an appropriate RF component exists.

A typical setup is shown in Figure 3-29a. The demultiplexer can be all-optical, as in the case of a loop mirror [180, 20, 21], or electro-optical as is the case for a lithium niobate or EA modulator [181].

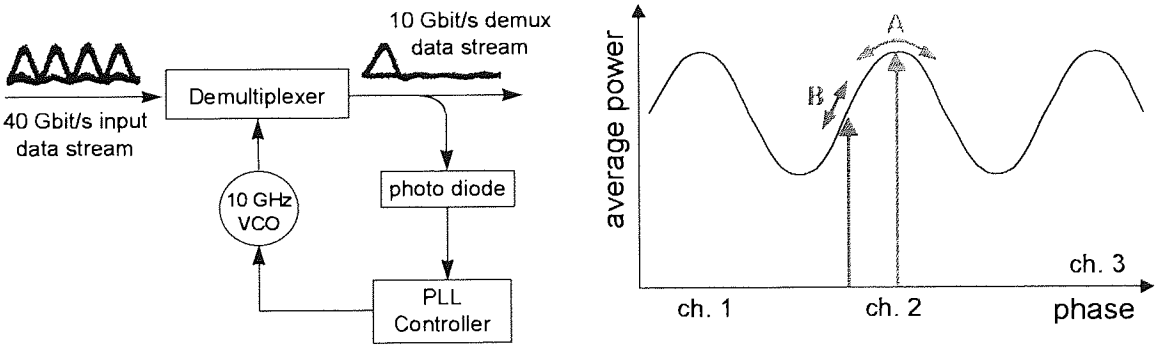

Figure 3-29. PLL clock recovery post demultiplexer: (a) schematic diagram; (b) phase-locking requirements.

The demultiplexer acts to take a time-slice of the incoming (e.g. 40 Gbit/s) data stream. That is, the demultiplexer samples the incoming signal. Under ideal conditions, this time-

slice corresponds to a single channel. As the phase shifts, the average power will vary periodically, see Figure 3-29b. For maximum switching efficiency and therefore minimum system penalty, the phase should be locked to the peak of the function (point A). This makes it difficult for the feedback electronics to tell, in which direction the phase has drifted. However, if the phase is locked to half way up the function (point B), then a change in power would indicate the direction of any phase drifts - but the switching efficiency would be degraded. Therefore, a trade-off is made between system stability, and switching efficiency.

The phase of the recovered clock can be locked to the centre of the demultiplexer switching window with increased stability, by using a technique known as *dithering* to obtain a differential error signal [182, 181, 183]. Dithering imposes a degree of phase modulation on the recovered clock, giving rise to a residual timing variation; it also increases the complexity of the drive electronics. The technique is explained in more detail in Chapter 5, which presents experimental results on simultaneous demultiplexing, data regeneration, and clock recovery using a single SOA-NOLM. Chapter 7 presents details on a novel experiment that achieves simultaneous demultiplexing and clock recovery using a single EA modulator in a novel bi-directional configuration. Independent control is achieve between the error-signal used in clock recovery, and demultiplexing operation, there by removing need for a dither signal.

To date, the most promising techniques of PLL clock recovery are based on either gain modulation [184, 185] or FWM within fibre [186] or within a semiconductor optical amplifier [121]. With gain modulation, the optical data stream and optical clock pulses generated via a VCO are combined, and introduced into an SOA. The gain of the SOA is saturated by the intense optical clock, which subsequently modulates the optical data stream, thus imparting a phase variation that represents the frequency difference between the two signals. In this way, gain modulation uses a cross-correlation component at the same wavelength as the signal, which subsequently becomes background optical noise.

The technique has been used to recover a 6.3 GHz pre-scaled clock from a 50 Gbit/s OTDM data stream [187].

The PLL operation speed can be improved by using the nonlinear process of FWM, see section 2.8. Background optical noise is suppressed, because the cross-correlation component is independent from the data and clock signals, and can therefore be selected by a bandpass optical filter. This greatly improves the SNR characteristics, and therefore phase-noise (or timing jitter) of the recovered clock. The technique has allowed a 6.3 GHz clock to be recovered from a 100 Gbit/s OTDM data stream, with a timing jitter of 0.34 ps [188]. More recently a 6.3 GHz clock was recovered from a 400 Gbit/s (all-mark) OTDM data stream, but with a large degree of timing jitter (1.3 ps) [102]. The main disadvantage of both of these techniques is that it was necessary to use dithering to improve the system stability.

3.6.4 Other techniques

One of the simplest forms of clock recovery is that based on a dielectric resonator narrow-band high Q filter. Such devices have allowed clock recovery at 20 GHz, with a timing jitter < 0.5 ps and was the subject of RACE 2011 project [189]. They do however have a fixed frequency response, and can only recover the OTDM line-rate, therefore requiring subsequent processing to recover the base-rate frequency.

3.7 System Impairments in an OTDM System

In addition to the traditional system impairments associated with optical transmission (i.e. amplitude noise, timing jitter, and inter-symbol interference), the multiplexing and demultiplexing of optical signals will cause finite levels of crosstalk between the various OTDM channels.

3.7.1 Multiplexer performance

For a multiplexer, incoherent interference between channel ' i ' and other channels may become critical. The SNR after demultiplexing must be calculated allowing for temporal overlap of the pulses. Assuming a fibre-based interleaver where the path length differences are in the order of nanoseconds, as used in this thesis, then penalties will arise from incoherent interference wherever temporal overlap occurs. The resultant signal to noise ratio of channel ' i ' in the case of incoherent interference in an n channel OTDM system is given by [84]:

$$SNR_i = \frac{\int P_i(t)dt}{\sum_{j=1}^{n}\sum_{k\neq j}\int\sqrt{P_j(t)P_k(t)}dt} \qquad \text{Equation 3-11}$$

where $P_j(t)$ and $P_k(t)$ are the time dependence of channel j and k after demultiplexing. Equation 3-11 dictates the pulse width required for a given crosstalk level when multiplexing ideal signals together, and the level of background radiation from a practical source which may be tolerated. However, in practice, the final penalty will also depend on the shape of the demultiplexer switching window, see section 3.7.2.

Figure 3-30 shows the pulse width and extinction ratio requirements of an optical source for use in a 40 Gbit/s (4×10 Gbit/s), and an 80 Gbit/s (8×10 Gbit/s) OTDM network [190, 236].

Figure 3-30. Theoretically predicted penalties for multiplexing from: (a) 10 Gbit/s to 40 Gbit/s; (b) 10 Gbit/s to 80 Gbit/s; Assuming PRBS=2^6-1; Data modulator ER=16 dB; From references [190, 236].

The simulation results were calculated by multiplexing a PRBS 10 Gbit/s *gaussian* pulse train with a flat background up to the required OTDM line-rate, i.e. 40 or 80 Gbit/s. BER measurements were calculated at the line-rate, and a multiplexing penalty was defined as the difference between the sensitivity of the receiver for a given extinction ratio and pulse width compared to the best receiver sensitivity for the complete simulation. This was repeated for a random set of relative delays between each of the channels, and an average penalty recorded. The process was then repeated for different pulse widths and extinction ratios.

The results indicate that a pulse width of 4-7 ps and an extinction ratio of greater than 38 dB is required for a multiplexing penalty of less than 0.5 dB in a 40 Gbit/s (4×10 Gbit/s) OTDM system. The pulse source characteristics become even more stringent for an 80 Gbit/s (8×10 Gbit/s) where for a penalty of less than 0.5 dB, the pulse width must be 3±1 ps and the extinction ratio greater than 48 dB. These requirements can be achieved using two cascaded, harmonically driven EA modulators, see section 7.2. If higher levels of multiplexing are required, then modelocked sources may have to be considered.

3.7.2 Demultiplexer performance

The two main causes of degradation associated with the demultiplexer are: channel crosstalk due to a finite demultiplexer extinction ratio, and intensity fluctuations as a result of timing jitter between the device switching window and the required target channel. The shape of the demultiplexer switching window, the associated timing jitter and the extinction ratio are therefore very important parameters.

3.7.2.1 Channel crosstalk

A finite demultiplexer extinction ratio results in incomplete rejection of the unwanted channels, see Figure 3-31.

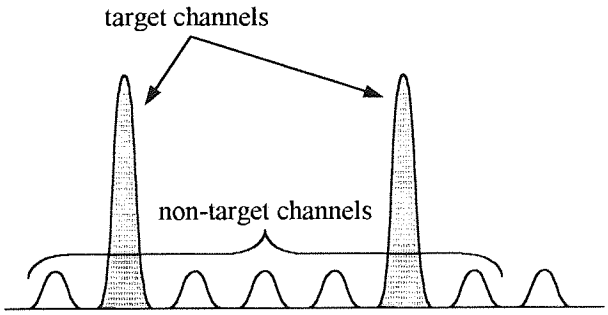

Figure 3-31. A finite demultiplexer extinction ratio results in incomplete rejection of unwanted channels and channel crosstalk.

The unwanted signals contribute to the total power incident on the receiver, and appear as additional noise. The receiver sensitivity is degraded, and a power penalty is recorded given by [84]:

$$\Delta P_{(dB)} = 10Log_{10}\left(\frac{SXR+1}{SXR-1}\right), SXR = \frac{P_i}{\sum_{k\neq i} P_k} \qquad \text{Equation 3-12}$$

where SXR is the 'signal to crosstalk' ratio, P_i is the signal power after demultiplexing and P_k is the power in the unwanted channels. To obtain a penalty of less than 0.5 dB, a SXR of greater than 12.5 dB is required. In addition to this power penalty, the unwanted channels may interact with noise originating from any optical amplifiers, reducing the SNR and resulting in an error-floor.

The extinction ratio, and the switching window needed to demultiplex a 10 Gbit/s channel from a 40 Gbit/s OTDM data stream, were calculated using a numerical simulation defined in MatLab [191]. A 10 GHz, 7 ps pulse stream was encoded with a 2^6-1 pseudo-random bit sequence using a modulator with a 16 dB extinction ratio. The resulting data stream was passively multiplexed up to 40 Gbit/s. Transmission was simulated by attenuating and amplifying the signal, therefore accumulating spontaneous emission noise. The data stream was then demultiplexed using a *raised-gaussian* switching window to simulate a finite device extinction ratio. The signal was detected on a 6 GHz receiver with a noise figure of 5.5 dB. Calculations assume signal-spontaneous beat noise only. The receiver sensitivity was estimated from BER curves, calculated by attenuating the received optical power. This process was repeated for different demultiplexer switching window widths, and extinction ratios. A demultiplexing penalty was then defined as the difference between the sensitivity of the receiver for a given extinction ratio and switching window width compared to the best receiver sensitivity for the complete simulation, (~15 ps window, and extinction ratio of 100 dB).

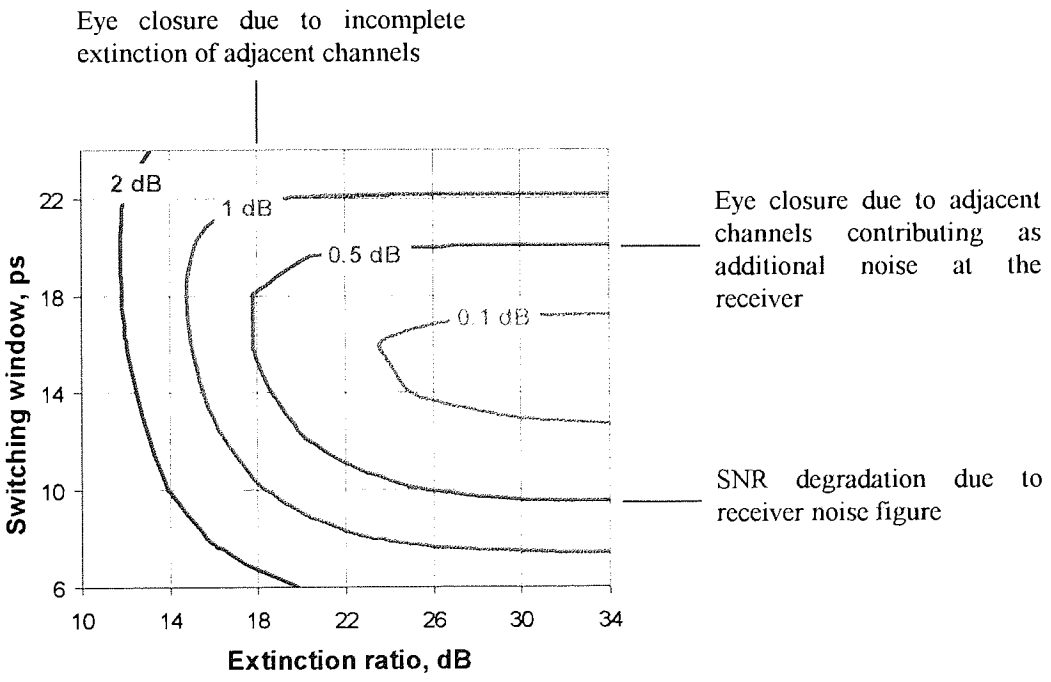

Figure 3-32. Theoretically predicted penalties when demultiplexing from 40 Gbit/s to 10 Gbit/s. Assuming 7 ps pulse width, 2^6-1 PRBS, 16 dB modulator ER, Pre-amp NF=5.5dB, Receiver BW=6 GHz;

The results indicate that for < 0.5 dB penalty then an extinction ratio of greater than 20 dB is required and an associated switching window of 14-18 ps. This is easily achievable using modern EA modulators. As the width of the switching window increases, for constant demultiplexer extinction ratio, then adjacent channels will be detected as additional noise at the receiver. This results in eye closure, and an upper limit in the width of the switching window for a given system penalty. Similarly, as the extinction ratio is decreased for a constant switching window width, then incomplete extinction of adjacent channels also causes additional noise at the receiver and eye closure. As the width of the switching window is decreased, then less signal is detected at the receiver and the noise associated with the receiver pre-amplifier degrades the SNR. This results in a lower limit in the switching window width for a given system penalty.

The above simulation was repeated for both an 80 Gbit/s and a 160 Gbit/s OTDM system. The results are shown below in Figure 3-33.

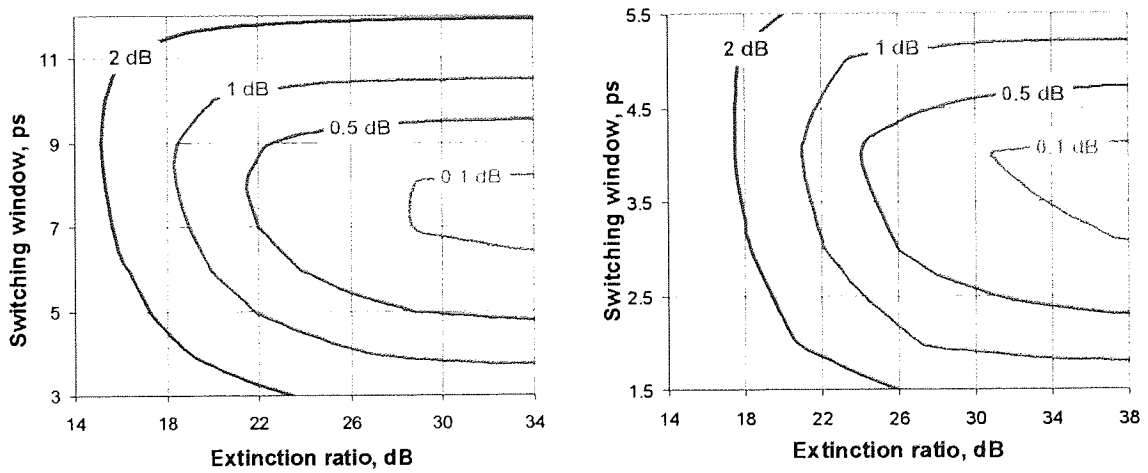

Figure 3-33. Theoretically predicted penalties for demultiplexing from: (a) 80 Gbit/s to 10 Gbit/s, $\Delta\tau$=3.5 ps; (b) 160 Gbit/s to 10 Gbit/s, $\Delta\tau$=1.5 ps; Assuming PRBS=2^6-1; Data modulator ER=16 dB; Pre-amp NF=5.5dB; Receiver BW=6 GHz;

These indicate that for demultiplexing from 80 Gbit/s to 10 Gbit/s a 6-9 ps switching window is necessary with an extinction ratio of ~22 dB. For the 16 channel system the requirements become even more stringent, requiring an extinction ratio of ~26 dB and a

switching window of 3.5 ps ± 1 ps. Two of the most promising devices that exhibit suitable switching characteristics, are the SOA-NOLM [209] and the EA modulator [236].

3.7.2.2 Intensity fluctuations resulting from demultiplexer timing jitter

Relative timing jitter between the non-flat demultiplexer switching window and the incoming OTDM data stream, induces intensity fluctuations in the demultiplexed signal and results in an additional power penalty [192]. This effect is shown in Figure 3-34.

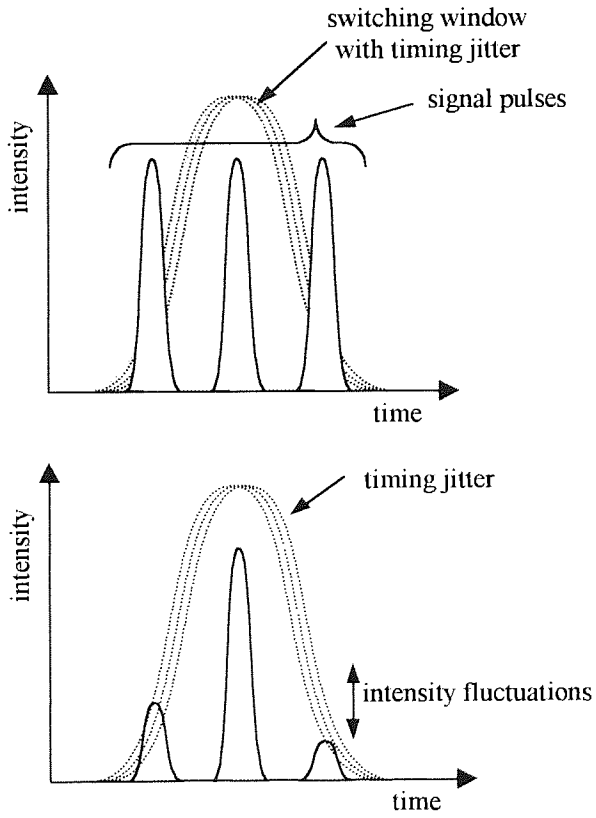

Figure 3-34. A finite demultiplexer timing jitter results in intensity fluctuations.

In addition to causing an additional power penalty, an error floor can also be introduced associated with the probability of the pulse arriving outside the switching window. This effect can be analysed by introducing a simplified model.

Three assumptions are made: (i) the width of the square switching window is larger than the signal pulse width; (ii) the distribution of the relative timing jitter is assumed

gaussian; (iii) each multiplexed signal has the same value of timing jitter σ. Figure 3-35 shows the OTDM multiplexed pulses, the square switching window, and the probability density function (PDF) of the relative timing jitter.

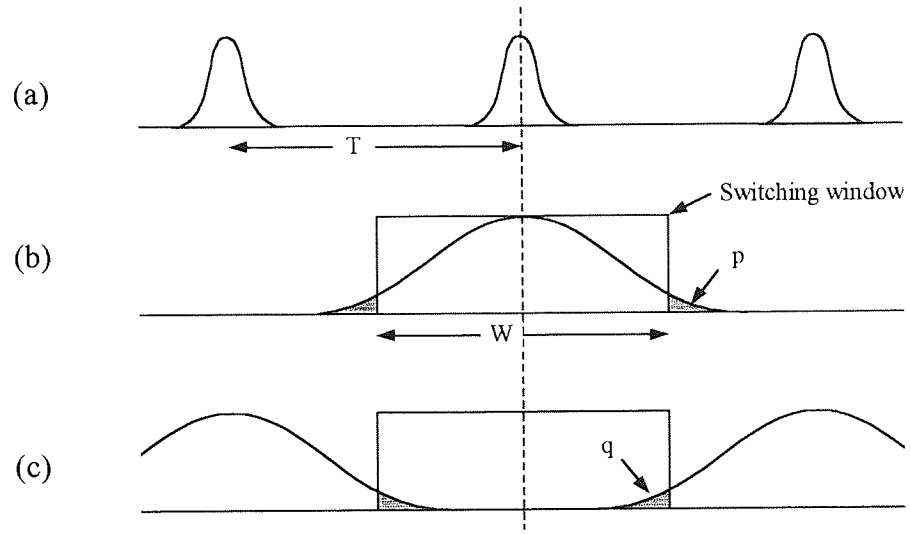

Figure 3-35. BER degradation due to demultiplexer timing jitter. (a) OTDM data stream; (b) Probability density function (PDF) of demultiplexed channel; (c) PDF of other channels

Errors may occur when the signal pulse deviates from the switching window, and when adjacent signal pulses enter the switching window. Let the error probabilities be p and q, given by [193]:

$$p = \frac{1}{\sqrt{2\pi}} \int_{W/2\sigma}^{\infty} \exp\left(-\frac{t^2}{2}\right) dt \qquad \text{Equation 3-13}$$

$$q = \frac{1}{\sqrt{2\pi}} \int_{W-}^{W+} \exp\left(-\frac{t^2}{2}\right) dt, \qquad W^{\pm} = \frac{T \pm W/2}{\sigma} \qquad \text{Equation 3-14}$$

Assuming a duty ratio of 2:1, the error probabilities for all the possible signal pattern combinations can be approximated by [193]:

$$BER = p + \frac{q}{2} \qquad \text{Equation 3-15}$$

Figure 3-36 shows the BER as a function of the window width W normalised to the time-slot width T for various values of rms timing jitter σ. Error probabilities p and q for $\sigma = T/12$ are also shown. As the duty ratio is increased then the error probability q

associated with adjacent signal pulses entering the switching window becomes less significant, and p dominates.

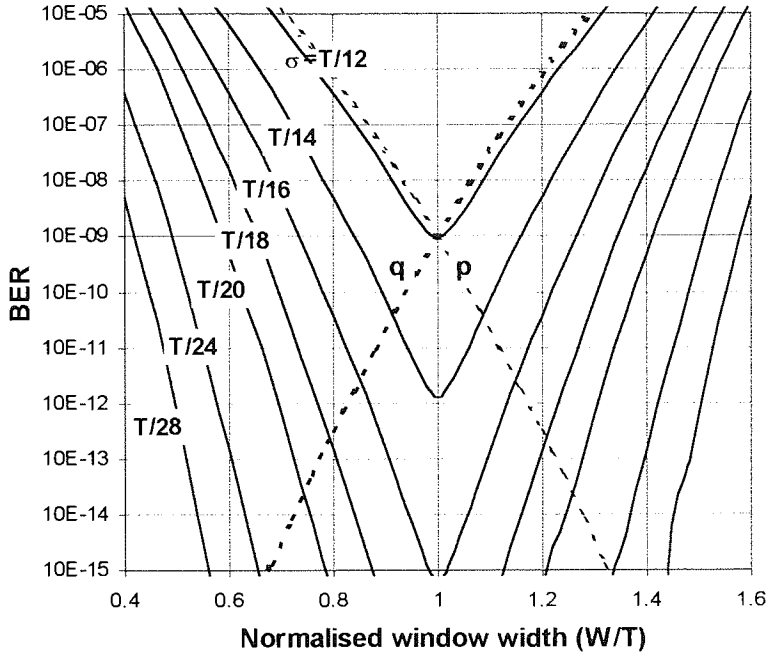

Figure 3-36. Analysis of demultiplexer timing jitter on BER performance and switching window width

The minimum BER is obtained when the window width W is equal to the time-slot width T. The rms value of the relative timing jitter should be less than $T/12$ to achieve a BER of 10^{-9}. Considering a generalised OTDM system. For a multiplexing penalty of less than 1 dB, then the pulse width should be less than one third of the bit period (i.e. $\frac{1}{3}T$), see Figure 3-30. For a demultiplexing penalty of 1 dB, then the switching window W should be twice the pulse width or two thirds the bit period (i.e. $\frac{2}{3}T$), see Figure 3-32. Therefore, from Figure 3-36, the timing jitter σ on the recovered clock should be less than $T/18$ for BER of 10^{-9}, and less than $T/22$ for a BER of 10^{-12}. For a 40 Gbit/s system with a pulse width of ~7 ps, a 15 ps switching window, the timing jitter should be ~1.2 ps. If the data-rate is increased to 100 Gbit/s (i.e. a 10 channel system), and the same assumptions are made, then the timing jitter $\sigma = 450$ fs.

3.7.3 System performance

When calculating the performance of a system, both multiplexer and demultiplexer degradations must be taken into account simultaneously, along with other system degradations, including dispersion, timing and amplitude jitter, amplified spontaneous emission, and noise originating in the receiver. With the above considerations in mind, Table 1 summarises an outline specification for an N channel OTDM network [84].

System Parameter	Specification
Transmitter extinction ratio	28.5 dB + 20 $Log_{10}(N-1)$
Transmitter pulse width	$< \frac{1}{3}T$
Demultiplexer extinction ratio	15 dB + 10 $Log_{10}(N-1)$
Demultiplexer switching window	$\frac{2}{3}T$
Demultiplexer timing jitter	$\frac{1}{22}T$ for BER 10^{-12}

Table 1. System specification for an *N* channel OTDM network. *T* is the bit period.

Table 1 was used as a basis for the design of a 40 Gbit/s (4×10 Gbit/s) OTDM system described in Chapter 7. It also helps to analyse the suitability of emerging device technology, and in the improvement of more developed solutions.

3.8 Chapter Summary

This chapter has outlined the key functionality that is required within an OTDM network, reviewed many of the possibilities and evaluated the existing literature. It has discussed in detail the characteristics of an ideal optical pulse source, and compared them with practical alternatives. Two optical sources that are used throughout this thesis were experimentally characterised, a third source based on an EA modulator is described in section 7.2. The different techniques of multiplexing, demultiplexing, and 'drop and insert' multiplexing have been discussed, with particular attention given to the operation of the NOLM as an all-optical switch. Such a device forms the basis for the SOA-

NOLM, which is described in detail in Chapter 4, and then used in an experiment, to perform simultaneous demultiplexing, data regeneration, and clock recovery in Chapter 5. The importance of data regeneration was then considered, with attention given to an optically amplified soliton system, where Gordon-Haus timing jitter severely affects the maximum achievable transmission distance. It is also important to consider what effect an inserted channel, of a slightly different wavelength, and temporal profile may have on subsequent transmission after a 'drop and insert' node. All-optical and electro-optical clock recovery techniques were then considered and compared. Finally the possible causes of system impairments were discussed, with emphasis given to the stringent requirements placed upon the duty-ratio and extinction ratio of the optical source and on the high-speed demultiplexer. The relative timing jitter between the OTDM data stream and the recovered clock was also analysed.

Chapter 4

Introduction to semiconductor optical amplifiers

4.1 Introduction

Since the development of the erbium-doped fibre amplifier (EDFA) in the late 1980's [194], the semiconductor optical amplifier (SOA) has been almost completely abandoned as an in-line amplifier in the 1.5 μm region. This is a direct consequence of the carrier dynamics of the device. When a signal pulse propagates through an amplifier, the carrier density is depleted such that a lower gain is available to subsequent parts of the pulse, or at high bit rates, subsequent pulses. Therefore, if the data rate is faster than the gain recovery time, the output signal will exhibit significant patterning effects, which will lead to a system penalty, or an error floor. More recently however, by understanding the carrier dynamics, significant optical nonlinearities within the SOA have been exploited [39, 195], with a goal to simplifying and integrating the architectural requirements of an all-optical network for the 21st century.

The problems associated with high-speed pulse amplification, can be overcome by either increasing the saturation intensity of the device or by dominating the evolution of the carrier density by an additional optical signal [39]. When an intense pulse propagates through a SOA, the carrier density reduces rapidly along the leading edge of the pulse and begins to increase again as the trailing edge leaves the device. As a pulse depletes the carriers, it influences its own propagation, produces a linear-phase shift across the pulse that spectrally-broadens the signal. This in turn may be used to compress the pulse by propagation through an appropriate dispersive media [39].

The nonlinear processes associated with an SOA can be classified as either, interband or intraband [196]. An interband process is associated with changes between the electron concentration in the conduction band and the valance band, whereas the intraband

process is connected with changes in the energy distribution of electrons within the conduction or valence band. The gain in an SOA is supplied by the interband optical transition between the valence and the conduction bands.

A 10 Gbit/s channel has been successfully demultiplexed from a 20 Gbit/s data-stream using the nonlinear process of polarisation rotation [197]. Polarisation-rotation is induced by periodically changing the carrier density of the SOA, leading to differential complex propagation constants for the TE- and TM- modes. Polarisation-insensitive wavelength-conversion of a 20 Gbit/s data signal over a range on 12 nm has been also been demonstrated using XPM in a SOA [198], and 60 Gbit/s operation is predicted possible [199]. Patterning is avoided by using an intense CW beam [200], allowing gain recovery time to be reduced to 50 ps. The configuration offers advantages over similar devices based on nonlinear effects in optical fibres in terms of size, environmental stability, and tuning range. An SOA has also been used to provide inter-cavity phase modulation allowing 20 Gbit/s clock recovery [179], see section 3.6.

A very promising nonlinear intraband effect within an SOA is FWM [201, 202, 195]. FWM has been used for all-optical modulation up to 100 GHz [203], demultiplexing and wavelength conversion of a 6.3 Gbit/s channel from a 200 Gbit/s OTDM data stream [122], 40 Gbit/s mid-span spectral inversion [111], and 10 GHz base-rate clock recovery from a 400 Gbit/s (all-mark) OTDM data stream [102].

All-optical switching based on the nonlinear optical loop mirror (NOLM) was outlined in detail in section 3.4.1. The NOLM utilises the nonlinear Kerr response of silica based fibre. The Kerr-effect in fibre is relatively small, and to achieve switching in a NOLM with practical input powers, long lengths are required. These long lengths of fibre lead to walk-off between control and data pulses, switching latency, and make the device sensitive to vibrations and temperature perturbations. Many of the disadvantages associated with the NOLM can be overcome by replacing the long lengths of fibre, by a highly nonlinear element (NLE). To date, this has taken the form of a SOA, which has

been investigated by a number of research groups world-wide, known in the literature as either the SLALOM (Semiconductor Laser Amplifier in a LOop Mirror) [204], or the TOAD (Terahertz Optical Asymmetric Demultiplexer) [205]. SLALOM and TOAD assume an N channel OTDM system. Each channel has a time-slot, T_{bit} and is multiplexed together on to a single fibre in a time-frame, T_{frame}. The system requires N demultiplexing switches (one for each channel), each is capable of switching out a time-slot T_{bit}, every T_{frame} [206]. Both configurations use low control pulse energies, but differ in the method used to apply the control pulse. SLALOM uses a control signal at an orthogonal polarisation to the data signal. TOAD uses an additional 3 dB coupler to apply the control signal at a second wavelength. The TOAD has been used to demultiplex a single data channel from a 4 ps time-slot, within a 10 ns time-frame. This corresponds to 2500, 100 Mbit/s multiplexed channels, and an aggregate throughput of 250 Gbit/s [207]. It has also been used in header recognition and subsequent self-routing of pulses in a packet switched system [208]. In these examples, the amplifier was allowed to recover completely between switching pulses, creating a guard-band and leading to a single channel rate of $\leq$ 1 Gbit/s. However, providing the switching pulse train is a regular clock, then the carrier density will respond in a periodic fashion. The amplifier no longer needs to recover fully between switching pulses, and much higher channel rates are possible. For the purpose of this text, such a device will be referred to as an SOA-NOLM. An SOA-NOLM has been used to demultiplex a 10 Gbit/s data stream from a 40 Gbit/s [116], and a 160 Gbit/s OTDM data stream [209]. Two SOA-NOLM arranged in a feed back configuration have also been used for pulse storage and regeneration in an all-optical memory [210]. The SOA-NOLM therefore has great potential for use in future generation OTDM networks.

The basic concepts of the SOA-NOLM, which is an asymmetric interferometer, can be extended to other types of interferometric configuration such as the SOA Mach-Zehnder interferometer (SOA-MZI). Many different configurations have been realised depending on the location of the SOAs within the interferometer, and on the direction of propagation of the switching and data signals [211]. The SOA-MZI was first

demonstrated using fibre based couplers and discrete SOAs [212], but has since been monolithically integrated into a single, stable, compact device [213]. A SOA-MZI has been used to demultiplex a 5 Gbit/s channel from a 40 Gbit/s OTDM data stream [213], and more recently a 10 Gbit/s data channel from an 80 Gbit/s data stream [214, 215]. It has also been used to demonstrate 20 Gbit/s 'drop and insert' multiplexing [117], wavelength conversion [216, 217], and 20 Gbit/s data regeneration [218].

This chapter outlines the basic properties and operating characteristics associated with an SOA. It considers in detail the evolution of the device carrier dynamics, including nonlinear saturation, and the gain recovery process. The operation of an SOA-NOLM is considered in detail, both as an all-optical demultiplexer and as an all-optical regenerator. Finally, two different SOA-NOLM configurations will be constructed and experimentally characterised. These devices are then used in Chapter 5, which experimentally analyses the SOA-NOLM as an all-optical regenerator, and then demonstrates for the first time, simultaneous demultiplexing, data regeneration, and clock recovery using a single SOA-NOLM [219].

4.2 Basic Operating Characteristics

If a semiconductor laser is biased slightly below threshold, then the laser will produce positive gain but cannot oscillate. Thus, light incident on the first facet will appear amplified at the second. Two types of SOA are commonly recognised, Fabry-Perot (FPSLA) and the travelling-wave (TWSLA) amplifiers. Both have the same semiconductor laser structure, but differ in the effective reflectivity of their facets. A Fabry-Perot amplifier is a resonant amplifier in which the factor $G_s\sqrt{R_1R_2}$ is close to unity, where G_s is the single pass gain through the device, and R_1 and R_2 are the reflectivities of the respective facets. In practical terms this means that R_1 and R_2 are of the order $0.01 \rightarrow 0.3$. Under these conditions, resonant internal gains of 25-30 dB can be achieved [220]. FPSLA are susceptible to fluctuations in bias current, temperature and signal polarisation.

The TWSLA on the other hand, has anti-reflective coatings applied to each facet. An amplifier with zero reflectivity is known as a TW amplifier. In practice, even with the best AR-coatings ($R = 1\times10^{-4}$) there is still some residual reflection, and the amplifier is known as a Near Travelling Wave SLA. The facet reflectivity can severely limit the maximum extinction ratio of an SOA-NOLM. Recently, by using angled-facet and tapered waveguide devices, the facet reflectivity has been decreased to almost a negligible amount, and the fibre-to-device coupling efficiency reduced to as little as 1 dB [221]. The main advantages associated with the TWSLA are wide bandwidth (less sensitive to current and temperature fluctuations), low sensitivity to signal polarisation, and improved gain saturation characteristics.

4.3 Nonlinear Gain Dynamics in a SOA

Generally, the gain of an SOA is a function of the inverted carrier distribution in the active region. The carrier density N in the conduction band is a measure of the device gain, and is related to the optical power of the incoming pulse stream $P(t)$ by the rate equation [222, 223]:

$$\frac{dN}{dt} = \underbrace{\frac{I}{eV}}_{\substack{\text{pumping}\\ \text{by}\\ \text{injection current}}} - \underbrace{\frac{N(t)}{\tau_e}}_{\substack{\text{spontaneous emission}\\ \text{and}\\ \text{nonradiative recombination}}} - \underbrace{\frac{P(t)\Gamma g[N(t)-N_T]}{h\nu A}}_{\substack{\text{stimulated emission}\\ \text{during amplification}}} \qquad \text{Equation 4-1}$$

where I is the effective injection current, e is the electron charge, V is volume of the active region, τ_e is the carrier lifetime, Γ is the mode confinement factor, g is the gain coefficient, N_T is the carrier density at transparency, $h\nu$ is the photon energy, and A is cross-section area of the active region. The first term in Equation 4-1 describes the pumping by the injection current that subsequently allows population inversion to be achieved. The second term accounts for the spontaneous emission and nonradiative recombination. The third term denotes the decrease in carrier density due to stimulated emission during the amplification process.

4.3.1 Saturation Process

An optical beam incident on one facet of an SOA will appear amplified at the second. If the intensity of the incident beam is increased above a certain threshold then the device will go into saturation. Here, the limited numbers of states in the conduction-band have been filled. Unless taken into account saturation can cause pulse distortion and frequency chirping during amplification [223].

4.3.2 Gain recovery

After the short optical pulse has saturated the SOA, the gain recovers due to injection of carriers by the injection current, see Equation 4-1. In this period, stimulated recombination can be ignored in Equation 4-1, and the gain during the recovery period is given by [222]:

$$G_{rec}(t) = G_0 + (G(t_s) - G_0)\exp(-(t - t_s)/\tau_e), \qquad t \geq t_s \qquad \text{Equation 4-2}$$

where G_0 is the unsaturated single-pass gain, $G(t_s)$ is the gain after saturation, t_s is the time when the recovery starts, and τ_e is the *1/e* gain recovery time. The gain recovery time decreases with increasing bias current, and can be considered to be equal to the spontaneous carrier lifetime [195]. Figure 4-1 shows the calculated gain change in the SOA using the above equations and a short optical input pulse.

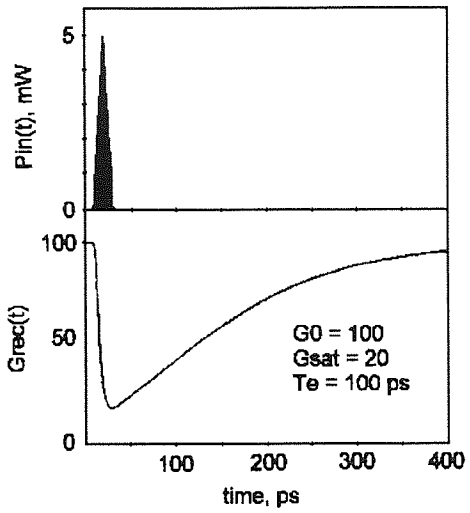

Figure 4-1. Saturation and gain recovery within a typical SOA.

It is clear that to avoid patterning effects during amplification, the bit period must be greater than the gain recovery time.

The gain recovery time of an SOA can be enhanced by optically pumping the device at a different wavelength [224]. A saturating holding beam at λ_1 is used to rapidly replenish the carrier population of the SOA after an intense clock pulse at λ_2 has affected the phase and amplitude of a data pulse at λ_3. Using a 30 mW holding beam and 200 mA bias current this technique has allowed a π recovery time in 12.5 ps [225]. This technique however, reduces the gain of the device, and adversely affects the life span of the SOA.

4.4 Operation Principles of an SOA-NOLM

Figure 4-2 shows the configuration of an SOA-NOLM. An intense control pulse introduced into the loop at WDM1 will traverse it in a clockwise direction leaving at WDM2. As the pulse passes through the SOA a rapid transition in its optical properties will occur.

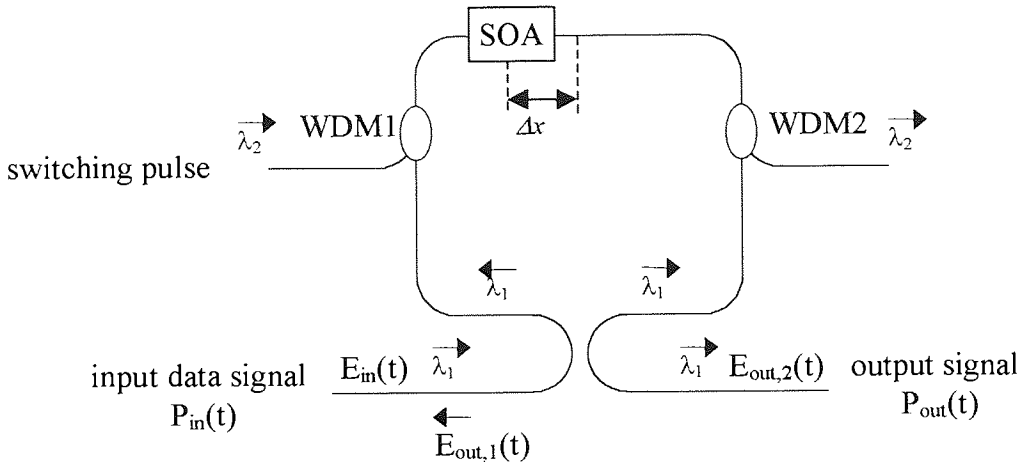

Figure 4-2. Configuration of the SOA-NOLM for switching with control pulse.

A low-intensity data pulse introduced at the loop input will be split into clockwise and anti-clockwise propagating components. If the data pulse enters the loop well in advance of the control pulse then both clockwise and anticlockwise components will have passed through the SOA before a change in its properties has occurred. Both components will interfere at the coupler, resulting in the input signal being reflected back along the input path. Similarly, if the data pulse lags the control pulse by a sufficient amount, then both pulse components will be subject to the same nonlinear properties. Each component will interfere at the coupler, and then be reflected back along the input arm.

If both clockwise and anticlockwise propagating components are at the centre of the loop when the control pulse propagates through the SOA, then the clockwise pulse will have passed through the SOA when the transition occurs, the anticlockwise component will have not. Consequently, as the anticlockwise component passes through the SOA, then it will experience different nonlinear properties compared with that of the clockwise travelling component. This will result in incomplete interference when the two components combine at the output of the coupler, and the pulse will emerge. The SOA-NOLM output exhibits a time window with rise and fall times in the order of picoseconds, and a flat top since the nonlinearity recovers on a nanosecond scale. The only data pulses that emerge from the loop are those within this window. The width of

the switching window can typically be varied from 10-100 ps by using a variable fibre stretcher placed in one arm of the loop mirror, see Figure 4-3.

Figure 4-3. Typical switching windows for an SOA-NOLM measured using a CW-DFB: (a) 60 ps; (b) 25 ps. From reference [39].

This is in contrast to a standard fibre NOLM, where the signal and clock wavelengths need to be matched carefully with respect to the fibre dispersion zero to ensure pulse 'walk through' each other by the required amount. Square switching windows are particularly useful because they offer a significant degree of jitter tolerance. Using a 1000 μm MQW SOA-NOLM, the switching energy is of the order of 400 fJ [39].

4.4.1 High-speed demultiplexing using an SOA-NOLM

Figure 4-4 shows the specific case when the SOA-NOLM is used as a high-speed demultiplexer. The incoming OTDM data stream at the line-rate is periodically switched to the output by an intense switching pulse stream operating at the OTDM base-rate, thus allowing a single channel to be demultiplexed. The remaining channels are reflected back along the input port, and can be separated using an optical circulator. This enables 'drop and insert' multiplexing to be achieved using a single device (see section 3.4). The intense switching pulse stream performs two roles; firstly, it strictly defines the temporal evolution of the SOA carrier density, independent of the incoming low-intensity data

signal. Secondly, the carrier density variation provides a periodic cross-phase modulation for the signal, which is exploited in the switching process.

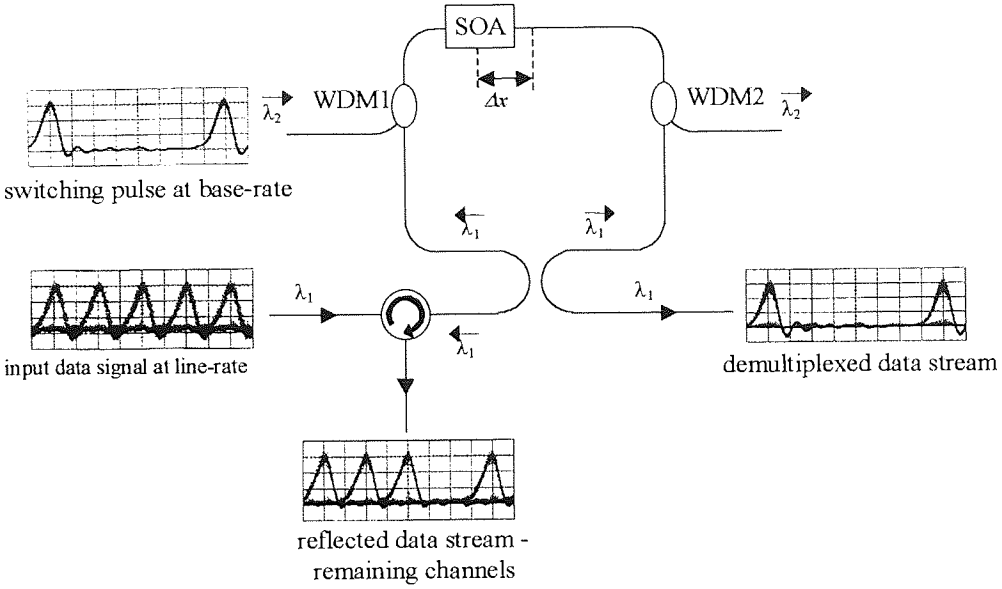

Figure 4-4. SOA-NOLM used as a high-speed demultiplexer. Insets intended to illustrate operation of demultiplexer.

Figure 4-5a shows the phase evolution of the clockwise and the anticlockwise propagating signals. The calculations assume that a 10 Gbit/s channel is being demultiplexed from a 40 Gbit/s OTDM data stream, and that the amplifier recovery time of the SOA is 500 ps. The switching signal repetition period is much less than the carrier lifetime, and the device never completely recovers and a saw-tooth phase variation is imposed on the signals, see Figure 4-5a. A relative phase difference exists between the two propagating components, which when the signals interfere at the 3-dB coupler, results in a square switching window at the loop output, see Figure 4-5b.

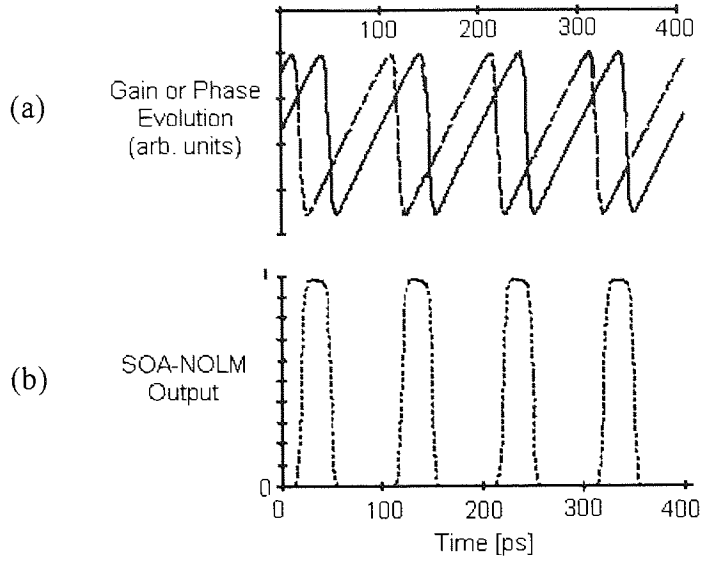

Figure 4-5. (a) Theoretical gain or phase evolution of the clockwise and anticlockwise signals in a periodically switched SOA-NOLM; (b) Phase difference results in a periodic switching window at the output of the SOA-NOLM.

The rise-time is determined by the control pulse width, and the switching window is determined by the phase difference, and therefore by the SOA offset from the centre of the loop.

4.4.2 All-optical data regeneration using an SOA-NOLM

All-optical data regeneration should re-time, re-shape and regenerate a transmitted data stream. This may be carried out midway through a point-to-point transmission link, or at a 'drop and insert' node within the network. Within a 'drop and insert' node, the inserted data channel may have a slightly different wavelength and temporal-profile from the data stream it is to be inserted into. This can lead to a group velocity mismatch and dispersive wave generation, which will degrade the receiver sensitivity, and limit the maximum transmission distance [108]. Data regeneration is covered in more detail in section 3.5.

As with a standard fibre NOLM, data regeneration can be achieved using an SOA-NOLM by letting the degraded input data stream switch a locally generated, high-quality

pulse stream into transmission, see Figure 4-7. If the locally generated pulse stream is operated at the incoming line-rate, then full data regeneration is achieved.

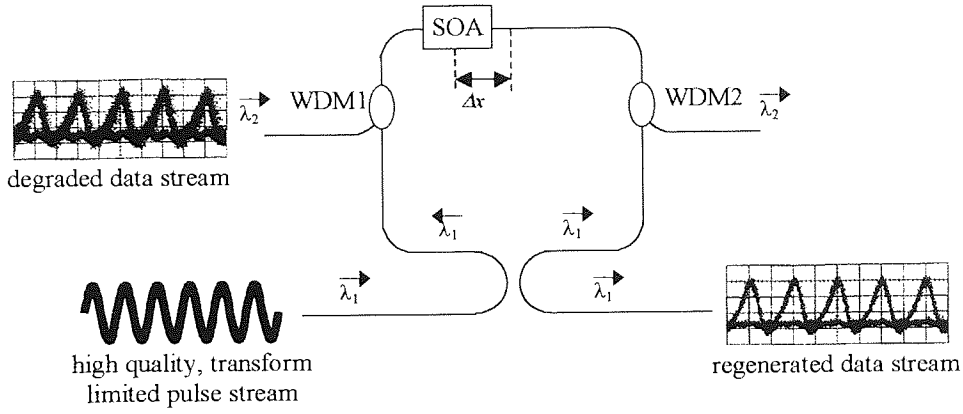

Figure 4-6. All-optical data regeneration using an SOA-NOLM. Insets intended to illustrate operation of regenerator.

If however, the locally generated pulse stream is operated at the base-rate, then all-optical demultiplexing with inherent data regeneration is achieved, see Figure 4-7. A high switching extinction ratio is ensured, and inter-channel crosstalk is eliminated, simply by the absence of light from the clock pulses used to probe the switching of the SOA-NOLM.

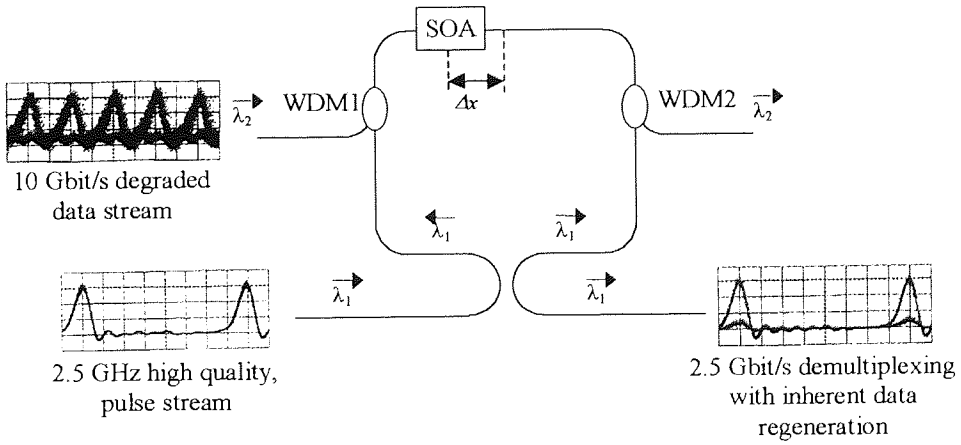

Figure 4-7. All-optical demultiplexing with inherent data regeneration.

Although high-speed data switching of an SOA-NOLM has been achieved at data rates that are significantly faster than the gain recovery time [226, 163, 227], the technique only allows *2R* data regeneration, and is limited to short pattern lengths. To achieve *3R* data regeneration using an SOA-NOLM, two criteria must be met. Firstly, the SOA must be situated within half a clock period of the loop centre, to ensure the

corresponding components of the same signal pulse experience the phase evolution induced by a single data (control) pulse [163]. Secondly, the gain recovery time must be less than the bit period of the switching pulse.

4.5 SOA-NOLM Experimental Characterisation

The remainder of this chapter describes two different SOA-NOLM configurations that are used in Chapter 5 to experimentally investigate all-optical demultiplexing, data regeneration, and clock recovery.

Two 1550 nm packaged SOAs were supplied by BT Laboratories. The first device is a 500 μm bulk SOA known throughout this thesis as SOA#1 (BT device number: SOA-01752), the second device is an angled-facet 1000 μm MQW SOA known as SOA#2 (BT device: SOA-01784). Each device is characterised in terms of fibre-to-fibre gain, saturated output power, facet reflectivity, and gain recovery time. A high facet reflectivity will cause incoherent interference and result in a degradation of the device extinction ratio, leading to a switching penalty. The gain recovery time will limit the maximum bit-rate before patterning effects have to be taken into consideration. The remainder of this chapter describes two different SOA-NOLM configurations. These are known throughout the remainder of this thesis as SOA-NOLM#1 and SOA-NOLM#2, and are used experimentally in Chapter 5 to demonstrated high-speed all-optical data regeneration.

4.5.1 500 μm bulk SOA - SOA#1

Figure 4-8 shows the experimental setup used to measure the fibre-to-fibre gain and the saturated output power.

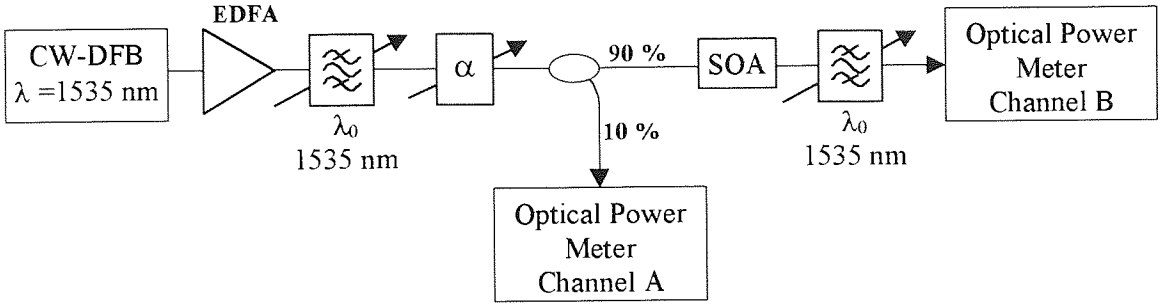

Figure 4-8. Experimental setup for the measurement of fibre-to-fibre gain and saturated output power.

A CW-DFB at 1535 nm was amplified using an EDFA, and a 3 nm *JDS Fitel* bandpass filter was used to reject any ASE. The signal was passed through a variable attenuator, before being split using a 90:10 coupler. 10 % was detected using channel A on a *Anritsu* optical power meter, and the remaining 90 % was coupled into the SOA under test. The output of the SOA was filtered using a second bandpass filter, thereby removing any ASE generated by the SOA. The output power was monitored on channel B of the power meter, and the fibre-to-fibre gain measured against input current using a fixed input power of –20 dBm to avoid device saturation. This procedure was repeated for different SOA operating temperatures, see Figure 4-11a. At 15 °C the fibre-to-fibre gain was 6 dB, and at 20 °C the gain decreased to 5 dB. The saturated output power was measured to be 5 dBm by varying the input power from –40 to +6 dBm, with a fixed SOA bias of 90 mA, see Figure 4-11b.

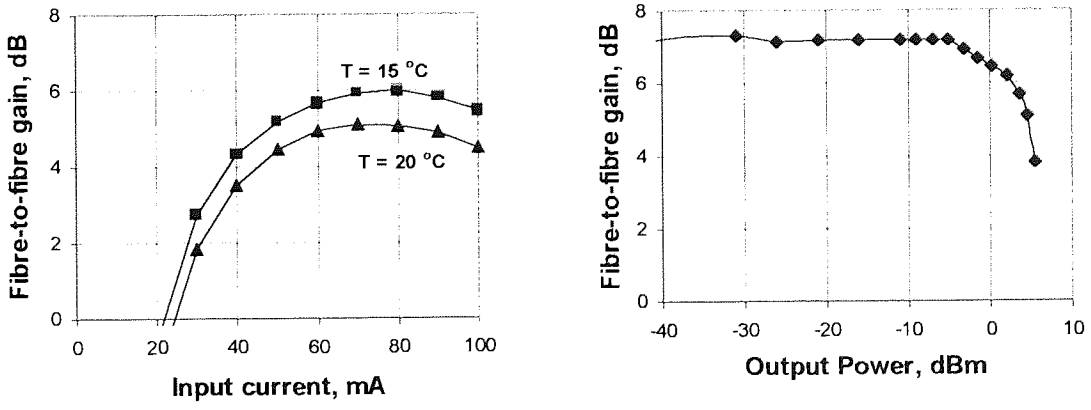

Figure 4-9. Characteristics of SOA#1, a 500 μm bulk SOA; (a) fibre-to-fibre gain; (b) saturated output power, input current = 70 mA, T = 20 °C;

The spontaneous emission spectrum of SOA#1 biased at 90 mA is shown in Figure 4-10. An isolator was placed either side of the SOA to prevent any residual reflections from

end connectors. The device has a gain peak at 1560 nm, and a minimum facet reflectivity at 1545 nm.

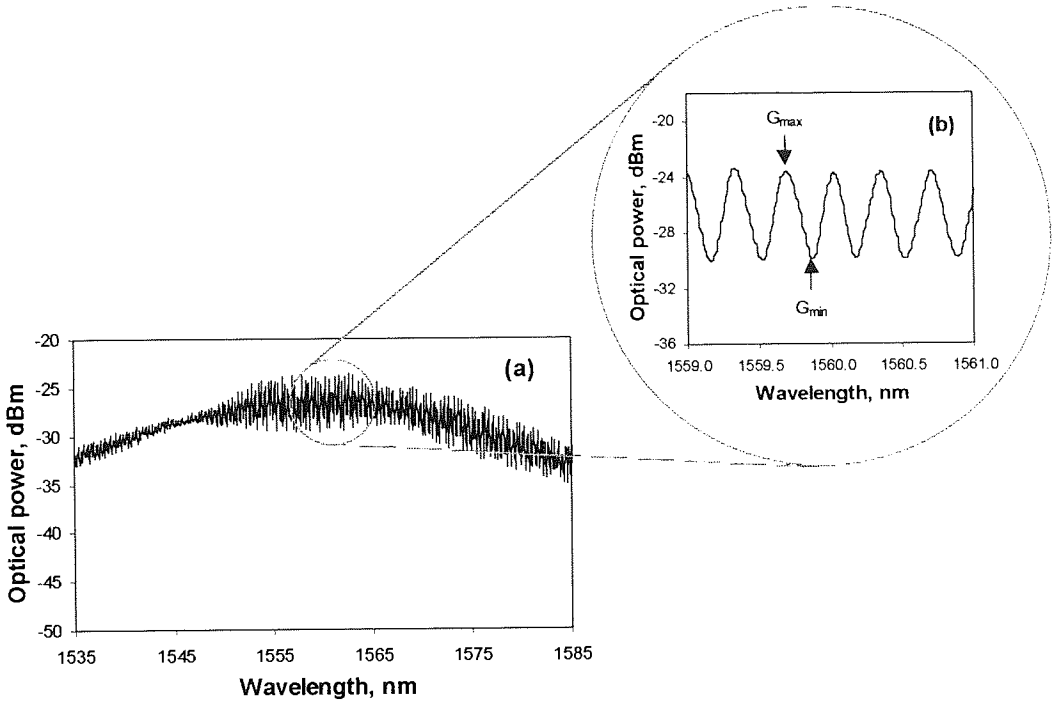

Figure 4-10. Spontaneous emission spectrum of a 500 μm semiconductor optical amplifier driven at 90 mA.

The actual facet reflectivity was obtained by measuring the resonant and antiresonant gain at different wavelengths across the gain curve. From this measurement, the geometric mean of the two facet reflectivities $R = \sqrt{R_1 R_2}$ can be obtained using [228]:

$$R = \frac{G_{\max} - G_{\min}}{4G_{\max}G_{\min}} \qquad \textbf{Equation 4-3}$$

where G_{max} and G_{min} are the resonant and antiresonant gains, respectively. The facet reflectivity was measured to be 2×10^{-4} at a wavelength of 1545 nm, assuming a 4 dB/facet fibre to device coupling loss.

The gain recovery time was measured using a simple pump-probe technique, illustrated in Figure 4-11. A CW-DFB operating at 1553 nm is combined using a fibre coupler with an intense 2.5 GHz, 15 ps control pulse at 1557 nm. As the intense pulse passes through the SOA, the device will go into saturation, and subsequently affect the phase and gain of the CW signal at 1553 nm. This is filtered and monitored using a sampling oscilloscope.

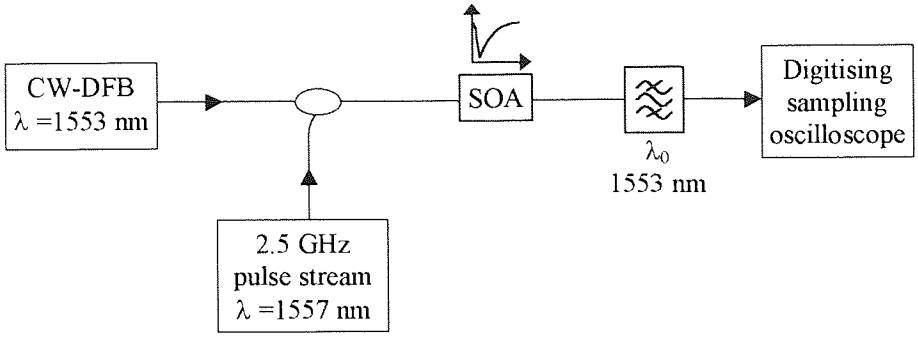

Figure 4-11. Pump-probe technique used to measure the gain recovery time of an SOA.

Figure 4-12 shows the gain recovery time of SOA#1. The recovery time is inversely proportional to the drive current, and is in good agreement with predicted shape in section 4.3.2. For a drive current of 90 mA, the gain recovery time is ~300 ps. This should allow a maximum switching speed of 3 Gbit/s.

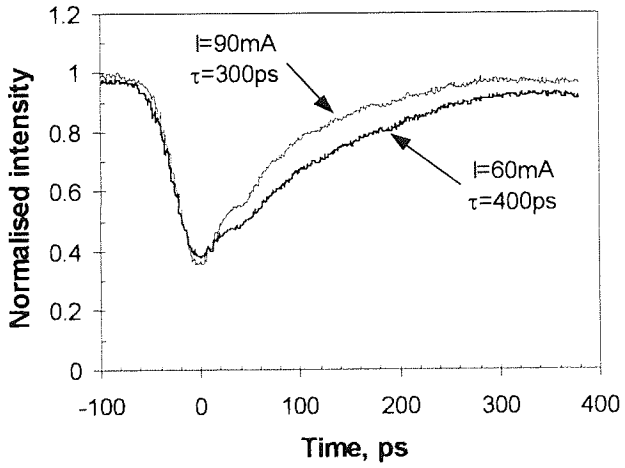

Figure 4-12. Gain recovery of SOA#1 for different bias currents: (a) 90 mA, τ_e = 300 ps; (b) 60 mA, τ_e = 400 ps.

SOA#1 is used as a nonlinear element in SOA-NOLM#1, which is described in section 4.5.3, and used experimentally in Chapter 5 to perform all-optical data regeneration at 2.5 Gbit/s.

4.5.2 Angled-facet 1000 μm MQW SOA - SOA#2

SOA#2 is an angled-facets 1000 μm MQW SOA with anti-reflection coated lens-ended fibre. The device has a fibre-to-fibre gain of 22 dB at 1555 nm, and 18 dB at 1538 nm for an input power of –25 dBm and a bias current of 160 mA.

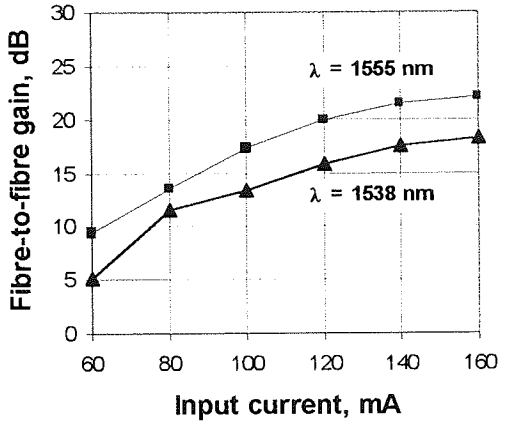

Figure 4-13. Fibre-to-fibre gain of SOA#2, an angled-facet 1000 μm MQW SOA. Input current = -20 dBm, T = 20 °C.

SOA#2 has a facet reflectivity of 1.3×10^{-3} at 1535 nm and a reflectivity of 7.2×10^{-4} at 1555 nm for a bias current of 150 mA. The gain recovery time was measured to be 100 ps, see Figure 4-14. This would allow a maximum switching speed of 10 Gbit/s.

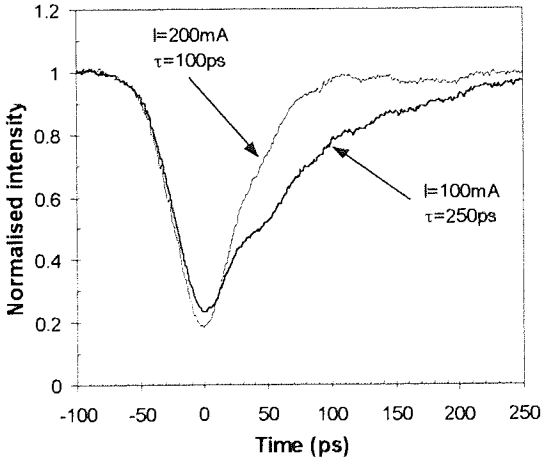

Figure 4-14. Gain recovery of a 1000 μm MQW SOA for different bias currents: (a) 100 mA, τ_e = 250 ps; (b) 200 mA, τ_e = 100 ps

SOA#2 is used as the nonlinear element in SOA-NOLM#2, which is described in section 4.5.4.

4.5.3 SOA-NOLM #1

Figure 4-15 shows the configuration of SOA-NOLM#1, which was built on a 1'×2' optical breadboard.. The wavelength of the data and control signals can be varied, depending on the pulse and data sources available. The SOA used in this configuration was the 500 μm bulk device outlined above as SOA#1. The SOA-NOLM could be easily changed from an all-optical demultiplexer to an all-optical regenerator, by simply tuning the bandpass filter.

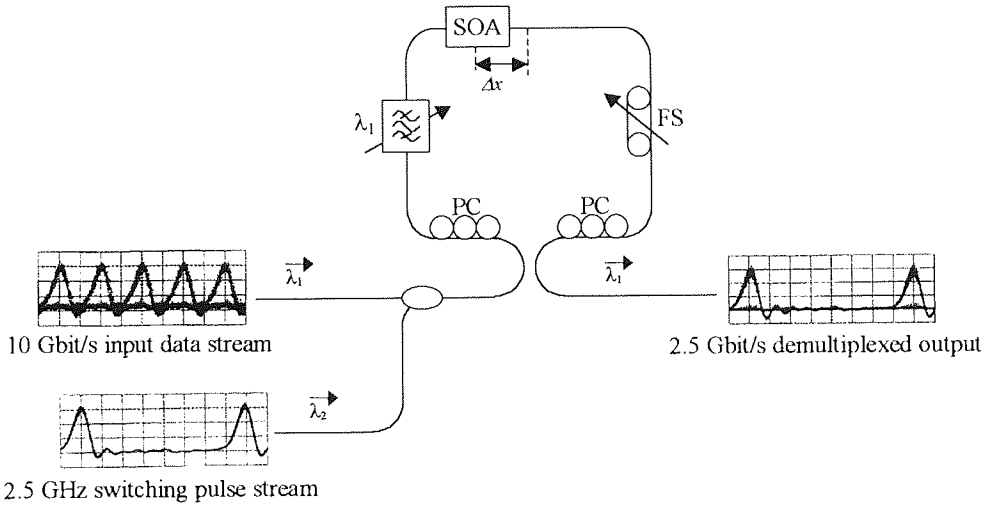

Figure 4-15. SOA-NOLM used as a high-speed demultiplexer.

A fibre coupler is used to combine a low intensity data stream at λ_1 with a high intensity control pulse stream at λ_2. The resulting signal is then coupled into the SOA-NOLM. The SOA-NOLM consists of a high quality *SIFAM* 3-dB coupler, two polarisation controllers, a 3 nm *JDS Fitel* tuneable bandpass filter, and a fibre stretcher. The fibre stretcher allows the switching window to be optimised by adjusting the distance the SOA is offset from the centre of the loop. The peak wavelength of the filter is set to the wavelength of the incoming data stream at λ_1, thereby extinguishing the clockwise component of the control pulse at λ_2. The symmetry of the loop is therefore broken and switching can be achieved. To ensure that the SOA was located at a fraction of the bit-period from the centre of the loop, a form of time domain reflectometry was used, and is shown in Figure 4-16.

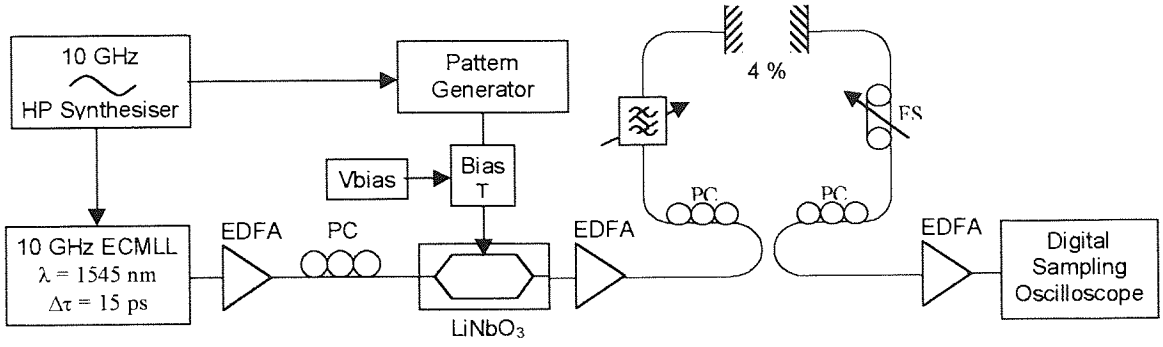

Figure 4-16. Time domain reflectometry used to ensure that the SOA is at the centre of the loop.

The loop was constructed to ensure that each arm was approximately the same length, but with one arm knowingly longer than the other. Before the SOA was spliced into place, the ends of each arm were cleaved to provide a 4 % reflection. A low repetition rate, 15 ps pulse stream was generated using an ECMLL, a $LiNbO_3$ amplitude modulator, and a pattern generator. These pulses were launched into the loop, and the reflections from each arm were monitored using a sampling oscilloscope. The time delay between the two reflected pulses allows the mismatch in the length of each arm to be calculated, using:

$$\Delta L = \Delta t \frac{c}{2n} \qquad \textbf{Equation 4-4}$$

where ΔL is the difference in length between the two arms, Δt is the time difference between the reflected pulses measured on the sampling oscilloscope, c is the speed of light in a vacuum, and n is the refractive index of the fibre. Once the length of each arm was equal, the SOA was spliced into place, and the fibre stretcher was used to finely adjust the device location for optimum switching.

The extinction ratio of the loop mirror was measured to assess the potential performance of the device for all-optical demultiplexing. A CW-DFB was coupled through a polarisation controller and into SOA-NOLM#1. The output from the SOA-NOLM was monitored on an optical spectrum analyser (span set to zero nm), and the polarisation controllers in the loop were used to bias the loop mirror from transmission into reflection, see Figure 4-17. The maximum extinction ratio was measured to be 25 dB,

making the device potentially suitable for demultiplexing in an eight channel OTDM system, (see section 3.7).

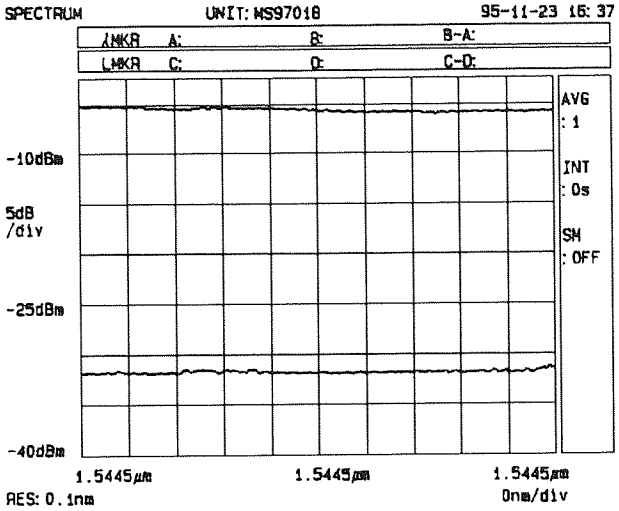

Figure 4-17. Extinction ratio measurements of SOA-NOLM#1.

In order to assess the switching window of the SOA-NOLM, a 5 GHz clock derived from an ECMLL was used to switch a low intensity CW signal from a 1545 nm DFB into transmission. The output from the SOA-NOLM was amplified, and detected using a 32 GHz pin-diode and a 50 GHz digital sampling oscilloscope. The switching window can be continuously tuned from 10 ps to 100 ps with no change in switching energy, simply by changing the device offset from the centre of the loop using the variable fibre stretcher. Figure 4-18 shows two different switching windows, with widths of 10 ps and 50 ps, respectively.

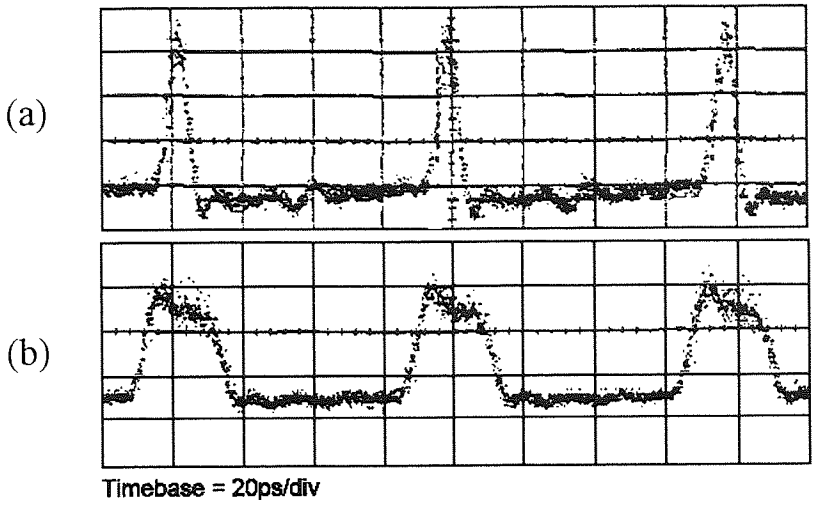

Figure 4-18. Switching window measurements of SOA-NOLM#1; (a) 10 ps; (b) 50 ps;

These measurement illustrate an almost square switching window, which is confirmed by a triangular autocorrelation shown in Figure 4-19.

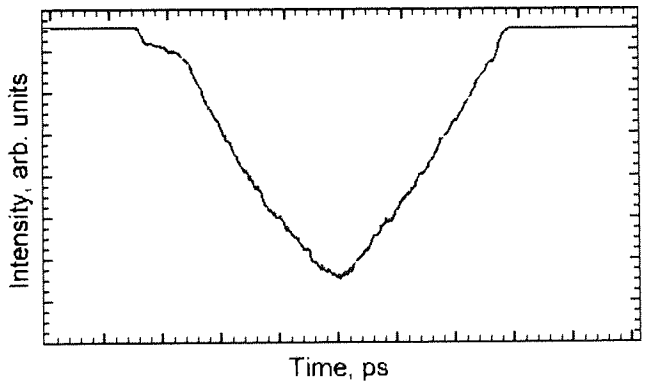

Figure 4-19. Triangular autocorrelation, indicating a square switching window.

Square switching windows are particularly useful because they offer a degree of jitter tolerance.

4.5.4 SOA-NOLM #2

Although SOA-NOLM#1 was flexible in terms of wavelength, it did however have the disadvantage that 6 dB of switching signal power was lost at the couplers and the gain recovery time limited the maximum switching speed to 3 Gbit/s. To overcome this

disadvantage a second SOA-NOLM was constructed using SOA#2, see section 4.5.2. This is shown in Figure 4-20, and is known as SOA-NOLM#2.

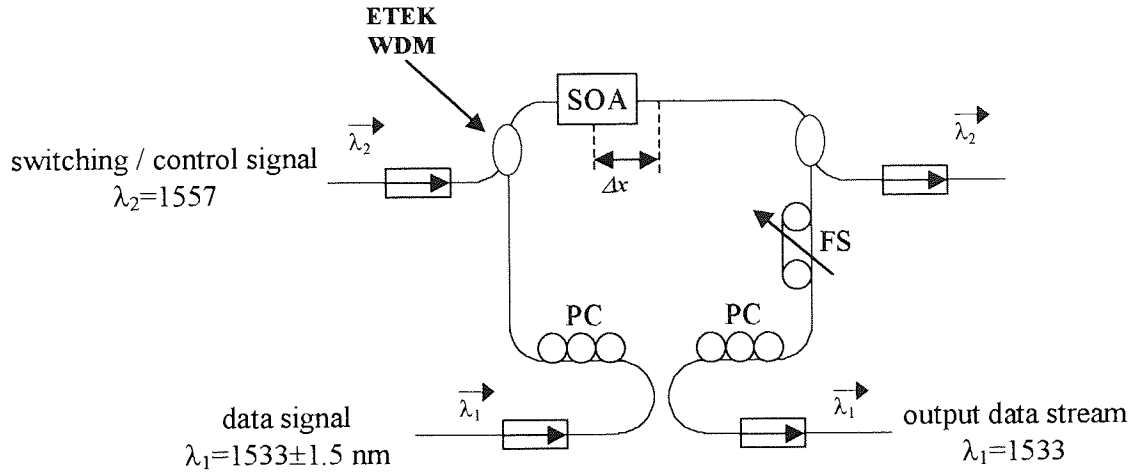

Figure 4-20. Configuration of SOA-NOLM #2.

Two ETEK 1533/1557 nm WDMs were used to couple the switching signal at 1557 nm into and out of the loop mirror. Similar switching window characteristics were observed as seen for SOA-NOLM#1.

The SOA had a 22 dB gain when biased at 200 mA, which was necessary to achieve a gain recovery of 100 ps. The gain caused the SOA to start lasing, making the system unstable. To reduce this effect, *ETEK* isolators were on the control signal input and output ports. Figure 4-21 shows the output of SOA-NOLM#2 when a 2.5 GHz pulse stream from an ECMLL was biased into transmission and reflection using the SOA-NOLM polarisation controllers. A residual facet reflection can be seen when the device is biased into reflection. This degrades Q measurements taken given in Chapter 5.

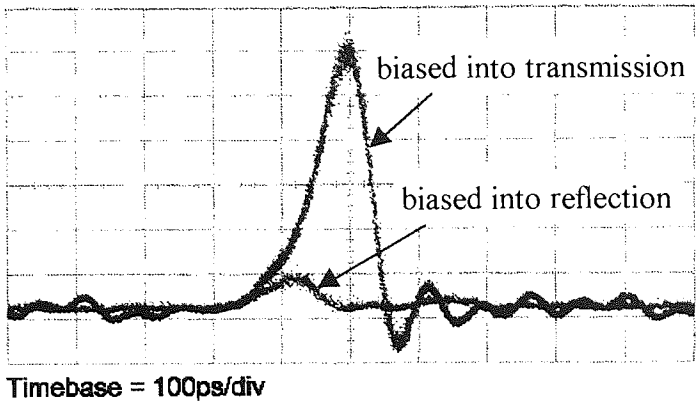

Figure 4-21. SOA-NOLM #2 biased into transmission and reflection.

In practice, the reflection also made the SOA-NOLM unstable, when biased to be normally reflective. Therefore in the experiments detailed in Chapter 5 the SOA-NOLM#2 was biased in transmission, and switched into reflection, therefore inverting the data stream.

4.6 Chapter Summary

This chapter has described how an SOA can be used as a nonlinear element within an OTDM network. The chapter started by outlining the nonlinear process of gain saturation, and the associated gain recovery time. The basic operating principles of an SOA-NOLM were described, and providing a periodic switching signal is used, the device can be operated at data rates that are faster than the characteristic recovery time. The use of an SOA-NOLM for all-optical data regeneration was then considered. Two SOAs were experimentally characterised, before being implemented into two different loop mirror configurations. These devices are used in Chapter 5 to perform simultaneous demultiplexing, data regeneration, and clock recovery using a single SOA-NOLM.

Chapter 5

Experimental investigation of simultaneous demultiplexing, data regeneration and clock recovery using a single SOA-NOLM

5.1 Introduction

One of the most promising all-optical processing elements for use in future high-speed OTDM networks is the semiconductor optical amplifier-based nonlinear optical loop mirror (SOA-NOLM). The SOA-NOLM is compact, and a relatively stable device that requires a low switching energy. It has been used for a variety of applications, including all-optical demultiplexing [116, 209], 2R data regeneration [162, 163], wavelength conversion [163], packet switching [208, 229], and all-optical memory [210].

This chapter will experimentally investigate the use of an SOA-NOLM as an all-optical data regenerator. It will then discuss how an SOA-NOLM can be used to achieve clock recovery by using the device as an all-optical mixer in a classical phase locked loop. Typically, the processes of demultiplexing, data regeneration, and clock recovery, are performed independently. The remainder of this chapter will present experimental results for the first time on simultaneous demultiplexing, data regeneration, and clock recovery using a single SOA-NOLM [20, 21].

5.2 All-optical Data Regeneration using an SOA-NOLM

5.2.1 Introduction

To demonstrate data regeneration using an SOA-NOLM the incoming degraded data stream is used to switch a locally generated high-quality pulse stream into transmission. To avoid patterning effects and obtain optimum regeneration, two criteria must be met.

Firstly the gain recovery time must be less than the bit-period of the incoming data signal, and secondly, the SOA must be positioned within half a clock period from the centre of the loop. The latter condition ensures that the clockwise and anticlockwise signal pulses experience the same phase evolution, induced by a single data pulse.

This section presents experimental results on 2.5 Gbit/s and 10 Gbit/s data regeneration, using the two SOA-NOLM configurations that are described in section 4.5. It then describes simultaneous demultiplexing with inherent data regeneration by extracting a 2.5 Gbit/s channel from a 10 Gbit/s OTDM data stream. To assess the degree of degradation, and the regeneration properties of the SOA-NOLM, Q measurements were made using a HP5420B 50 GHz digital-sampling oscilloscope and HP11982A 30 GHz lightwave converter. Assuming gaussian statistics and the decision threshold is set midway between the *one* and *zero* levels, the Q-value can be related to the BER using Figure 2-19. A Q of 6 is equal to a BER of 10^{-9}, while a Q of 7 is equal to a BER of 10^{-12}.

5.2.2 Experimental details of 2.5 Gbit/s data regeneration

The experimental setup used to analyse all-optical data regeneration with an SOA-NOLM is shown in Figure 5-1. This consists of an incoming 2.5 Gbit/s degraded data stream, a 2.5 GHz locally generated pulse stream, and SOA-NOLM #1.

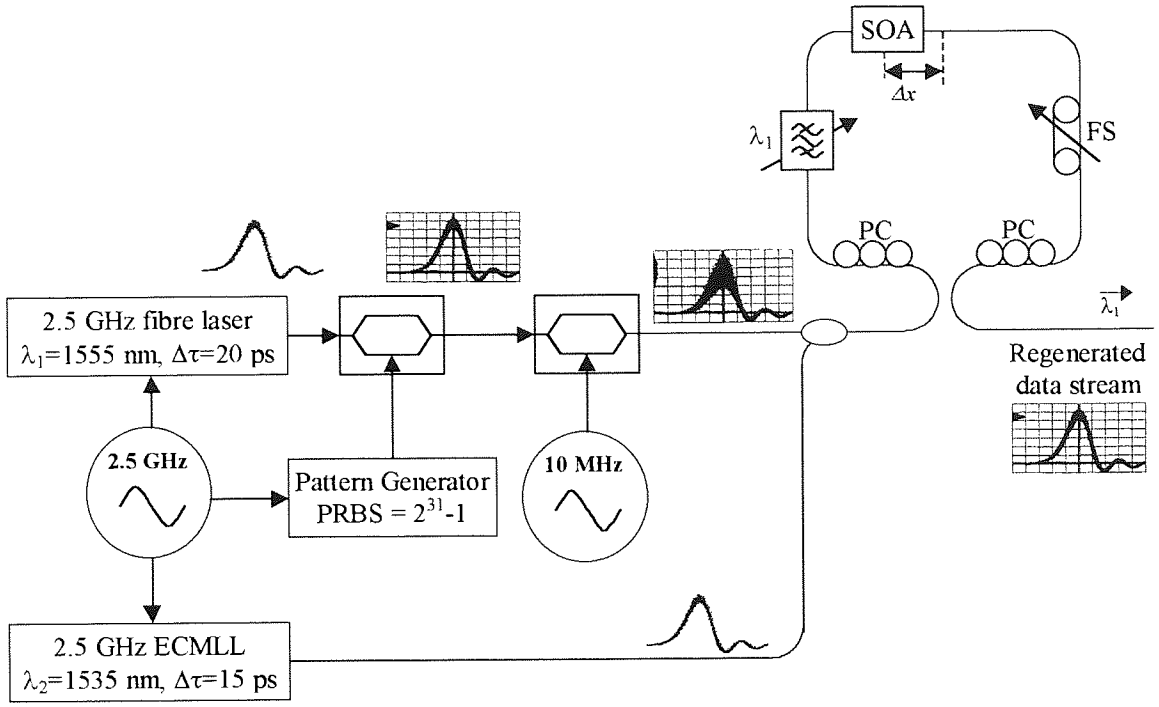

Figure 5-1. Experimental setup used to analyses all-optical data regeneration using an SOA-NOLM.

SOA-NOLM #1 consists of a 500 μm bulk SOA, a variable fibre stretcher, two polarisation controllers, and a 3 nm *JDS Fitel* bandpass filter (see section 4.5.3). The wavelength of the bandpass filter was tuned to 1535 nm, to equal that of the locally generated pulse stream. The SOA was biased at 100 mA, and the gain recovery time was measured to be 300 ps (see Figure 4-12). The maximum switching speed is therefore 3.3 Gbit/s.

The incoming degraded data stream was derived from a 2.5 GHz actively modelocked fibre ring laser which was optimised to produce ~20 ps pulses at 1555 nm. This was encoded with a 2^{31}-1 PRBS data sequence using a HP pattern generator and an *ETEK* $LiNbO_3$ amplitude modulator ($LiNbO_3$-AM#1), see section 3.3.2. The output data stream was amplified and fed through a *BT* $LiNbO_3$ amplitude modulator ($LiNbO_3$-AM#2) with an insertion loss of 13 dB. $LiNbO_3$-AM#2 was driven by a 10 MHz ramp function and biased to produce varying depths of modulation. This enabled the effects of amplitude jitter on data 1's to be simulated, see Figure 5-2.

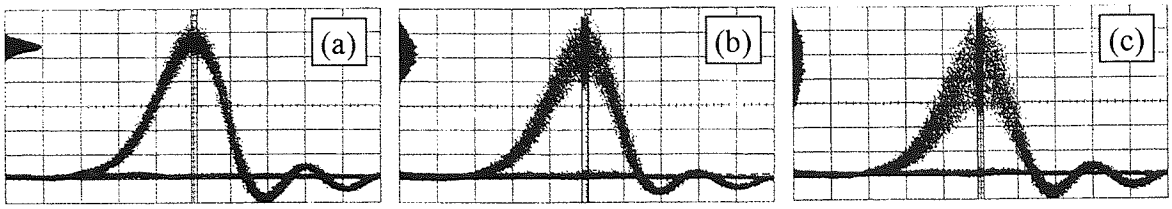

Figure 5-2. Simulation of amplitude jitter using an amplitude modulator: (a) input data stream, Q = 22.5; (b) 20 % modulation, Q = 7.8; (c) 40 % modulation, Q = 4.6.

The locally generated optical clock was generated using an ECMLL running at 1535 nm. The device was driven at the cavity fundamental to produce a 2.5 GHz, 15 ps pulse stream with a timing jitter of less than 150 fs, see section 3.3.1.

5.2.3 Results of 2.5 Gbit/s data regeneration using SOA-NOLM #1

The fibre stretcher was used to adjust the SOA-NOLM switching window to ~35 ps, which was measured using a CW-DFB and a sampling oscilloscope. The polarisation controllers in the loop mirror were used to bias the interferometer into reflection. The incoming data stream was used to switch the ECMLL into transmission, enabling non-inverting data regeneration at the transmitted output. A mean power of 8 dBm (–1 dBm at device facet) was required for the switching 2.5 Gbit/s PRBS data stream, which gives assuming, equal ones and zeros, a switching energy of 635 fJ. Figure 5-3 and Figure 5-4 show the eye diagrams of the incoming degraded data stream, and the regenerated output data stream.

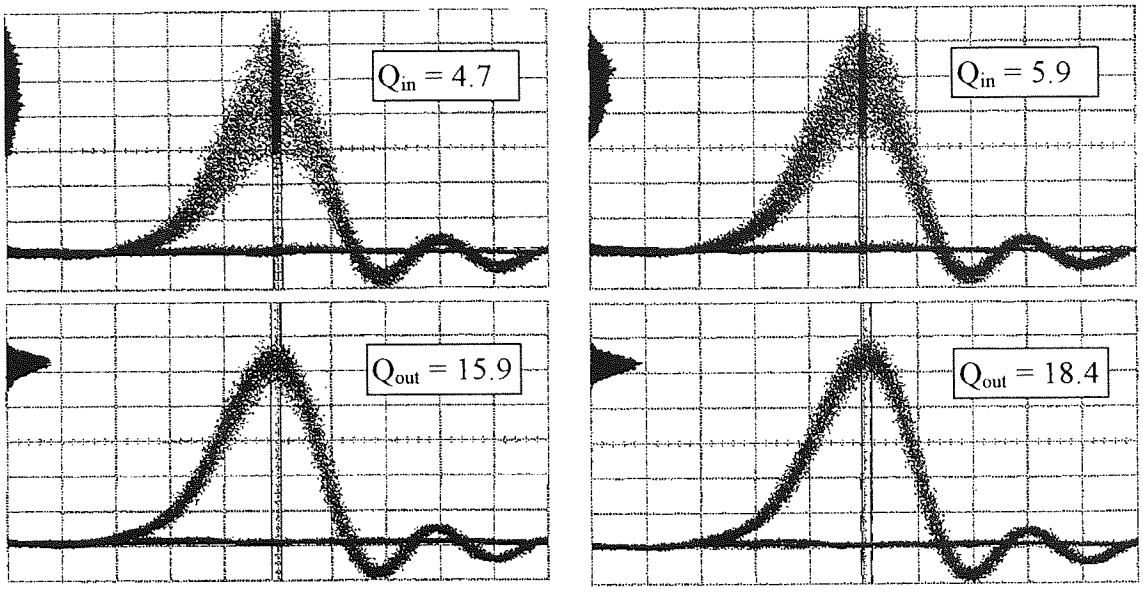

Figure 5-3. All-optical data regeneration at 2.5 Gbit/s, using SOA-NOLM #1: (a) Q_{in} = 4.7, Q_{out} = 15.9; (b) Q_{in} = 5.9, Q_{out} = 18.4.

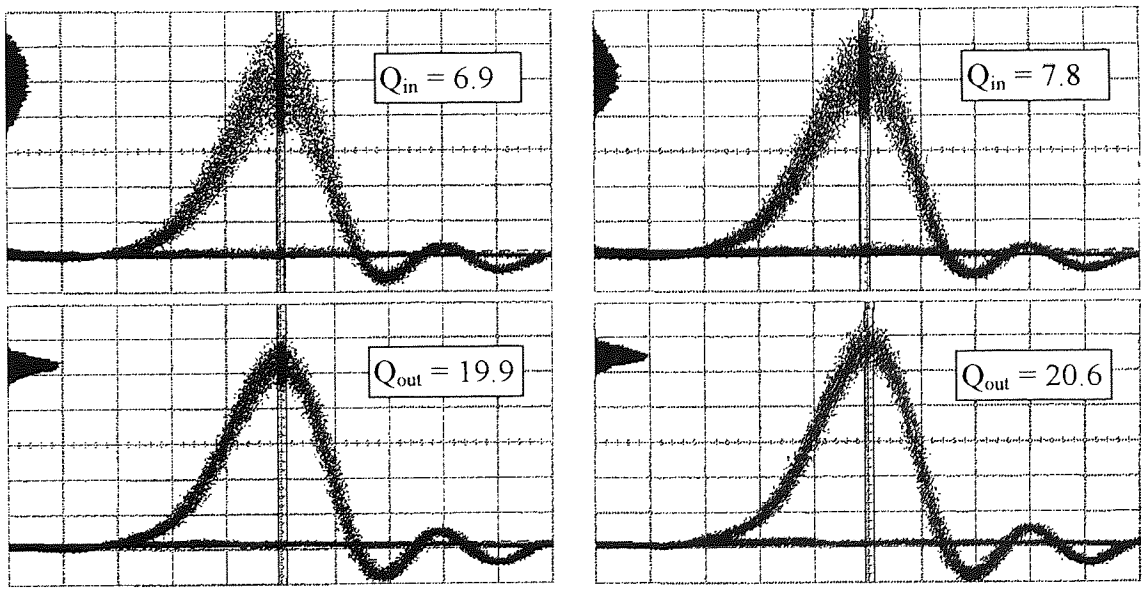

Figure 5-4. All-optical data regeneration at 2.5 Gbit/s, using SOA-NOLM #1: (a) Q_{in} = 6.9, Q_{out} = 19.9; (b) Q_{in} = 7.8, Q_{out} = 20.6.

The Q values indicate excellent system performance, from Figure 5-3a showing an input Q of 4.7 and a regenerated output Q of 15.9 to Figure 5-4b showing an input Q of 7.8

regenerated to a Q of 20.6. However, the role and location of a regenerator within an optical network must be considered in more detail. Namely, a regenerator should retime, reshape, and re-amplify a data signal *before* an error has occurred, or more importantly a regenerator *cannot* correct errors once they have occurred. The regenerator makes a decision like an electrical detector, and could transmit a zero when a data one is input, or vice versa. At 2.5 Gbit/s a BER of 10^{-9} corresponds to a Q of 6, or an error every 0.4 seconds, and a BER of 10^{-12} (Q=7), corresponds to one error every 400 seconds. The results shown in Figure 5-3a indicate that an input Q of 4.7 is regenerated to a Q of 15.9. In practice, if BER measurements were made, an error-floor would probably be observed. The regenerator redistributes the probability density function of the incoming data stream. Therefore, unless the decision threshold is midway between the one and zero states it is unreliable to infer a BER from a regenerated Q using Figure 2-19.

To assess the performance of the SOA-NOLM to regenerate a signal which has been degraded due to timing jitter, the fibre laser was replaced with a *NEL* 10 GHz DFB. When the DFB was driven at 2.5 GHz, it exhibited a large degree of timing jitter. Figure 5-5a shows the degraded input data stream with a Q of 7.8 and a rms timing jitter of 4.7 ps, and the regenerated output data stream with a Q of 14.0 and a timing jitter (measurement limited) of < 1.6 ps. The actual timing jitter on the transmitted data stream should be equal to that of the 2.5 GHz ECMLL measured in section 3.3.1 to be 140 fs.

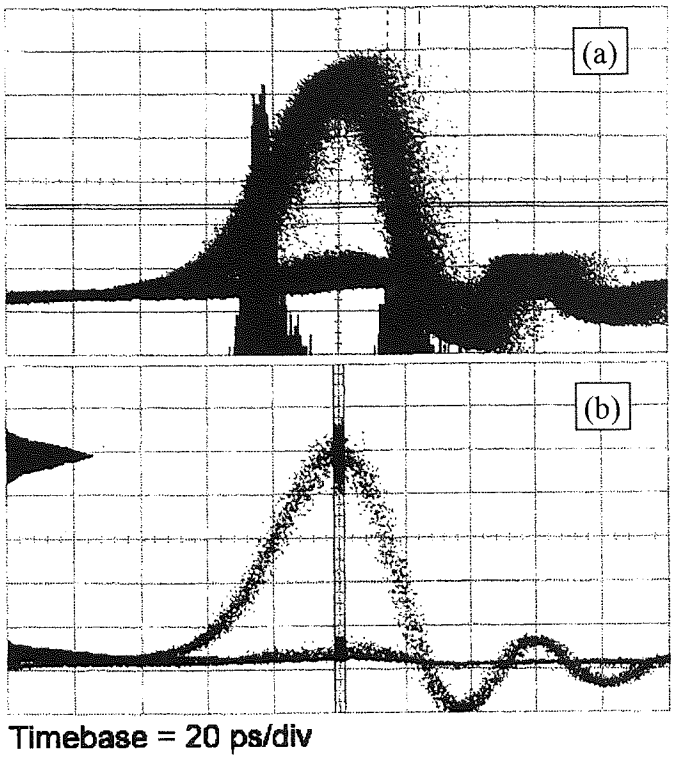

Figure 5-5. Performance of SOA-NOLM #1 to regenerate a signal subject to a large degree of timing jitter: (a) Q_{in} = 7.8, timing jitter = 4.7 ps; (b) Q_{out} = 14.0, measurement-limited timing jitter < 1.6 ps.

The SOA-NOLM therefore demonstrates excellent amplitude and timing restoration at 2.5 Gbit/s. Q measurements confirm a high quality output from which we would not anticipate additional errors from electronic detection. However, BER measurements are required to determine if the regenerator itself has erroneously transmitted (or reflected) a pulse.

To assess the regenerative properties of SOA-NOLM #1 at higher data rates, the fibre laser was passively multiplexed up to 5 Gbit/s and 10 Gbit/s using a fibre-based interleaver. Figure 5-6a shows the patterning effects that occur when SOA-NOLM #1 was driven by a 5 Gbit/s PRBS data stream. Two distinct levels are observed, resulting from the gain recovery time of the SOA. When operated at 10 Gbit/s almost complete eye closure is observed, see Figure 5-6b.

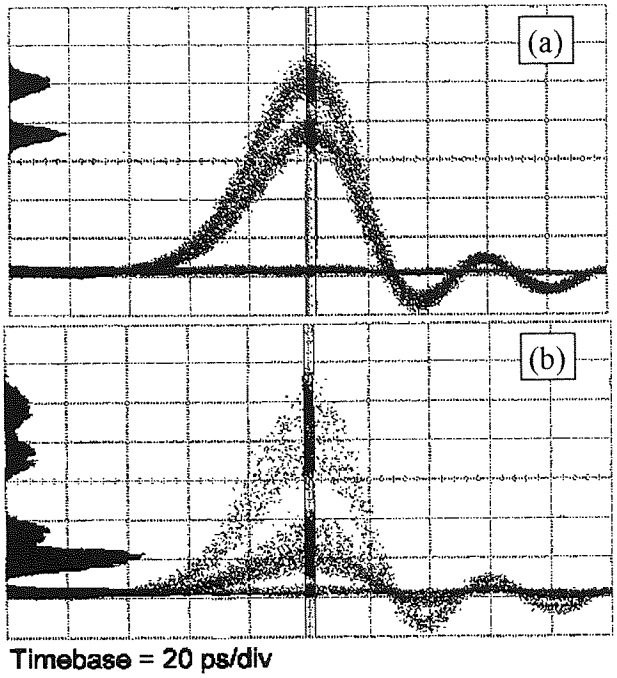

Figure 5-6. Patterning effects using SOA-NOLM #1. Each pulse experiences a different gain due to incomplete gain recovery before the device is re-switched: (a) 5 Gbit/s switching; (b) 10 Gbit/s switching.

To analyse the patterning effects in more detail, a 5 Gbit/s and 10 Gbit/s pulse burst was used to switch the SOA-NOLM; the output was monitored on a high-speed sampling oscilloscope. The pulse burst was realised using the 2.5 GHz fibre laser, and an amplitude modulator (AM). The AM was driven by a HP pattern generator configured to produce a single bit followed by a long string of zeros. This was then multiplexed up to the desired bit rate, either 5 Gbit/s or 10 Gbit/s. The SOA-NOLM #1 was biased into reflection and the 5 Gbit/s pulse burst (see Figure 5-7a) was used to switch the 2.5 GHz ECMLL into transmission.

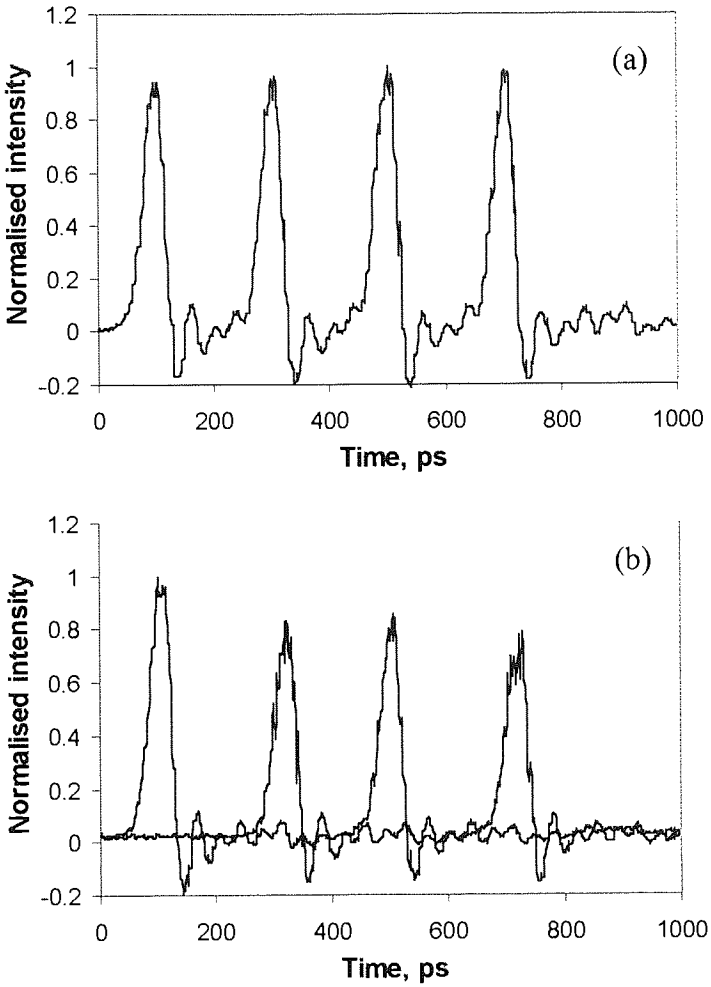

Figure 5-7. Analysis of patterning in SOA-NOLM #1: (a) 5 Gbit/s input pulse burst; (b) each pulse experiences a different gain due to the finite gain recovery time of the device.

The phase of the 2.5 GHz drive signal to the ECMLL was tuned to each of the transmission peaks generated by the switching pulse burst, see Figure 5-7b. Each pulse experiences a different loop transmission due to the finite recovery time of the SOA. Two distinct pulse amplitudes are observed, which agree closely with those obtained when the SOA-NOLM was switched with a PRBS data stream (Figure 5-6a), and correspond to the previous pulse being a zero and a one, respectively.

A 10 Gbit/s pulse burst was used to switch SOA-NOLM #1, and is shown in Figure 5-8a. The effects of device saturation, and subsequent gain recovery are much more pronounced. Four different pulse amplitudes are observed (see Figure 5-8b), accounting

for the almost complete eye closure that was observed when the loop mirror was driven by a PRBS data sequence, see Figure 5-6b.

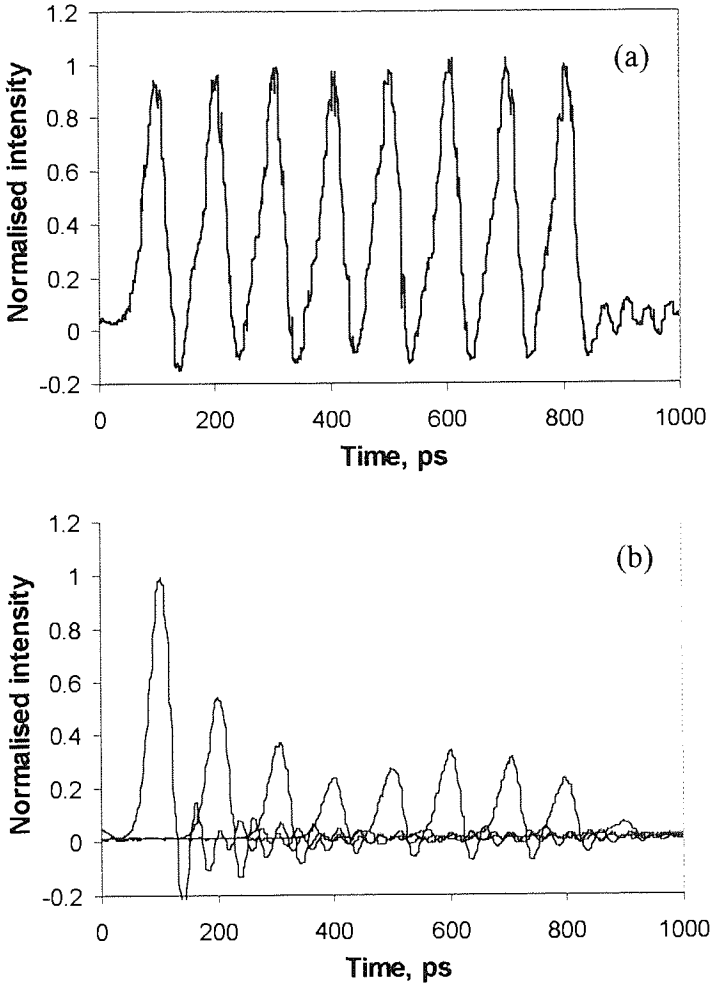

Figure 5-8. Analysis of patterning effects using SOA-NOLM #1: (a) 10 Gbit/s input pulse burst; (b) each pulse experiences a different gain due to finite gain recovery time.

To assess the feasibility of achieving data switching at higher bit-rates, SOA-NOLM #2 was constructed, see section 4.5.4. The loop mirror consisted of a 1000 μm MQW SOA that had a gain recovery time of ~100 ps. Such a device should allow data regeneration at bit -rates up to 10 Gbit/s. To confirm this, a 10 GHz low intensity pulse stream from the ECMLL described in section 3.3.1 was used to probe the loop mirror. Due to facet reflections and high device gain, the SOA-NOLM was biased in transmission, see Figure 5-9b. A 10 Gbit/s, 4-bit pulse burst was used to switch the loop mirror into reflection. The pulse burst shown in Figure 5-9a was derived from a 10 GHz fibre laser and a

$LiNbO_3$ amplitude modulator, which was driven by a 10 Gbit/s *Anritsu* (A3H2107) pattern generator. The different pulse amplitudes are due to a poor frequency response of the $LiNbO_3$ amplitude modulator.

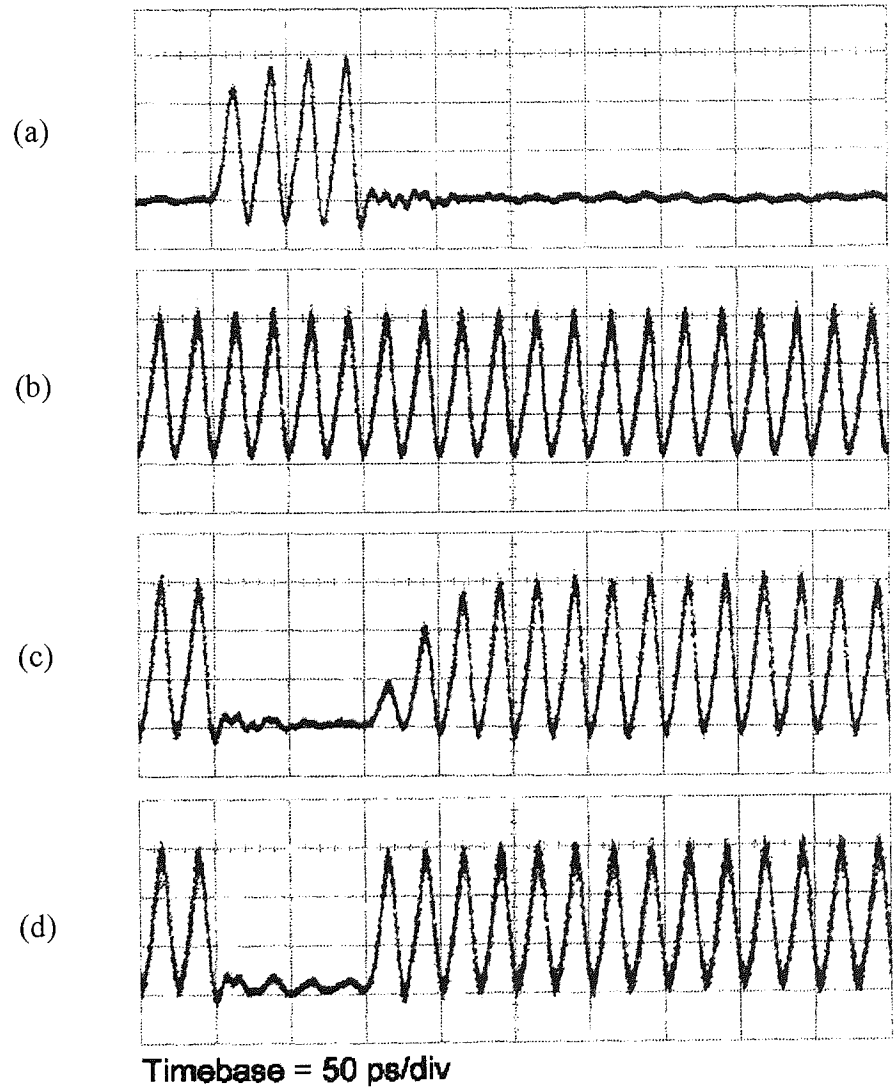

Figure 5-9. Analysis of patterning in SOA-NOLM #2: (a) 10 Gbit/s input 4-bit pulse burst; (b) SOA-NOLM biased into transmission, no switching pulse burst; (c) 10 Gbit/s, 4-bit pulse burst periodically switching the loop mirror into reflection, I_{SOA} = 100 mA, corresponding to a gain recovery of 250 ps; (d) 10 Gbit/s, 4-bit pulse burst periodically switching the loop mirror into reflection, I_{SOA} = 200 mA, corresponding gain recovery of 100 ps.

Figure 5-9c shows the output from SOA-NOLM #2, when the SOA was biased at 100 mA. The gain recovery time was measured to be 250 ps (see Figure 4-14), and different pulse amplitudes are observed. Figure 5-9d shows the result of increasing the SOA bias current to 200 mA, giving a gain recovery time of 100 ps. The gain fully

recovery between pulses, therefore each pulse experiences a similar gain, and patterning effects are eliminated.

5.2.4 All-optical regeneration at 10 Gbit/s using SOA-NOLM #2

The 2.5 GHz fibre laser was modulated with a 2^{31}-1 PRBS data sequence and passively multiplexed up to 10 Gbit/s. The quality of the data sequence was degraded by reducing the amplitude of the drive signal to the modulator. The ECMLL was tuned to 1535 nm, and sinusoidally modulated at 10 GHz, producing 15 ps pulses with a timing jitter of less than 300 fs. Figure 5-10 shows the results of 10 Gbit/s data regeneration using SOA-NOLM #2. It must be noted that due to the frequency response and noise figure of the HP digital sampling oscilloscope and lightwave converter, the maximum measurable Q was ~15 at 10 Gbit/s.

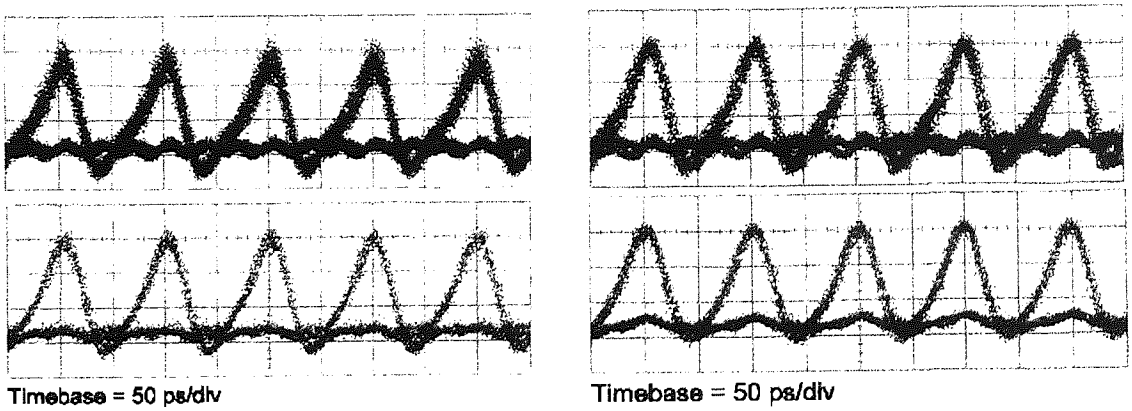

Figure 5-10. All-optical data regeneration at 10 Gbit/s, using SOA-NOLM #2: (a) Q_{in} = 6.4, Q_{out} = 10.3; (b) Q_{in} = 10.5, Q_{out} = 14.4.

The figure shows that an input Q of 6.4 was regenerated to a Q of 10.3, and an input Q of 10.5 was regenerated to a Q of 14.4. The SOA had a finite facet reflection, which caused the switching process to become unstable. This was overcome by using the polarisation controllers to bias the loop into transmission and switch it into reflection, effectively performing data inversion. A small residual reflection is still evident on the zero base line, which slightly degrades the accuracy of any Q measurement. Assuming a

PRBS 10 Gbit/s switching data stream, the switching energy on the device facet was ~100 fJ.

5.2.5 Demultiplexing with inherent data regeneration using SOA-NOLM #2

By decreasing the modulation speed of the ECMLL to 2.5 GHz, and letting the degraded 10 Gbit/s data stream switch the SOA-NOLM, then 10 Gbit/s to 2.5 Gbit/s demultiplexing can be achieved with inherent data regeneration. This is shown in Figure 5-11. For demultiplexing applications it is essential to maintain a good extinction ratio to ensure unwanted channels are completely removed. Interchannel cross talk is eliminated simply by the absence of light from the clock pulses used to probe the switching of the SOA-NOLM.

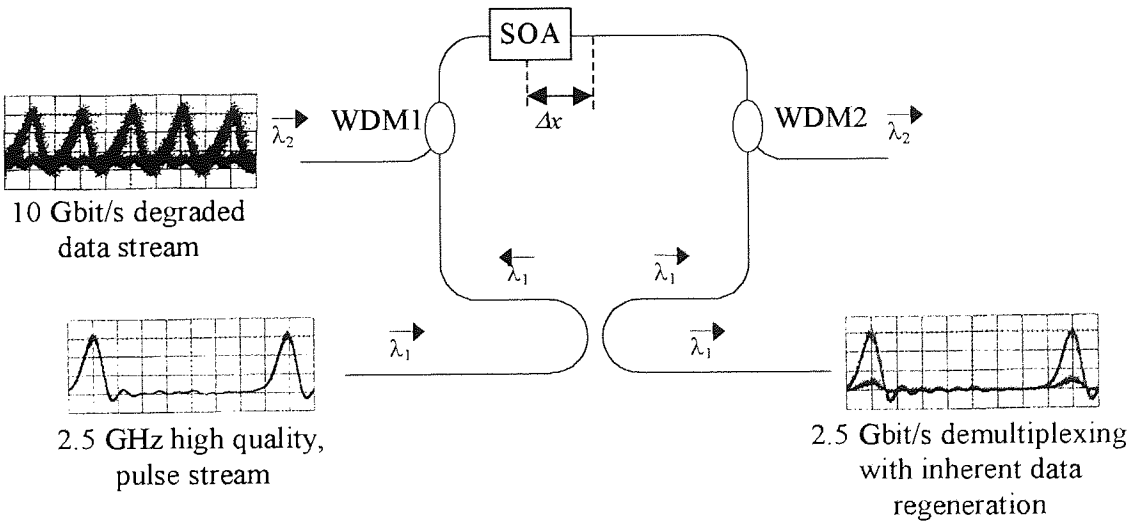

Figure 5-11. Demultiplexing with inherent data regeneration.

Figure 5-12 and Figure 5-13 shows the results of 10 Gbit/s to 2.5 Gbit/s demultiplexing with inherent data regeneration. To improve the stability of the SOA-NOLM, it was biased into transmission and switched into reflection; therefore achieving data inversion. A residual reflection on the base line degrades the measured Q of the demultiplexed signal.

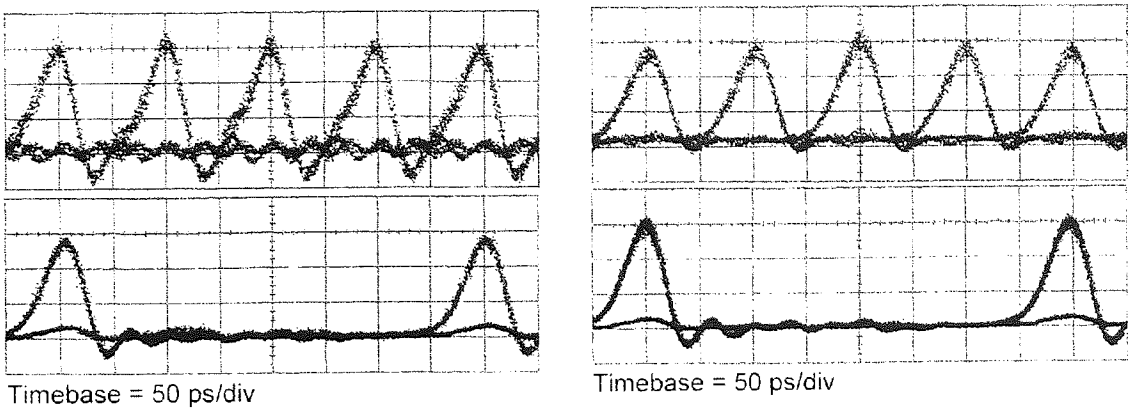

Figure 5-12. All-optical 10 Gbit/s to 2.5 Gbit/s demultiplexing with inherent data regeneration, using SOA-NOLM #2: (a) Q_{in} (10 Gbit/s) = 9.7, Q_{out} (2.5 Gbit/s) = 24.0; (b) Q_{in} = 8.5, Q_{out} = 19.8.

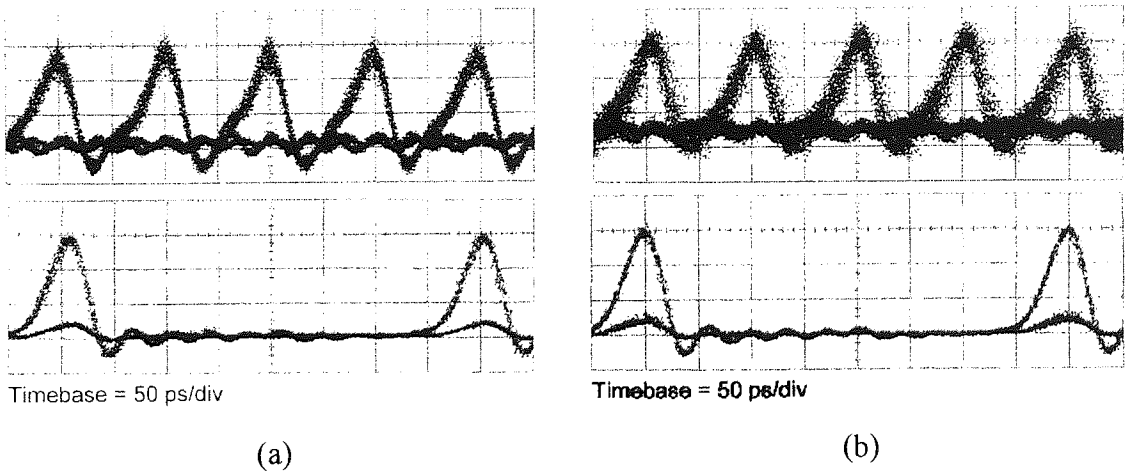

Figure 5-13. All-optical 10 Gbit/s to 2.5 Gbit/s demultiplexing with inherent data regeneration, using SOA-NOLM #2:
(a) Q_{in} (10 Gbit/s) = 7.0, Q_{out} (2.5 Gbit/s) = 15.3;
(b) Q_{in} (10 Gbit/s) = 7.0, timing jitter = 6.0 ps, Q_{out} (2.5 Gbit/s) = 13.9, timing jitter = 1.5 ps.

The Q values indicate excellent system performance. This is especially true in Figure 5-13b, which demonstrates all-optical data regeneration and demultiplexing. A 10 Gbit/s input with a Q of 7.0 and a timing jitter of 6.0 ps, is demultiplexed, and regenerated to a 2.5 Gbit/s output with a Q of 13.9 and a timing jitter of 1.5 ps.

5.3 Simultaneous Demultiplexing, Data Regeneration, and Clock Recovery using a Single SOA-NOLM

5.3.1 Introduction

A typical network architecture consists of a number of network nodes. It is recognised that each node needs to perform basic functions including demultiplexing, 'drop and insert' multiplexing, and clock recovery. Data regeneration may also be required to combat transmission impairments and ensure that each channel within the OTDM data stream has the same spectral and temporal characteristics. Conventionally each process is performed independently. This section demonstrated experimentally, simultaneous demultiplexing, data regeneration and clock recovery using a single SOA-NOLM.

5.3.2 All-optical sampling using an SOA-NOLM

If a train of ultra-short pulses is used as the control signal for an SOA-NOLM that has a periodic signal at its input (Figure 5-14), the output will consist of a series of pulses with amplitudes proportional to the magnitude of the input signal, at the temporal position of the control pulses [230]. In other words, the control pulses *sample* the signal pulses, see Figure 5-15a.

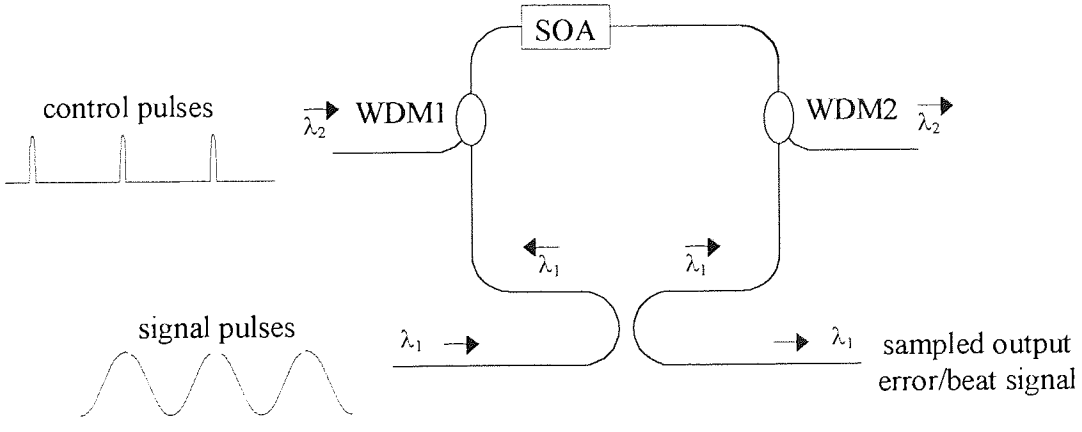

Figure 5-14. All-optical sampling using a SOA-NOLM.

If there is a frequency mismatch between the signal and the control pulse streams, then the output when detected on a photodiode will be full scale oscillations at the frequency difference between the two signals. This can therefore be used as an error signal to control a VCO, which drives either of the two input pulse streams. A closed loop is formed, with the SOA-NOLM acting as an all-optical phase detector analogous to a mixer in a classical electronic PLL.

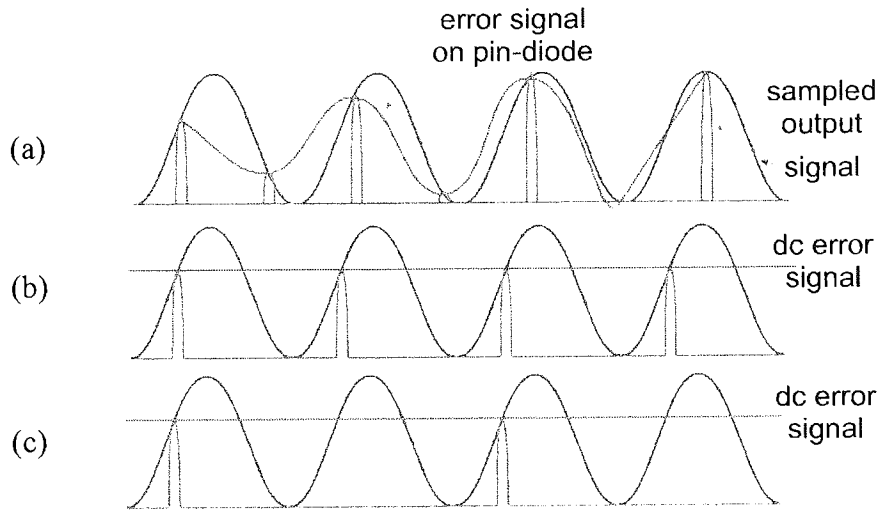

Figure 5-15. All-optical sampling: (a) frequency mismatch between signal and control pulse streams; (b) PLL converges to a dc level which represents a point of constant phase; (c) PLL can lock to sub-harmonics of the control pulse stream.

The PLL will converge to a dc level that represents a point of constant phase between the signal and control pulse streams, thus achieving clock recovery, see Figure 5-15b. The PLL will also lock to sub-harmonics of the signal pulse stream, see Figure 5-15c. Clock recovery can still be achieved if the periodic signal is replaced by a PRBS data sequence, and indeed, if the data sequence is used as the intense control signal used to switch the SOA-NOLM. This is the case with data regeneration. The main advantage of this technique is that it requires very simple low-speed control electronics.

5.3.3 Clock recovery using all-optical sampling

The experimental set-up is shown in Figure 5-20. The local optical clock was generated by an ECMLL modulated at 2.5 GHz by a VCO, producing 20 ps pulses at 1535 nm. The 10 Gbit/s control-pulse data-stream was produced by an actively stabilised fibre-

laser at 1555 nm producing 15 ps pulses. The two signals were all-optically mixed using the SOA-NOLM, which acts as an all-optical sampler, see section 5.3.2.

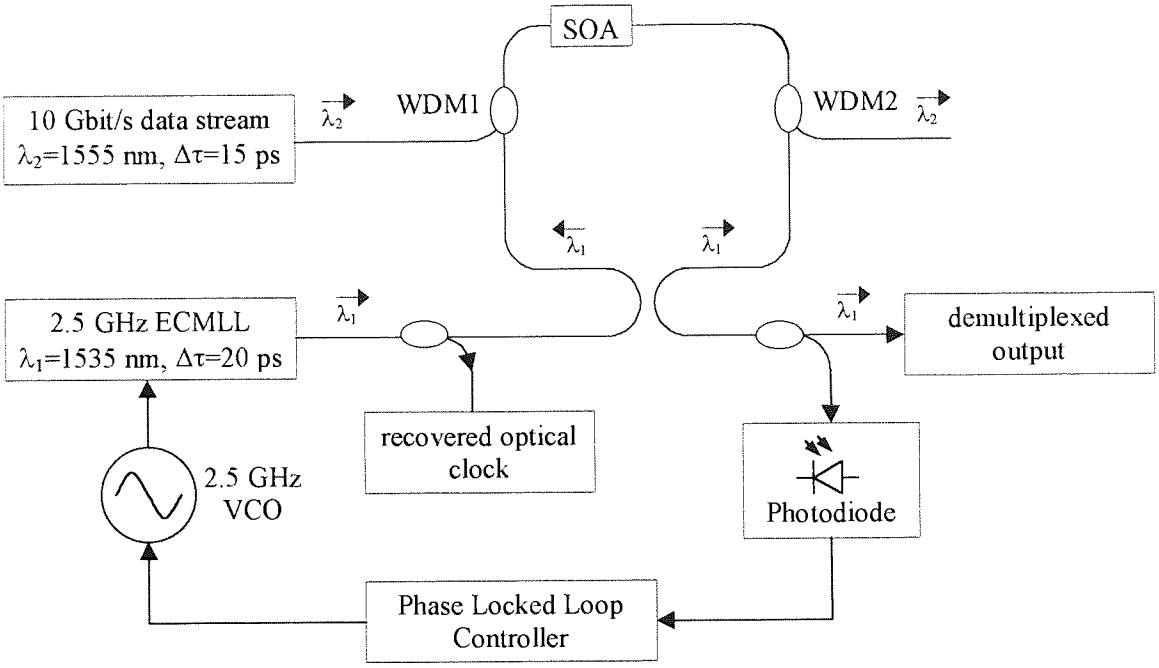

Figure 5-16. Experimental setup for simultaneous demultiplexing and clock recovery.

The output was amplified and split, 90% was monitored on a sampling oscilloscope and 10% detected on a 125 MHz photodiode. The frequency of the ECMLL was adjusted using the offset-bias on the PLL controller to be approximately 2.5 GHz. The output detected on the photodiode is shown in Figure 5-17, and is proportional to the phase difference between the two sources. This was fed through standard PLL controller electronics and into the VCO driving the ECMLL.

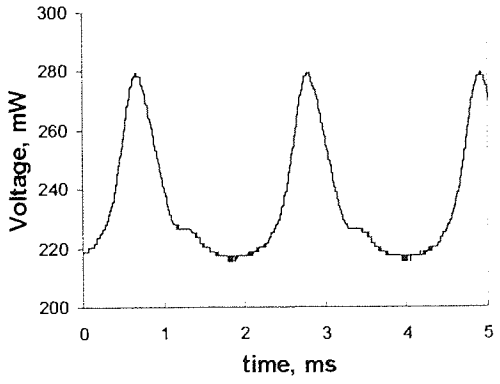

Figure 5-17. Beat signal between 10 Gbit/s fibre laser and 2.5 GHz ECMLL.

The microwave spectrum of the output from the 2.5 GHz VCO is shown in Figure 5-18a. The spectrum is unstable and has a frequency jitter of 40-50 kHz. Figure 5-18b shows the output from the VCO when the PLL was closed, and the 2.5 GHz base-rate clock has been recovered from the 10 Gbit/s OTDM data stream. The 2.5 GHz output from the unlocked VCO shown in Figure 5-18a appears to have a narrower linewidth than that of the recovered 2.5 GHz clock shown in Figure 5-18b. This is due to the sampling operation of the electrical spectrum analyser.

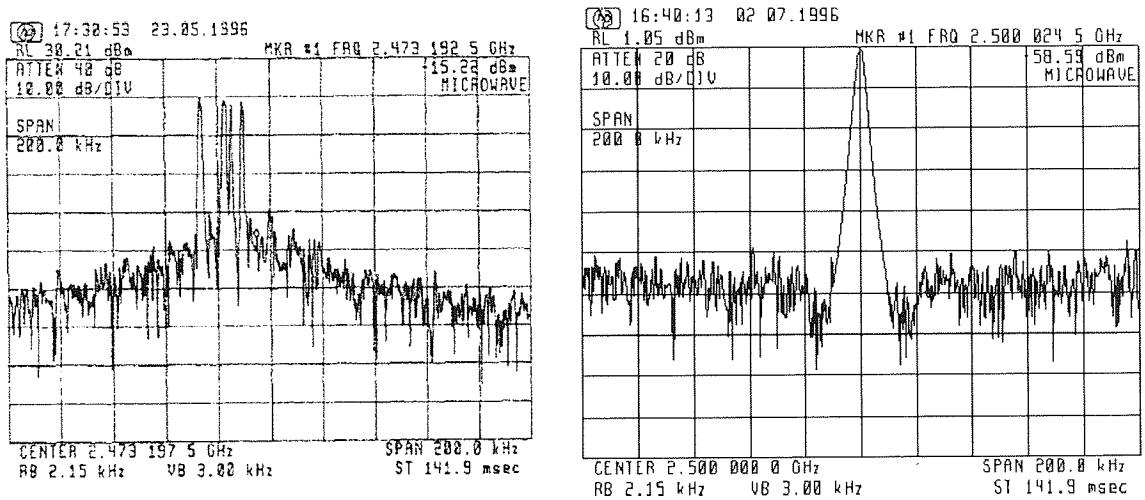

Figure 5-18. (a) 2.5 GHz output from VCO – PLL open; (b) 2.5 GHz recovered clock – PLL closed.

For maximum stability, the phase of the recovered clock must lock to the edge of the switching window, see section 3.6.3. Imperfect demultiplexing leads to eye closure, and a system penalty. This is illustrated in Figure 5-19, which shows a 10 Gbit/s OTDM input data stream, and the corresponding demultiplexed 2.5 Gbit/s output data stream. A distinct eye closure is observed on the 2.5 Gbit/s demultiplexed data stream.

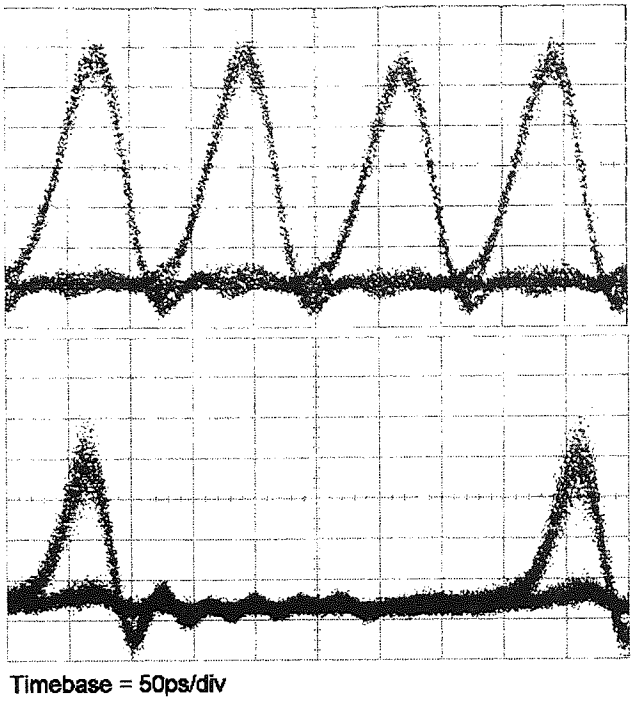

Figure 5-19. All-optical demultiplexing from 10 Gbit/s to 2.5 Gbit/s using SOA-NOLM#2.

Attempts to lock to the centre of the switching window, lead to instability problems because the system can not identify the direction of any phase drift; again this leads to a system penalty, and typically loss of clock recovery.

The phase of the recovered clock can be locked to the centre of the demultiplexer switching window with increased stability, by using a technique known as *dithering* to obtain a differential error signal [182, 181, 183]. This is covered in detail in the next section.

5.3.4 Stable clock recovery using a differential error signal

The experimental set-up is shown in Figure 5-20, and is based around that described in section 5.3.3. The local optical clock was generated by an ECMLL modulated at 2.5 GHz by a VCO, producing 20 ps pulses at 1533 nm. The 10 Gbit/s control-pulse data-stream was produced by an actively stabilised fibre-laser at 1555 nm producing 15 ps pulses. The two signals were all-optically mixed using the SOA-NOLM.

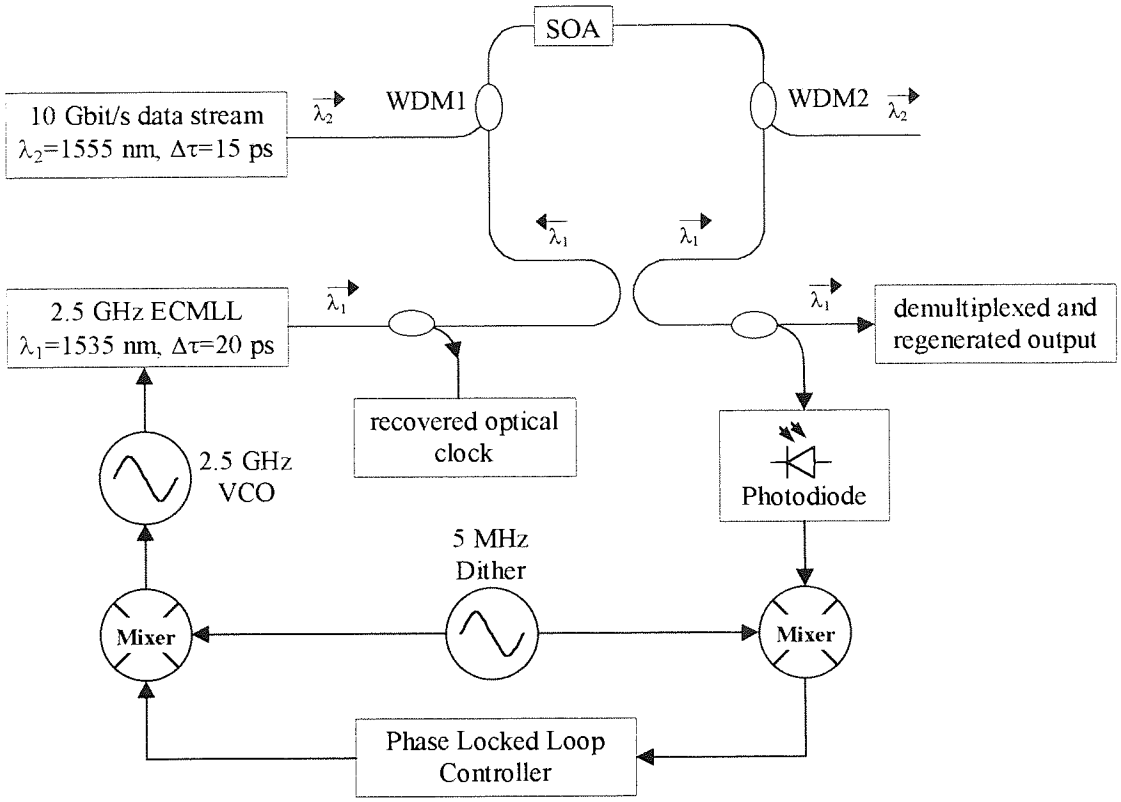

Figure 5-20. Experimental setup for simultaneous demultiplexing, data regeneration, and clock recovery.

A 5 MHz frequency dither was applied to the optical clock via the VCO used to drive the ECMLL. The signal detected on the slow photodiode consists of two complex components. The first is a large beat signal (and harmonics of) at the frequency difference between the two optical input signals. The second is a small error signal at the dither frequency of 5 MHz, which is proportional to the phase difference between the two signals. The dither signal component was extracted using a photodiode and a very narrow band electrical filter constructed from a *MAXIM* wideband transconductance amplifier (MAX435). The measured frequency response is shown in Figure 5-21.

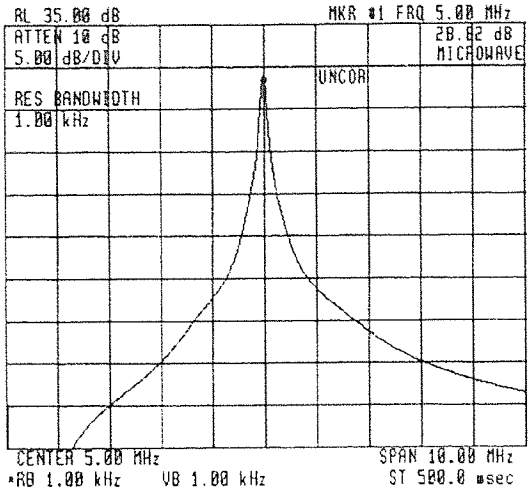

Figure 5-21. 5 MHz Narrow bandpass electrical filter. Gain = 28 dB, 3 dB bandwidth = 200 kHz.

The filter had a gain of 28 dB, a 3 dB bandwidth of 200 kHz, and could be tuned from 4 MHz to 6 MHz. The output from the filter was fed through a 5 MHz mixer driven by the local oscillator. The output was then fed to standard PLL control electronics, and used to drive the VCO. This can be seen schematically in the lower half of Figure 5-20.

Figure 5-22 shows the results of simultaneous demultiplexing, data regeneration and clock recovery. A 10 Gbit/s degraded data stream with a Q of 7.3 is demultiplexed to 2.5 Gbit/s and regenerated to a Q of 15.7. The recovered 2.5 GHz optical clock has a timing jitter of only 1.5 ps.

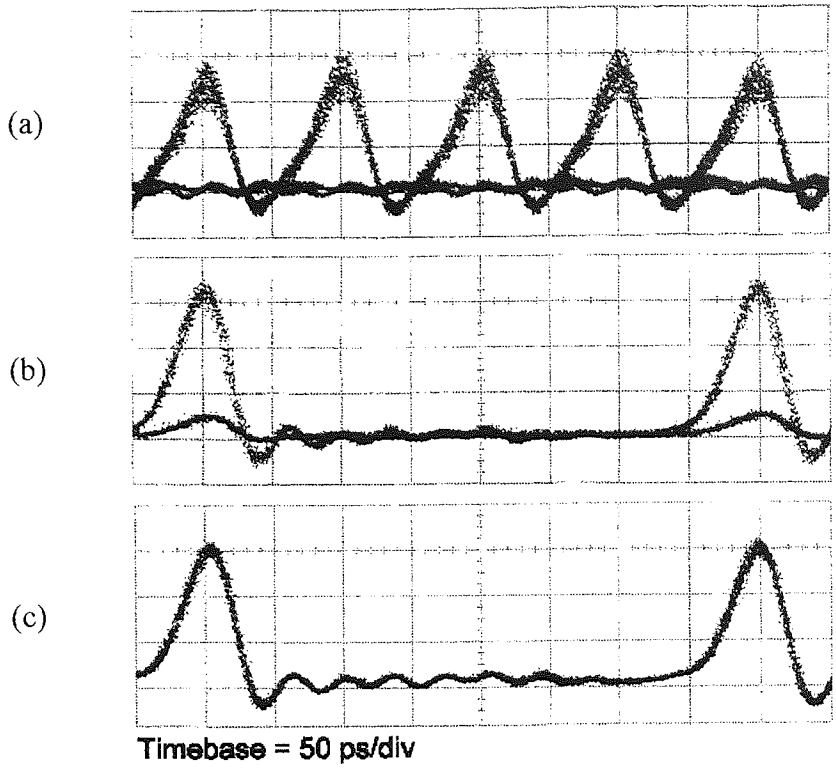

Figure 5-22. Simultaneous demultiplexing, data regeneration, and clock recovery: (a) 10 Gbit/s degraded input data-stream, Q=7.22; (b) 2.5 Gbit/s demultiplexed and regenerated data-stream, Q=15.66; (c) 2.5 GHz recovered clock, timing jitter=1.5 ps.

Figure 5-23 shows the microwave spectrum of the recovered electrical clock. At a span of 200 kHz the noise pedestal is 35 dB down. Increasing the span to 10 MHz reveals two side-bands components, which are 30 dB below the peak of the 10 GHz recovered clock.

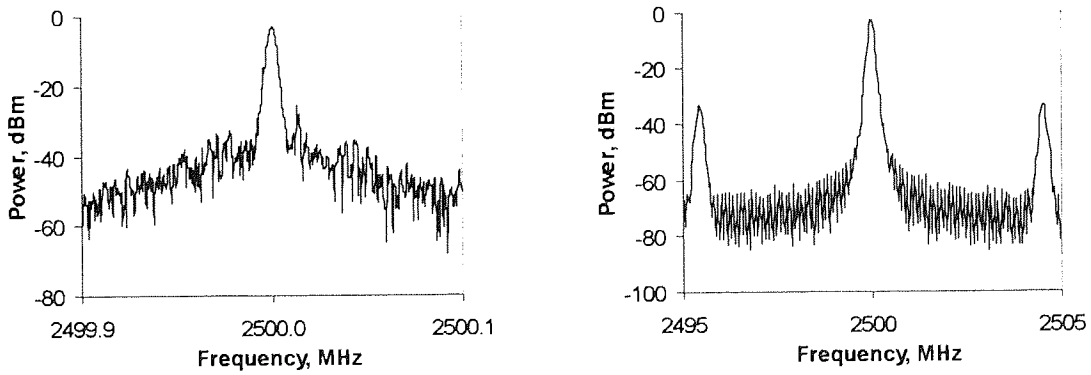

Figure 5-23. Microwave spectrum of the recovered electrical clock: (a) span 200 kHz, noise pedestal is 35 dB down; (b) span 10 MHz, dither components at fc ± 5 MHz are 30 dB down.

The components are a direct result of the *dithering* technique used in the clock recovery process, and cause a timing variation of 6 ps on the recovered clock. The timing variation can be minimised for measurement purposes by ensuring the optical and electrical clocks are in-phase, see Figure 5-24.

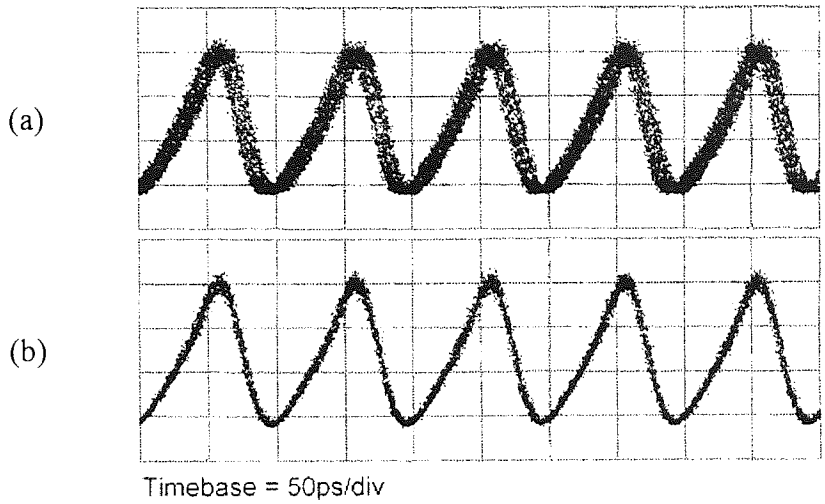

Figure 5-24. Recovered optical clock showing timing variation caused by frequency dithering: (a) Optical clock out-of-phase with trigger, timing jitter = 6 ps; (b) Optical clock in-phase with trigger, timing jitter < 1.5 ps.

5.4 Chapter Summary

This chapter has given details of the experimental analysis of the use of an SOA-NOLM as an all-optical data regenerator. This was achieved by letting the degraded data stream switch a locally generated high quality pulse stream into transmission. If the clock was operated at the OTDM line-rate, then full data regeneration was achieved. Alternatively, if the locally generated clock was operated at the OTDM base-rate, then simultaneous demultiplexing and data regeneration was achieved. The regenerative behaviour was quantified by comparing the input and output Q-values, measured using a HP 50 GHz digital sampling oscilloscope and a 30 GHz lightwave converter.

If the bit period of the switching data stream is less than the gain recovery time of the SOA, then patterning effects severely affect the regenerative performance of the device. 2.5 Gbit/s data regeneration was achieved using a 500 μm bulk SOA with a gain

recovery time of 300 ps. Excellent system performance was observed, with a degraded input data stream with a Q of 5.9 being regenerated to a Q of 18.4. 10 Gbit/s data regeneration was demonstrated using a 1000 μm MQW-SOA with a gain recovery time of 100 ps. Similar regenerative behaviour was observed, however a small facet reflection artificially degraded the results obtained. Since this experiment, BT Laboratories have developed high gain SOAs with tapered waveguides and angle facets [221]. The gain ripple on such devices is almost zero, making measurements of the facet reflectivity almost impossible. It is anticipated that such devices would have superior regenerating properties.

A degraded 10 Gbit/s data stream with a Q of 7.0 and a timing jitter of 6.0 ps was demultiplexed and simultaneously regenerated to a 2.5 Gbit/s data stream with a Q of 13.9 and a timing jitter of 1.5 ps. A high switching extinction ratio was achieved and interchannel crosstalk eliminated, simply by the absence of light from the clock pulses used to probe the switching of the SOA-NOLM. Such a configuration would be advantageous within an OTDM 'drop and insert' node.

To achieve data regeneration at higher data-rates, the SOA gain recovery time must be reduced. This maybe achieved by optimising the SOA design. For example, a low temperature grown strained MQW InGaAs/InAlAs doped with Beryllium [231] has been demonstrated with a recovery time of around 1ps. This should allow all-optical switching and data regeneration up to 1 Tbit/s.

The experimental setup was extended to enable simultaneous clock recovery. This was achieved by exploiting the inherent sampling ability of the SOA-NOLM, and using it as an all-optical mixer in a PLL configuration. A 10 Gbit/s degraded input data stream with a Q of 7.3 was demultiplexed to 2.5 Gbit/s and simultaneously regenerated to a Q of 15.7, while recovering the optical and electrical clocks. A technique known as dithering was used to ensure that the phase of the recovered clock locked to the centre of the switching window, therefore enabling full switching and optimum data regeneration. The

clock recovery technique used low-speed control electronics, but exhibited a relatively large timing variation due to the dithering process. This was minimised for measurement purposes by ensuring that the optical and electrical clocks were in-phase. Although relatively stable, the clock recovery system was susceptible to changes in input power. In the long term, these problems could be overcome by improved control electronics.

Chapter 6

Introduction to electroabsorption modulators

6.1 Introduction

Electroabsorption (EA) modulators are stable, compact devices requiring simple sinusoidal drive electronics, and have been used in impressive OTDM network demonstrations [73, 74, 111, 181]. They are therefore very promising candidates for use as a principal component within the next generation (> 100 Gbit/s) of OTDM networks. Applications include, low-chirp picosecond optical-pulse generation [232, 233, 234, 235], data modulation [248], simultaneous pulse generation and data encoding using a single device [84], 80-10 Gbit/s OTDM demultiplexing [236], actively mode-locked ring laser incorporating an EA modulator [237], analogue transmission [238, 239], and wavelength conversion [240]. Another attractive feature is that they can be monolithically integrated with other semiconductor optical devices. To date an EA modulator has been integrated with a CW-DFB [241, 242, 235], an SOA [243], and more recently a fully integrated optical data source has been produced [244]. Here, the light from a CW-DFB was modulated by an EA modulator to produce transform-limited picosecond pulses, which were then amplified using a SOA, before being modulated using a second EA modulator to produce a high quality data-stream. Five 20 GHz modulators have also been integrated on an InP-based passive-multiplexer for use in a 100 Gbit/s OTDM network [245]. The disadvantage with device integration is that as the number of elements increases, then the yield falls. Device reliability may also be an issue, i.e. if a single device fails, then the complete integrated device would need to be replaced.

This chapter discusses the basic operating characteristics of an EA modulator with an emphasis on its use in an OTDM network. It outlines the fundamental physical processes

behind such a device, before discussing some typical structures and associated operating parameters.

It then outlines in theory and confirms experimentally, the use of such a device as a picosecond optical-pulse source, before discussing its use as an electro-optical switch, for either demultiplexing or 'drop and insert' multiplexing. The next chapter draws upon the fundamental operating characteristics outlined in this, by demonstrating three novel experiments that utilise the device in a bi-directional configuration, with an aim to reduce network management, complexity, and cost.

6.2 Electroabsorption Modulator Design and Characterisation

Although the design and fabrication of EA modulators is in its infancy, devices have already been demonstrated with superb operating characteristics. Recently, packaged devices have been demonstrated with modulation bandwidths in excess of 40 GHz, low driving voltages (~2V), and low polarisation sensitivity (<1 dB) [246, 247, 248]. This section starts by describing the electroabsorption effect, the fundamental principle behind all EA modulators. It then describes the different types of EA modulator available, before concentrating on the design and optimisation of a MQW EA modulators.

6.2.1 Electroabsorption effect

The complex refractive index of a semiconductor material can be divided into real and imaginary components. The real part of the complex index determines the velocity of the light propagating through the material, and the imaginary part determines the attenuation of the propagating light. If the semiconductor material is placed in an electric field, then both the real and imaginary parts of the refractive index maybe modified. Electro-optic devices, (e.g. $LiNbO_3$ AM modulator) exploit a change in velocity of light through the material [249]. Electro-absorption devices exploit the changes in materials optical absorption characteristics [106]. This effect is illustrated with reference to Figure 6-1. As the magnitude of the electric field is increased, then the absorption edge of the

semiconductor will shift to higher wavelengths, which results in a change in the optical absorption coefficient at a particular operating wavelength. In bulk materials, the phenomenon is associated with the Franz-Keldysh effect [250], and in MQW regions it is associated with the quantum-confined Stark effect (QCSE) [251, 252]. Electro-absorption due to the QCSE can be up to fours larger than for similar bulk materials [249].

Figure 6-1. Absorption spectra illustrating the electro-absorption effect. Figure is based on data for a MQW device, where electro-absorption is due to the quantum confined Stark effect, see reference [256].

An EA modulator is a semiconductor device in which an undoped absorber layer is sandwiched between extrinsically p- and n- doped semiconductor layers to form a pin junction, see Figure 6-2a. The absorption layer can be either a bulk material, or based on a MQW configuration. When the device is reverse biased, the voltage is dropped directly across the absorber layer, generating a high-electric field that in a MQW device, results in a increase in the absorption coefficient, as shown in Figure 6-2b.

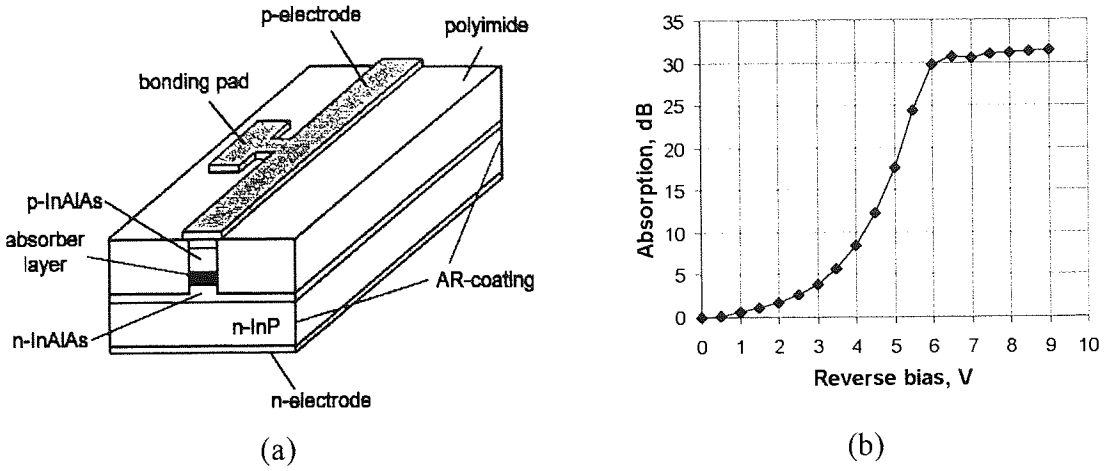

Figure 6-2. (a) A typical structure of a lumped-element (LE) electrode EA modulator; (b) Absorption characteristics of an EA modulator.

Relatively little work has been devoted to bulk EA modulators, although recently a polarisation-insensitive EA modulator was demonstrated with an extinction ratio of 40 dB, an insertion-loss of 11 dB, and a 20 GHz bandwidth [253]. MQW EA modulators are used throughout this thesis, and are considered in more detail in the following section.

The modulator shown in Figure 6-2a uses a lumped-element (LE) electrode to apply the electric field. Devices of this kind suffer from bandwidth limitations due to CR constants. A relatively new type of EA modulator that avoids this limitation, is known as a travelling-wave (TW) device, and is shown in Figure 6-3.

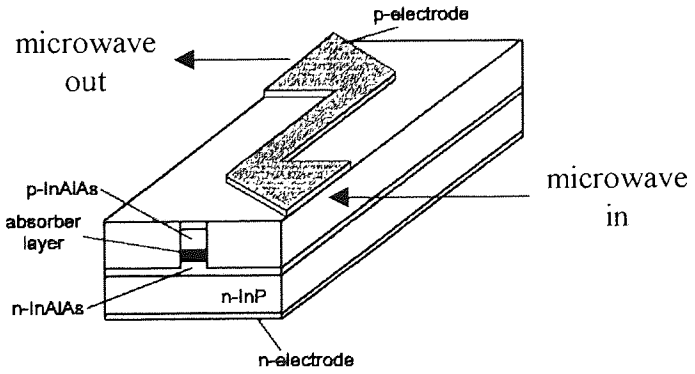

Figure 6-3. Typical structures of a travelling-wave EA modulator;

TW-EA modulators consist of an optical waveguide (i.e. the absorption layer) and a parallel electrical waveguide. Optical and electrical field co-propagate through the

device. TW-EA modulators, unlike LE-EA modulators do not suffer from CR-constant limitations. They do however suffer from a 'walk-off' effect between the two fields, which limits the interaction length and therefore the maximum extinction ratio. Recently, a polarisation-insensitive MQW TW-EA modulator was demonstrated with a bandwidth of 25 GHz, and an extinction ratio of 30 dB, for a driving voltage of 4 V [254]. It is predicted that such a device should allow EA modulators to be developed with bandwidths greater than 100 Gbit/s [254].

6.2.2 MQW EA modulator design and optimisation

Figure 6-4 shows a ridge buried heterostructure electroabsorption modulator fabricated using metallorganic vapour phase epitaxy (MOVPE), consisting of an InGaAsP/InGaAsP MQW absorber layer, comprising seventeen 95 Å wells (λ_g = 1.55 μm) separated by 55 Å barriers (λ_g = 1.10 μm) [232, 233]. This is embedded in a Fe-doped InP current blocking structure, which ensures that the modulating voltage is efficiently applied across the depleted absorption layer.

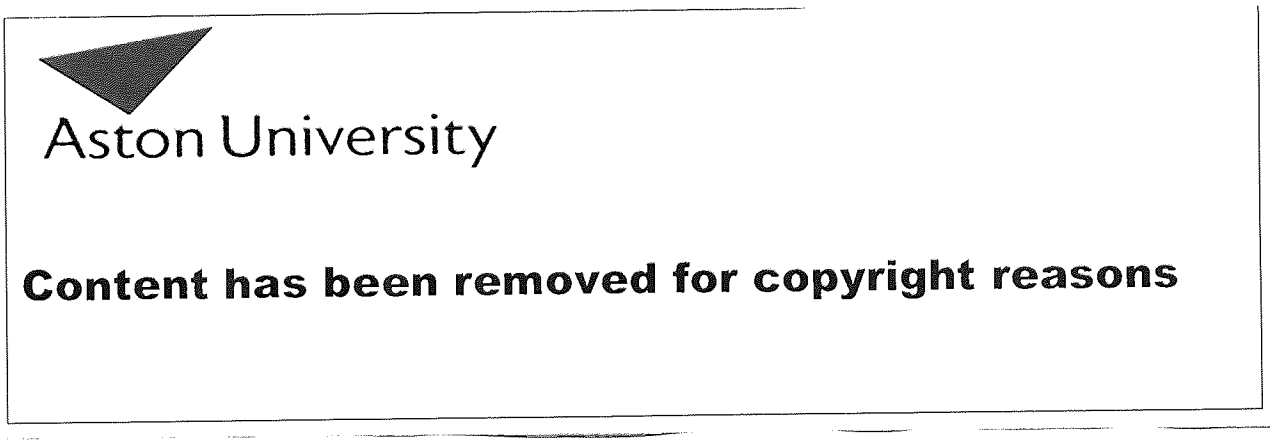

Figure 6-4. Cross-section of a ridge-buried heterostructure electroabsorption modulator. See reference [233]

The cross-sectional geometry was designed to minimise device capacitance and was measured to be 1.33 pF/mm. A 325 μm packaged device had a bandwidth in excess of 10 GHz, an insertion loss of ~10.5 dB, and a modulation depth of 25 dB.

As discussed in the introduction, the most promising use of an EA modulator within an OTDM network is as a picosecond pulse source or as a high-speed demultiplexer. With this in mind the following attributes or parameters must be considered and optimised.

a) modulation speed or frequency response
b) modulation efficiency and driving voltage
c) extinction ratio or modulation depth
d) insertion loss
e) device saturation power
f) polarisation sensitivity
g) chirp parameter

The design of an EA modulator is complex, and a trade-off is typically made between the above parameters, depending on the exact application. The following section is intended to outline the importance of the above parameters, and indicate how they can be optimised.

a) Modulation speed or frequency response

Within an OTDM network, the required extinction ratio of an optical pulse source, and a high-speed demultiplexer will depend on the number of OTDM channels (see section 3.7). High-bandwidth devices are therefore desirable, allowing the OTDM base-rate to be maximised, while reducing the number of channels necessary to achieve the required line-rate, and so relaxing the device extinction ratio requirements. Bandwidths of greater than 10 GHz are common, but devices of 40 GHz have been demonstrated [246]. It must also be pointed out that this also places stringent requirement on the electronic equipment necessary to encode the data at such high data-rates, in which case all-optical data-encoding techniques may have to be employed [112, 115]. Optimisation of the device bandwidth is discussed below.

The frequency response of an EA modulator is primarily limited by the capacitance of the device and the associated packaging. The capacitance is inversely proportional to the device length, (but also depends on the precise structure); therefore, high modulation

speeds can be achieved by decreasing the length of the active modulation region. At frequencies of > 40 GHz a device length of ~100 μm is required, making it harder to cleave and package. This limit has recently been overcome by sandwiching the active modulation region within a passive integrated waveguide that is used to couple light into, and out of the device [248]. The total device length is kept long enough for easy fabrication and packaging, while enabling independent control of the length of the modulation region to be achieved. An optimised packaged EA modulator with a device length of 1.5mm and a 63 μm active region exhibited a 3 dB electrical bandwidth of greater than 40 GHz [248]. The device had a relatively low driving voltage of 3V, an extinction ratio of 15 dB, and an insertion loss of 8 dB was achieved. A present this device is unstable for use in an OTDM network due to the relatively low extinction ratio.

b) Modulation efficiency

The modulation efficiency of an EA modulator is given by the highest gradient of the absorption vs. reverse bias characteristic, see Figure 6-2b. The higher the modulation efficiency the lower the duty-cycle, which in turn gives the minimum obtainable pulse width, or switching window at a given drive frequency. Increasing the device modulation efficiency also relaxes the requirements of any high-speed electronic amplifiers used. At 10 GHz a modulation efficiency of 10 dB/V is common, but devices with 20 dB/V have been reported [255, 256].

c) Extinction ratio or modulation depth

As the number of channels in an OTDM system is increased, inter-channel interference becomes more significant, and the extinction ratio becomes an increasingly important parameter. High modulation-depth EA modulators are therefore required for the tasks of demultiplexing and pulse generation. Section 3.7 outlines the extinction ratio requirements for both the optical pulse source and the demultiplexer. For error-free operation a picosecond pulse source suitable for use in an 8×10 Gbit/s OTDM system requires a background intensity or extinction ratio of > 44 dB. The demultiplexer should have an extinction ratio of > 22 dB to give a penalty of < 0.5 dB.

The device extinction ratio depends on the length of the modulation region [248], with a longer device resulting in a higher extinction ratio. However, to increase the frequency response, the length of the active modulation region is typically decreased, and so these two parameters are traded-off depending on the required application. The extinction ratio can also be improved by increasing the number of MQW within the active region [248].

Another factor that limits the device extinction ratio, is a mismatch between the numerical aperture (spot-size) of the fibre and of the modulator. A proportion of the light that is not coupled into the fundamental mode of the modulator, may pass through the device as a higher-order parasitic-mode, and be subsequently coupled into the fibre at the output of the device. To overcome this limitation a new high-modulation depth EA modulator has recently been demonstrated [233], and is illustrated below.

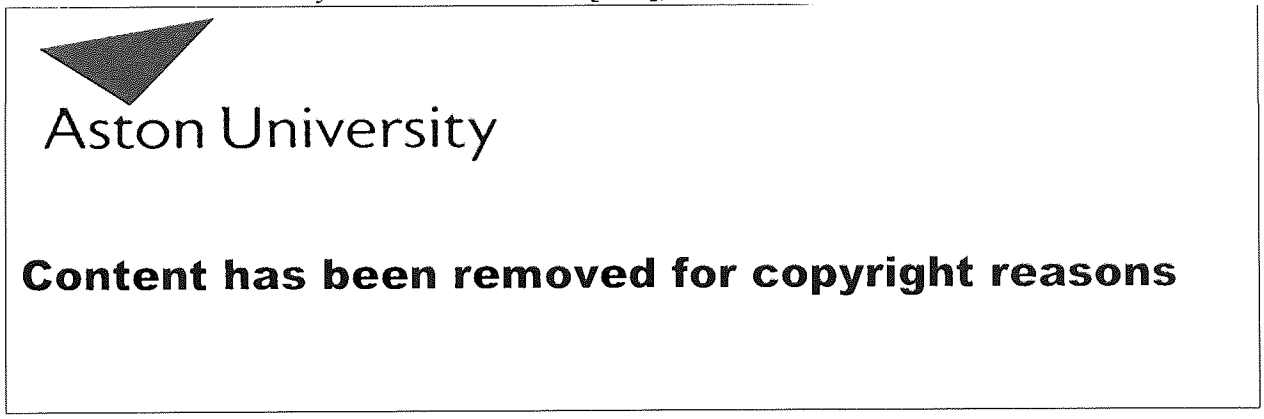

Figure 6-5. Deeply ridge buried heterostructure electroabsorption modulator. From reference [233].

Figure 6-5 shows a deeply ridge buried heterostructure electroabsorption modulator, designed to remove stray light from the vicinity of the MQW. The device structure is based on ridge-buried heterostructure shown in Figure 6-4. The thickness of the Fe-InP blocking layer was doubled to 5 μm, and the lateral profile was extended to 25 μm, while the width of the p-InP mesa was decreased to 6.5 μm. The MQW absorber layer remained unchanged for a direct device comparison. Increasing the thickness of the Fe-doped InP layer has the added benefit of significantly reducing the device capacitance by 30% to 0.92 pF/mm. Packaged 371 μm long devices had a 3-dB bandwidth of 14 GHz,

a 7 dB insertion loss, and a 40-50 dB extinction ratio. A device of this kind was used in the experiments detailed in the next chapter.

d) Insertion loss and, e) Device saturation power

An ideal modulator should have zero insertion loss and a high saturation power that is less than the damage threshold of the device. Typical EA modulators, exhibit a high insertion-loss (~10 dB), but a low saturation power, commonly + 6 dBm. Optical amplifiers are therefore necessary both before and after the modulator; this dramatically increases the system cost.

A typical EA modulator has an insertion loss of 7-12 dB, of which MQW and carrier absorption can account for less than $1/3^{rd}$ of this value, the remaining loss is dominated by fibre coupling losses of around ~3 dB per facet. This is due to a numerical aperture mismatch between the optical fibre and the modulator, outlined previously, and in theory could be reduced by using a tapered waveguide each side of the modulator, which are designed to expand the modulator spot size to match that of the fibre. A similar technique has been demonstrated with semiconductor optical amplifiers, where the coupling loss per facet was reduced from 3–4 dB to less than 1 dB [221]. The technique also has the added advantage that the facet reflectivity is reduced to an almost immeasurable value, which becomes an important parameter when the device is operated in a bi-directional configuration, as described in the next chapter.

f) Device polarisation-sensitivity

MQW EA modulators are typically sensitive to polarisation, which is due to a polarisation-dependence in the optical-confinement factor and field distribution of the waveguide. It can be minimised by matching the energy of the light- and heavy-hole transitions to reduce band discontinuities, in practice this is achieved by introducing tensile-strain and optimising the layer composition of the MQW [247, 256, 257]. Device optical saturation power can also be improved using the same technique [258].

g) Chirp parameter

The chirp parameter α of an optical transmitter, together with the dispersion D of the optical fibre will set the upper limit on the maximum transmission distance.

Chirp is an inherent property of intensity modulated light, originating as a phase shift as the intensity is varied. The chirp parameter α is the derivative of the n verses k curve, where n and k are the real and imaginary parts of the modal index of the electroabsorption waveguide [259].

$$\alpha = \frac{\partial n}{\partial k} \qquad \text{Equation 6-1}$$

A simple and fast method of measuring the chirp-parameter of an externally modulated CW source, is performed using a network analyser. The network analyser is used to measure the small-signal frequency response of the optical source under test, a dispersive medium, and a high-speed receiver [260]. Sharp resonance frequencies are observed originating from an interference effect between carrier and sideband wavelengths. From this, both the fibre dispersion and chirp-parameter can be easily calculated, using [260]:

$$f_u^2 L = \frac{c}{2D\lambda^2}\left(1 - \frac{2}{\pi}\arctan(\alpha)\right) + \frac{c}{2D\lambda^2}(2u) \qquad \text{Equation 6-2}$$

where f_u is the resonance frequency, D is the dispersion of the fibre, L is the fibre length, λ is the operating wavelength, and α is the chirp parameter. Plotting $f_u^2 L$ verses $2u$ gives a straight line whose slope and position yield the dispersion and chirp parameter. The technique should be restricted for measurements of $-10 < \alpha < 10$, and has an uncertainty of ± 0.1. The chirp-parameter varies with reverse bias, and is commonly less than 0.7 for an EA modulator.

6.3 Pulse Generation and Switching using an EA Modulator

The EA modulator has been used primarily for low-chirp picosecond optical pulse generation [232, 234], high-speed (80×10 Gbit/s) OTDM demultiplexing [236], and has been the key component in a number of impressive OTDM system experiments [73, 74,

111, 181]. This section describes how such a device is used for the above applications; it outlines the fundamental operating characteristics and compares then with experimental results.

6.3.1 Picosecond pulse generation using an EA modulator

In contrast with modulators that use the electro-optic effect, the EA modulator exhibits absorption characteristics that increase exponentially with reverse bias voltage, a characteristic that can be exploited for ultra-short optical pulse generation. Figure 6-6 shows the experimental setup of a picosecond pulse source based on the external modulation of a CW laser by an EA modulator.

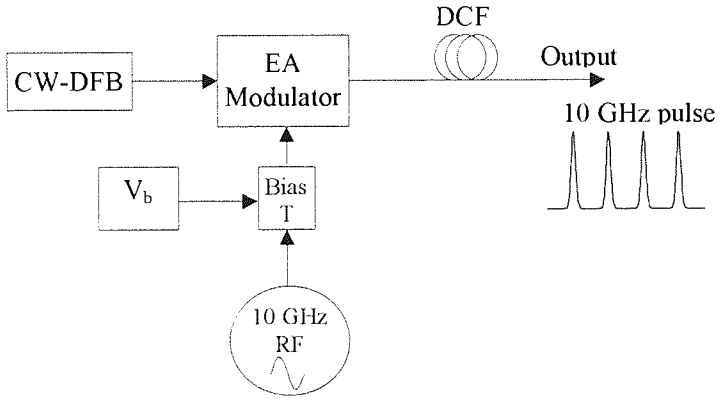

Figure 6-6. Experimental setup of a 10 GHz pulse source based on an EA modulator.

A CW-DFB is incident on one facet of the EA modulator. The device is biased into absorption, and a sinusoidal voltage is applied to the reverse bias, see Figure 6-7. This periodically switches the EA modulator into transmission, and the CW signal at the input to the device, emerges at the output as a high-speed optical pulse stream.

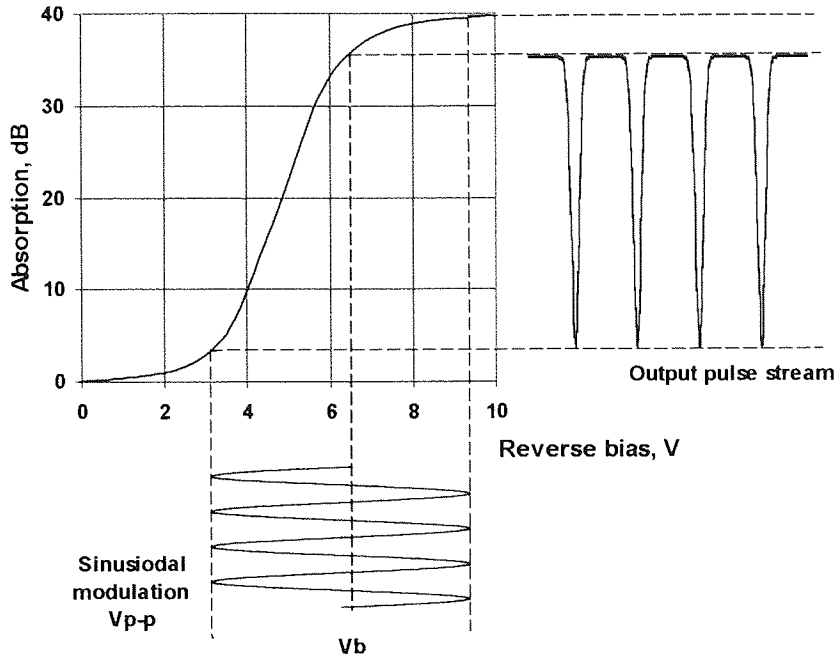

Figure 6-7. Nonlinear absorption characteristics of an electroabsorption modulator used to generate an ultra-short pulse stream with a sinusoidal drive signal.

The exact temporal profile of the pulse stream depends on the reverse bias voltage V_b, the modulation voltage $V_{p\text{-}p}$, and the modulation coefficient k_1, defined as the peak gradient of the absorption characteristics. The experimental setup shown in Figure 6-6 was used to investigate the use of an EA modulator as a pulse source.

A packaged 370 μm deeply-ridged, MQW buried heterostructure EA modulator was supplied by *Dave Moodie* at BT Laboratories. The device is similar in design to that shown in Figure 6-5, however the MQW absorption layer is strained to reduce the polarisation sensitivity of the device. The device packaging allows the EA modulator to be externally terminated at 50 Ω. This increases the device frequency response. It also enables two RF drive signals to be applied simultaneously, therefore allowing simultaneous pulse generation and encoding [84]. The device (BT device number: MV2276A12-11) is referred to as EAM#1 throughout the remainder of this thesis. The measured insertion-loss characteristics of the device are shown in Figure 6-8.

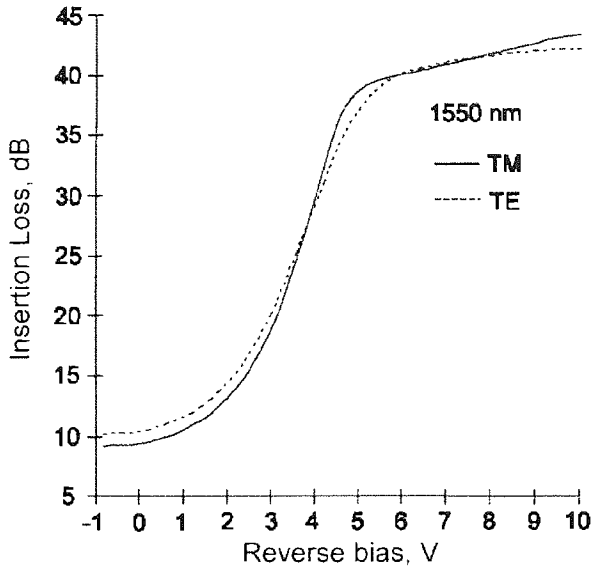

Figure 6-8. Insertion-loss characteristics of a 372 μm deeply-ridged polarisation-insensitive MQW buried heterostructure, with a ~12 GHz electrical bandwidth and a modulation efficiency, k=10 dB/V. BT Device number: MV2276A12-11

The device has an insertion loss of ~10 dB, a modulation coefficient of 10 dB/V, and a polarisation sensitivity of less than 1 dB. The frequency response characteristics are shown in Figure 6-9.

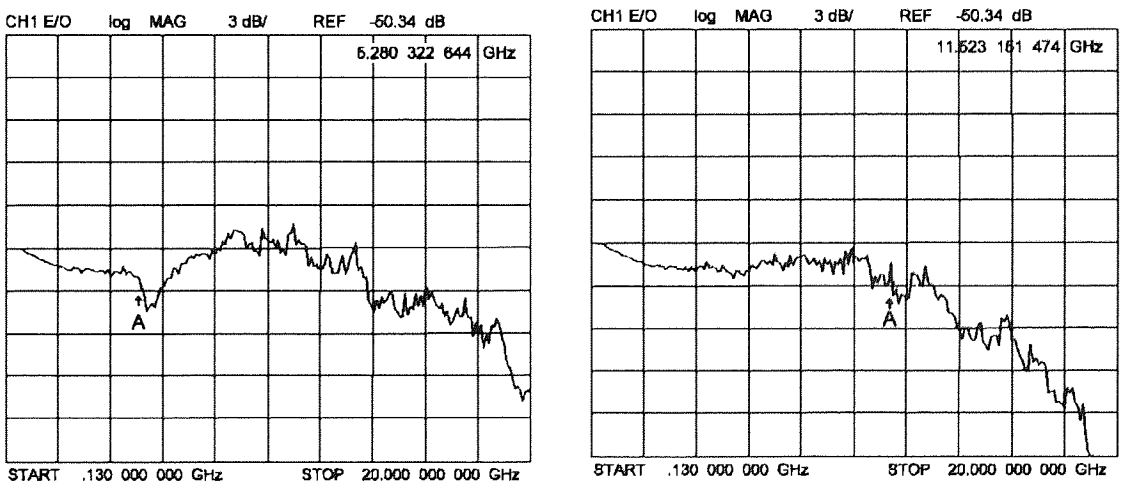

Figure 6-9. Frequency response characteristics of EAM#1; (a) RF input #1, 3-dB bandwidth = 5.3 GHz; (b) RF input #2, 3-dB bandwidth = 11.5 GHz; A 370 μm deeply-ridged polarisation-insensitive MQW buried heterostructure. BT Device number: MV2276A12-11

The 3-dB electrical bandwidth of RF input#1 is ~5 GHz, and the bandwidth of RF input#2 is ~12 GHz. Therefore, to obtain optimum device performance, RF input#1 was terminated using a bias-T to remove the DC component and was then terminated at

50 Ω. The device was reverse biased at ~7 V using a bias-T, and sinusoidally modulated using a 10 V_{p-p}, 10 GHz drive signal derived from a HP synthesiser and a 10 GHz narrow band MITEQ amplifier. A polarisation controller was used at the input to maximise the output power and optimise the pulse characteristics. The pulse width was measured to be ~14.4 ps using an autocorrelator. The spectral width was 0.35 nm, given a time-bandwidth product of 0.62, indicating the pulses contained a small amount of chirp. The characteristics are shown below in Figure 6-10.

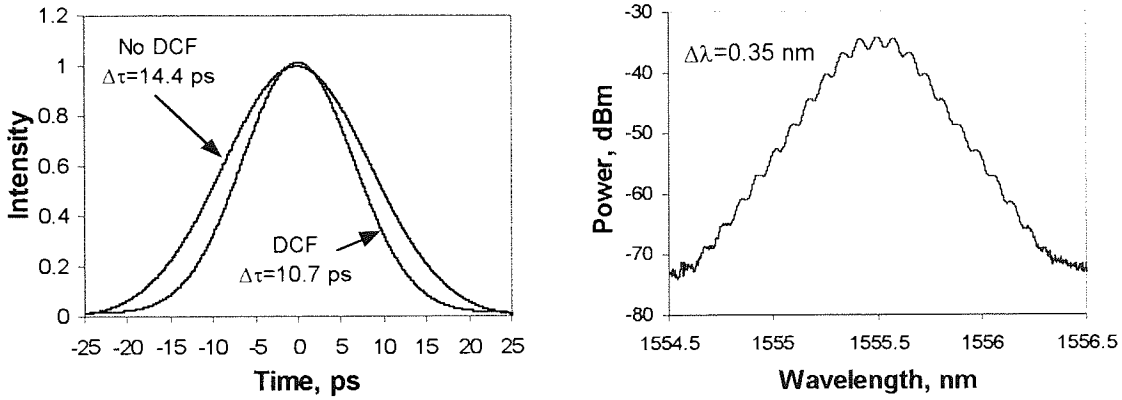

Figure 6-10. Autocorrelation and optical spectrum of a 10 GHz pulse generated using an EAM#1, V_b = 6.8 volts, V_{p-p} = 10 volts.

The pulses were compressed using DCF with a total dispersion of –20 ps/nm/km, producing 10.7 ps pulses with a time-bandwidth product of 0.46.

6.3.2 Optical switching or gating using an EA modulator

For demultiplexing applications, the transmission window must be approximately rectangular and narrow enough to select the required channel, while the extinction ratio must be high, to sufficiently reject any remaining channels. For channel-drop functionality the transmission window must be wide enough to allow all but one channel to pass, while selectively absorbing the remaining channel. The transmission window of a sinusoidally driven EA modulator can be modified to meet these conditions by simply changing the reverse bias voltage [261]. Figure 6-11 shows a typical experimental setup, indicating the required switching functions for both demultiplexing and the drop functionality.

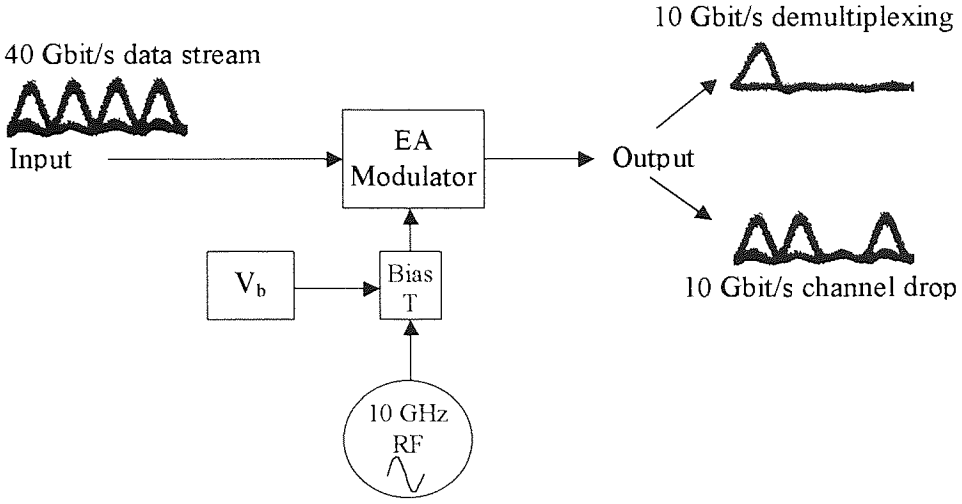

Figure 6-11. Optical switching to achieve either demultiplexing with device biased into absorption and modulated into transmission, or channel-drop functionality with the device biased into transmission and modulated into absorption.

To analyse the switching characteristics in more detail, the same assumptions will be adopted as for those investigated using an EA modulator as a pulse source, namely: (i) the extinction ratio is proportional to reverse bias, and can be approximated by a linear ramp function with a modulation coefficient, k_1 equal to 10 dB/V; and in addition (ii) loss in forward bias is constant (i.e. free-carrier absorption in forward bias is negligible) (iii) device insertion loss will be ignored.

The EA modulator drive voltage V_{in}, can be denoted by:

$$V_{in} = V_b - \frac{V_{p-p}}{2}\sin\theta \qquad \textbf{Equation 6-3}$$

And consists of a sinusoidal drive voltage of phase θ, and amplitude V_{p-p} which is superimposed onto a small reverse bias V_b, see Figure 6-12a. The output power from the modulator P_{out}, assuming a CW input P_{in} is given by:

$$P_{out} = P_{in}\,10^{k_1(V_{in}-V_1)/10} \qquad \textbf{Equation 6-4}$$

Where k_1 is the modulation or absorption coefficient, and V_1 is intercept of the ramp function, shown in Figure 6-8. The output from the modulator will be in general a train of near rectangular pulses, see Figure 6-12b, whose width is determined by the drive parameters, V_b, V_{p-p}, and the modulation coefficient, k_1.

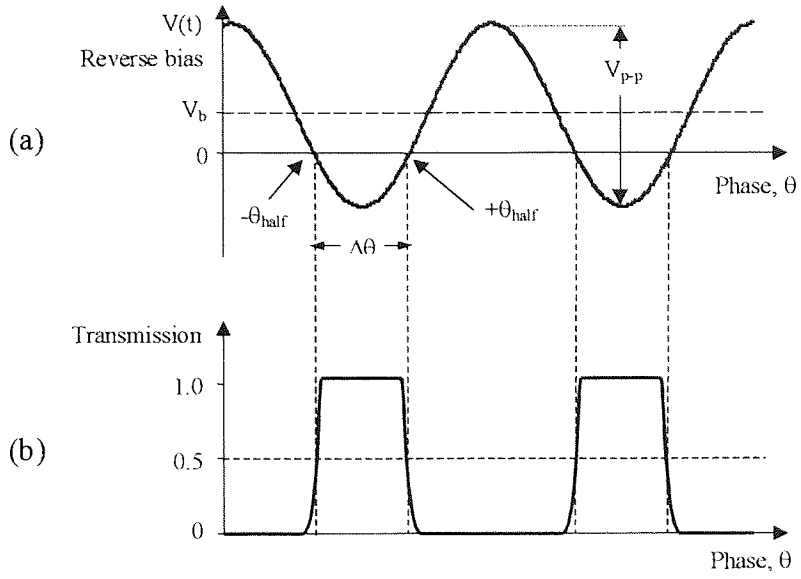

Figure 6-12. Drive signal applied to the modulator, and the optical output from the modulator, exhibiting optical gating

The full-wave half-maximum switching window width can be calculated by defining θ_{half} as the phase where the optical power at the output of the EA modulator is half that of the input power, i.e. $P_{out} = \frac{P_{in}}{2}$. Substituting into Equation 6-4 gives the corresponding voltage at the θ_{half} point.

$$V_{in-half} = V_1 - \frac{10\log 2}{k_1} \qquad \textbf{Equation 6-5}$$

θ_{half} can then be calculated by rearranging Equation 6-3 and substituting Equation 6-5.

$$\theta_{half} = \sin^{-1}\left(\frac{20\cdot\log 2 + k\cdot V_b - k\cdot V_1}{k_1\cdot V_{p-p}}\right) \qquad \textbf{Equation 6-6}$$

The phase, $\Delta\theta$ which is equal to the switching window width is then given by:

$$\Delta\theta = \pi - 2\cdot\theta_{half} \qquad \textbf{Equation 6-7}$$

And the switching window width, $\Delta\tau$ is then given by:

$$\Delta\tau = \frac{\Delta\theta}{2\pi}T$$
$$= \frac{\pi - 2\sin^{-1}\left(\frac{20\cdot\log 2 + k\cdot V_b - k\cdot V_1}{k\cdot V_{p-p}}\right)}{2\pi}T \qquad \text{Equation 6-8}$$

Figure 6-13 shows an example of the calculated switching windows, for a 10 GHz sinusoidal modulation voltage of 10 V_{p-p}, and various dc bias voltages of 1, 3, 5, and 7 V. A narrower optical gate is obtained with increasing reverse bias.

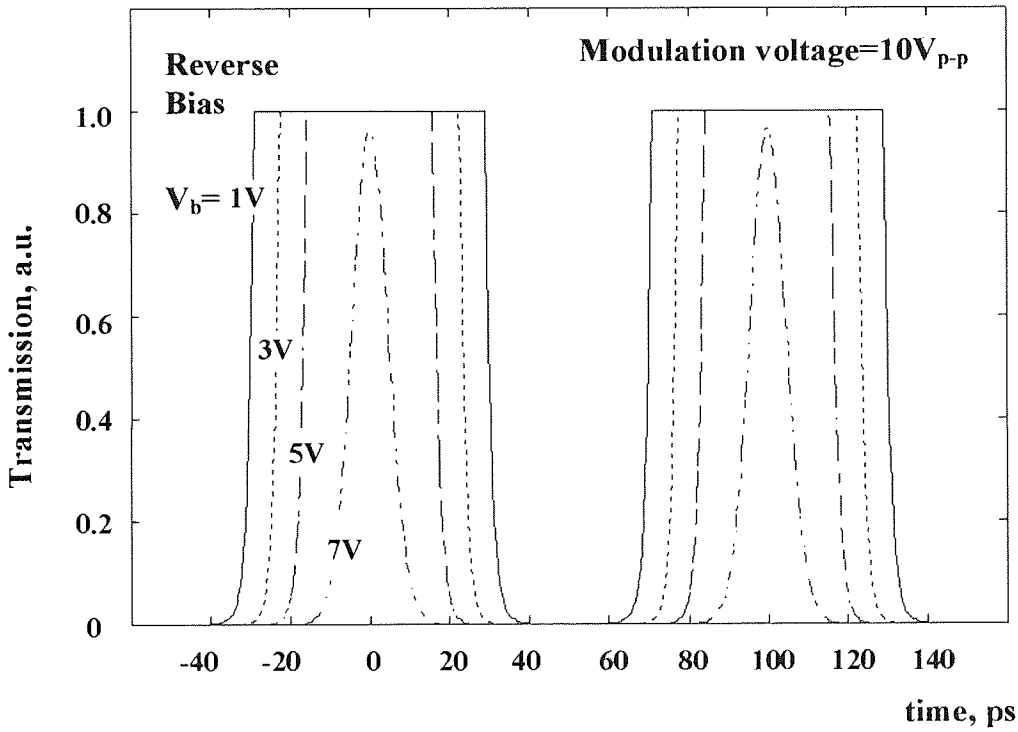

Figure 6-13. Switching window function for a constant sinusoidal voltage, V_{p-p}=10 V and various reverse bias voltages, V_b=1, 3, 5, and 7 V.

To confirm the theoretical calculations on the switching window width detailed above, a second EA modulator (EAM#2) was configured similar to that shown in Figure 6-6. Here, a CW-DFB is incident on one facet of the EAM#2, the output was detected using a HP83440D 32 GHz pin-diode and a HP5420B 50 GHz digital sampling oscilloscope. EAM#2 (BT device number: AT2032D4-11) was a 325 μm deeply-ridged MQW buried heterostructure device with a ~14 GHz electrical bandwidth, and a modulation efficiency, k_I = ~10 dB/V, see Figure 6-5. The measured insertion loss characteristics of the device

are shown in Figure 6-8, indicating a loss of between 7 dB and 10 dB, depending on polarisation. At high reverse bias the polarisation sensitivity was 10-15 dB.

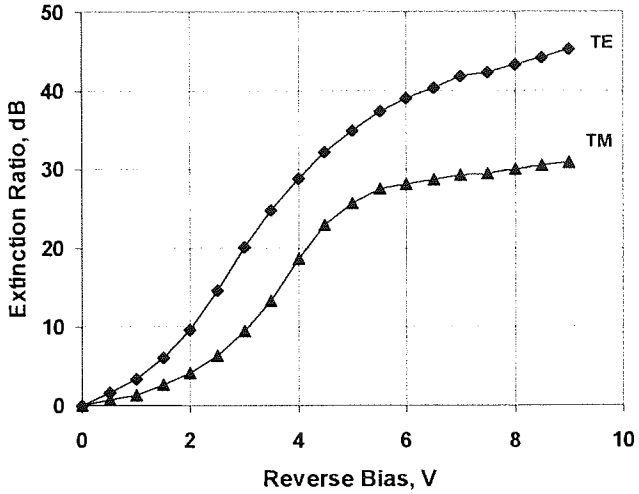

Figure 6-14. Insertion-loss characteristics of EAM#2, a 325 μm deeply-ridged MQW buried heterostructure, with a ~14 GHz electrical bandwidth and a modulation efficiency, k=10 dB/V. BT Device number: AT2032D4-11

EAM#2 was sinusoidally modulated using a 10 GHz, 14 $V_{p\text{-}p}$ drive signal, derived from a HP synthesiser and a MITEQ amplifier. The reverse bias V_b was varied, and the switching window width was measured using a digital sampling oscilloscope, see Figure 6-15. The switching window could be varied from 60 to 20 ps for corresponding reverse bias voltages of 1V to 7V. When the modulator was biased at a low reverse bias of 1V, a flat response was obtained, although a forward bias of up to 6V was applied. This indicates that the free-carrier absorption in forward bias was negligible, therefore the assumptions made previously appear to be correct.

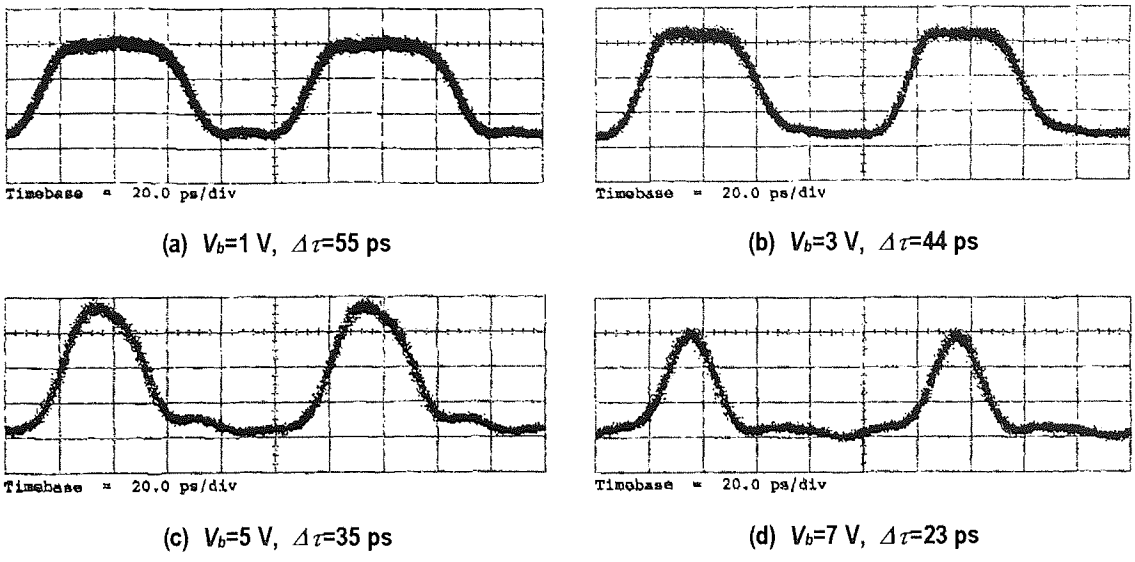

(a) V_b=1 V, $\Delta\tau$=55 ps (b) V_b=3 V, $\Delta\tau$=44 ps

(c) V_b=5 V, $\Delta\tau$=35 ps (d) V_b=7 V, $\Delta\tau$=23 ps

Figure 6-15. Various switching windows obtained by sinusoidally driving EAM#2 with a constant modulation voltage of 14 $V_{p\text{-}p}$ and different reverse bias voltages of 1, 3, 5, 7 V.

The experimental switching window FWHM widths taken from the measurements above for different reverse bias voltages and a constant 10 GHz sinusoidal drive signal with a fixed modulation voltage of 14 $V_{p\text{-}p}$, is shown in Figure 6-16, along with the theoretically predicted switching window width calculated using Equation 6-8. The modulation coefficient, k_I and V_I were calculated from the insertion loss characteristics shown in Figure 6-14, k_I =10 dB/V, and V_I=2.3V.

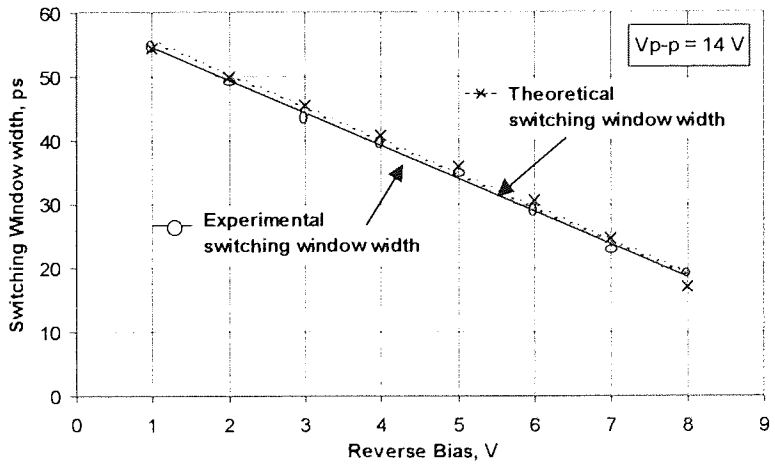

Figure 6-16. Experimental (using EAM#2) and theoretical switching window widths for different reverse bias voltages, V_b.

The graph shows excellent agreement between the theoretically calculated results, and the experimental results.

The dynamic extinction ratio of EAM#2 for different reverse bias voltage conditions was measured using the experimental setup shown in Figure 6-17. A 10 GHz, high extinction (>40 dB), 5 ps pulse stream, derived from the source described in section 7.2, was passed through the EA modulator and detected on an optical power meter. The reverse bias voltage was set to 1V, and the pulse was tuned through the transmission window of the EA modulator using a variable electrical delay line. This was repeated for different reverse voltages.

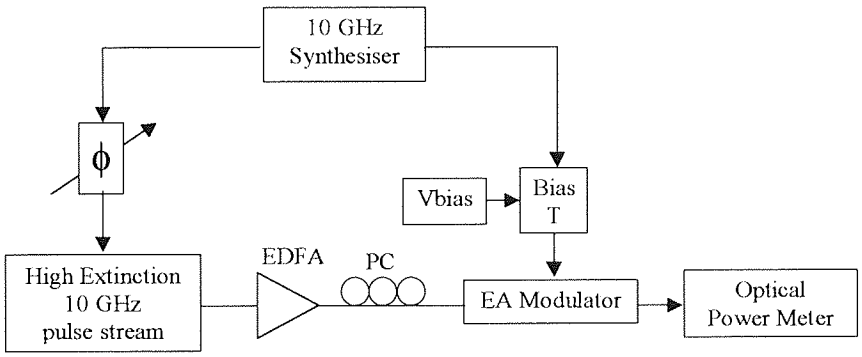

Figure 6-17. Experimental setup for extinction ratio measurements of the 'drop' channel function.

The results are shown in Figure 6-18, indicating a fairly constant dynamic extinction of ~28 dB, for reverse bias voltages over the range 1-5 V.

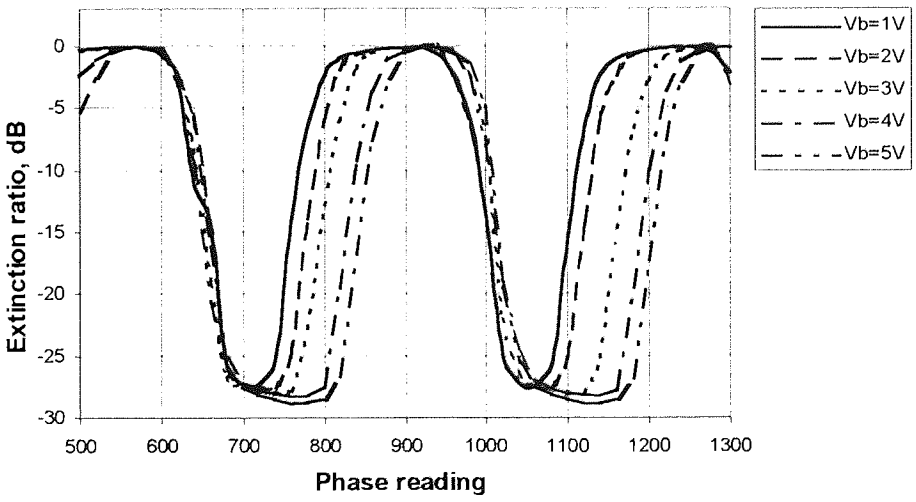

Figure 6-18. Dynamic extinction ratio measurements for different reverse bias voltages.

This indicates that the EAM#2 is suitable for use as a high-speed demultiplexer or 'drop and insert' multiplexing in OTDM network with sixteen channels or more.

6.4 Chapter Summary

In summary, this chapter was intended to give an overview of the EA modulator. It summarised current applications, and then outlined some common device structures, before discussing EA modulator design and optimisation. The main content emphasised the use of such a device within an OTDM network as either an optical pulse source, or a high-speed optical demultiplexer. Experimental results were outlined and compared with those predicted in theory. The next chapter assumes the basic knowledge outlined in this, and discusses the use of an EA modulator in a novel bi-directional configuration.

Chapter 7

Experimental bi-directional operation of EA modulators in an OTDM network

7.1 Introduction

EA modulators are set to become key functional components in future high-speed OTDM networks, due to impressive demonstrations in a number of recent system experiments [111]. They are ideally suited to pulse generation [232], data encoding, demultiplexing [236, 262], and 'drop and insert' multiplexing [263]. All of these applications use the EA modulator in a unidirectional configuration, but there is no inherent reason for this limitation. In this chapter, an EA modulator is used for the first time in a novel bi-directional configuration to achieve additional functionality.

Bit-error rate measurements are presented on the use of a single EA modulator to simultaneously demultiplex two 10 Gbit/s channels from a 40 Gbit/s OTDM data stream [22]. Error free operation is observed, and the effects of incoherent interference between the demultiplexed channel and residual facet reflections are investigated.

If one of the demultiplexed channels is used as an error signal to form a simple phase-locked loop feedback circuit, then simultaneous demultiplexing and clock recovery can be achieved. By utilising the inherent bi-directionality of an EA modulator, we can derive an error signal that is independent from the switching process, making the clock recovery process very stable with extremely low jitter. Operation was demonstrated by using a single EA modulator to demultiplex a 10 Gbit/s channel from a 40 Gbit/s OTDM data stream, whilst simultaneously recovering the 10 GHz electrical clock [23]. The technique was extremely stable, exhibited ultra-low timing jitter, and used low-speed electronics.

40 Gbit/s 'drop and insert' multiplexing is also demonstrated using the same EA modulator under different dc bias conditions. The performance is analysed using BER measurements [24]. Clock recovery is achieved using the technique detailed above.

The last experiment presents preliminary results on a high-extinction optical pulse source, suitable for use in an 80 Gbit/s OTDM system. High-extinction pulses source can be realised by cascading two EA modulators in series, details of this technique are given in the next section. An alternative to this method, is to double-pass a single modulator. Initial results indicate that the system suffers from amplified facet reflections which lead to incoherent interference, and a large degree of amplitude jitter.

The next section outlines a high-extinction, low-duty ratio high-quality pulse source, based on EA modulators. The source is then used in the following experiments which were outlined above.

7.2 A High-Extinction, Low Duty-Cycle Optical Pulse Source

7.2.1 Introduction

The characteristics of an optical pulse source suitable for an OTDM network were discussed in detail in section 3.7. The pulse width must be less than $1/3^{rd}$ of the bit period, (8 ps in a 4×10 Gbit/s system and 4 ps in a 8×10 Gbit/s system), and the extinction ratio must be greater than 36 dB for a 4×10 Gbit/s system and >44 dB for a 8×10 Gbit/s system. These requirements are difficult to realise using a sinusoidally driven EA modulator, which typically produces pulses with a width of 15 ps (uncompressed), and exhibits a 30 dB extinction ratio. The main long term method to overcome these limitations is the optimisation of device design parameters, outlined in section 6.2.2, however alternative techniques do exist and are outlined below.

The simplest way to overcome the extinction ratio limitations is to cascade two synchronously driven modulators [236]. The pulse width or duty-cycle is inversely

proportional to the frequency of the drive signal [106], that is, the higher the frequency, the shorter the pulses. The duty-ratio can therefore be reduced by driving the modulator with a combination of the fundamental operating frequency and its first harmonic [264], producing a pulsed drive signal, see Figure 7-1.

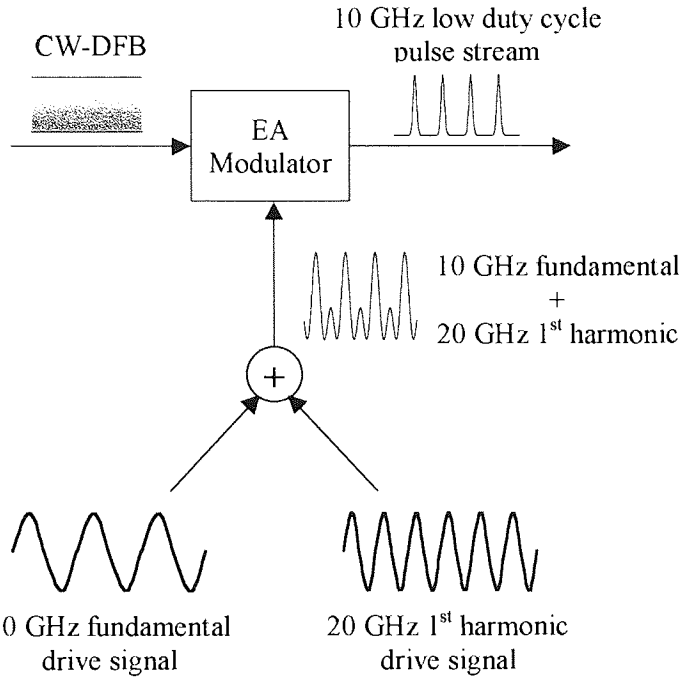

Figure 7-1. Harmonically driven EA modulator to reduce duty cycle.

These two techniques were recently combined to produce high-extinction, low-duty cycle, 4 ps pulses at 10 GHz, suitable for multiplexing up to 80 Gbit/s [236], and is described in more detail below.

7.2.2 Experimental details

The experimental setup is shown in Figure 7-2. A 10 GHz pulse stream was generated using a 1557 nm CW-DFB incident on a packaged high-modulation depth EA modulator. The device was a ridged deeply buried heterostructure MQW (see Figure 6-5) and had a dc extinction ratio of 35 dB, fibre-to-fibre insertion loss of 7.2 dB and a 3-dB electrical bandwidth of ~14 GHz. The modulator was harmonically driven [265] using a 10 GHz synthesiser, a passive frequency doubler and a 20 GHz wideband amplifier, allowing both 10 GHz and 20 GHz components to be applied to the device.

The duty-cycle was reduced and 5.5 ps pulses produced, which were measured using an autocorrelator, see Figure 7-3. The output was then amplified and coupled into a second EA-modulator (dc extinction ratio of 25 dB), allowing pulses with an extremely low background intensity to be produced.

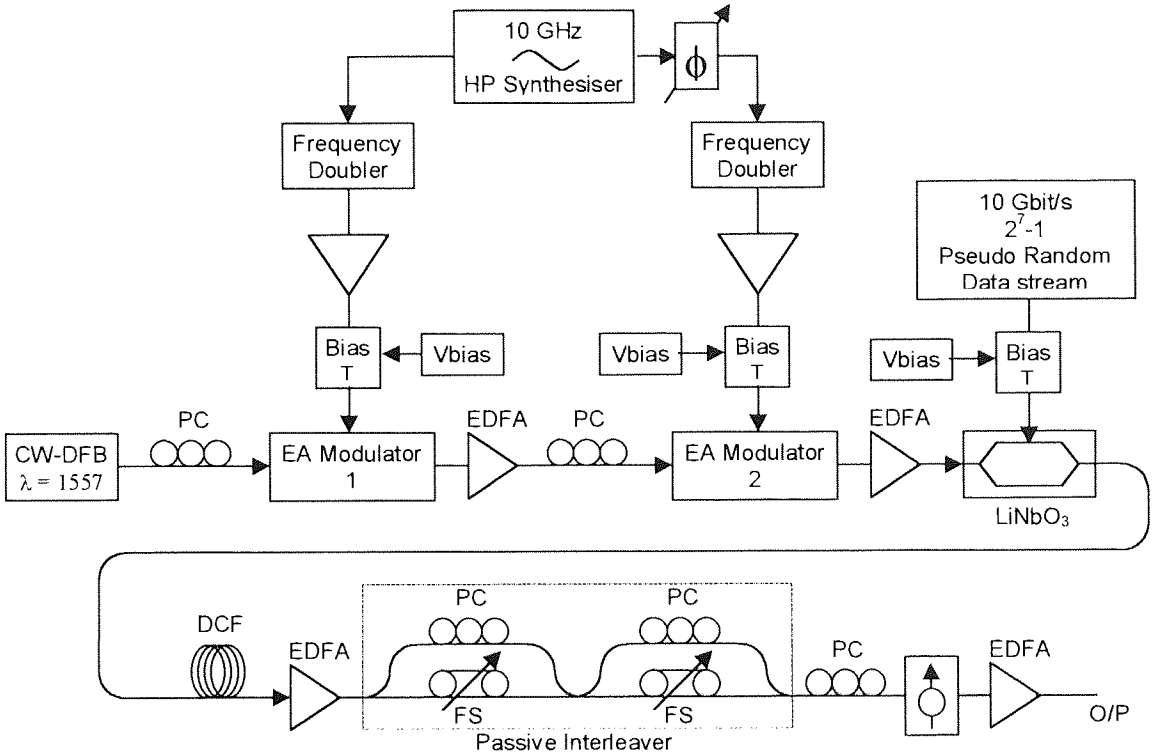

Figure 7-2. 40 Gbit/s high extinction ratio, low duty cycle data source, based on two harmonically driven EA modulators.

Dispersion compensating fibre (DCF) was used to remove residual chirp, producing $sech^2$ transform-limited pulses, compressing the pulse width to 3.7 ps, see Figure 7-3b.

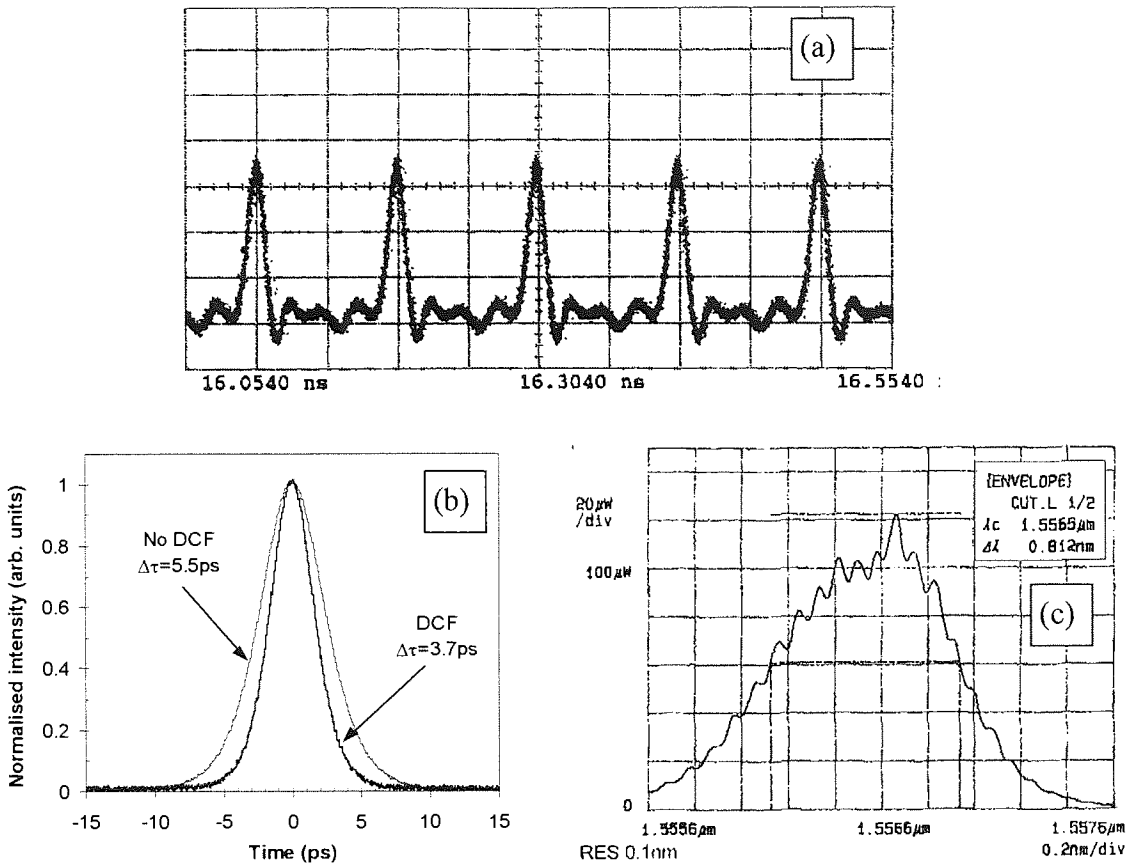

Figure 7-3. Characteristics of a high-extinction, low duty-cycle, 10 GHz optical pulse stream, generated using two synchronously driven EA modulators: (a) pulse stream; (b) auto-correlation; (c) optical spectrum.

Figure 7-3 shows the characteristics of the high extinction, low duty cycle, 10 GHz pulse stream which was generated using setup shown in Figure 7-2. The rms timing jitter was calculated to be 350 fs using an RF spectrum analyser and the technique outlined in section 3.3, and was limited by the jitter of the HP synthesiser which was measured to be 300 fs.

A 2^7-1 pseudo-random data stream was applied, the word length of which was limited by the low frequency response of the lithium niobate ($LiNbO_3$) amplitude modulator. The overall extinction of the resulting 10 Gbit/s data stream was measured using an all-fibre coherence time analyser [266]. The principle is shown in Figure 7-4, and is based on a cross-correlation technique.

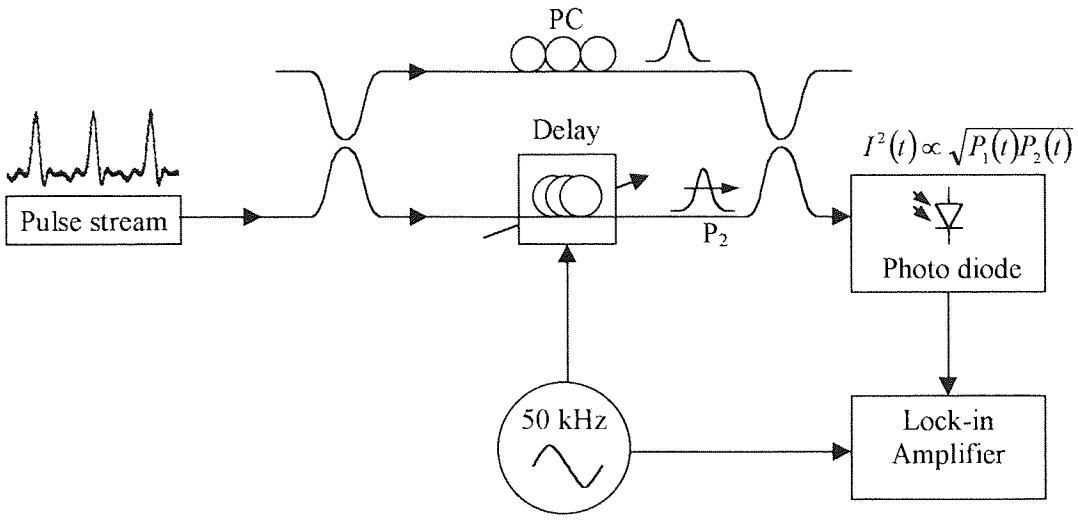

Figure 7-4. A coherence time analyser based on a Mach-Zehnder interferometer, used to measure extinction ratio of optical source.

A Mach-Zehnder interferometer is formed by using a 3-dB coupler to split the incoming signal into two components. The first component is passed through a polarisation controller, before being recombined with the second component which has passed through a variable optical delay and a phase modulator. The resulting signal detected on a photodiode is given by:

$$I^2(t) \propto \sqrt{P_1(t)P_2(t)} \qquad \textbf{Equation 7-1}$$

where P_1 and P_2 are the powers in each of the arms of the interferometer. A lock-in amplifier is used to measure the amplitude of the 50 kHz beat frequency. A maximum beat signal will be detected when the delay-line is adjusted so that the two pulse components overlap:

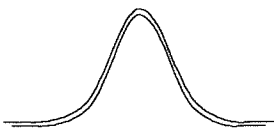

$$I_{\max}{}^2 \propto \sqrt{P_{1peak} \cdot P_{2peak}} \cdot \sqrt{S_1 \cdot S_2} \qquad \textbf{Equation 7-2}$$

where P_{1peak} and P_{2peak} are the peak power of each component. Similarly, P_{1back} and P_{2back} are the background radiation of each pulse component, due to the exponential decay in the tail of the pulse, and a finite extinction ratio. S_1 and S_2 are correction factors to account for different pulse shapes. A minimum signal will be obtained when the two pulses are completely separated:

$$I_{\min}{}^2 \propto \sqrt{P_{1peak} \cdot S_1 \cdot P_{2back}} + \sqrt{P_{2peak} \cdot S_2 \cdot P_{1back}} \qquad \text{Equation 7-3}$$

If the two arms of the interferometer are equal, and the fibre delay is used to walk the same pulse through itself, then $P_{peak} = P_{1peak} = P_{2peak}$, $P_{back} = P_{1back} = P_{2back}$ and $S = S_1 = S_2$. The pulse extinction ratio can then be calculated as follows:

$$\frac{V_{\max}{}^2}{V_{\min}{}^2} \propto \frac{I_{\max}{}^2}{I_{\min}{}^2} = \frac{S \cdot P_{peak}}{2\sqrt{S} \cdot \sqrt{P_{peak} \cdot P_{back}}} = \frac{1}{2}\sqrt{S} \cdot \sqrt{\frac{P_{peak}}{P_{back}}} \qquad \text{Equation 7-4}$$

$$10\log\left(\frac{V_{\max}}{V_{\min}}\right)^2 = 10\log\frac{\sqrt{S}}{2} + 10\log\sqrt{\frac{P_{peak}}{P_{back}}} \qquad \text{Equation 7-5}$$

$$\text{Electrical XR} = 10\log\frac{\sqrt{S}}{2} + \frac{1}{2}(\text{Optical XR}) \qquad \text{Equation 7-6}$$

$$\text{Optical XR} = 2\left(\text{Electrical XR} - 10\log\left(\frac{\sqrt{S}}{2}\right)\right) \qquad \text{Equation 7-7}$$

where $S = 1.5$ (2.1 dB) for a gaussian pulse stream and $S = 1.76$ (1.7 dB) for a $sech^2$ pulse stream.

The optical extinction ratio of the 10 Gbit/s data stream was measured to > 50 dB, this combined with a pulse width of ~ 4 ps, makes the source suitable for use in a 80 Gbit/s OTDM system.

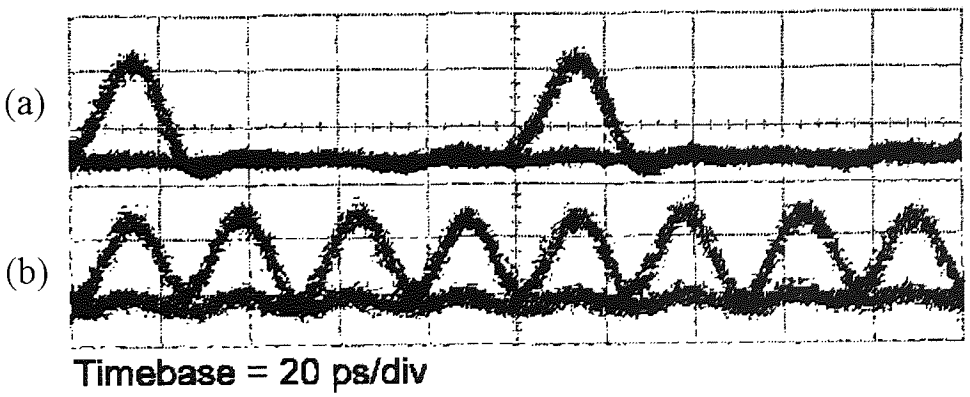

Figure 7-5. (a) 10 Gbit/s data stream; (b) 40 Gbit/s data stream.

The 10 Gbit/s data stream (see Figure 7-5a) was passively multiplexed up to 40 Gbit/s, before being passed through a polariser to ensure single polarisation operation (see Figure 7-5b). This source was used in the following experiments.

7.3 Two Channel Demultiplexing using a Single EA Modulator

7.3.1 Introduction

For full demultiplexing, a separate EA modulator would be used to select each channel, therefore requiring 4 modulators for a 40-10 Gbit/s system, or 8 modulators for a 80-10 Gbit/s OTDM system [236]. This section will present experimental results on the use of a single electroabsorption modulator to simultaneously demultiplex two 10 Gbit/s channels from a 40 Gbit/s OTDM data stream [22]. Error-free operation is observed, and the effects of incoherent interference between the demultiplexed channel and residual facet reflections investigated. This technique will improve network reliability whilst also representing a substantial cost saving.

7.3.2 Experimental details

The experimental setup is shown in Figure 7-6. The 40 Gbit/s data stream (Figure 7-7a) was split using a 3 dB coupler, 50% being fed in a clockwise direction through the EA modulator, and detected at port B. The remaining 50% was fed in an anti-clockwise direction back through the same EA modulator, and monitored at port A. Isolators were used to prevent the output at port A from getting to port B and creating interference effects. Alternatively, a 3-port circulator could be used in place of the second coupler, decreasing the overall loss.

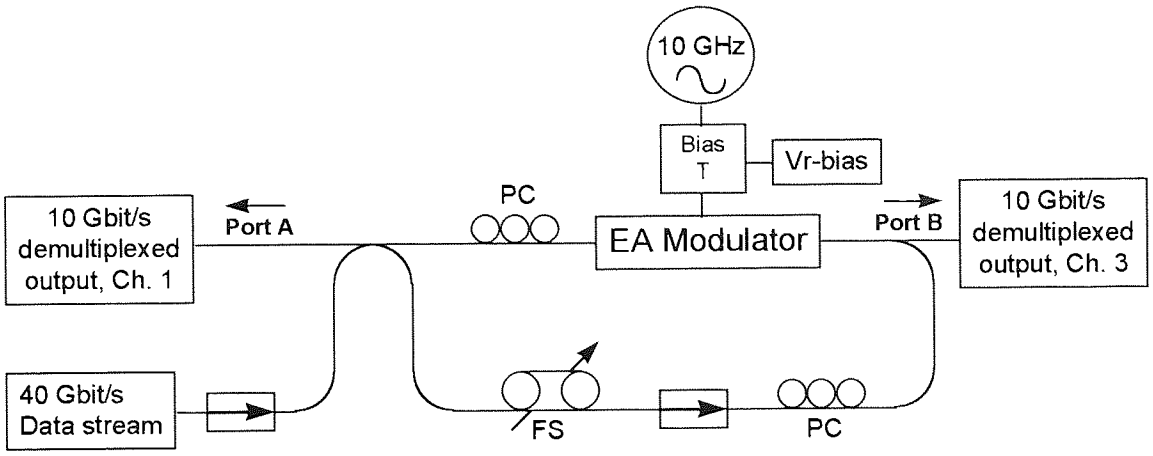

Figure 7-6. Experimental setup of two channel demultiplexer. PC - polarisation controller, FS - fibre stretcher.

EAM#2 (see section 6.3.2) was sinusoidally driven at 10 GHz to produce a 20 ps transmission window, enabling a single 10 Gbit/s channel to be demultiplexed at port A (see Figure 7-7b).

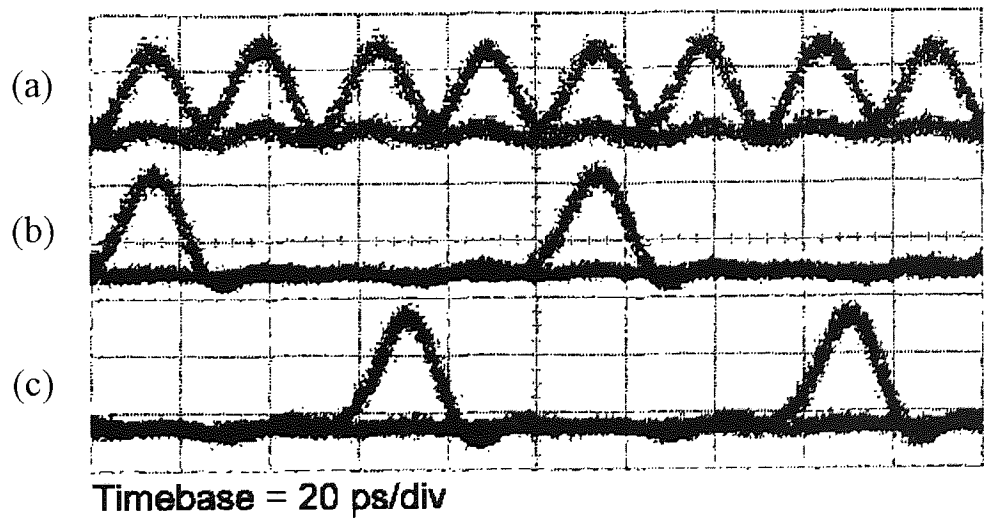

Figure 7-7. (a) 40 Gbit/s OTDM input data stream. (b) 10 Gbit/s demultiplexed channel 1, Port A. (c) 10 Gbit/s demultiplexed channel 3, Port B.

Demultiplexing of a second 10 Gbit/s channel was simultaneously achieved at port B (Figure 7-7c), by adjusting the phase of the 40 Gbit/s signal fed in the anti-clockwise direction using the variable fibre stretcher.

7.3.3 Analysis of expected system penalty

The dynamic extinction ratio of EAM#2 was measured in section 6.3.2, and is shown in Figure 6-18 to be greater than 28 dB. Figure 3-32 indicates that under normal operation the modulator should give a demultiplexing penalty of less than 0.1 dB.

Each facet of the EA-modulator had an anti-reflective coating, and a measured residual reflectivity of –30 dB. This caused incoherent interference between the reflected and required signals, causing an additional crosstalk penalty at each of the output ports [267]. Figure 7-8 shows the various signals entering and leaving the EA modulator, and the residual signals caused by finite facet reflectivities.

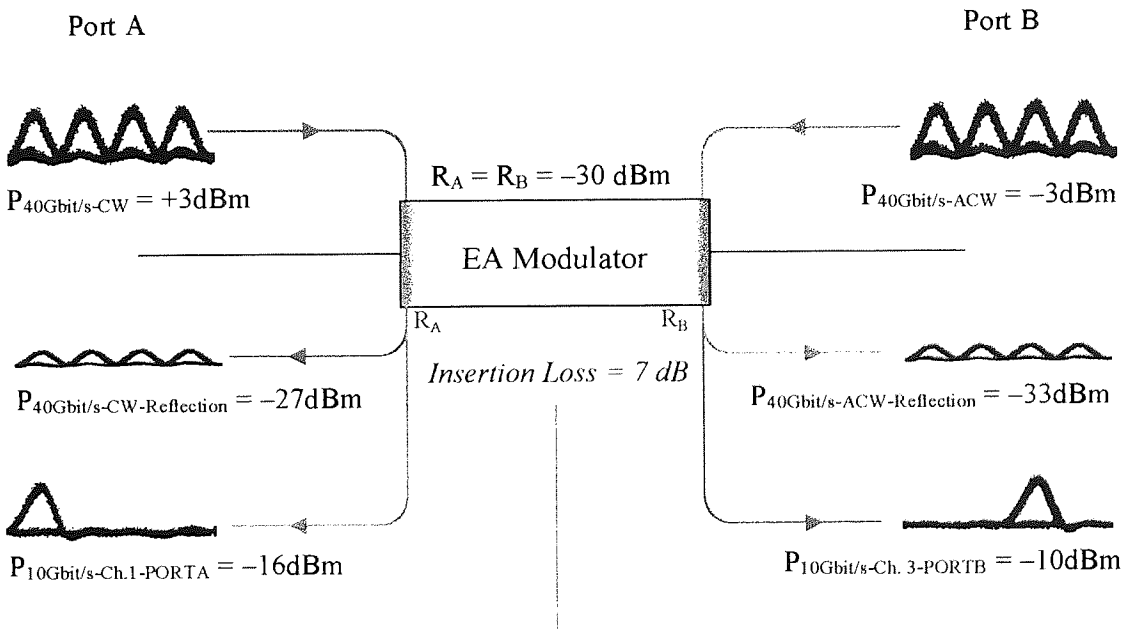

Figure 7-8. Analysis of incoherent interference due to residual facet reflections.

The unwanted reflections at each facet contributes to the total power incident on the receiver, causing a simple power penalty. To obtain a power penalty of less than 0.5 dB, then the 'signal to crosstalk' ratio (SXR) should be greater than 12.4 dB, see section 3.7.2. The SXR at Port A is calculated to be 11 dB, giving a power penalty of ~0.7 dB. Incoherent interference between the demultiplexed channel and the residual facet reflection also results in a degradation of the apparent SNR. This leads to a system penalty and a worsening of any error floor. A SNR of 16.4 dB gives a BER of 10^{-9}, and

a SNR of 18.5 dB gives a BER of 10^{-15}. The calculated SNR at the receiver is given by Equation 3-11 and at port *A* is calculated to be 17 dB, indicating that the system will suffer an additional penalty, and may be subject to an error floor. Port *B* has a SXR of 23 dB, indicating that the channel should result in a negligible power penalty. The SNR is calculated to be 29 dB, indicating no additional penalty due to incoherent interference on this port.

The interference effect can be minimised using the polarisation controllers, by ensuring that the reflected wave is orthogonally polarised to the demultiplexed signal. However, this then removes the polarisation insensitivity of the demultiplexer, which is undesirable.

7.3.4 Bit error rate measurements of two channel demultiplexer

Figure 7-9 shows the results of BER measurements made on the two 10 Gbit/s demultiplexed channels. A 10 Gbit/s optimised data signal is used as a back-to-back reference of the receiver sensitivity.

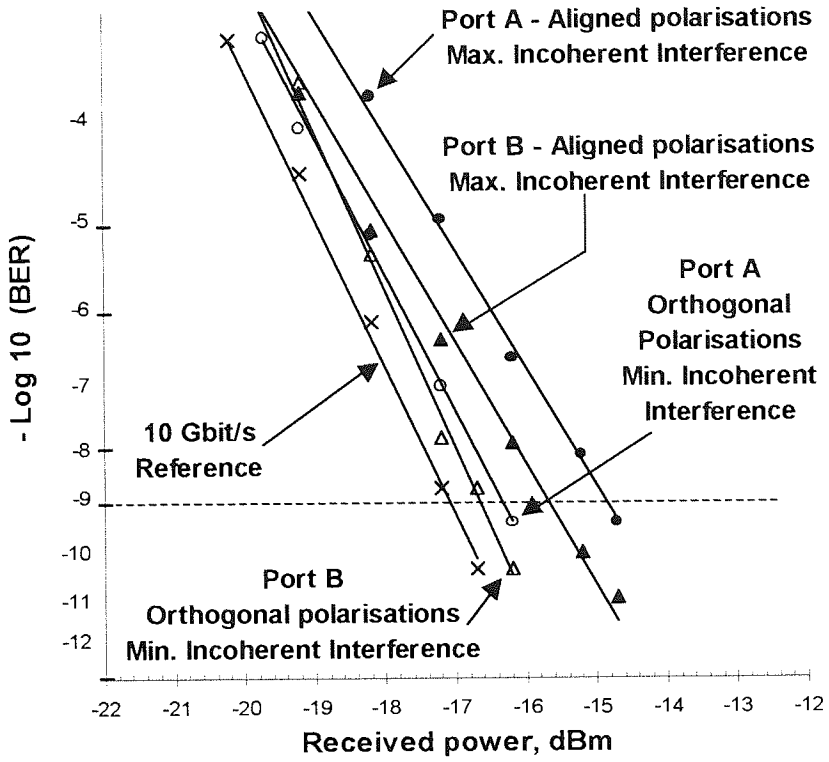

Figure 7-9. Bit error rate measurements of simultaneous two channel demultiplexer:

x (cross) : 10 Gbit/s optimised data (reference);
O (outlined circle) : 40-10Gbit/s demultiplexed output, port A - Orthogonal polarisation, min. incoherent interference;
Δ (outlined Triangle) : 40-10Gbit/s demultiplexed output, port B - Orthogonal polarisation, min. incoherent interference;
● (solid Circle) : 40-10Gbit/s demultiplexed output, port A - aligned polarisation, maximum incoherent interference.
▲ (solid Triangle) : 40-10Gbit/s demultiplexed output, port B - aligned polarisation, maximum incoherent interference;

With the polarisation states set to minimise incoherent interference, no additional penalty was observed when compared to the same modulator operating as a traditional uni-direction demultiplexer. This was true for both ports A and B. With the signals aligned for maximum incoherent interference the system still operated error-free, albeit with a 1.6 dB penalty. These results agree closely with the theoretical analysis detailed in section 7.3.3.

For aligned polarisations, port A has a measured system penalty of 1.6 dB, and port B has a penalty of 0.8 dB. The differences in system penalties between the two channels is because different optical power levels are incident in each direction through the modulator. By ensuring that these power levels are the same, then the penalty on port A

should be reduced in-line with that of port B. To reduce the effects of incoherent interference further, then angle facet devices may be required.

7.4 Simultaneous Clock Recovery and Demultiplexing

The different techniques of clock recovery were discussed in section 3.6. Chapter 5 presented results that demonstrated simultaneous demultiplexing, data regeneration, and clock recovery using a semiconductor optical amplifier based nonlinear optical loop mirror (SOA-NOLM) [21]. In order to lock the peak of the switching window of the device, it was necessary to dither the local clock to obtain a differential error signal, giving the direction and magnitude of any phase drift. The dithering process imposes a degree of phase modulation on the recovered clock, giving rise to a residual but deterministic timing variance. The following section outlines novel results of simultaneous 'dither free' clock recovery and demultiplexing [23] by extending the experimental setup outlined in section 7.3.

7.4.1 Experimental details

The experimental set-up is shown below in Figure 7-10. To achieve clock recovery, the demultiplexed output at port B was detected on a low-speed photodiode and used as an error signal. This was fed through standard PLL electronics which were used to control a 10 GHz VCO driving the modulator, thus creating a closed loop.

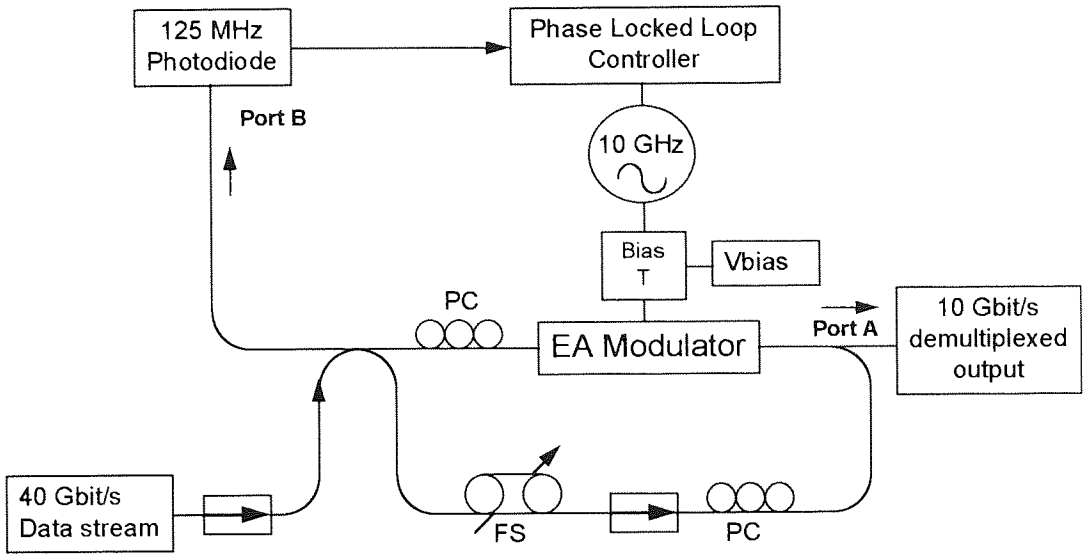

Figure 7-10. Experimental setup of simultaneous clock recovery and demultiplexer. PC - polarisation controller, FS - fibre stretcher.

The EA modulator acts as an electro-optic sampler, whose time averaged intensity is a function determined by the phase / frequency difference between the 40 Gbit/s OTDM data stream and the locally generated 10 GHz electrical clock. A variable fibre stretcher is used to adjust the phase of the 40 Gbit/s signal fed in the anti-clockwise direction through EAM#2. The resulting 10 Gbit/s channel then forms an error signal which can be offset from the centre of the transmission window by a small fraction of the clock period, allowing the sampling process to be achieved on the edge of the data stream, and the feedback circuit to determine the amplitude and direction of any phase drift. Independent control of the sampling point is achieved between the error signal used in clock recovery, and the demultiplexed signal, this makes the system extremely stable.

Incoherent interference effects between the required 10 Gbit/s demultiplexed signal at port A, and residual reflections (-30.5 dBm) from the EA modulator resulted in a small degradation in performance, the effects could be minimised by ensuring that the signals were at orthogonal polarisations, as before. Alternatively, the problems associated with incoherent interference can be almost eliminated by reducing the optical power of the anti-clockwise travelling error signal. Clock recovery will still be maintained, because a much smaller signal power can be used compared with that required for BER measurements.

7.4.2 Results of simultaneous demultiplexing and clock recovery

Figure 7-11a shows the 40 Gbit/s OTDM data stream. Figure 7-11b shows a 10 Gbit/s demultiplexed channel, and Figure 7-11c shows the 10 GHz recovered electrical clock. Jitter analysis of the recovered clock was performed using an RF spectrum analyser, by measuring the noise spectral density and the total power of each signal harmonic [104].

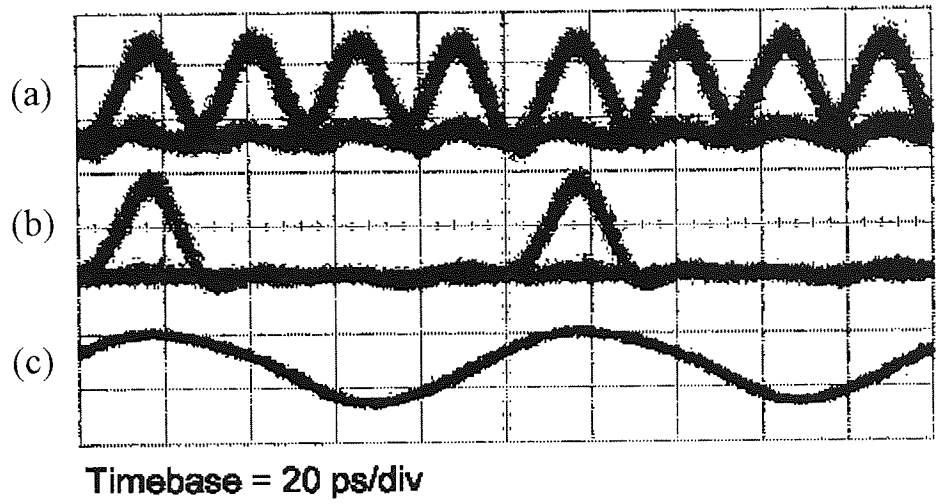

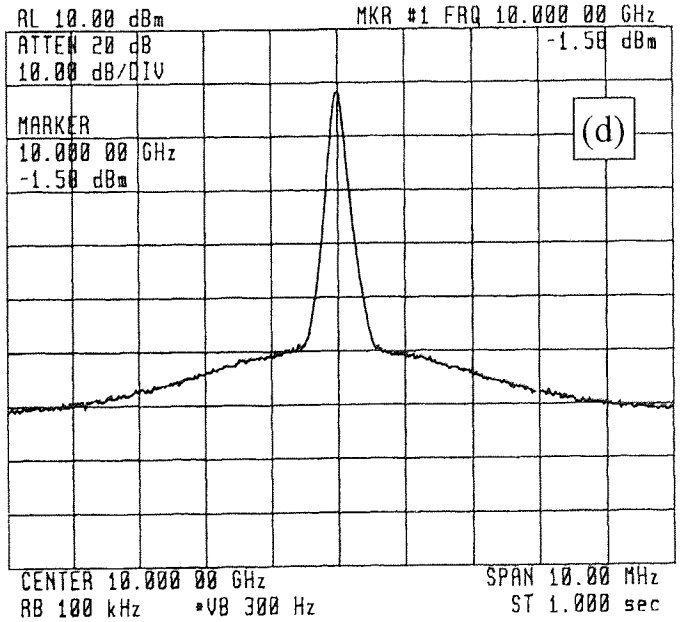

Figure 7-11. (a) 40 Gbit/s OTDM input data stream. (b) 10 Gbit/s demultiplexed channel 1, Port A. (c) 10 GHz recovered electrical clock, (d) microwave spectrum of recovered 10 GHz clock

The RF spectrum of the recovered clock is shown in Figure 7-11d; the phase noise pedestal is 50 dB below the peak of the recovered clock. The rms timing jitter was

calculated to be ~150 fs, which is less than that of the incoming data (350 fs), making this form of clock recovery suitable for use in an OTDM network operating at >100 Gbit/s [102].

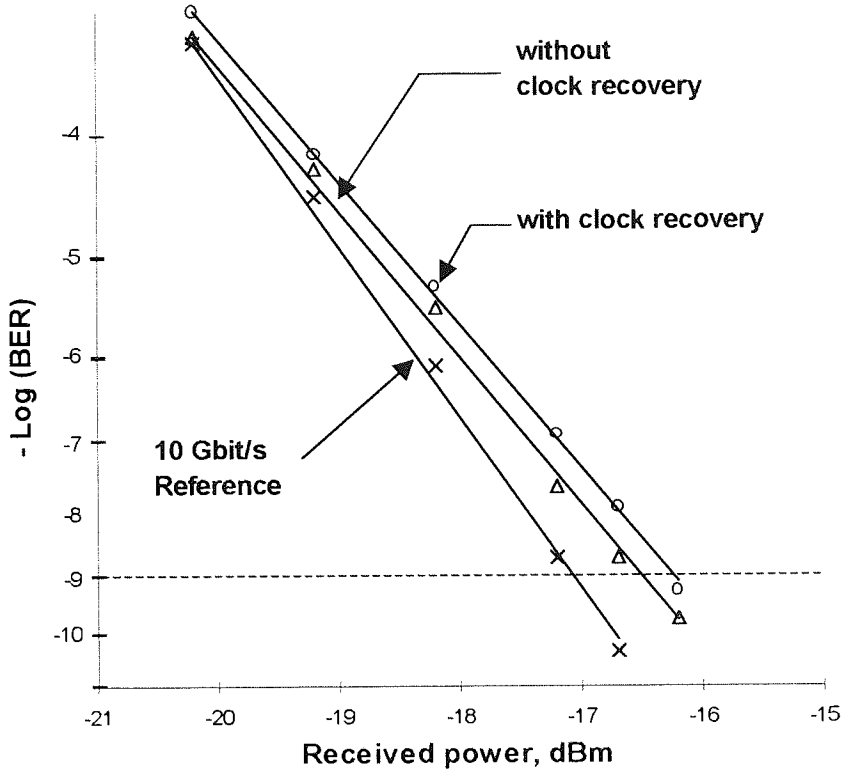

Figure 7-12. Bit-error-rate of the 10 Gbit/s demultiplexed channel.

X (cross) : 10 Gbit/s optimised data (reference);
Δ (outlined Triangle) : 40-10 Gbit/s demultiplexed output - without clock recovery;
O (outlined circle) : 40-10 Gbit/s demultiplexed output - with novel clock recovery;

Figure 7-12 shows the results of BER measurements made on the 10 Gbit/s demultiplexed channels, with and without clock recovery. A 10 Gbit/s optimised data signal is used as a back-to-back reference to indicate receiver sensitivity. The system operated error free, with minimal penalty and no indication of an error floor.

To achieve clock recovery, the gain, RC time constant, and damping of the feedback electronics had to be manually optimised. Changes in the optical power incident on the photodiode would disturb this condition, and result in additional phase noise. Therefore, further work should involve the development of the feedback electronics to account for variations in input power levels.

In conclusion, simultaneous demultiplexing and clock recovery has been demonstrated using a single EA modulator in a novel bi-directional configuration. The clock recovery exhibited excellent stability, using low speed electronics, and had an extremely low timing jitter on 150 fs.

7.5 Drop & Insert Multiplexing using EA Modulators

7.5.1 Introduction

To perform effective 'drop and insert' multiplexing the EA modulator must completely remove a single data stream (the 'drop'), whilst leaving the remaining channels undisturbed. It is then a simple matter to insert a data stream into the vacant time-slot (the 'insert'). If the dropped channel is not completely removed, then crosstalk between the inserted channel and the remaining signal can cause incoherent interference, effectively degrading the system performance and subsequently limiting the maximum transmission distance. The extinction ratio and the shape of the transmission window are therefore important device parameters and are analysed in Chapter 6. 'Drop and insert' multiplexing is discussed in more detail Chapter 3.

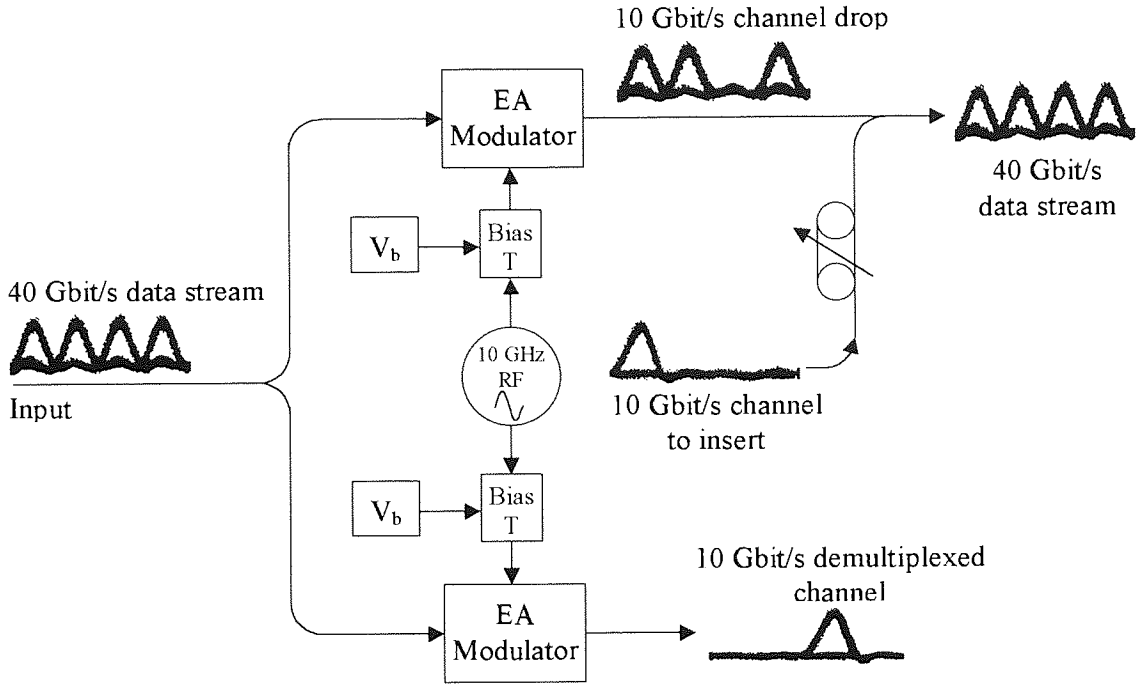

Figure 7-13. Full 'drop and insert' multiplexing using two synchronously driven EA modulators, with complementary transmission windows.

For full 'drop and insert' multiplexing, at least two synchronously driven modulators are necessary, each with a complementary switching function. The first modulator performs the 'drop' function, and the second modulator performs the demultiplexing operation (see Figure 7-13).

To analyse the effectiveness of the 'drop and insert' process, a 3-node OTDM network demonstration was devised, each node is self-contained and performs its own clock recovery [24]. Node 1 uses two EA modulators to generate a 40 Gbit/s OTDM data stream, node 2 performs the 'drop' function on a single channel, whilst simultaneously recovering the 10 GHz clock by exploiting the bi-directionality of the EA modulator as described in section 7.4. Node 3 uses an EA-Modulator based demultiplexer with independent electrical clock recovery to extract a 10 Gbit/s channel [110].

7.5.2 Experimental details

The experimental set-up is shown in Figure 7-14. At node 1 a 40 Gbit/s OTDM data stream was generated using the source outlined in section 7.2. This was amplified and fed into the input of the 'drop' section of the OTDM node 2.

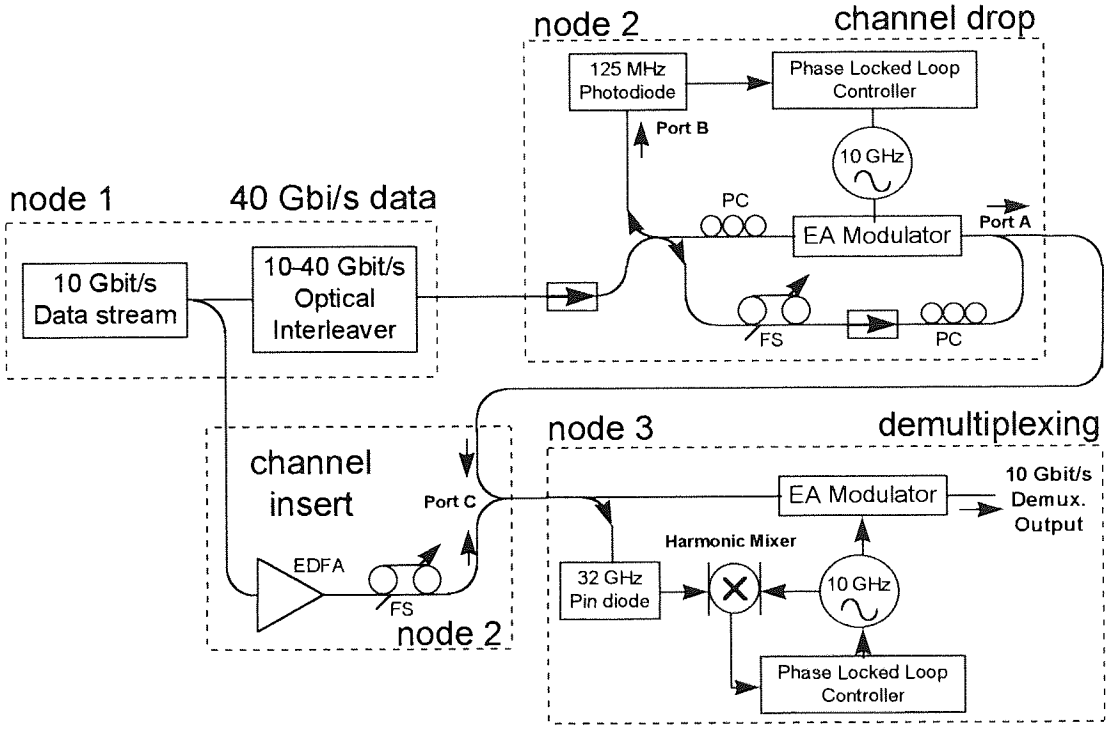

Figure 7-14. Experimental setup of a 3-node OTDM network, demonstrating 'drop and insert' multiplexing. PC - polarisation controller, FS - fibre stretcher.

The EAM#2 used to achieve demultiplexing and clock recovery in section 7.4 was damaged, and was replaced by a different device of unknown specification, called EAM#3. EAM#3 insertion loss characteristics are shown in Figure 7-15.

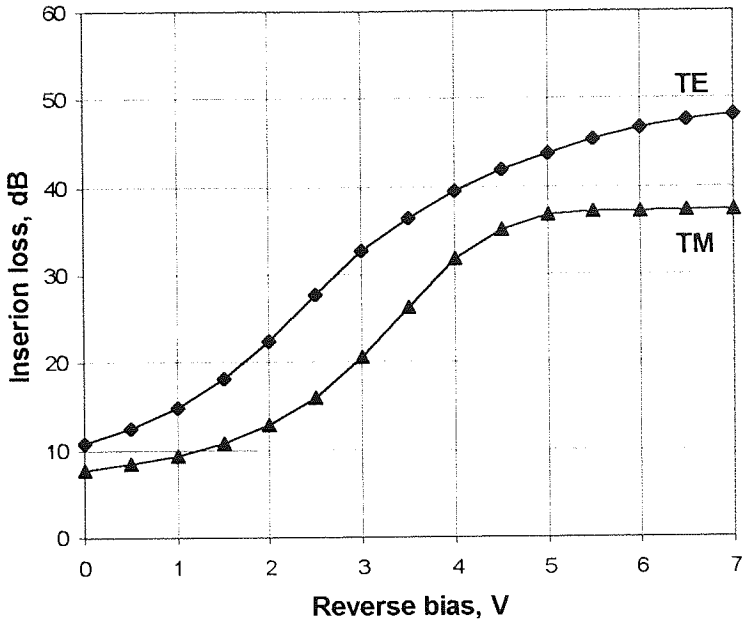

Figure 7-15. Insertion loss characteristics of EAM#3.

The EA modulator was reversed biased at 1V and sinusoidally driven using a voltage controlled oscillator (VCO) at 10 GHz, producing a 75 ps rectangular transmission window. This enabled three 10 Gbit/s channels to pass through the device unaffected, while almost completely removing (dropping) the remaining 10 Gbit/s channel. The 40 Gbit/s OTDM input data stream is shown in Figure 7-16a. Figure 7-16b shows the 75 ps transmission window for the 'drop' process, measured using a CW-DFB. Figure 7-16c shows the remaining three channels after channel 3 has been dropped. A clear open eye is observed, with excellent extinction of the dropped channel. An imperfect transmission window leads to a small attenuation of the two adjacent channels.

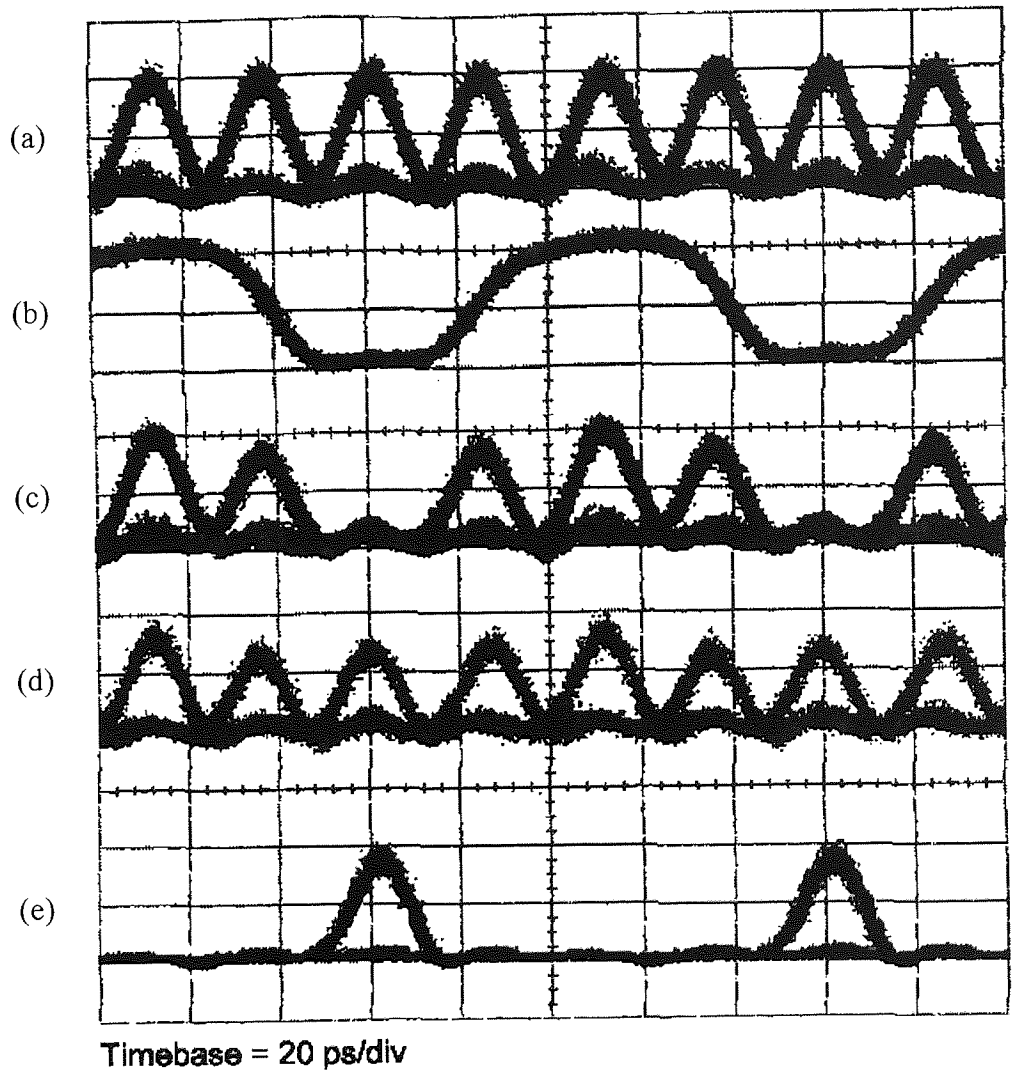

Figure 7-16. (a) 40 Gbit/s OTDM input data stream. (b) transmission window, indicating that channel 3 is to be dropped. (c) 40 Gbit/s OTDM data stream with channel 3 dropped. (d) 40 Gbit/s OTDM data stream with channel 3 re-inserted. (e) 10 Gbit/s demultiplexed data stream at Port D

A different 10 Gbit/s channel was inserted into the vacant time slot using a 3 dB coupler and a variable fibre stretcher to adjust its phase. The resulting 40 Gbit/s data stream (see Figure 7-16d) was fed into node 3. This consisted of an EA modulator-based demultiplexer driven by a 10 GHz VCO. Clock recovery was achieved electrically, using a 32 GHz high-speed photo-detector, an electrical mixer and the appropriate phase locked loop control circuitry [110]. Figure 7-16e shows an example of a demultiplexed channel. Different channels could be selected for demultiplexing using an electrical phase

shifter. BER of each 10 Gbit/s channel are presented in the next section, to confirm that the 'drop and insert' process does not significantly degrade the signal.

7.5.3 BER measurements for 'drop and insert' functionality

Figure 7-17 shows the results of BER measurements made on each of the 10 Gbit/s demultiplexed channels. An optimised 10 Gbit/s channel is used as a receiver sensitivity reference. When the polarisation of the inserted channel is aligned with the polarisation of the remaining channels, then a significant penalty and an error floor is observed. However, if the polarisation of the inserted channel is orthogonal to the remaining undropped channels, then the inserted channel suffers from no or minimal penalty. Each of the undropped 10 Gbit/s channels operated error-free with no indication of an error floor, but incurred a 1 dB penalty. This is thought to be due to the extra optical processing on these channels and the imperfect transmission window at the 'drop' stage.

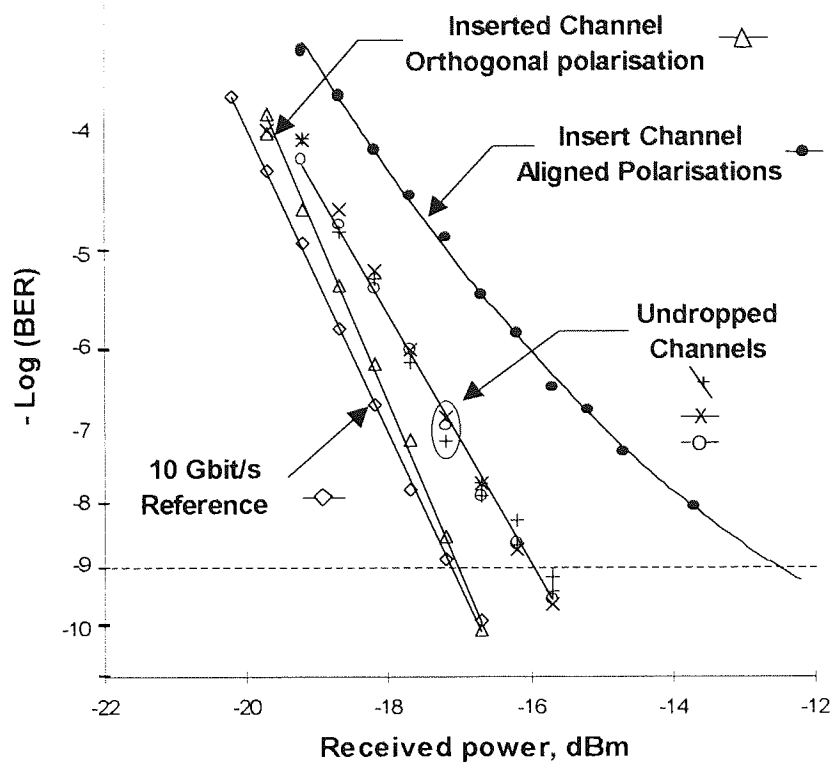

Figure 7-17. Bit-error-rate of the each 10 Gbit/s demultiplexed channel.

◊ (outlined diamond): 10 Gbit/s optimised back-to-back reference;
Δ (outlined Triangle) : 10 Gbit/s demultiplexed output - inserted channel 3 (Orthogonal polarisations);
O (outlined circle), x (cross), + (plus symbol): 10 Gbit/s demultiplexed output - three undropped channels (Orthogonal polarisations);
● (solid circle) 10 Gbit/s demultiplexed output - inserted channel 3 (Aligned polarisations);

To assess the dynamic extinction ratio of the channel 'drop' function, a high extinction (>40 dB), 10 GHz, 5 ps pulse was passed through the EA modulator and detected on an optical power meter. The pulse was tuned through the transmission window of the EA modulator using a variable electrical delay line. A similar procedure is outlined in section 6.3.2, and is shown in Figure 6-17.

The results are shown in Figure 7-18, indicating a maximum extinction of the dropped channel of ~14 dB. Ordinarily, this would result in incoherent interference between the residual undropped signal and the inserted channel, and cause a switching penalty. As described above, to avoid this effect the polarisation of the inserted channel was optimised so that it was orthogonal to the original data stream. The dynamic extinction

ratio of improved EA modulators (EAM#2) has since been measured under the same drive conditions to be in excess of 28 dB, which would reduce such effects to an insignificant level.

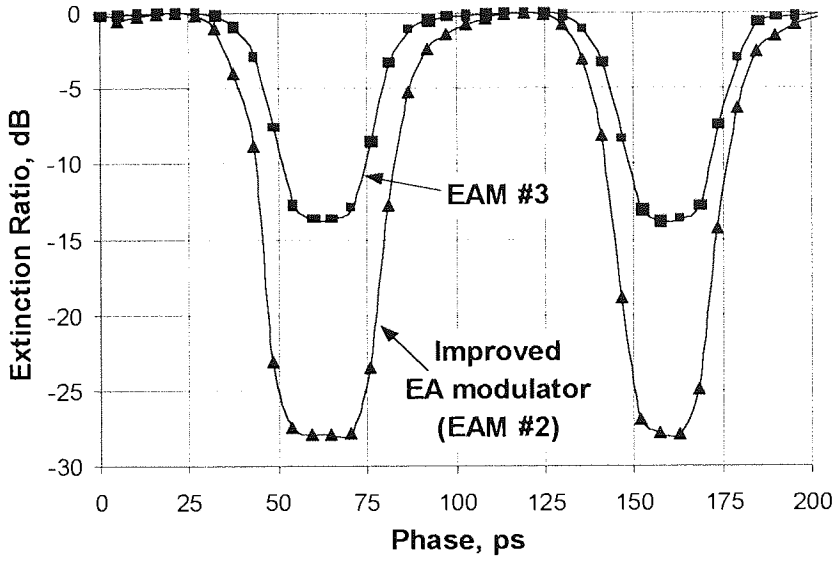

Figure 7-18. Extinction ratio measurements of the 'drop' process. ■ (solid square) : EAM#3 used in D&I experiments; ▲ (solid triangle) : Improved EA modulator;

In conclusion, 'drop and insert' functionality was demonstrated using an EA modulator, for the first time. A 3-node OTDM network was demonstrated, where each node was self-contained and performed its own clock recovery. To access the performance of the 'drop and insert' process, each channel was demultiplexed and bit-error-rates measurements taken. The system showed excellent performance, with a clear open eye and no indication of an error floor, provided the inserted channel was orthogonal.

7.5.4 Full 'drop and insert' multiplexing

As stated in section 7.5.1, full 'drop and insert' multiplexing requires two synchronously driven modulators, each with a complementary switching duration. The first modulator performs the 'drop' function, and the second modulator performs the demultiplexing operation (see Figure 7-13).

An EA modulator can be considered as a high-speed pin-diode. This property has recently been proposed to allow full 'drop and insert' multiplexing using a single EA modulator via novel photo-detection [84]. The principle is outlined in Figure 7-19.

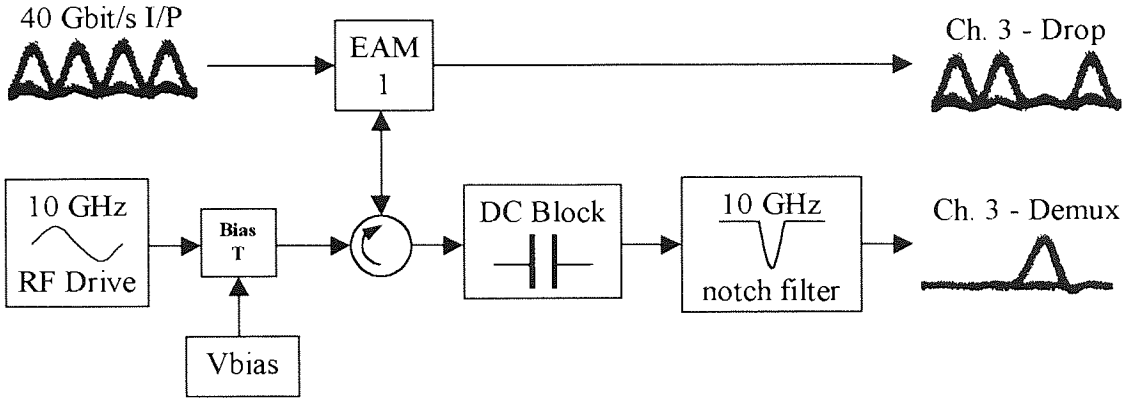

Figure 7-19. Full D&I multiplexing using photo-detection.

Here the EA modulator is biased into transmission, and switched into absorption for a fraction of the drive cycle. The enables a single channel to be dropped, and three channels to pass unaffected to the output. If there is a data 'one' in the time-slot of the dropped channel, it will be absorbed generating carriers within the active region of the modulator. This can then be detected as a voltage across the device, using appropriate filters to remove the residual 10 GHz RF drive signal. Preliminary results indicate that error free operation is not feasible given current device operating characteristics. This is due to background absorption leading to signal crosstalk [84]. The technique is the subject of further investigations.

7.6 High Extinction Pulse Source using a Single EA Modulator

7.6.1 Introduction

The characteristics of an optical pulse source suitable for use in an OTDM network were discussed in section 3.7. One of the most important parameters is the optical extinction ratio, for a 4×10 Gbit/s system this must be greater than 36 dB, and for a 8×10 Gbit/s system it must be >44 dB, and therefore represents a difficult, although not impossible

target for device fabrication. The simplest way to overcome the extinction ratio limitations, is to cascade two synchronously driven modulators, as detailed in section 7.2.

This technique doubles the number of modulators, and therefore increases the system complexity and cost. A much better solution is to adopt a double-pass strategy of a single modulator. The principles of this technique were first demonstrated by measuring the *dc* extinction ratio of a 130 μm bulk EA modulator with a high-reflectivity coating on the back-facet [268]. The device had a bandwidth of 20 GHz, and had a single-pass dc extinction ratio of 10 dB, which was doubled to 20 dB in a double-pass configuration. Conventionally to achieve this level of extinction ratio, a 260 μm device would have had to be adopted, resulting in a corresponding decrease in the device modulation bandwidth. The technique therefore allows a trade-off between device extinction ratio and required bandwidth.

The following experiment extends the ideas detailed above to generate high extinction ratio optical pulses suitable for use in a 40 or 80 Gbit/s OTDM system.

7.6.2 Experimental setup

Figure 7-20 shows the experimental setup. A 1557 nm CW-DFB is incident on EAM#2 which was driven at 10 GHz using a HP synthesiser. The 10 GHz, 12 ps pulse stream generated at the output was amplified, 10% was detected at output port A via a 90/10 coupler, the remaining signal was fed through an isolator before being coupled back through the same EA modulator.

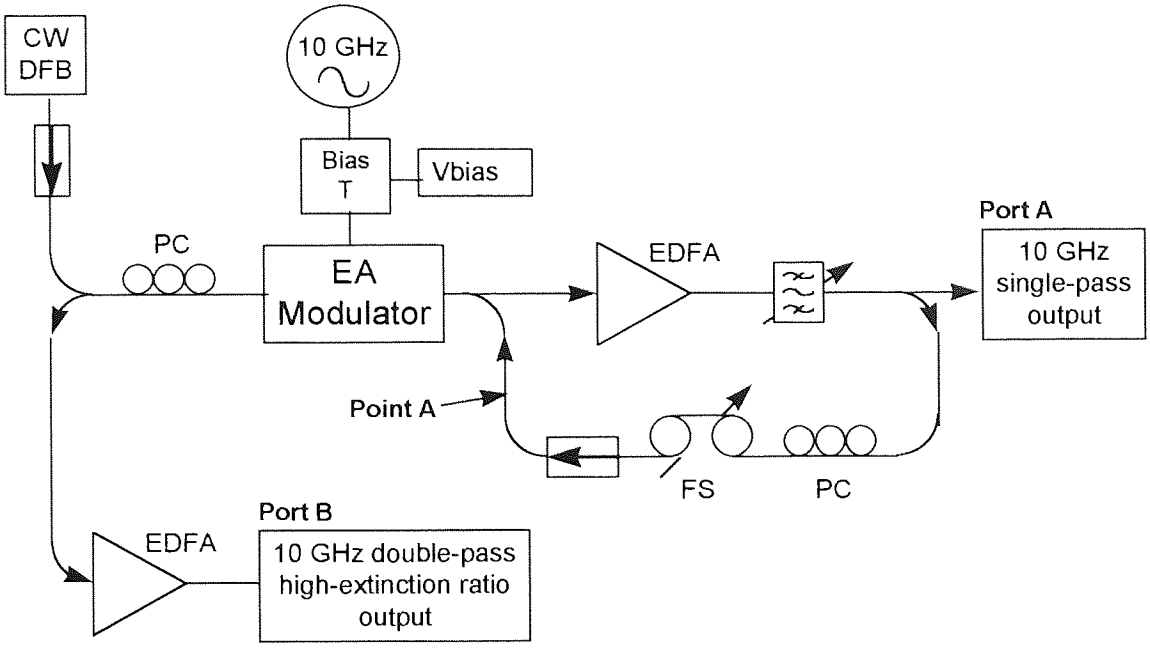

Figure 7-20. Experimental setup of a high extinction ratio double-pass optical source

The final output was amplified and compressed using dispersion compensating fibre, before being detected at port B.

7.6.3 Results

Preliminarily results indicated that the source suffered from a large degree of amplitude jitter. Figure 7-21a shows the output of Port A monitored on a 50 GHz sampling oscilloscope and a 32 GHz pin diode. Intrinsic phase noise from the DFB laser source is converted into excess intensity noise due to incoherent interference between the single-pass signal, and a reflection from the same signal [267], returned to the device in the opposite direction for the second pass. The effect is greatly intensified due to the amplifier gain, and also because of the additional presence of signal-spontaneous emission beat noise [269].

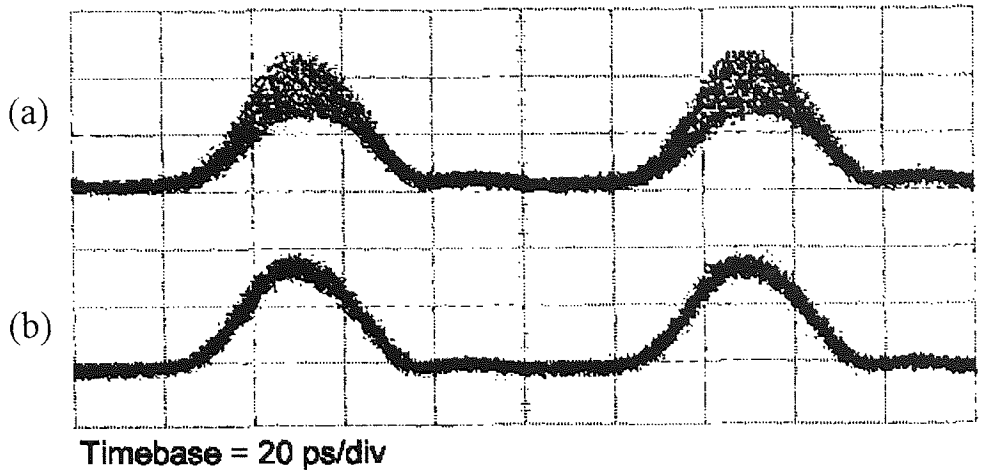

Figure 7-21. Results of the output at Port A. (a) maximum incoherent interference – aligned polarisations; (b) minimum incoherent interference – orthogonal polarisations.

The effect can be almost eliminated (see Figure 7-21b) by firstly arranging that the two signals were at orthogonal polarisations [267], and secondly using a large transmission window which on each pass of the modulator could be used to shape the signal into a very narrow pulse stream [270], the principle is illustrated in Figure 7-21.

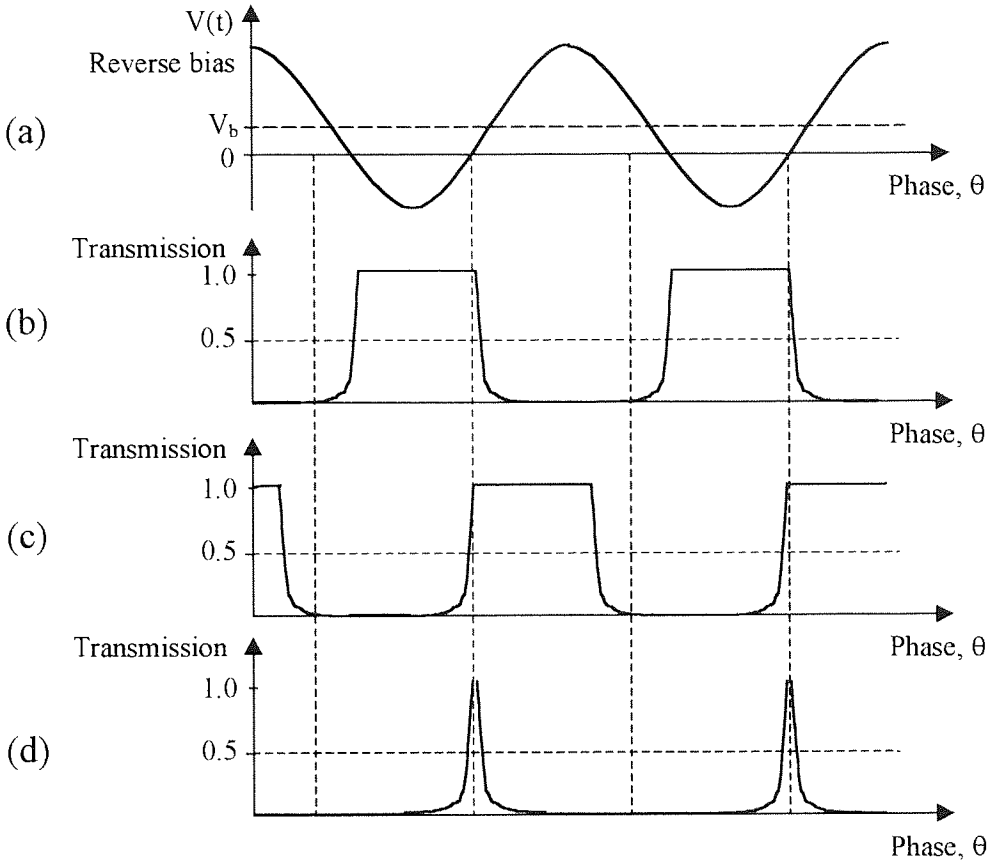

Figure 7-22. Analysis of the operation of a double-pass, high-extinction pulse source; a) sinusoidal voltage supplied to EA modulator; b) single-pass output from EA modulator, with large transmission window to avoid incoherent interference; c) transmission window seen on second-pass of EA modulator; d) output after double-pass of EA modulator

On the first pass of the modulator the CW light is shaped by the nonlinear absorption characteristics of the EA modulator to produce a rectangular stream of pulses, see Figure 7-22b. If the rectangular stream of pulses is fed back through the modulator at the correct instance, then they will pass through the device relatively unaffected, apart from an increase in pulse extinction ratio. If however the phase of the returning pulse stream is adjusted so that it is on the edge of the modulator switching window, see Figure 7-22c, then the output will be a stream of high quality optical pulses with a extremely low duty cycle, given by Equation 7-8 [270], and a high extinction ratio, see Figure 7-22d.

$$\Delta\tau \approx \frac{20\log 2}{\pi k V_{p-p}} \qquad \textbf{Equation 7-8}$$

To more accurately access the degradation due to incoherent interference, the output of Port A was monitored between 50 kHz and 1 MHz using an electrical spectrum analyser and a low frequency photodiode.

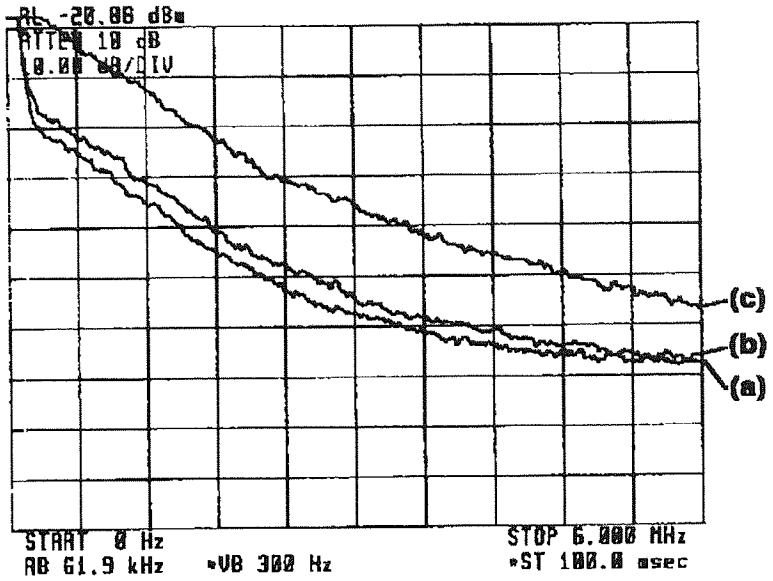

Figure 7-23. Microwave spectrum used to analysis incoherent interference between the wanted pulse stream and the reflected signal. (a) EA modulator used as a conventional single pass pulse source, power density = 2.0×10^{-4}; (b) EA modulator used as a double pass pulse source, when signal and unwanted reflection are at orthogonal polarisations, power density = 5.6×10^{-4}; (c) EA modulator used as a double pass pulse source, when signal and unwanted reflection are aligned in polarisation, power density = 7.4×10^{-2}.

The power spectral density was measured by integrating the area below the curve. Figure 7-23a has a power density of 2.0×10^{-4} and shows the results when the EA modulator is operated as a conventional single-pass source (i.e. with point A disconnected). Figure 7-23b shows the results when point A is connected. The required 10 GHz signal and the reflected signal are at orthogonal polarisations, representing a point of minimum interference and an associated power density of 5.6×10^{-4}. Figure 7-23c represents the point of maximum interference (polarisations aligned) and has an associated power density of 7.4×10^{-2} showing significant degradation.

These preliminary results indicate that the main limiting factor is the residual facet reflectively. Further work is continuing in this area, initially using a fibre polariser to prevent the amplified reflection from causing any interference, and secondly using a new packaged EA modulator which has AR-coated lens-ended fibre, which is hoped to have a

lower associated reflectivity. Once these effects have been reduced, then the configuration should allow high extinction pulses to be produced. Such a source should be suitable for use in an 80 Gbit/s OTDM network.

7.7 Chapter Summary

This chapter demonstrated for the first time, the use of an EA modulator in a bi-directional configuration for use within an OTDM network. Two independent 10 Gbit/s channels were demultiplexed from a 40 Gbit/s OTDM data stream. The effects of incoherent interference between the demultiplexed channels and residual facet reflections were investigated. BER measurements showed, even at a point of maximum incoherent interference the system operated error-free, with less than 1.6-dB penalty. This configuration allows the number of high-speed components to be reduced, therefore improving system reliability, whilst also significantly reducing costs.

A novel method of clock recovery was demonstrated that exploited the bi-directionality of the EA modulator, to derive an error signal which was independent from the switching process. Operation was demonstrated by using a single EA modulator to demultiplex a 10 Gbit/s channel from a 40 Gbit/s OTDM data stream, whilst simultaneously recovering the 10 GHz electrical clock. The system showed excellent stability and used reliable low-speed inexpensive components. The recovered clock had a phase noise-induced timing jitter of <150 fs, indicating operation up to and beyond 100 Gbit/s is possible.

40 Gbit/s 'drop and insert' multiplexing was demonstrated for the first time, using an EA modulator. Excellent performance was observed, and confirmed using BER measurements. Each of the undropped 10 Gbit/s channels operated error-free with no indication of an error floor, but incurred a 1-dB penalty. This is thought to be due to the extra processing on these channels and the imperfect transmission window at the 'drop' stage. The inserted channel however suffered from no significant penalty.

Finally preliminary results on a high extinction, 10 GHz pulse source were presented. The source suffered from a large degree of amplitude jitter as a result of residual reflection from the EA modulator, causing incoherent interference. In practice this effect could be minimised by using angle-facet devices or tapered waveguides similar to those used with lasers and semiconductor optical amplifiers [221]. Once this problem has been overcome, a high extinction ratio source for use in >40 Gbit/s OTDM network should be possible. The technique will also allows for a trade-off between device extinction ratio and required bandwidth.

In summary, bi-directional operation of any electro-optic modulator (at the same or at a different wavelength) will allow the number of high-speed components with the network to be reduced, therefore improving reliability, whilst substantially reducing costs.

Chapter 8

Summary and conclusions

8.1 General Summary

This thesis explored the use of optical time division multiplexing (OTDM) as a possible solution to overcome the exponentially increasing bandwidth requirements that are being placed upon the current telecommunications network.

After Chapter 2, which introduced the fundamental concepts and limitations associated with single-mode optical communications, Chapter 3 outlined the basic functionality of an OTDM network. The building blocks from which an OTDM network may be constructed were identified. Each function was described in detail, and the most promising solutions were outlined and compared. The basic building blocks are a picosecond optical pulse source, a demultiplexer, a 'drop and insert' multiplexer, and a clock recovery unit. In practice, a data regenerator may also be required.

Three of the most promising optical sources were used throughout this thesis. These were the fibre ring laser, the external cavity modelocked laser (ECMLL), and the external modulation of a CW by an electroabsorption (EA) modulator. The fibre ring laser and the ECMLL are ideal laboratory sources, but are relatively bulky and complex to setup, and therefore are unlikely to be deployed in the field. The external modulation by an EA modulator is a very promising alternative, offering wide bandwidths, low-drive voltages, polarisation insensitivity, wide wavelength operation and high extinction ratios. Such devices have been used to generate transform-limited pulses with $sech^2$ to *gaussian* intensity profiles. They have also been integrated with CW-DFB lasers to produce stable, reliable, monolithic devices. However, as the number of channels in an OTDM network is increased, the multiplexing constraints impose very stringent requirements on the extinction ratio and the duty-cycle of the optical pulse source. The extinction ratio

requirements can be achieved by cascading two EA modulators, and the duty-cycle reduced by using a harmonic drive signal. EA modulators were also used for high-speed optical switching, and were described in detail in Chapter 6, and then used experimentally in Chapter 7.

Another very promising device that has been used extensively for optical switching is the semiconductor optical amplifier-based nonlinear optical loop mirror (SOA-NOLM). The SOA-NOLM overcomes the disadvantages associated with the standard fibre-NOLM, by replacing the long lengths of fibre necessary to achieve switching with a short semiconductor optical amplifier (SOA). The SOA-NOLM has a fundamentally square switching window determined by SOA offset from the centre of the loop, and not by carefully selecting operating wavelengths to obtain the desired walk-off effect, as with the standard fibre-NOLM. Other advantages with the SOA-NOLM include a low switching energy, and improved environmental stability due to shorter loop length. Chapter 4 introduced the SOA and describes different applications of its use as a nonlinear element within an OTDM network. Before describing the basic operation of an SOA-NOLM, the nonlinear processes of gain saturation and gain recovery were outlined. To achieve all-optical demultiplexing, an intense clock at the OTDM base-rate was used to switch a single channel from an incoming OTDM data-stream into transmission. The intense clock pulse defines the temporal evolution of the SOA carrier density, while also providing a periodic cross-phase modulation of the low intensity signal, which was exploited in the switching process.

Periodically amplified RZ transmission systems are essentially analogue in nature, and therefore accumulate transmission impairments over the system length. In a linear transmission system, this will be due to a combination of group velocity dispersion resulting in inter-symbol interference and signal-to-noise degradations due to spontaneous-emission from the optical amplifiers. If soliton transmission is considered, the temporal profile of the pulse will be maintained, but it will however acquire a random timing jitter. To extend the maximum transmission distance, it is often desirable to

regenerate the transmitted data stream. This may be carried out midway through a point-to-point transmission link, or at a 'drop and insert' node within the network. At a 'drop and insert' node, if the inserted channel has a slightly different centre wavelength from the data stream it is inserted into, then group velocity dispersion may result in the channel 'walking out' of its own time slot. If the inserted data channel has a different temporal profile, then energy will be shed in the form of a dispersive wave, which will interfere with the other signals and degrade the receiver sensitivity.

Data regeneration can be achieved using an SOA-NOLM, by letting the incoming degraded data stream switch a clean locally generated clock into transmission. If the clock operates at the OTDM line-rate then full data regeneration is achieved. However, if the clock is set to the OTDM base-rate, then demultiplexing with inherent data regeneration is achieved. A high switching extinction ratio is ensured, and interchannel crosstalk is eliminated simply by the absence of light from the clock pulses used to probe the switching of the SOA-NOLM.

Demultiplexing has been investigated by other authors, with impressive results. An SOA-NOLM has been used to demultiplex a 10 Gbit/s channel from a 160 Gbit/s OTDM data stream. Although data regeneration has been proposed and demonstrated, it has not been fully analysed. Chapter 5 presents experimental results on all-optical data regeneration using an SOA-NOLM at both 2.5 Gbit/s and 10 Gbit/s. The results of 10 Gbit/s to 2.5 Gbit/s demultiplexing, with data regeneration are also investigated. Q-measurements were made to assess the regeneration process. A 2.5 Gbit/s input data stream with a Q of 5.9 was regenerated to a Q of 18.4. At 10 Gbit/s a Q of 6.4 was regenerated to a Q of 10.3. Similar impressive results were observed for simultaneous demultiplexing and regeneration, where an input data stream with a Q of 7.0 and a timing jitter of 6.0 ps was regenerated to a Q of 13.9 and a timing jitter of less than 1.5 ps. The SOA-NOLM demonstrated excellent regenerative properties for signals degraded by both amplitude and timing jitter.

To synchronise the switching and detection processes, the clock recovery unit must extract a low-jitter, base-rate clock from the transmitted data stream operating at a higher line-rate. One of the most promising methods of clock recovery is based on a phase locked loop (PLL), which relies on a phase detector (electrical or optical) to determine the frequency mismatch between the incoming data stream and a locally generated clock. An important feature of an interleaved OTDM data signal is that it does not contain a RF component at the base-rate clock frequency, only at the higher line-rate. Therefore, high-speed electronic receivers and mixers are required to determine the frequency mismatch. Alternatively, base-rate clock recovery can be achieved after the demultiplexer, where an appropriate RF component exists.

The demultiplexer takes a time-slice of the incoming data stream, and under ideal conditions this time-slice corresponds to a single channel. As the phase shifts between the incoming signal and the locally generated clock, the average power will vary similar to a *raised-cosine*. For maximum switching efficiency and therefore minimum system penalty, the phase of the recovered clock should ideally lock to the peak of the *cosine* function. This makes it difficult for the feedback electronics to tell in which direction the phase has drifted. Locking to halfway down the function where the gradient is a maximum, a change in power will indicate the magnitude and direction of any phase drifts, but the switching efficiency will be degraded. Therefore, a trade-off is made between switching efficiency and system stability.

By using the SOA-NOLM switching properties with its inherent sampling ability, the reminder of Chapter 5 demonstrated for the first time, simultaneous demultiplexing, data regeneration and clock recovery using a single SOA-NOLM [20, 21]. A 2.5 Gbit/s channel is demultiplexed from a 10 Gbit/s OTDM data stream while simultaneously recovering the 2.5 GHz clock.

To achieve optimum switching, and therefore data regeneration, it is necessary to phase lock to the peak of the switching window. This was achieved by adopting a technique

known as 'dithering'. By frequency modulating the local clock, a differential error signal was obtained, which was used to correct for the direction and magnitude of any phase drifts. The technique however imposes a large timing variance on the recovered clock, which at higher data rates would degrade the system performance.

EA modulators have been used in a number of impressive OTDM system experiments. They are ideally suited to pulse generation, data encoding, demultiplexing, and 'drop and insert' multiplexing. All of these applications use the EA modulator in a unidirectional configuration, but there is no inherent reason for this limitation. Before Chapter 7, which presented experimental results on the use of an EA modulator in a novel bi-directional configuration, Chapter 6 outlined the fundamental properties of the EA modulator. It described how such a device was used for picosecond pulse generation, and high-speed demultiplexing. For full demultiplexing within an OTDM node, a different EA modulator would be required for each channel, therefore eight modulators are needed for an 80 Gbit/s (8×10 Gbit/s) OTDM system. Chapter 7 demonstrated how a single EA modulator can be used in a bi-directional configuration to demultiplex two independent 10 Gbit/s channels from a 40 Gbit/s OTDM data stream [22]. The effects of incoherent interference between the demultiplexed channels and residual facet reflections were investigated. BER measurements show that even at a point of maximum incoherent interference, the system operated error-free with no indication of an error floor, and less than a 1.6-dB penalty.

The clock recovery unit in an OTDM node must extract a low-jitter, base-rate clock from the transmitted data stream operating at a higher line-rate. To date, the only possible solution to this problem was to adopt the technique known as 'dithering', which allowed a differential error signal to be obtained. This technique was adopted in Chapter 5, where an SOA-NOLM was used to perform simultaneous demultiplexing, data regeneration, and clock recovery. The technique however imposes a large timing variance on the recovered clock.

This thesis presented a novel form of clock recovery, which exploits the bi-directionality of an EA modulator to derive an error signal that is independent from the switching process. A 10 Gbit/s channel was demultiplexed from a 40 Gbit/s OTDM data stream, whilst simultaneous recovering the 10 GHz base-rate electrical clock [23]. The system showed excellent stability, and used low-speed electronics for the clock recovery process. BER measurements indicated no additional switching penalty compared with the same device operating with a clock derived from the original data stream. Operation at 100 Gbit/s is predicted to be possible using devices similar to those used in these experiments.

An important functionality within an OTDM node is 'drop and insert' multiplexing. Here, the optical switch must completely remove a single data channel (the 'drop'), while leaving the remaining channels undisturbed. It is then a simple matter to insert a different data stream into the vacant time-slot (the 'insert'). If the dropped channel is not completely removed, then crosstalk between the inserted channel and the remaining signal can cause incoherent interference, effectively degrading the system performance. A 40 Gbit/s 'drop and insert' node was demonstrated using EA modulators [24]. Clock recovery was achieved using the bi-directionality of an EA modulator as outlined above, thus demonstrating the flexibility of such a technique. A 10 Gbit/s channel was completely removed from a 40 Gbit/s OTDM data stream. A different channel was then inserted into the vacant time-slot. Each channel was then demultiplexed, and the effects of incoherent interference were analysed. Excellent performance was observed, and confirmed using BER measurements. Each of the 'undropped' 10 Gbit/s channels operated error-free with no indication of an error floor but they incurred a 1-dB penalty. This is thought to be due to the extra processing on these channels and the imperfect transmission window at the 'drop' stage. The inserted channel however suffered from no significant penalty.

It must be noted that to achieve full 'drop and insert' functionality, two synchronously driven electro-optic modulators are necessary, each with a complementary switching

duration. The first modulator performs the 'drop' function, and the second modulator performs the demultiplexing operation. All-optical switching devices (e.g. SOA-NOLM) on the other hand, perform both demultiplexing and 'drop' functionality using a single device.

In order to generate a 10 GHz optical pulse stream with an extinction ratio that is suitable for encoding and multiplexing up to 40 Gbit/s, then two synchronously driven EA modulators must be cascaded in series (see section 7.2). Section 7.6 demonstrated, how in theory, a high extinction pulse stream could be generated using a single EA modulator. A CW-DFB was passed through an EA modulator, the pulse stream generated on the first pass, was then fed back through the same device in the opposite direction. The source suffered from a large degree of amplitude jitter caused by incoherent interference from residual facet reflection. It is predicted that once this effect has been reduced by using, for example, angle facet devices, then the configuration should allow high extinction pulses to be produced. Such a source should be suitable for use in an 80 Gbit/s OTDM network.

By exploiting the bi-directionality of an EA modulator, the number of high-speed components can be reduced, therefore increasing system reliability, whilst also substantially reducing system costs.

8.2 Future Experiments

The remainder of this chapter outlines general developments that are required to allow an ultra high speed (>100 Gbit/s) OTDM network to be realised. It then describes further work relating specifically to the development of the ideas presented in this thesis.

8.2.1 Developments in optical switching technology

One of the main factors which limits the wide-spread deployment of a high speed OTDM network is the practical realisation of a transform-limited optical pulse source. Such a

source should be stable, compact, and relatively easy to use. It should also exhibit a low duty-cycle combined with a high extinction ratio. The EA modulator is a very promising candidate. However, further developments still need to be made. Important parameters that need to be improved and optimised are the device bandwidth, modulation efficiency, extinction ratio, polarisation sensitivity, wavelength sensitivity, and device insertion loss. Another factor that must be considered if the EA modulator is to be used in a bi-directional configuration, is the device facet reflectivity. There are various solutions to this problem, from using angle facet devices to tapered waveguides. The latter of which should also decrease the fibre-to-device coupling losses and therefore modulator insertion loss.

The EA modulator has also been used extensively as a high-speed optical switch, and has been used to achieve data encoding, demultiplexing, and 'drop and insert' multiplexing. 40 GHz packaged devices have already been demonstrated, although at present they suffer from a relatively low extinction ratio. However, in principle as 40 Gbit/s chip-sets become available, then a 320 Gbit/s (8×40 Gbit/s) OTDM network should be feasible. Therefore, it is predicted that the EA modulator will be an integral part of the next generation of an OTDM network. Above this rate, all-optical switching technologies may have to be employed.

One of the most promising all-optical switching technologies is the SOA-NOLM, which has been used to demultiplex a 10 Gbit/s channel from a 160 Gbit/s OTDM data stream. Such a configuration uses a regular intense control pulse to periodically define the carrier evolution of the semiconductor optical amplifier. However, if a data stream is used to switch an SOA-NOLM, then the carrier evolution is no longer periodic, and the gain recovery time of the device can result in severe patterning effects. This effect was observed in Chapter 5, where an SOA-NOLM was used to perform data regeneration. Data pattering an be avoided by ensuring that the gain recovery time is less than the bit-period of the switching data stream. The gain recovery time of the devices used in this thesis was approximately 100 ps, limiting the data regeneration rate to 10 Gbit/s.

Therefore, further research should aim to reduce the gain recovery time. To increase the data regeneration rate up to 100 Gbit/s, a recovery time of less than 10 ps is required. This is a challenging target, and in practice, other nonlinear elements may have to be explored.

The interferometric nature of the SOA-NOLM makes it susceptible to environmental fluctuations, and therefore unlikely to be deployed in the field. The SOA-NOLM used in this thesis also performs wavelength conversion. This would be undesirable if the device was used to perform data regeneration in a point-to-point transmission link. Efforts to avoid wavelength conversion involve complex polarisation-maintaining components.

A very promising alternative to the SOA-NOLM is the SOA Mach-Zehnder interferometer (SOA-MZI). Environmental instabilities have been substantially reduced by monolithically integrating the device. Wavelength conversion and polarisation issues can be avoided by arranging that the control and signal pulses propagate in opposite directions.

8.2.2 Extensions to work outlined in this thesis

A major part of this thesis was based on all-optical data regeneration using an SOA-NOLM. The performance of the regeneration process was assessed by measuring the Q-value of an artificially degraded input data stream, and comparing it with the Q-value at the output of the regenerator. When analysing Q-measurements it is important to note that a regenerator cannot correct an error once it has occurred, only prevent it from happening. Therefore, an input Q of 5 that is regenerated to an output Q of 15 can give misleading results. The only reliable way to confirm the performance of a regenerator is to perform BER measurements in conjunction with real transmission impairments. Here, the transmitted data stream will be subjected to true transmission impairments, such as dispersion, SNR degradations, timing jitter, and nonlinear propagation effects. Using a recirculating loop experiment, the system penalty should be plotted against transmission

distance, both with and without the regenerator present. Further research should investigate increasing the bit-rate to 20 Gbit/s and 40 Gbit/s.

The SOA-NOLM was also used to perform simultaneous clock recovery. To improve system stability and obtain optimum regeneration, a technique known as dithering was used. This resulted in a large timing variance on the recovered clock, which limited the system performance. Further work should look into optimising the feedback electronics, and explore the possibility of using a high-speed (200 MHz) lock-in amplifier. The other disadvantage with this technique of clock recovery, is that it arbitrarily locks to any channel. Further work should explore the possibility of 'dithering' each channel at a different frequency before multiplexing, and then using the lock-in amplifier to select each channel as required [271].

The remainder of this thesis was based on the bi-directional operation of an EA modulator. The main limiting factor in using an EA modulator in a bi-directional configuration was that residual facet reflections caused incoherent interference effects, thereby degrading the system performance. The design and packaging of subsequent devices should concentrate on reducing this effect.

In its simplest configuration, bi-directional operation allowed two independent 10 Gbit/s channels to be demultiplexed from a 40 Gbit/s OTDM data stream. A simple extension to this work would be to demonstrate two-channel 'drop' functionality. Further work should aim to increase the data rate up to at least 80 Gbit/s. This should be feasible using the same optical pulse source, simply by adding an extra multiplexing stage. The EA modulator would need to be harmonically driven in order to obtain the required switching window.

Electronic based clock recovery using a harmonic mixer, and a high-speed pin diode is only expected to be possible up to 100 Gbit/s. Beyond this, device packaging would be almost impossible. This thesis presented a novel method of clock recovery, which

exploited the EA modulators bi-directionality to obtain an error signal that was independent from the switching process. The system used low-speed electronics, was extremely stable, exhibited no additional switching penalty, and operated with ultra-low timing jitter on the recovered clock. Further work should involve the development of the feedback electronics to account for variations in input power levels. The capture and locking should be measured and maximised. The effects of timing jitter on the clock recovery process should also be analysed.

This thesis demonstrated a self contained 40 Gbit/s 'drop and insert' node using an EA modulator. To maximise the effects of incoherent interference (for analysis purposes), the inserted channel was derived from the same optical source as the OTDM data stream. All channels therefore had the same temporal and spectral characteristics. The experiment should be extended so that the inserted channel is derived from a different pulse source, with a slightly different centre wavelength and pulse width. This would better simulate the conditions that are present in an installed OTDM network. Pulse 'walk-off' due to group velocity dispersion could then be analysed, and the effects of nonlinear power evolution could be assessed. The scalability of the node should also be measured. Data regeneration at the output of the 'drop and insert' node should be analysed.

Full 'drop and insert' multiplexing requires two synchronously driven modulators, each with a complementary switching duration. The first modulator performs the 'drop' function, and the second modulator performs the demultiplexing operation. An EA modulator can be considered as a high-speed pin-diode. Further research should investigate the use of the photo-detection properties of the EA modulator to allow full 'drop and insert' multiplexing using a single device.

The final long term goal would be to develop a 320 Gbit/s (8×40 Gbit/s) OTDM test bed. The optical source and demultiplexer requirements are obtained with reference to section 3.7. For less than a 1 dB penalty, the pulse source must generate a 40 GHz pulse

stream with a pulse width of < 1 ps, and an extinction ratio of > 45 dB. These are quite challenging goals, and a mode-locked device may have to be used. The first possible candidate is an actively mode-locked ring-laser employing an EA modulator and an SOA, which has recently been shown to demonstrate picosecond pulses [272]. Alternatively, with improved packaging technology based on that used in the *SANTEC* ECL-100 [273], a 40 GHz ECMLL may become a very promising alternative. To demultiplex a 40 Gbit/s channel from a 320 Gbit/s OTDM data stream with less than a 1 dB penalty, an extinction ratio of greater than 18 dB and a switching window of less than 2.5 ps is required. To achieve this using an EA modulator, improvements in modulation efficiency and frequency response will be required. However, recent results indicate that such devices will probably be demonstrated within the next 2-3 years [246, 248].

Appendix A

Journal Publications and Conference Presentations

Journal Publications

1. I. D. Phillips, A. Gloag, D. G. Moodie, N. J. Doran, I. Bennion, and A. D. Ellis, "Drop and insert multiplexing with simultaneous clock recovery using an electroabsorption modulator", *IEEE Photonics Technology Letters*, vol. 10, no. 2, pp. 291—293, (1998)

2. I. D. Phillips, A. Gloag, D. G. Moodie, N. J. Doran, I. Bennion, and A. D. Ellis, "Simultaneous demultiplexing and clock recovery using a single electroabsorption modulator in a bi-directional configuration", *Accepted from publication in Optics Communications June 1998*

3. I. D. Phillips, A. Gloag, D. G. Moodie, N. J. Doran, I. Bennion, and A. D. Ellis, "Simultaneous two channel OTDM demultiplexing using a single electroabsorption modulator in a novel bi-directional configuration", *Electronics* Letters, vol. 33, no. 21, pp. 1811—1812, (1997)

4. I. D. Phillips, A. Gloag, P. N. Kean, N. J. Doran, I. Bennion, and A. D. Ellis, "Simultaneous demultiplexing, data regeneration, and clock recovery with a single semiconductor optical amplifier-based nonlinear-optical loop mirror", *Optics Letters*, vol. 22, no. 17, pp. 1326—1328, (1997)

5. I. D. Phillips, A. Gloag, P. N. Kean, N. J. Doran, I. Bennion, and A. D. Ellis, "Simultaneous clock recovery and data regeneration using a nonlinear optical loop mirror as an all-optical mixer", *OSA TOPS – System Technologies*, vol. 12, pp. 423—426, (1997)

Patents

July 1997 — BT Patent number: 25454 - Covers work from publications [1, 2, 3]
D. G. Moodie, A. D. Ellis, A. Gloag, and I. D. Phillips
"Simultaneous bi-directional operation of an electroabsorption within an OTDM network"

Conference Presentations

Sept 1997 — **IOOC-ECOC '97,** Edinburgh, (Post-deadline oral presentation)
I. D. Phillips, A. Gloag, D. G. Moodie, N. J. Doran, I. Bennion, and A. D. Ellis, "40 Gbit/s 'drop and insert' multiplexing with novel clock recovery using an electroabsorption modulator in a bi-directional configuration", *Technical Digest ECOC 1997*, vol. 5, paper TH3A-PD, pp. 81—84

Feb 1997 — **OFC '97**, Dallas, Texas (Oral presentation)
I. D. Phillips, A. Gloag, P. N. Kean, N. J. Doran, I. Bennion, and A. D. Ellis, "Simultaneous clock recovery and data regeneration using a nonlinear optical loop mirror as an all-optical mixer", *Technical Digest OFC 1997*, paper ThH5, pp. 273—274

References

1. "Synchronous Transmission Systems", Northern Telecom Europe, Oakleigh Raod South, New Southgate, London, N11 1HB, UK, Doc – GH9, Issue 3.1

2. K. Runge, R. L. Pierson, P. J. Zampardi, P. B. Thomas, J. Yu, and K. C. Wang, "40 Gbit/s AlGaAs/GaAs HBT 4/1 multiplexer IC", *Electronics Letters*, vol. 31, no. 11, pp. 876—877, (1995)

3. C. Svensson, "The limits to high-speed electronics", *Technical Digest ECOC 1997*, vol. 4, paper TH2C, pp. 85—89

4. A. Felder, M. Moller, J. Popp, J. Bock, and H. M. Rein, "46 Gb/s demux, 50 Gb/s mux, and 30 GHz static frequency-divider in Silicon bipolar technology", *IEICE Transactions on Electronics*, paper E79C, pp. 892—897, (1996)

5. M. Moller, H. M. Rein, A. Felder, J. Popp, and J. Bock, "50 Gbit/s time-division multiplexer in Si-bipolar technology", *Electronics Letters*, vol. 31, no. 17, pp. 1431—1433, (1995)

6. N. S. Bergano, and C. R. Davidson, "Wavelength division multiplexing in long-haul transmission systems", *Journal of Lightwave Technology*, vol. 14, no. 6, pp. 1299—1308, (1996)

7. P. E. Green, "Fibre Optic Networks", (Prentice Hall, Englewood, Cliffs, NJ, 1993)

8. C. A. Brackett, "Dense wavelength division multiplexing networks - principles and applications", *IEEE Journal On Selected Areas in Communications*, vol. 8, no. 6, pp. 948—964, (1990)

9. V. Mizrahi, S. Alexander, J. Berthold, S. Chaddick, W. Jones, "The future of WDM systems", *Technical Digest ECOC 1997*, paper MO4A, pp. 137—141

10. S. Merli, F. Arecco, A. Mariconda, F. Pozzi, F. Veghini, and E. Iannone, "The "Prometeo" test bed: A unidirectional WDM transparent self healing ring in a field environment", *Technical Digest ECOC 1997*, paper WE4C, pp. 347—350

11. A. A. Dealbuquerque, A. J. N. Houghton, and S. Malmros, "Field trials for fiber access in the EC", *IEEE Communications Magazine*, vol. 32, no. 2, pp. 40—48, (1994)

12. T. Lynch, et al, "Experimental field demonstration of a managed multinoded, reconfigurable, wavelength-routed optical network", *Technical Digest ECOC 1992*

13. CIENA Corporation, 920 Elkridge Landing Road, Linthicum, MD 21090, USA. Tel: 410-865-8500, Fax: 410-865-6800, Email: marketing@ciena.com, Web: www.ciena.com

14. D. A. Cleland, A. D. Ellis, and C. H. F. Sturrock, "Precise modeling of 4-wave-mixing products over 400km of step-index fiber", *Electronics Letters*, vol. 28, no. 12, pp. 1171—1173, (1992)

15. J. C. Feggeler, D. G. Duff, N. S. Bergano, C. C. Chen, Y. C. Chen, et al, "WDM transmission measurements on installed optical amplifier undersea cable systems", *Technical Digest OFC 1996*, paper TuN3, pp. 72—73

16. S. Bigo, A. Bertaina, M. Chbat, S. Gurib, J. D. Loura, J. C. Jacquinot, J. Hervo, P. Bousselet, S. Borne, D. Bayart, L. Gasca, and J. L. Beylat, "320 Gbit/s WDM transmission over 500 km of conventional single-mode fibre with 125-km amplifier spacing", *Technical Digest ECOC 1997*, vol. PD, paper TH3A, pp. 17—22

17. H. Taga, T. Miyakawa, K. Murashige, N. Edagawa, M. Suzuki, H. Tanaka, K. Goto, and S. Yamamoto, "A half Tbit/s (50x10.66 Gbit/s), over 1600 km transmission experiment using widely gain-flattened EDFA chains", *Technical Digest ECOC 1997*, vol. PD, paper TH3A, pp. 13—18

18. D. M. Spirit, and L. C. Blank, "Optical-time division multiplexing for future high-capacity network applications", *British Telecommunications Technology Journal*, vol. 11, no. 2, pp. 35—45, (1993)

19. D. M. Spirit, A. D. Ellis, and P. E. Barnsley, "Optical-time division multiplexing - systems and networks", *IEEE Communications*, vol. 32, no. 12, pp. 56—62, (1994)

20. I. D. Phillips, A. Gloag, P. N. Kean, N. J. Doran, I. Bennion, and A. D. Ellis, "Simultaneous clock recovery and data regeneration using a nonlinear optical loop mirror as an all-optical mixer", *Technical Digest OFC 1997*, paper ThH5, pp. 273—274

21. I. D. Phillips, A. Gloag, P. N. Kean, N. J. Doran, I. Bennion, and A. D. Ellis, "Simultaneous demultiplexing, data regeneration, and clock recovery with a single semiconductor optical amplifier-based nonlinear-optical loop mirror", *Optics Letters*, vol. 22, no. 17, pp. 1326—1328, (1997)

22. I. D. Phillips, A. Gloag, D. G. Moodie, N. J. Doran, I. Bennion, and A. D. Ellis, "Simultaneous two channel OTDM demultiplexing using a single electroabsorption modulator in a novel bi-directional configuration", *Electronics Letters*, vol. 33, no. 21, pp. 1811—1812, (1997)

23. I. D. Phillips, A. Gloag, D. G. Moodie, N. J. Doran, I. Bennion, and A. D. Ellis, "Simultaneous demultiplexing and clock recovery using a single electroabsorption modulator in a bi-directional configuration", *Electronics Letters*, In review October 1997

24. I. D. Phillips, A. Gloag, D. G. Moodie, N. J. Doran, I. Bennion, and A. D. Ellis, "Drop and insert multiplexing with simultaneous clock recovery using an electroabsorption modulator", *IEEE Photonics Technology Letters*, Accepted for publication October 1997

25. J. M. Senior, *Optical Fibre Communications - Principles and Practice*, (Prentice Hall, New York, USA, 1992, ISBN: 0-13-635426-2)

26. J. M. Dugan, A. J. Price, M. Ramadan, D. L. Wolf, E. F. Murphy, A. J. Antos, D. K. Smith, and D. W. Hall, "All-optical, fibre-based 1550nm dispersion compensation in a 10 Gbit/s, 150 km transmission experiment over 1310 nm optimised fibre", *Technical Digest OFC 1992*, paper PD14

27. M. Onishi, Y. Koyano, M. Shigematsu, H. Kanamori, and M. Nishimura, "Dispersion compensating fibre with a high figure of merit of 250 ps/nm/km/dB", *Electronics Letters*, vol. 30, no. 2, pp. 161—163, (1994.)

28. I. Bennion, J. A. R. Williams, L. Zhang, K. Sugden, and N. J. Doran, "UV-written in-fiber Bragg gratings", *Optical Quantum Electronics*, vol. 28, no. 2, pp. 93—135, (1996)

29. D. Garthe, W. S. Lee, R. E. Epsworth, T. Bricheno, and C. P. Chew, "Practical dispersion equaliser based on fibre Bragg gratings with a bit rate length product of 1.6 Tbit/s.km", *Technical Digest ECOC 1994*, vol. 4, paper PD11

30. A. D. Ellis, and D. M. Spirit, "Unrepeatered transmission over 80km standard fiber at 40 Gbit/s", *Electronics Letters*, vol. 30, no. 1, pp. 72—74, (1994)

31. G. P. Agrawl, "Nonlinear Fibre Optics", (Academic Press, 1995, isbn: 0-12-045142-5)

32. M. Nakazawa, E. Yamada, H. Kubota, and K. Suzuki, "10 Gbit/s soliton data-transmission over one million kilometers", *Electronics Letters*, vol. 27, no. 14, pp. 1270—1272, (1991)

33. T. Miya, Y. Terunuma, T. Hosaka, and T. Miyashita, "Ultimate low-loss single mode fibre at 1.55 um", *Electronics Letters*, vol. 15, no. 4, pp. 106—107, (1979)

34. L. F. Tiemeijer, P. J. A. Thijs, T. Dongen, J. J. M. Binsma, E. J. Jansen, and H. R. J. R. Vanhelleputte, "Reduced intermodulation distortion in 1300-nm gain-clamped MQW laser-amplifiers", *IEEE Photonics Technology Letters*, vol. 7, no. 3, pp. 284—286, (1995)

35. M. Settembre, M. Tamburrini, F. Matera, H. Haunstein, B. Teichmann, I. Gabitov, E. Laedke , K. Spatschek, S. K. Turitsyn, J.J.E. Reid, "Evaluation of 10 Gbit/s @ 1.3 μm signal transmission in fibre link using semiconductor optical amplifiers", *Technical Digest ECOC 1997*, vol. 1, paper MO3A, pp. 75—79

36. P. I. Kuindersma, G. P. J. M. Cuijpers, J. J. E. Reid, G. N. van den Hoven, and S. Walczyk, "An experimental analysis of the system performance of cascades of 1.3-um semiconductor optical amplifiers", *Technical Digest ECOC 1997*, vol. 1, paper MO3A, pp. 79—82

37. J. J. E. Reid, P. I. Kuindersma, G. P. J. M. Cuijpers, G. N. van den Hoven, S. Walczyk, B. Teichmann, C. Dorschky, R. Seitz, C. Schulien, L. Cucala, H. Gruhl, R. Leppla, and A. Mattheus, "High bit-rate 1.3-um optical transmission in the field using cascaded semiconductor optical amplifiers", *Technical Digest ECOC 1997*, session MO3A, pp. 83—86

38. G. N. Van den Hoven, P. I. Iiuindersma, G. P. Cuijpers, L.F. Tiemeijer, T. Van Dongen, J. J. Binsma, E.J. Jansen, and S. Walczyk,, "Optimizing semiconductor optical amplifiers for transmission systems", *Technical Digest ECOC 1997*, vol. 2, paper TU2B, pp. 90—94

39. A. D. Ellis, D. M. Patrick, D. Flannery, R. J. Manning, D. A. O. Davies, and D. M. Spirit, "Ultra-high speed OTDM networks using semiconductor amplifier based processing nodes", *Journal of Lightwave Technology*, vol. 13, no. 5, pp. 761—770, (1995)

40. Y. Ohishi, T. Kanamori, T. Kitagawa, S. Takahashi, E. Snitzer, and G. H. Sigel, "Pr3+ doped fluoride fibre amplifier operating at 1.3 um", *Optics Letters*, vol. 16, no. 22, pp. 1747—1749, (1991)

41. Y. Miyajima, T.Sugawa, and Y. Fukasaku, "38.2 dB amplification at 1.31 um and possibility of 0.98 pumping in Pr3+ doped fluoride fibre", *Electronics Letters*, vol. 27, no. 19, pp. 1706—1708, (1991)

42. T. Whitley, "1.3 micron optical amplifiers", *Focus Magazine*, no. 22, pp. 2—15, (1995)

43. M. C. Brierley, and C. A Millar, "Amplification and lasing at 1350 nm in Neodymium doped fluorozirconate fibre", *Electronics Letters*, vol. 24, no. 7, pp. 438—440, (1988)

44. H. Y. Tam, "Erbium-doped fiber amplifiers", *GEC Journal of Research*, vol. 10, no. 2, pp. 101—105, (1993)

45. E. Desurvire, "Erbium Doped Fibre Amplifiers – Principles and Applications", John Wiley & Sons, New York, isbn: 0-471-58977-2, 1994)

46. I. Bennion, "Lecture notes on Erbium doped fibre amplifiers", Lecture Course: E585, Department of Electronic Engineering & Apllied Physics, Aston University, Birmingham, England.

47. R. G. Smart, J. L. Zyskind, J. W. Sulhoff, and D. J. Digiovanni, "An investigation of the noise-figure and conversion efficiency of 0.98-um pumped erbium-doped fiber amplifiers under saturated conditions", *IEEE Photonics Technology Letters*, vol. 4, no. 11, pp. 1261—1264, (1992)

48. P. S. Henry, "Lightwave primer", *IEEE Journal of Quantum Electronics*, vol. 21, no. 12, pp. 1862—1879, (1985)

49. I. H. Malitson, et al, *Journal of the Optical Society of America*, vol. 55, pp. 1205—1207, (1965)

50. M. J. Adams, "An introduction to Optical Waveguides", (Wiley, New York, 1981)

51. C. R. South, "Total dispersion in step-index monomode fibres", *Electronics Letters*, vol. 15, no. 13, pp. 394—396, (1979)

52. K. I. White, and B. P. Nelson, "Zero total dispersion in step-index monomode fibres at 1.30 um and 1.55 um.", *Electronics Letters*, vol. 15, no. 13, pp. 396—398, (1979)

53. L. B. Jeunhomme, "Single-Mode Fibre Optics", (Marcel Dekker Inc., 1983)

54. B. J. Ainslie, and C. R. Day, "A review of single-mode fibres with modified dispersion charactersistics", *Journal of Lightwave Technology*, vol. 4, no. 8, pp. 967—979, (1986)

55. D. M. Spirit, and M. J. O'Mahony, "High Capacity Optical Transmission – Explained", (BT Series, J. Wiley & Sons, Sussex, England, ISBN: 0-471-95117-X, 1995)

56. C. Hentschel, "Fibre Optics Handbook – An Introduction and Reference Guide to Fibre Optic Technology and Measurement Techniques", Hewlett Packard GmbH, Germany, ISBN: 3-9801677-0-4, (1989)

57. N. J. Doran, "Nonlinear phenomena in optical fibres", *Electronic Engineering*, vol. 1, pp. 1—28, (1990)

58. H. A. Haus, "Optical-fiber solitons, their properties and uses", *Proceedings of the IEEE*, vol. 81, no. 7, pp. 970—983, (1993)

59. A. Hasagawa, and F. Tappert, "Transmission of stationary nonlinear pulse in dispersive dielectric fibres", *Applied Physics Letters*, vol. 23, pp. 142—144, (1973)

60. L. F. Mollenauer, R. H. Stolen, and J. P. Gordon, "Experimental observation of picosecond pulse narrowing and solitons in optical fibres", *Physical Review Letters*, vol. 45, pp. 1095—1097, (1980)

61. L. F. Mollenauer, E. Lichtman, M. J. Neubelt, and G. T. Harvey, "Demonstration using sliding frequency guiding filters, or error free soliton transmission over more than 20 Mm at 10 Gbit/s. single channel, and over more than 13 Mm at 20 Gbit/s using two 10 Gbit/s channels", *Electronics Letters*, vol. 29, pp. 910—911, (1993)

62. M. Nakazawa, Y. Kimura, K. Suzuki, H. Kubota, T. Komukai, and E. Yamada, "Field demonstration of soliton transmission at 10 Gbit/s over 2000km in Tokyo metropolitan optical loop network", *Electronics Letters*, vol. 31, no. 12, pp. 992—994, (1995)

63. M. Nakazawa, Y. Kimura, K. Suzuki, H. Kubota, T. Komukai, E. Yamada, T. Sugawa, E. Yoshida, T. Yamamoto, T. Imai, A. Sahara, O. Yamauchi, and M. Umezawa, "Soliton transmission at 20 Gbit/s over 2000 km in Tokyo metropolitan optical network", *Electronics Letters*, vol. 31, no. 17, pp. 1478—1479, (1995)

64. J. R. Taylor, "Optical solitons – theory and experiment", (Cambridge University Press, Cambridge, 1992)

65. N. J. Doran, "Nonlinear fibre devices and soliton communications", *Guided Wave Nonlinear Optics*, pp. 535—551, (1992)

66. Created with the help of Donald Govan, Aston University, Birmingham, England

67. A. Altuncu, L. Noel, W. A. Pender, A. S. Siddiqui, T. Widdowson, A. D. Ellis, M. A. Newhouse, A. J. Antos, G. Kar, and P. W. Chu, "40 Gbit/s error-free transmission over a 68km distributed erbium-doped fiber amplifier", *Electronics Letters*, vol. 32, no. 3, pp. 233—234, (1996)

68. K. J. Blow, and N. J. Doran, "Average soliton dynamics and the operation of soliton systems with lumped amplifiers", *IEEE Photonics Technology Letters*, vol. 3, no. 4, pp. 369—371, (1991)

69. A. Yariv, "Signal-to-noise considerations in fibre links with periodic or distributed optical amplification", *Optics Letters*, vol. 15, no. 19, pp. 1064—1066, (1990)

70. J. V. Wright, S. F. Carter, "Contraints on the design of long-haul soliton systems", *Technical Digest NLGW 1991*, paper MA2-1, pp. 6—9

71. A. F. Mitchell, J. V. Wright, S. F. Carter, A. D. Ellis, A. Lord, J. Lyke, and J. M. Scott, "The future of optically amplified submarine systems", *Technical digest on the Future of Optically Amplified Submarine Systems*, vol. S3, no. 2, pp. 49—54, (1993)

72. J. P. Gordon, "Theory of the soliton self-frequency shift", *Optics Letters*, vol. 11, no. 10, pp. 662—664, (1986)

73. G. Aubin, E. Jeanney, T. Montalant, J. Moulu, F. Pirio, J. B. Thomine, and F. Devaux, "20 Gbit/s soliton transmission over transoceanic distances with a 105km amplifier span", *Electronics Letters*, vol. 31, no. 13, pp. 1079—1080, (1995)

74. G. Aubin, T. Montalant, J. Moulu, F. Pirio, J. B. Thomine, and F. Devaux, "40 Gbit/s OTDM soliton transmission over transoceanic distances", *Electronics Letters*, vol. 32, no. 24, pp. 2188—2189, (1996)

75. G. Waters, and N. Wotherspoon, "Q measurement in high-speed optical amplified networks", *European Lightwave Transmission Seminar*, Hewlett-Packard (1996)

76. G. P. Agrawal, "Fibre Optic Comunications Systems", (J. Wiley & Sons, 1992)

77. X. Shan, T. Widdowson, D. J. Malyon, A. D. Ellis, and D. M. Spirit, "Comparison of soliton sources for communication applications", (IEE Colloqium on High Capcity Optical Communications, London, May '94), *IEE Proceedings J*, vol. 120, no. 6, (1994)

78. S. Tarucha, and K. Otsuka, "Response of semiconductor-laser to deep sinusoidal injection current modulation", *IEEE Journal of Quantum Electronics*, vol. 17, no. 5, pp. 810—816, (1981)

79. A. Takada, T. Sugie, and Saruwatari, "High-speed picosecond optical pulse compression from a gain-switched 1.3um distributed feedback-laser diode (DFB) through highly dispersive single mode fibre", *Journal of Lightwave Technology*, vol. 5, pp. 1525—1533, (1987)

80. M. Nakazawa, K. Suzuki, and Y. Kimura, "Transform-limited pulse generation in the gigahertz region from a gain-switched distributed-feedback laser diode using spectral windowing", *Optics Letters*, vol. 15, pp. 715—717, (1990)

81. J. Chung, N. Kikuchi, and S. Sasaki, "Generation of transform-limited optical pulses using a combination of a gain-switched diode-laser and a semiconductor optical amplifier", *IEEE Photonics Technology Letters*, vol. 7, no. 8, pp. 860—862, (1995)

82. M. Schell, D. Huhse, and D. Bimbarg, "Generation of 2.5 ps light pulses with 15 nm wavelength tunability at 1.3 mm by self seeded gain switched semiconductor laser", *IEEE Photonics Technology Letters*, vol. 5, no. 11, pp. 1267—1269, (1993)

83. K. A. Williams, I. H. White, D. Burns, and W. Sibbett, "Jitter reduction through feedback for picosecond pulsed InGaAsP lasers", *IEEE Journal of Quantum Electronics*, vol. 32, no. 11, pp. 1988—1994, (1996)

84. A. D. Ellis, "All-optical networking beyond 10 Gbit/s; OTDM networks based on electro-optic modulators and fibre ring lasers", *PhD Thesis*, Aston University, (1997)

85. L. C. Blank, "Multi-gbit/s optical-time division multiplexing employing LiNbO3 switches with low-frequency sinewave drive", *Electronics Letters*, vol. 24, no. 25, pp. 1543—1544, (1988)

86. J. J. Veselka, S. K. Korotky, P. V. Mamyshev, A. H. Gnauck, G. Raybon, and N. M. Froberg, "A soliton transmitter using a CW laser and an NRZ driven Mach-Zehnder modulator", *IEEE Photonics Technology Letters*, vol. 8, no. 7, pp. 950—952, (1996)

87. A. D. Ellis, T. Widdowson, X. Shan, and D. G. Moodie, "3-node, 40-Gbit/s OTDM network experiment using electro-optic switches", *Electronics Letters*, vol. 30, no. 16, pp. 1333—1334, (1994)

88. A. Mar, D. Derickson, R. Helkey, J. Bowers, R. T. Huang, and D. Wolf, "Actively mode-locked external-cavity semiconductor-lasers with transform-limited single-pulse output", *Optics Letters*, vol. 17, no. 12, pp. 868—870, (1992)

89. E. Muller, W. Reichert, C. Ruck, and R. Steiner, "External-cavity laser design and wavelength calibration", *Hewlett-Packard* Journal, vol. 44, no. 1, pp. 20—27, (1993)

90. P. B. Hansen, G. Raybon, U. Koren, B. I. Miller, M. G. Young, M. Chien, and X. X. Burrus, "5.5-mm long InGaAsP monolithic extended-cavity laser with an integrated bragg-reflector for active mode-locking", *IEEE Photonics Technology Letters*, vol. 4, no. 3, pp. 215—217, (1992)

91. R. P. Davey, K. Smith, and A. Mcguire, "High-speed, mode-locked, tunable, integrated erbium fiber laser", *Electronics Letters*, vol. 28, no. 5, pp. 482—484, (1992)

92. E. J. Greer, Y. Kimura, K. Suzuki, E. Yoshida, and M. Nakazawa, "Generation of 1.2ps, 10 Ghz pulse-train from all-optically modelocked, erbium fiber ring laser with active nonlinear polarization rotation", *Electronics Letters*, vol. 30, no. 21, pp. 1764—1765, (1994)

93. D. M. Patrick, "Modelocked ring laser using nonlinearity in a semiconductor-laser amplifier", *Electronics Letters*, vol. 30, no. 1, pp. 43—44, (1994)

94. X. Shan, D. Cleland, and A. Ellis, "Stabilizing erbium fiber soliton laser with pulse phase locking", *Electronics Letters*, vol. 28, no. 2, pp. 182—184, (1992)

95. X. Shan, "Stabilisation of a 10 GHz mode-locked erbium fibre laser and its applications in 4x10 Gbit/s soliton transmission", *Technical Digest NGWP 1993*, paper TuD4

96. A. Takada, and H. Miyazawa, "30 GHz picosecond pulse generation from actively mode-locked erbium-doped fiber laser", *Electronics Letters*, vol. 26, no. 3, pp. 216—217, (1990)

97. T. Pfeiffer, and G. Veith, "40 GHz pulse generation using a widely tunable all-polarization preserving erbium fiber ring laser", *Electronics Letters*, vol. 29, no. 21, pp. 1849—1850, (1993)

98. P. N. Kean, J. W. D. Gray, I. Bennion, and N. J. Doran, "Dispersion-modified actively modelocked erbium fiber laser using a chirped fiber grating", *Electronics Letters*, vol. 30, no. 25, pp. 2133—2135, (1994)

99. PriTel Inc., P. O. Box 4025, Naperville, IL 60567-4025 USA, Tel: 630-961-5660, Fax: 630-961-1105, Email: pritel@xnet.com

100. G. E. Wickens, D. M. Spirit, and L. C. Blank, "20 Gbit/s, 205-km optical-time division multiplexed transmission-system", *Electronics Letters*, vol. 27, no. 11, pp. 973—974, (1991)

101. N. Takato, K. Jinguji, M. Yasu, H. Toba, and M. Kawachi, "Silica-based single-mode waveguides on silicon and their application to guided-wave optical interferometers", *Journal of Lightwave Technology*, vol. 6, no. 6, pp. 1003—1010, (1988)

102. O. Kamatani, and S. Kawanishi, "Prescaled timing extraction from 400 Gbit/s optical signal using a phase locked loop based on four-wave-mixing in a laser diode amplifier", *IEEE Photonics Technology Letters*, vol. 8, no. 8, pp. 1094—1096, (1996)

103. D. M. Bird, R. M. Fatah, M. K. Cox, P. D. Constantine, J. C. Regnault, and K. H. Cameron, "Miniature packaged actively mode-locked semiconductor-laser with tunable 20 ps transform limited pulses", *Electronics Letters*, vol. 26, no. 25, pp. 2086—2087, (1990)

104. A. J. Taylor, J. M. Wiesenfeld, G. Eisenstein, and R. S. Tucker, "Timing jitter in mode locked and gain switched InGaAsP injection lasers", *Applied Physics Letters*, vol. 49, no. 12, pp. 681—683, (1986)

105. J. A. R. Williams, I. Bennion, K. Sugden, and N. J. Doran, "Fiber dispersion compensation using a chirped in-fiber Bragg grating", *Electronics Letters*, vol. 30, no. 12, pp. 985—987, (1994)

106. D. G. Moodie, "Electroabsorption modulators and their impact on future telecommunication networks", MSc Thesis, Electronic and Electrical Engineering Department, University College London, London, UK, (1994)

107. P. Harper, F. M. Know, P. N. Kean, I. Bennion, and N. J. Doran, "10 Gbit/s soliton propagation over 5250 km in standard fibre with dispersion compresation", *Technical Digest OFC 1997*, paper ThN1, pp. 304—305

108. A. D. Ellis, and T. Widdowson, "690-node global OTDM network demonstration", *Electronics Letters*, vol. 31, no. 14, pp. 1171—1172, (1995)

109. T. S. Kinsel, and F. S. Chen, "Experimental evaluation of an optical time division demultiplexer for twenty-four channels", *Applied Optics*, vol. 11, no. 6, pp. 1411—1418, (1972)

110. A. D. Ellis, T. Widdowson, X. Shan, G. E. Wickens, and D. M. Spirit, "Transmission of a true single-polarization 40 Gbit/s soliton data signal over 205km using a stabilized erbium fiber ring laser and 40 GHz electronic timing recovery", *Electronics Letters*, vol. 29, no. 11, pp. 990—992, (1993)

111. D. D. Marcenac, D. Nesset, A. E. Kelly, M. Brierley, A. D. Ellis, D. G. Moodie, and C. W. Ford, "40Gbit/s transmission over 406km of NDFS using mid-span spectral inversion by four-wave-mixing in a 2mm long semiconductor optical amplifier", *Electronics Letters*, vol. 33, no. 10, pp. 879—880, (1997)

112. D. M. Patrick, and A. D. Ellis, "Demultiplexing using cross-phase modulation-induced spectral shifts and kerr polarisation rotation in optical fibre", *Electronics Letters*, vol. 29, no. 2, pp. 227—228, (1993)

113. O. Kamatani, and S. Kawanishi, "Add/drop operation for 100 Gbit/s optical signal based on optical wavelength conversion by 4-wave-mixing", *Electronics Letters*, vol. 32, no. 10, pp. 911—913, (1996)

114. K. J. Blow, N. J. Doran, and B. P. Nelson, "Demonstration of the nonlinear fiber loop mirror as an ultrafast all-optical demultiplexer", *Electronics Letters*, vol. 26, no. 14, pp. 962—964, (1990)

115. D. M. Patrick, A. D. Ellis, and D. M. Spirit, "Bit-rate flexible all-optical demultiplexing using a nonlinear-optical loop mirror", *Electronics Letters*, vol. 29, no. 8, pp. 702—703, (1993)

116. A. D. Ellis, and D. M. Spirit, "Compact 40 Gbit/s optical demultiplexer using a GaInAsP optical amplifier", *Electronics Letters*, vol. 29, no. 24, pp. 2115—2116, (1993)

117. E. Jahn, N. Agrawal, H. J. Ehrke, R. Ludwig, W. Pieper, and H. G. Weber, "Monolithically integrated asymmetric mach-zehnder interferometer as a 20 Gbit/s all-optical add/drop multiplexer for OTDM systems", *Electronics Letters*, vol. 32, no. 3, pp. 216—217, (1996)

118. D. M. Patrick, A. D. Ellis, D. A. O. Davies, M. C. Tatham, and G. Sherlock, "Demultiplexing using polarization rotation in a semiconductor-laser amplifier", *Electronics* Letters, vol. 30, no. 4, pp. 341—342, (1994)

119. T. Morioka, K. Mori, and M. Saruwatari, "Ultrafast polarization-independent optical demultiplexer using optical carrier frequency-shift through crossphase modulation", *Electronics Letters*, vol. 28, no. 11, pp. 1069—1070, (1992)

120. P. A. Andrekson, N. A. Olsson, J. R. Simpson, T. Tanbunek, R. A. Logan, and M. Haner, "16 Gbit/s all-optical demultiplexing using 4-wave-mixing", *Electronics Letters*, vol. 27, no. 11, pp. 922—924, (1991)

121. S. Kawanishi, T. Morioka, O. Kamatani, H. Takara, and M. Saruwatari, "100 Gbit/s, 200 km optical transmission experiment using extremely low jitter PLL timing extraction and all-optical demultiplexing based on polarization-insensitive 4-wave-mixing", *Electronics Letters*, vol. 30, no. 10, pp. 800—801, (1994)

122. T. Morioka, H. Takara, S. Kawanishi, K. Uchiyama, and M. Saruwatari, "Polarisation-independent all-optical demultiplexing up to 200 Gbit/s using four-wave mixing in a semiconductor laser amplifier", *Technical Digest OFC 1996*, paper WH1, pp. 131—132

123. T. Morioka, H. Takara, S. Kawanishi, T. Kitoh, and M. Saruwatari, "Error-free 500 Gbit/s all-optical demultiplexing using low-noise, low-jitter supercontinuum short pulses", *Electronics Letters*, vol. 32, no. 9, pp. 833—834, (1996)

124. D. B. Mortimore, "Fiber loop reflectors", *Journal of Lightwave Technology*, vol. 6, no. 7, pp. 1217—1224, (1988)

125. N. Finlayson, B. K. Nayar, and N. J. Doran, "Switch inversion and polarization sensitivity of the nonlinear-optical loop mirror", *Optics Letters*, vol. 17, no. 2, pp. 112—114, (1992)

126. N. J. Doran, and D. Wood, "Nonlinear-optical loop mirror", *Optics Letters*, vol. 13, no. 1, (1988)

127. N. J. Doran, D. S. Forrester, and B. K. Nayar, "Experimental investigation of all-optical switching in fiber loop mirror device", *Electronics Letters*, vol. 25, no. 4, pp. 267—269, (1989)

128. K. J. Blow, N. J. Doran, and B. K. Nayar, "Experimental demonstration of optical soliton switching in an all-fiber nonlinear sagnac interferometer", *Optics Letters*, vol. 14, no. 14, pp. 754—756, (1989)

129. A. W. O'Neill, and R. P. Webb, "All-optical loop mirror switch employing an asymmetric amplifier attenuator combination", *Electronics* Letters, vol. 26, no. 24, pp. 2008—2009, (1990)

130. M. E. Fermann, F. Haberl, M. Hofer, and H. Hochreiter, "Nonlinear amplifying loop mirror", *Optics* Letters, vol. 15, no. 13, pp. 752—754, (1990)

131. D. A. Pattison, P. N. Kean, W. Forysiak, I. Bennion, and N. J. Doran, "Bandpass switching in a nonlinear-optical loop mirror", *Optics* Letters, vol. 20, no. 4, pp. 362—364, (1995)

132. K. J. Blow, N. J. Doran, B. K. Nayar, and B. P. Nelson, "2-wavelength operation of the nonlinear fiber loop mirror", *Optics Letters*, vol. 15, no. 4, pp. 248—250, (1990)

133. A. D. Ellis, and D. A. Cleland, "Ultrafast all-optical switching in two wavelength amplifying nonlinear optical loop mirror", *Electronics Letters*, vol. 28, no. 4, pp. 405—407, (1992)

134. K. Uchiyama, S. Kawanishi, H. Takara, T. Morioka, and M. Saruwatari, "100 Gbit/s to 6.3 Gbit/s demultiplexing experiment using polarization-independent nonlinear-optical loop mirror", *Electronics Letters*, vol. 30, no. 11, pp. 873—875, (1994)

135. D. A. Pattison, "Switching and generation of ultrashort pulses using all-fibre devices", *PhD Thesis*, Aston University, Birmingham, England, (1995)

136. B. P. Nelson, K. Smith, and K. J. Blow, "Mode-locked erbium fiber laser using all-optical nonlinear loop modulator", *Electronics Letters*, vol. 28, no. 7, pp. 656—658, (1992)

137. K. J. Blow, and K. Smith, "Nonlinear loop mirror devices and applications", *British Telecommunications Technology Journal*, vol. 11, no. 2, pp. 99—107, (1993)

138. S. Bigo, E. Desurvire, and B. Desruelle, "All-optical RZ-to-NRZ format conversion at 10 Gbit/s with nonlinear-optical loop mirror", *Electronics Letters*, vol. 30, no. 22, pp. 1868—1869, (1994)

139. D. Mahgerefteh, and M. W. Chbat, "All-optical 1.5-um to 1.3-um wavelength conversion in a walk-off compensating nonlinear-optical loop mirror", *IEEE Photonics Technology Letters*, vol. 7, no. 5, pp. 497—499, (1995)

140. K. Smith, N. J. Doran, and P. G. J. Wigley, "Pulse shaping, compression, and pedestal suppression employing a nonlinear-optical loop mirror", *Optics Letters*, vol. 15, no. 22, pp. 1294—1296, (1990)

141. M. Jinno, and T. Matsumoto, "Ultrafast all-optical logic operations in a nonlinear sagnac interferometer with 2 control beams", *Optics Letters*, vol. 16, no. 4, pp. 220—222, (1991)

142. J. P. Gordon, and H. A. Haus, "Random-walk of coherently amplified solitons in optical fiber transmission", *Optics Letters*, vol. 11, no. 10, pp. 665—667, (1986)

143. A. Mecozzi, J. D. Moores, H. A. Haus, and Y. Lai, "Soliton transmission control", *Optics Letters*, vol. 16, no. 23, pp. 1841—1843, (1991)

144. Y. Kodama, and A. Hasegawa, "Generation of asymptotically stable optical solitons and suppression of the Gordon-Haus effect", *Optics Letters*, vol. 17, pp. 31—33, (1992)

145. L. F. Mollenauer, J. P. Gordon, and S. G. Evangelides, "The sliding-frequency guiding filter - an improved form of soliton jitter control", *Optics Letters*, vol. 17, no. 22, pp. 1575—1577, (1992)

146. D. LeGuen, F. Farve, R. Boittin, J. Debeau, F. Devaux, M. Henry, C. Thebault, and T. Georges, "Demonstration of sliding-filter-controlled soliton transmission at 20 Gbit/s over 14 Mm", *Electronics Letters*, vol. 15, no. 6, pp. 314—316, (1995)

147. N. J. Smith, and N. J. Doran, "Picosecond soliton transmission using concatenated nonlinear-optical loop-mirror intensity filters", *Journal of the Optical Society of America, B*, vol. 12, no. 6, pp. 1117—1125, (1995)

148. E. Brunmaunand, P. Brindel, O. Leclerc, F. Pitel, and E. Desurvire, "Parametric study of chromatic dispersion influence in 20 Gbit/s, 20 Mm regenerated soliton systems with up to 140km amplifier spacing", *Electronics Letters*, vol. 32, no. 11, pp. 1022—1023, (1996)

149. J. P. King, I. Hardcastle, H. J. Harvey, P. D. Greene, B. J. Shaw, M. G. Jones, D. J. Forbes, and M. C. Wright, "Polarization-independent 20 Gbit/s soliton data-transmission over 12500 km using amplitude and phase modulation soliton transmission control", *Electronics Letters*, vol. 31, no. 13, pp. 1090—1091, (1995)

150. S. Bigo, O. Audouin, and E. Desurvire, "Analysis of soliton in-line regeneration through 2-wavelength nonlinear loop mirror as synchronous amplitude-phase modulator", *Electronics Letters*, vol. 31, no. 25, pp. 2191—2192, (1995)

151. S. Bigo, E. Desurvire, and O. Audouin, "Dual-control nonlinear-optical loop mirrors for all-optical soliton synchronous modulation", *Optics Letters*, vol. 21, no. 18, pp. 1463—1465, (1996)

152. T. Widdowson, D. J. Malyon, A. D. Ellis, K. Smith, and K. J. Blow, "Soliton shepherding - all-optical active soliton control over global distances", *Electronics Letters*, vol. 30, no. 12, pp. 990—991, (1994)

153. W. Pohlmann, E. Schlag, K. Koffers, B. Wedding, and J. Albers, "10 Gbit/s silicon bipolar optical receiver and regenerator", *Electronics Letters*, vol. 29, no. 24, pp. 2146—2148, (1993)

154. J. P. Hueting, T. Widdowson, and A. D. Ellis, "10 Gbit/s NRZ global transmission using optically amplified electronic regeneration", *Electronics Letters*, vol. 31, no. 13, pp. 1075—1076, (1995)

155. M. Yoneyama, A. Sano, T. Kataoka, A. Hirano, T. Otsuji, K. Sato, H. miyazawa, and K. Hagimoto, "40 Gbit/s optical repeater circuit using InAlAs/InGaAs HEMT digital IC module", *Electronics Letters*, vol. 33, no. 23, pp. 1977—1979, (1997)

156. A. Felder, M. Moller, M. Wurzer, M. Rest, T. F. Meister, and H. M. Rein, "60 Gbit/s regenerating demultiplexer in SiGe bipolar technology", *Electronics Letters*, vol. 33, no. 23, pp. 1984—1986, (1997)

157. W. A. Pender, P. J. Watkinson, E. J. Greer, and A. D. Ellis, "10 Gbit/s all-optical regenerator", *Electronics Letters*, vol. 31, no. 18, pp. 1587—1588, (1995)

158. W. A. Pender, T. Widdowson, and A. D. Ellis, "Error-free operation of a 40 Gbit/s all-optical regenerator", *Electronics Letters*, vol. 32, no. 6, pp. 567—569, (1996)

159. M. Jinno, and M. Abe, "All-optical regenerator based on nonlinear fiber sagnac interferometer", *Electronics Letters*, vol. 28, no. 14, pp. 1350—1352, (1992)

160. J. K. Lucek, and K. Smith, "All-optical Signal Regenerator", *Optics Letters*, vol. 18, no. 15, pp. 1226—1228, (1993)

161. M. Jinno, "All-optical signal regularizing/regeneration using a nonlinear fiber sagnac interferometer switch with signal-clock walk-off", *Journal of Lightwave Technology*, vol. 12, no. 9, pp. 1648—1659, (1994)

162. M. Eiselt, W. Pieper, G. Grosskopf, R. Ludwig, and H. G. Weber, "One million pulse circulations in a fiber ring using a slalom for pulse shaping and noise-reduction", *IEEE Photonics Technology Letters*, vol. 5, no. 4, pp. 422—424, (1993)

163. D. A. O. Davies, A. D. Ellis, and G. Sherlock, "Regenerative 20 Gbit/s wavelength conversion and demultiplexing using a semiconductor-laser amplifier nonlinear loop mirror", *Electronics Letters*, vol. 31, no. 12, pp. 1000—1001, (1995)

164. S. Bigo, O. Leclerc, P. Brindel, G. Vendrome, E. Desurvire, P. Doussiere, and T. Ducellier, "All-optical regenerator for 20 Gbit/s transoceanic transmission", *Electronics Letters*, vol. 33, no. 11, pp. 975—976, (1997)

165. D. Chiaroni, B. Lavigne, A. Jourdan, L. Hamon, C. Janz, and M. Renaud, "New 10 Gbit/s 3R NRZ optical regenerator interface based on semiconductor optical amplifiers for all-optical networks", *Technical Digest ECOC 1997*, paper PD-TH3B, pp. 41—46

166. R. J. Manning, A. J. Poustie, and K. J. Blow, "All-optical clock division using a semiconductor optical amplifier loop mirror with feedback", *Electronics Letters*, vol. 32, no. 16, pp. 1504—1506, (1996)

167. M. Jinno, and T. Matsumoto, "All-optical timing extraction using a 1.5-um self pulsating multielectrode DFB-LD", *Electronics Letters*, vol. 24, no. 23, pp. 1427—1429, (1988)

168. P. E. Barnsley, G. E. Wickens, H. J. Wickes, and D. M. Spirit, "A 4x5 Gbit/s transmission-system with all-optical clock recovery", *IEEE Photonics Technology Letters*, vol. 4, no. 1, pp. 83—86, (1992)

169. P. Barnsley, "All-optical clock extraction using two-contact devices", *IEE Proceedings Journal*, vol. 140, no. 5, pp. 325—336, (1993)

170. U. Feiste, D. J. As, and A. Ehrhardt, "18 GHz all-optical frequency locking and clock recovery using a self-pulsating two-section DFB-laser", *IEEE Photonics Technology Letters*, vol. 6, no. 1, pp. 106—108, (1994)

171. R. Ludwig, W. Pieper, E. Jahn, N. Agrawal, A. Ehrhardt, L. Kuller, H. G. Weber, "10 GHz all-optical clock recovery using a mode-locked semiconductor laser in a 40 Gbit/s, 100-km transmission experiment", *Technical Digest OFC 1996*, paper WH2

172. I. Ogura, H. Kurita, Y. Hashimoto, T. Shimizu, and H. Yokoyama, "Demonstration of all-optical clock recovery and demultiplexing with a simple-geometry utilising mode-locked laser diodes", *Technical Digest ECOC 1997*, vol. 2, paper TU2A, pp. 77—81

173. H. Kurita, T. shimizu, and H. Yokoyama, "All-optical clock extraction at bit rates upto 80 Gbit/s with monolithic mode-locked laser diodes", *Conference on Lasers and Electroptics*, CTuJ5, pp. 96—97, (1997)

174. A. D. Ellis, K. Smith, and D. M. Patrick, "All-optical clock recovery at bit rates up to 40 Gbit/s", *Electronics Letters*, vol. 29, no. 15, pp. 1323—1324, (1993)

175. S. Bigo, and E. Desurvire, "20 GHz all-optical clock recovery based on fiber laser mode-locking with fiber nonlinear loop mirror as variable intensity phase modulator", *Electronics Letters*, vol. 31, no. 21, pp. 1855—1857, (1995)

176. L. E. Adams, E. S. Kintzer, and J. G. Fujimoto, "All-optical timing extraction at 40-GHz using a mode-locked figure-8 laser with an sla", *Electronics Letters*, vol. 31, no. 20, pp. 1759—1761, (1995)

177. L. E. Adams, E. S. Kintzer, and J. G. Fujimoto, "Performance and scalability of an all-optical clock recovery figure 8 laser", *IEEE Photonics Technology Letters*, vol. 8, no. 1, pp. 55—57, (1996)

178. K. Smith, and J. K. Lucek, "All-optical clock recovery using a mode-locked laser", *Electronics Letters*, vol. 28, no. 19, pp. 1814—1816, (1992)

179. D. M. Patrick, and R. J. Manning, "20 Gbit/s all-optical clock recovery using semiconductor nonlinearity", *Electronics Letters*, vol. 30, no. 2, pp. 151—152, (1994)

180. K. L. Hall, K. A. Rauschenbach, E. A. Swanson, S. R. Chinn, and G. Raybon, "Picosecond-accuracy all-optical bit phase sensing using a nonlinear-optical loop mirror", *IEEE Photonics Technology Letters*, vol. 7, no. 8, pp. 935—937, (1995)

181. K. Suzuki, N. Ohkawa, M. Murakami, and K. Aida, "Unrepeated 40 Gbit/s RZ signal transmission over 240 km of conventional single mode fibre", *Technical Digest ECOC 1997*, vol. 3, paper WE1B, pp. 27—31

182. S. Kawanishi, and M. Saruwatari, "New-type phase-locked loop using traveling-wave laser-diode optical amplifier for very high-speed optical-transmission", *Electronics Letters*, vol. 24, no. 23, pp. 1452—1453, (1988)

183. H. Bulow, "Optoelectronic synchronization scheme for ultrahigh-speed optical demultiplexer", *Electronics Letters*, vol. 31, no. 22, pp. 1937—1938, (1995)

184. S. Kawanishi, and M. Saruwatari, "10 GHz timing extraction from randomly modulated optical pulses using phase-locked loop with traveling-wave laser-diode optical amplifier using optical gain modulation", *Electronics Letters*, vol. 28, no. 5, pp. 510—511, (1992)

185. S. Kawanishi, and M. Saruwatari, "Ultra-high-speed PLL-type clock recovery circuit based on all-optical gain modulation in a travelling-wave laser diode amplifier", *Journal of Lightwave Technology*, vol. 11, no. 12, pp. 2123—2129, (1993)

186. S. Kawanishi, H. Takara, T. Morioka, O. Kamatani, and M. Saruwatari, "200 Gbit/s, 100km time division multiplexed optical transmission using supercontinuum pulses with prescaled pll timing extraction and all optical demultiplexing", *Electronics Letters*, vol. 31, no. 10, pp. 816—817, (1995)

187. S. Kawanishi, H. Takara, M. Saruwatari, and T. Kitoh, "Ultrahigh-speed phaselocked-loop-type clock recovery circuit using a traveling-wave laser-diode amplifier as a 50 Ghz phase-detector", *Electronics Letters*, vol. 29, no. 19, pp. 1714—1716, (1993)

188. O. Kamatani, and S. Kawanishi, "Ultrahigh-speed clock recovery with phase-lock loop based on 4-wave-mixing in a traveling-wave laser-diode amplifier", *Journal of Lightwave Technology*, vol. 14, no. 8, pp. 1757—1767, (1996)

189. P. Monteiro, J. N. Matos, A. Gameiro, and J. R. F. Darocha, "20 Gbit/s DR based timing recovery circuit", *Electronics Letters*, vol. 30, no. 10, pp. 799—800, (1994)

190. Results were kindly provided by Dominique Marcenac, BT Laboratories, Martlesham, Ipswich, England. These results were presented at ECOC 1997, see paper:

191. Personal communication and MatLab code provided by Dominique Marcenac, BT Laboratories, Martlesham, Ipswich

192. K. Uchiyama, T. Morioka, S. Kawanishi, H. Takara, and M. Saruwatari, "Signal-to-noise ratio analysis of 100 Gbit/s demultiplexing using nonlinear optical loop mirror", *Journal of Lightwave Technology*, vol. 15, no. 2, pp. 194—201, (1997)

193. M. Jinno, "Effects of crosstalk and timing jitter on all-optical time-division demultiplexing using a nonlinear fiber sagnac interferometer switch", *IEEE Journal of Quantum Electronics*, vol. 30, no. 12, pp. 2842—2853, (1994)

194. R. J. Mears, L. Reekie, I. M. Jauncey, and D. N. Payne, "Low-noise erbium-doped fiber amplifier operating at 1.54-um", *Electronics Letters*, vol. 23, no. 19, pp. 1026—1028, (1987)

195. J. M. Wiesenfeld, "Gain dynamics and associated nonlinearities in semiconductor optical amplifiers", *Journal of High Speed Electronics and Systems*, vol. 7, no. 1, pp. 179—222, (1996)

196. M. J. Adams, D. A. O. Davies, M. C. Tatham, and M. A. Fisher, "Nonlinearities in semiconductor-laser amplifiers", *Optical Quantum Electronics*, vol. 27, no. 1, pp. 1—13, (1995)

197. D. M. Patrick, A. D. Ellis, D. A. O. Davies, M. C. Tatham, and G. Sherlock, "Demultiplexing using polarization rotation in a semiconductor-laser amplifier", *Electronics Letters*, vol. 30, no. 4, pp. 341—342, (1994)

198. D. M. Patrick, and R. J. Manning, "20 Gbit/s wavelength conversion using semiconductor nonlinearity", *Electronics Letters*, vol. 30, no. 3, pp. 252—253, (1994)

199. M. Asghari, I. H. White, and R. V. Penty, "Wavelength conversion using semiconductor optical amplifiers", *Journal of Lightwave Technology*, vol. 15, no. 7, pp. 1181—1190, (1997)

200. R. J. Manning, D. A. O. Davies, D. Cotter, and J. K. Lucek, "Enhanced recovery rates in semiconductor-laser amplifiers using optical-pumping", *Electronics Letters*, vol. 30, no. 10, pp. 787—788, (1994)

201. G. P. Agrawal, "4-wave mixing and phase conjugation in semiconductor-laser media", *Optics Letters*, vol. 12, no. 4, pp. 260—262, (1987)

202. G. P. Agrawal, "Highly nondegenerate 4-wave mixing in semiconductor-lasers due to spectral hole burning", *Applied Physics Letters*, vol. 51, no. 5, pp. 302—304, (1987)

203. S. Kawanishi, K. Okamoto, M. Ishii, O. Kamatani, H. Takara, and K. Uchiyama, "All-optical time-division-multiplexing of 100 Gbit/s signal based on four-wave mixing in a travelling-wave semiconductor laser amplifier", *Electronics Letters*, vol. 33, no. 11, pp. 976—977, (1997)

204. M. Eiselt, "Optical loop mirror with semiconductor-laser amplifier", *Electronics Letters*, vol. 28, no. 16, pp. 1505—1507, (1992)

205. J. P. Sokoloff, P. R. Prucnal, I. Glesk, and M. Kane, "A terahertz optical asymmetric demultiplexer (TOAD)", *IEEE Photonics Technology Letters*, vol. 5, no. 7, pp. 787—790, (1993)

206. J. P. Sokoloff, I. Glesk, P. R. Prucnal, and R. K. Boncek, "Performance of a 50 Gbit/s optical-time domain multiplexed system using a terahertz optical asymmetric demultiplexer", *IEEE Photonics Technology Letters*, vol. 6, no. 1, pp. 98—100, (1994)

207. I. Glesk, J. P. Sokoloff, and P. R. Prucnal, "Demonstration of all-optical demultiplexing of TDM data at 250 Gbit/s", *Electronics Letters*, vol. 30, no. 4, pp. 339—341, (1994)

208. I. Glesk, J. P. Solokoff, and P. R. Prucnal, "All-optical address recognition and self-routing in a 250 Gbit/s packet-switched network", *Electronics Letters*, vol. 30, no. 16, pp. 1322—1323, (1994)

209. K. Suzuki, K. Iwatsuki, S. Nishi, M. Saruwatari, and T. Kitoh, "160 Gbit/s single-polarization subpicosecond transform-limited pulse signal demultiplexing using ultrafast optical loop mirror including MQW traveling-wave semiconductor-laser amplifier", *Electronics Letters*, vol. 30, no. 12, pp. 660—661, (1994)

210. A. J. Poustie, K. J. Blow, and R. J. Manning, "Amplitude restoration and storage threshold in an all-optical memory", *Technical Digest ECOC 1997*, vol. 2, paper TU2A, pp. 69—72

211. K. I. Kang, I. Glesk, P. R. Prucnal, "Ultrafast optical time demultiplexers using semiconductor optical amplifiers", *International Journal of High Speed Electronics and Systems*, vol. 7, no. 1, pp. 125—151, (1996)

212. K. I. Kang, I. Glesk, T. G. Chang, P. R. Prucnal, and R. K. Boncek, "Demonstration of all-optical mach-zehnder demultiplexer", *Electronics Letters*, vol. 31, no. 9, pp. 749—750, (1995)

213. E. Jahn, N. Agrawal, M. Arbert, H. J. Ehrke, D. Franke, R. Ludwig, and W. Pieper, "40 Gbit/s all-optical demultiplexing using a monolithically integrated Mach-Zehnder interferometer with semiconductor-laser amplifiers", *Electronics Letters*, vol. 31, no. 21, pp. 1857—1858, (1995)

214. M. Vaa, B. Mikkelsen, K. S. Jepsen, K. E. Stubkjaer, R. Hess, M. Duelk, W. Vogt, E. Gamper, E. Gini, P. A. Besse and H. Melchior, and S. Bouchoule, "Bit-error-rate assessment of 80 Gbit/s all-optical demultiplexing by a monolithically integrated Mach-Zehnder interferometer with semiconductor optical amplifiers", *Technical Digest ECOC 1997*, vol. 3, paper WE1B, pp. 31—34

215. R. Hess, M. Caracciagross, W. Vogt, E. Gamper, P. A. Besse, M. Duelk, E. Gini, H. Melchior, B. Mikkelsen, M. Vaa, K. S. Jepsen, K. E. Stubkjaer, and S. Bouchoule, "All-optical demultiplexing of 80 to 10 Gb/s signals with monolithic integrated high-performance Mach-Zehnder interferometer", *IEEE Photonics Technology Letters*, vol. 10, no. 1, pp. 165—167, (1998)

216. W. Idler, K. Daub, G. Laube, M. Schilling, P. Wiedemann, K. Dutting, M. Klenk, E. Lach, and K. Wunstel, "10 Gbit/s wavelength conversion with integrated multiquantum-well-based 3-port mach-zehnder interferometer", *IEEE Photonics Technology Letters*, vol. 8, no. 9, pp. 1163—1165, (1996)

217. L. H. Spiekman, U. Koren, M. D. Chien, B. I. Miller, J. M. Wiesenfeld, and J. S. Perino, "All-optical Mach-Zehnder wavelength converter with monolithically integrated DFB probe source", *IEEE Photonics Technology Letters*, vol. 9, no. 10, pp. 1349—1351, (1997)

218. L. Billes, J.C. Simon, B, Kowalski, M. Henry, G. Michaud, P. Lamouler and F. Alard, "20 Gbit/s optical 3R regenerator using SOA based Mach-Zehnder interferometer gate", *Technical Digest ECOC 1997*, vol. 2, paper Tu4B, pp. 269—272

219. I. D. Phillips, A. Gloag, P. N. Kean, N. J. Doran, I. Bennion, and A. D. Ellis, "Simultaneous demultiplexing, data regeneration, and clock recovery with a single semiconductor optical amplifier-based nonlinear-optical loop mirror", *Optics Letters*, vol. 22, no. 17, pp. 1326—1328, (1997)

220. M. J. O'Mahony, "Semiconductor-laser optical amplifiers for use in future fiber systems", *Journal of Lightwave Technology*, vol. 6, no. 4, pp. 531—544, (1988)

221. A. E. Kelly, I. F. Lealman, L. J. Rivers, S. D. Perrin, and M. Silver, "Polarization-insensitive, 25dB gain semiconductor-laser amplifier without antireflection coatings", *Electronics Letters*, vol. 32, no. 19, pp. 1835—1836, (1996)

222. M. Eiselt, W. Pieper, and H. G. Weber, "SLALOM - Semiconductor laser amplifier in a loop mirror", *Journal of Lightwave Technology*, vol. 13, no. 10, pp. 2099—2112, (1995)

223. G. P. Agrawal, and N. A. Olsson, "Self-phase modulation and spectral broadening of optical pulses in semiconductors laser amplifiers", *IEEE Journal of Quantum Electronics*, vol. 25, no. 11, pp. 2297—2306, (1989)

224. R. J. Manning, and D. A. O. Davies, "3-wavelength device for all-optical signal-processing", *Optics Letters*, vol. 19, no. 12, pp. 889—891, (1994)

225. R. J. Manning, and G. Sherlock, "Recovery of a pi-phase-shift in approximate-to-12.5ps in a semiconductor-laser amplifier", *Electronics Letters*, vol. 31, no. 4, pp. 307—308, (1995)

226. D. A. O. Davies, A. D. Ellis, T. Widdowson, and G. Sherlock, "10 Gbit/s data switched semiconductor-laser amplifier nonlinear loop mirror", *Electronics Letters*, vol. 31, no. 2, pp. 111—112, (1995)

227. A. D. Ellis, D. A. O. Davies, A. Kelly, and W. A. Pender, "Data-driven operation of semiconductor amplifier loop mirror at 40 Gbit/s", *Electronics Letters*, vol. 31, no. 15, pp. 1245—1247, (1995)

228. N. A. Olsson, "Lightwave systems with optical amplifiers", *Journal of Lightwave Technology*, vol. 7, no. 7, pp. 1071—1082, (1989)

229. D. Cotter, J. K. Lucek, M. Shabeer, K. Smith, D. C. Rogers, D. Nesset, and P. Gunning, "Self-routing of 100 Gbit/s packets using 6 bit keyword address recognition", *Electronics Letters*, vol. 31, no. 17, pp. 1475—1476, (1995)

230. B. P. Nelson, K. J. Blow, P. D. Constantine, N. J. Doran, J. K. Lucek, and I. W. Marshall, "All-optical Gbit/s switching using nonlinear optical loop mirror", *Electronics Letters*, vol. 27, no. 9, pp. 704—705, (1991)

231. R. Takahashi, Y. Kawamura, and H. Iwamura, "Ultrafast 1.55 um all-optical switching using low-temperature-grown multiple-quantum wells", *Applied Physics Letters*, vol. 68, no. 2, pp. 153—155, (1996)

232. D. G. Moodie, A. D. Ellis, and C. W. Ford, "Generation of 6.3ps optical pulses at a 10 GHz repetition rate using a packaged electroabsorption modulator and dispersion compensating fiber", *Electronics Letters*, vol. 30, no. 20, pp. 1700—1701, (1994)

233. D. G. Moodie, M. J. Harlow, M. J. Guy, S. D. Perrin, C. W. Ford, and M. J. Robertson, "Discrete electroabsorption modulators with enhanced modulation depth", *Journal of Lightwave Technology*, vol. 14, no. 9, pp. 2035—2043, (1996)

234. S. Oshiba, K. Nakamura, H. Horikawa, "High-efficient electroabsorption modulator to generate 20 GHz 3.6ps transform limited optical pulses", *Technical Digest OFC 1997*, pp. 136—137

235. H. Takeuchi, K. Tsuzuki, K. Sato, M. Yamamoto, Y. Itaya, A. Sano, M. Yoneyama, and T. Otsuji, "NRZ operation at 40 Gb/s of a compact module containing an MQW electroabsorption modulator integrated with a DFB laser", *IEEE Photonics Technology Letters*, vol. 9, no. 5, pp. 572—574, (1997)

236. D. D. Marcenac, A. D. Ellis, and D. G. Moodie, "80 Gbit/s OTDM using electroabsorption modulators", *Technical Digest ECOC 1997*, vol. 3, paper WE1B, pp. 23—26

237. M. J. Guy, J. R. Taylor, D. G. Moodie, and A. E. Kelly, "10 GHz 3 ps actively mode-locked ring laser incorporating a semiconductor laser amplifier and an electroabsorption modulator", *Electronics Letters*, vol. 32, no. 24, pp. 2240—2241, (1996)

238. L. D. Westbrook, and D. G. Moodie, "Simultaneous bidirectional analog fiberoptic transmission using an electroabsorption modulator", *Electronics Letters*, vol. 32, no. 19, pp. 1806—1807, (1996)

239. L. D. Westbrook, L. Noel, and D. G. Moodie, "Full-duplex, 25km analogue fibre transmission at 120 Mbit/s with simultaneous modulation and detection in an electroabsorption modulator", *Electronics Letters*, vol. 33, no. 8, pp. 694—695, (1997)

240. N. Edagawa, M. Suzuki, S. Yamamoto, "Novel wavelength conversion using an electroabsorption modulator: conversion experiments at upto 40 Gbit/s", *Technical Digest OFC 1997*, paper TuO5, pp. 77—78

241. K. Wakita, K. Sato, I. Kotaka, M. Yamamoto, and T. Kataoka, "20 Gbit/s, 1.55-um strained-InGaAsP MQW modulator integrated DFB laser module", *Electronics Letters*, vol. 30, no. 4, pp. 302—303, (1994)

242. M. Ishizaka, M. Yamaguchi, Y. Sakata, Y. Inomoto, J. Shimizu, and K. Komatsu, "Modulator integrated DFB lasers with more than 600km transmission capability at 2.5 Gbit/s", *Technical Digest ECOC 1997*, vol. 1, paper MO4B, pp. 163—167

243. U. Koren, B. I. Miller, M. G. Young, M. Chien, G. Raybon, T. Brenner, R. Benmichael, K. Dreyer, and R. J. Capik, "Polarization-insensitive semiconductor optical amplifier with integrated electroabsorption modulators", *Electronics Letters*, vol. 32, no. 2, pp. 111—112, (1996)

244. A. Ramdane, F. Devaux, N. Souli, D. Delprat, and A. Ougazzaden, "Monolithic integration of multiple-quantum-well lasers and modulators for high-speed transmission", *IEEE Journal Of Selected Topics In Quantum Electronics*, vol. 2, no. 2, pp. 326—335, (1996)

245. F. Zamkotsian, K. Sato, H. Okamoto, K. Kishi, I. Kotaka, M. Yamamoto, Y. Kondo, H. Yasaka, Y. Yoshikumi, and K. Oe, "Monolithic integration of a MQW modulators on an optical multiplexer on InP for 100 Gbit/s transmission", *Journal of Lightwave Technology*, vol. 14, no. 10, pp. 2344—2352, (1996)

246. F. Devaux, P. Bordes, A. Ougazzaden, M. Carre, and F. Huet, "Experimental optimization of mqw electroabsorption modulators with up to 40 GHz bandwidths", *Electronics Letters*, vol. 30, no. 16, pp. 1347—1348, (1994)

247. R. Weinmann, D. Baums, U. Cebulla, H. Haisch, D. Kaiser, E. Kuhn, E. Lach, K. Satzke, J. Weber, P. Wiedemann, and E. Zielinski, "Polarization-independent and ultra-high bandwidth electroabsorption modulator in multi-quantum-well deep-ridge wave-guide technology", *IEEE Photonics Technology Letters*, vol. 8, no. 7, pp. 891—893, (1996)

248. T. Ido, S. Tanaka, M. Suzuki, M. Koizumi, H. Sano, and H. Inoue, "Ultra-high-speed multiple-quantum-well electroabsorption optical modulators with integrated wave-guides", *Journal of Lightwave Technology*, vol. 14, no. 9, pp. 2026—2034, (1996)

249. J. Singh, "Semiconductor Optoelectronics – Physics and Technology", (McGraw-Hill International, isbn: 0-07-057637-8, 1995)

250. H. Shen, and F. H. Pollak, "Generalized Franz-Keldysh theory of electromodulation", *Physical Review B-condensed Matter*, vol. 42, no. 11, pp. 7097—7102, (1990)

251. D.A. B. Miller, and D. S. Chemla, "Optical Nonlinearities and Instabilities in Semiconductors", (Academic Press, 1988)

252. L. A Coldren, "Integrated Optoelectronics, Quantum Electronics – Principles and Applications", (Academic Press, Edited by: M. Dagenais, R. F. Leheny, J. Crow, isbn: 0-12-200420-5, 1995)

253. C, Duchet, P. Brindel, M. Goix, and O. Leclerc, "Polarization-insensitive bulk modulator module with high extinction ratio for soliton demultiplexing from 40 to 10 Gbit/s", *Technical Digest ECOC 1997*, vol. 1, paper MO4B, pp. 179—182

254. K. Kawano, M. Kohtoku, M. Ueki, T. Ito, S. Kondoh, Y. Noguchi, and Y. Hasumi, "Polarisation-insensitive travelling-wave electrode electroabsorption (TW-EA) modulator with bandwidth over 50 GHz and driving voltage less than 2V", *Electronics Letters*, vol. 33, no. 18, pp. 1580—1582, (1997)

255. F. Devaux, S. Chelles, A. Ougazzaden, A. Mircea, M. Carre, F. Huet, A. Carenco, Y. Sorel, J. F. Kerdiles, and M. Henry, "Full polarization insensitivity of a 20 Gbit/s strained-MQW electroabsorption modulator", *IEEE Photonics Technology Letters*, vol. 6, no. 10, pp. 1203—1206, (1994)

256. T. Ido, H. Sano, D. J. Moss, S. Tanaka, and A. Takai, "Strained InGaAs/InalAs MQW electroabsorption modulators with large bandwidth and low driving voltage", *IEEE Photonics Technology Letters*, vol. 6, no. 10, pp. 1207—1209, (1994)

257. K. Yamada, K. Nakamura, H. Murai, T. Kunii, and Y. Ogawa, "Polarization insensitive electroabsorption modulators for high-speed optical gating", *IEICE Transactions on Electronics*, vol. E80C, no. 1, pp. 62—68, (1997)

258. D. J. Moss, T. Ido, and H.sano, "Photogenerated carrier sweep-out times in strained InGaAs/InAl as quantum well modulators", *Electronics Letters*, vol. 30, pp. 405—406, (1994)

259. F. Koyama, and K. Iga, "Frequency chirping in external modulators", *Journal of Lightwave Technology*, vol. 6, no. 1, pp. 87—93, (1988)

260. F. Devaux, Y. Sorel, and J. F. Kerdiles, "Simple measurement of fibre dispersion and of chirp parameter of intensity modulated light", *Journal of Lightwave Technology*, vol. 11, no. 12, pp. 1937—1940, (1993)

261. M. Suzuki, H. Tanaka, N. Edagawa, and Y. Matsushima, "New applications of a sinusoidally driven InGaasP electroabsorption modulator to in-line optical gates with ASE noise-reduction effect", *Journal of Lightwave Technology*, vol. 10, no. 12, pp. 1912—1918, (1992)

262. D. G. Moodie, P. J. Cannard, A. J. Dann, D. D. Marcenac, C. W. Ford, J. Reed, T. R. Moore, J. K. Lucek, and A. D. Ellis, "Low polarisation sensitivity buried heterostructure electroabsorption modulators for ultra high speed netwroks", *23rd European Conference On Communications technical digest*, vol. MO4B, (1997)

263. M. Suzuki, H. Tanaka, and Y. Matsushima, "10 Gbit/s optical demultiplexing and switching by sinusoidally driven InGaAsP electroabsorption modulators", *Electronics Letters*, vol. 28, no. 10, pp. 934—935, (1992)

264. N. M. Froberg, G. Raybon, A. M. Johnson, Y. K. Chen, T. Tanbunek, R. A. Logan, A. Tate, A. M. Sargent, K. Wecht, and P. F. Sciortino, "Pulse generation by harmonic modulation of an integrated DBR laser-modulator", *Electronics Letters*, vol. 30, no. 8, pp. 650—651, (1994)

265. M. J. Guy, S. V. Chernikov, J. R. Taylor, and D. G. Moodie, "Demonstration of the feasibility of dual-frequency operation of an electroabsorption modulator for demultiplexing in a 16-channel 40-Gbit/s otdm system", *Electronics Letters*, vol. 32, no. 12, pp. 1138—1139, (1996)

266. Personal communication with A. D. Ellis, BT Laboratories, Martlesham, Ipswich

267. J. L. Gimlett, and N. K. Cheung, "Effects of phase-to-intensity noise conversion by multiple reflections on gigabit-per-second DFB laser transmission systems", *Journal of Lightwave Technology*, vol. 7, no. 6, pp. 888—895, (1989)

268. K. Yamada, K. Nakamura, and Y. Ogawa, "Improvement of bandwidth-to-drive-voltage of an electroabsorption modulator employing a double-pass configuration", *IEEE Photonics Technology Letters*, vol. 8, no. 8, pp. 1021—1023, (1996)

269. J. L. Gimlett, M. Z. Iqbal, L. Curtis, N. K. Cheung, A. Righetti, F. Fontana, and G. Grasso, "Impact of multiple reflection noise in Gbit/s lightwave systems with optical fiber amplifiers", *Electronics Letters*, vol. 25, no. 20, pp. 1393—1394, (1989)

270. H. Tanaka, S. Takagi, M. Suzuki, and Y. Matsushima, "Optical short-pulse generation by double gate operation of tandem connected electroabsorption modulators driven by sinusoidal voltages", *Electronics Letters*, vol. 29, no. 16, pp. 1449—1451, (1993)

271. Personal communication with A. D. Ellis, BT Laboratories, Martlesham, Ipswich, England

272. M. J. Guy, J. R. Taylor, D. G. Moodie, A. E. Kelly, "A 10-GHz 2-ps actively modelocked fibre-integrated semiconductor laser employing an electroabsorption modulator", *Technical Digest CLEO 1997*, paper CTuH5, pp. 86—87

273. Santec USA, Holmdel Corporation Plaza, HWY. 35 & Union Avenue, Holmdel, NJ 07733, Tel: 1-908-739-5505, Fax: 1-9080739-5506, Email: santec@po.infosphere.or.jp, WWW: http://www.santec.com/